

Ghent University
Faculty of Pharmaceutical Sciences

Design and evaluation of drug loaded microbubbles for ultrasound guided cancer therapy

**Ontwikkeling en evaluatie van geneesmiddel
bevattende microbubbels voor ultrasound
geleide kankertherapie**

Ine Lentacker

Pharmacist

Thesis submitted to obtain the degree of
Doctor in Pharmaceutical Sciences

Proefschrift voorgedragen tot het bekomen van de graad van
Doctor in de Farmaceutische Wetenschappen

2009

Dean:

Prof. dr. apr. Jean Paul Remon

Promoters:

Prof. dr. apr. Niek N. Sanders
Prof. dr. apr. Stefaan C. De Smedt

Co-promoter:

Prof. dr. apr. Jo Demeester

*Laboratory of General Biochemistry
and Physical Pharmacy*

The author and the (co-)promoters give the authorization to consult and to copy parts of this thesis for personal use only. Any other use is limited by the Laws of Copyright, especially the obligation to refer to the source whenever results from this thesis are cited.

De auteur en de (co-)promotoren geven de toelating dit proefschrift voor consultering beschikbaar te stellen en delen ervan te kopiëren voor persoonlijk gebruik. Elk ander gebruik valt onder de beperkingen van het auteursrecht, in het bijzonder met betrekking tot de verplichting uitdrukkelijk de bron te vermelden bij het aanhalen van resultaten uit dit proefschrift.

Gent, 4 februari 2009

De promotoren:

Prof. dr. apr. Niek N. Sanders

De auteur:

Ine Lentacker

Prof. dr. apr. Stefaan C. De Smedt

De co-promotor:

Prof. dr. apr. Jo Demeester

JORGE CHAM © 2009



THE ORIGIN OF THE THESES

WWW.PHDCOMICS.COM

Eerst het stukje tekst waar ik het hardst op gezwoegd heb in héél dit doctoraat, het dankwoord!

Stefaan en Jo, jullie gaven mij de kans om zelfstandig onderzoek te verrichten en lieten mij steeds vrij om nieuwe onderzoekswegen in te slaan. **Stefaan**, door jouw geanimeerde lessen wou ik absoluut “thesesen” op de tweede verdieping. Een beslissing waar ik nog geen moment spijt van gehad heb. Ik ben er zeker van dat jouw enthousiasme nog talloze studenten zal motiveren om zich in te zetten voor de wetenschap. **Niek**, bedankt voor de ideeën en suggesties tijdens mijn doctoraat. Ik hoop dat jouw Gentherapie labo in de diergeneeskunde snel groeit. **Kevin Br.**, ik wens je nog veel succes de komende jaren op het FFW.

Zonder de inzet en werkhijver van ons secretariaatsteam zouden vele dingen in het honderd lopen! **Katharine en Bruno**, merci voor de vele registraties, bonnetjes en het oplossen van “voornaam-problemen”, maar vooral voor de gezellige babbels en grapjes tussendoor!

Katrien, Joanna and Zanna, I already feel “at home” in my new office, thanks to you.

Veel collega’s hebben ondertussen het labo verlaten, maar zijn daarom zeker niet vergeten! **Barbara en Tinneke** merci voor de leuke koffiepauzes en gezellige lunches! **Stefaan D.**, ik zal jou ongetwijfeld nog wel eens zien, maar in ieder geval nog veel succes aan ‘den overkant’ en merci voor de aangename babbels! Dear **Farzaneh**, I’m sure we will meet again in the near future.

Kevin B., Broes, Dries and Chaobo, thank you for contributing to the pleasant atmosphere in the lab!

Hendrik, Geertrui en Oliwia, jullie zijn hier nog maar een jaartje, maar ik ben blij dat jullie zo’n sociale collega’s zijn, altijd bereid om deel te nemen aan één of andere labo-activiteit!

Bart G., ik ben heel blij dat ik niet meer de enige ben om te “bubbelen”. Het voorbije jaar was het al zeer aangenaam om met jou samen te werken en ik ben er zeker van dat het de komende jaren niet anders zal zijn.

Marie-Luce en Nathalie, jullie zijn fantastische collega’s en ik hoop dat jullie onderzoek binnenkort als een sneltrein vooruit schiet!

Ik weet nog hoe Bart ervoor zorgde dat ik een plaatsje kreeg in de “polyvalente zaal” waar **Bruno, Lies en Roos** zetelden en erbij vertelde dat ik me daar wel snel thuis zou voelen. **Lies en Roos**, jullie zorgden er inderdaad voor dat ik mij onmiddellijk thuis voelde in het labo en “den buro”. Jullie leerden mij alle kneepjes van het vak! Gelukkig zien we elkaar nog regelmatig om alle nieuwtjes uit te wisselen en ik denk dat het wel zo zal blijven! **Sofie**, ik ben zo blij dat we alletwee nog een tijdje op het FFW zullen rondlopen. Bedankt voor de zovele gesprekjes over kinderen, interieurinrichting en zoveel meer!

Koen, ik heb jou (helaas) pas leren kennen tijdens de full-time in ons laatste jaar. Maar ondertussen ben je een heel goeie vriend geworden. Hopelijk is jullie huizenjacht binnenkort succesvol afgerond en wonen jullie niet te ver uit de buurt!

Bart, jij bent zoveel meer dan een fantastische collega! Eerst en vooral was het door jou als thesisbegeleider te hebben dat ik gebeten werd door het wetenschappelijk onderzoek en daardoor met volle goesting aan mijn doctoraat begon. Ondertussen zien we elkaar bijna meer naast het labo dan in het labo en zorg jij, samen met de andere vriendjes, altijd voor de nodige ontspanning en relativering. Een vriend waar we altijd op kunnen rekenen... Siebe kan zich geen betere peter wensen!

Sofie, ons wekelijks (in theorie althans;-)) zwempartijtje is ook altijd iets om naar uit te kijken. Ik ben blij dat je binnenkort zo dichtbij komt wonen en ben er zeker van dat jij een SUPER-meter zal worden voor onze dochter!

Er waren altijd genoeg feestjes en gelegenheden om te vieren en te ontspannen: Merci **Jo, Evelien, Griet, Lieven, Julie, Evie, Olivier, Patricia, Marjan, Sylvie, Margriet, Ilse, Kwinten, Els, Manu** en al wie ik nog vergeten ben.

Janine, Robert en Christophe, ik ben heel gelukkig met zo'n lieve schoonouders en schoonbroer. Merci om er altijd voor ons te zijn!

Mama en papa, ik hoop dat we Siebe een even warme thuis zullen kunnen geven als ik altijd gehad heb! **Bram en Hanne**, ondanks het feit dat we alledrie totaal verschillend zijn, kunnen we het toch ongelofelijk goed vinden met elkaar. Bedankt om Siebe zoveel te entertainen!

Chouke, jij kent als geen ander de (kleine) frustraties van onderzoek. Merci om iedere dag opnieuw mijn steun en toeverlaat te zijn! Ook al zucht ik regelmatig als je weer gaat "wijnbouwen", uiteindelijk zal ik wel trots zijn als je een lekker wijntje kan produceren. Al zal het dan geen pinot noir zijn... ;-) Lieve kleine **Siebe** ("Wiebje"), mijn relativeringsvermogen is nog nooit groter geweest, sinds jij er bent! Ik ben ontzettend gelukkig dat ik jou iedere morgen mag wakker maken. Nu maar hopen dat jouw zusje even schattig en lief zal zijn!

Ine

TABLE OF CONTENTS

Table of Contents	11
List of Abbreviations and Symbols	13
General Introduction: Aim and Outline of this Thesis	17
Chapter 1: Introduction	21
Chapter 2: Polymer-coated albumin microbubbles that bind and protect plasmid DNA	71
Chapter 3: Transfection properties of uncoated and polymer coated albumin microbubbles	89
Chapter 4: Lipoplex loaded microbubbles for ultrasound targeted gene delivery	105
Chapter 5: Ultrasound exposure of lipoplex loaded microbubbles facilitates direct cytoplasmic entry of the lipoplexes	125
Chapter 6: Ultrasound assisted siRNA delivery using PEG-siPlex Loaded microbubbles	151
Chapter 7: Design and evaluation of doxorubicin containing microbubbles for ultrasound triggered doxorubicin delivery: cytotoxicity and mechanisms involved	173
Summary & General Conclusions	195
Samenvatting & Algemene Besluiten	201
Curriculum Vitae	209

LIST OF ABBREVIATIONS

A	Amplitude
AALS	Acoustically Active Liposphere
AAV	Adeno-Associated Virus
Ad	Adenovirus
ATP	Adenosine Triphosphate
BBB	Blood Brain Barrier
BCA	Bicinchoninic Acid
bp	Basepair
BSA	Bovine Serum Albumin
CCLR	Cell Culture Lysis Reagent
C₃F₅	Perfluoropropane
C₅F₁₂	Perfluoropentane
C₆F₁₄	Perfluorohexane
C_nF_{n+2}	Perfluorocarbons
Cholesteryl Bodipy FLC12	Cholesteryl 4,4-difluoro-5,7-dimethyl-4-bora-3a,4a-diaza-s-indacene-3-dodecanoate
CLSM	Confocal Laser Scanning Microscopy
CMV	Cytomegalovirus
DF	Duty Factor
DIC	Differential Interference Contrast
DLS	Dynamic Light Scattering
DMEM	Dulbecco's Modified Eagle's Medium
DNA	Desoxyribonucleic Acid
DOPE	1,2-Dioleoyl-sn-Glycero-3-Phosphoethanolamine
DOTAP	N-(1-(2,3-Dioleoyloxy)propyl)-N,N,N-Trimethylammoniumchloride
DOX	Doxorubicin
DPPE	1,2-Dipalmitoyl-sn-Glycero-3-Phosphocholine
dsDNA	Double Stranded DNA
dsRNA	Double Stranded RNA
DSPE-PEG	1,2-Distearoyl-sn-Phosphatidylethanolamine PEG
DSPE-PEG₂₀₀₀-biotin	DSPE-[biotinyl PEG ₂₀₀₀]
DTT	Dithiothreitol
EDTA	Ethylenediaminetetraacetic Acid
ELIP	Echogenic liposome
EtBr	Ethidium Bromide
f	Frequency
FBS	Fetal Bovine Serum
FFS	Fluorescence Fluctuation Spectroscopy
FITC	Fluorescein Isothiocyanate

gDNA	Genomic DNA
Hepes	4-(2-Hydroxyethyl)-1-Piperazineethanesulfonic Acid
HIFU	High Intensity Focused Ultrasound
HSV	Herpes Simplex Virus
HuH-7	Human Hepatoma-7
IFN	Interferon
IL-12	Interleukine 12
kb	Kilobase
kDa	Kilodalton
kPa	Kilopascal
MPa	Megapascal
LB	Luria–Bertani Medium
LBL	Layer-by-layer
LBGT	Laser Beam Gene Transduction
L-Gln	L-Glutamine
LPS	Liposome
LPX	Lipoplex
mβCD	Methyl- β -Cyclodextrin
mRNA	Messenger RNA
MTT	3-(4,5-Dimethylthiazol-2-yl)-2,5-Diphenyltetrazolium Bromide
MW	Molecular Weight
N:P ratio	Nitrogen to Phosphate Ratio
NSAID	Non-Steroidal Anti-Inflammatory Drugs
ONs	Antisense Oligonucleotides
PAGE	Polyacrylamide Gel Electrophoresis
PAH	Poly-(allylamine Hydrochloride)
PBS	Phosphate Buffered Saline
PCI	Photochemical Internalization
PCS	Photon Correlation Spectroscopy
pDMAEMA	Poly(2-Dimethylaminoethyl Methacrylate)
pDNA	Plasmid DNA
PEG	Poly(ethylene Glycol)
PEG-siPlexes	PEGylated siRNA-Liposome Complexes
pEI	Poly(ethyleneimine)
PLB	Passive Lysis Buffer
pLGA	Poly-(D,L-lactide-coglycolide)
pLL	Poly-(L-lysine)
PRF	Pulse Repetition Frequency
PRP	Pulse Repetition Period
PS	Photosensitizer

PW	Pulsed Wave
P/S	Penicilline-Streptomycine
RISC	RNA Induced Silencing Complex
RITC	Rhodamine isothiocyanate
RLU	Relative Light Units
RNA	Ribonucleic Acid
RNAi	RNA Interference
RNase	Ribonuclease
SD	Standard Deviation
SDS	Sodiumdodecylsulfate
SEAP	Secreted Alkaline Phosphatase
SF₆	Hexafluoride
shRNA	Short Hairpin RNA
siRNA	Short Interfering RNA
siPlexes	SiRNA-Liposome Complexes
ssDNA	Single Stranded RNA
ssRNA	Single Stranded DNA
SV40	Simian Virus 40
T	Period
TBE	Tris, Boric acid and EDTA buffer
TE	Tris and EDTA buffer
TIMP-1	Tissue Inhibitor of Metalloproteinase-1
TPPS2a	Meso-tetraphenylporphyrine Sulphonate
TRITC	Tetramethylrhodamineisothiocyanate
USE	Ultrasound Exposure
UV	Ultraviolet
v	Velocity
VEGF	Vascular Growth Factor
VSMC	Vascular Smooth Muscle Cells

LIST OF SYMBOLS

λ	Wavelength
τ	Pulse Duration
ζ	Zeta Potential

General Introduction

Aim and Outline of this Thesis

General Introduction

Aim and Outline of this Thesis

Elucidation of the cellular and genetic molecular mechanisms involved in cancer onset has provided several targets for the development of genetic and chemotherapeutic drugs. After surgical removal and/or radiation of the primary tumor, the remaining cancer cells can be treated with a variety of chemotoxic or genetic drugs. Despite the identification and development of several new drugs, cancer therapy encounters several barriers to become really effective. Due to the abnormalities and deficiencies in tumor vasculature and interstitial transport, current chemotherapeutic treatments are hampered by the non-uniform and insufficient delivery of anti-cancer agents to tumor cells. Due to the non-selective nature of several chemotherapeutics, resulting in neutropenia, therapies are often delayed and drug doses limited. This can result in the development of multi-drug resistance in a variety of tumors, responsible for treatment failure and non-responsive recurrence in several patients.

Treatment of cancers by gene therapy requires the development of intelligent delivery systems that are able to selectively stimulate gene uptake in cancer cells. To be effective, genetic drugs must conquer several barriers before reaching their intracellular target site. Although, viral gene carriers are by far the most efficient gene delivery carriers, their clinical use is hampered by the risk of insertional mutagenesis and severe immune responses. As a consequence, several non-viral gene carriers are currently under development, although their transfection efficiencies remain rather low. Intravenous administration of microbubbles combined with ultrasound radiation of the tumor has been recently proposed as a strategy to help non-viral gene carriers to (a) overcome biological barriers in drug delivery and (b) selectively enhance drug uptake in cancer cells. As current cancer treatments are hampered by the lack of an efficient and targeted delivery of drugs or genes to cancer cells, the general aim of this thesis was to design drug carrying microbubbles that are able to selectively deliver their content to cancer cells upon ultrasound radiation.

Chapter 1 gives a short overview of treatment strategies currently developed or employed in cancer therapy. Also, the basic concepts regarding the interaction between ultrasound energy and microbubbles as well as the clinical applications of microbubbles are summarized. As drug loaded

microbubbles show potential for ultrasound guided drug delivery we aimed at developing cationic charged albumin-shelled microbubbles to enable electrostatic loading of plasmid DNA (**chapter 2**). Although the microbubbles could be efficiently loaded with plasmid DNA, and though the loaded DNA seemed well protected against degradation by nucleases, transfection efficiencies obtained after ultrasound exposure of this microbubbles remained rather low (**chapter 3**). We showed that this is due to the formation of large aggregates consisting of microbubble shell fragments and plasmid DNA, which seemed to be too large to enter the cells. To tackle this problem we aimed at developing a new concept in **chapter 4**, in which pre-defined plasmid DNA-liposome complexes (lipoplexes) were attached onto the surface of a lipid shelled polymer. In **chapter 5** of this thesis we demonstrate that ultrasound exposure of such lipoplex loaded microbubbles results in the release of intact lipoplexes, which are immediately deposited inside the cytoplasm of the target cells, making an endocytic uptake and release redundant. The same microbubbles were loaded with short interfering RNA and evaluated for gene silencing purposes (**chapter 6**). Finally, in **chapter 7** we tried to answer the question whether this type of microbubbles is also promising for the ultrasound triggered delivery of doxorubicin to cancer cells.

Chapter 1

Introduction

Part of this chapter has been accepted for publication in *Soft Matter* (invited review).

Lentacker I.¹, De Smedt S.C.¹, Sanders N.N.² Drug loaded microbubbles for ultrasound triggered delivery.

¹ Laboratory of General Biochemistry and Physical Pharmacy, Department of Pharmaceutics, Ghent University, Ghent, Belgium.

² Laboratory of Gene Therapy, Department of Nutrition, Genetics and Ethology, Ghent University, Heidestraat 19, B-9820 Merelbeke, Belgium

ABSTRACT

Cancer is a major cause of death in the world. Nearly 13% of all deaths in 2007 were caused by cancer according to the World Health Organization. The recent advances in understanding the basic molecular mechanisms involved in the onset of cancer provide a framework for the pharmacological and genetic treatment of cancer. Several anti-neoplastic agents, acting at several stages in tumor development, have been developed. The identification of some important genes involved in the genetic onset of several cancers, like the p53 tumor suppressor gene and the ras oncogene, has led to a growing interest in cancer gene therapy.

Ultrasound has recently gained attention in the drug delivery field. Its non-invasive nature, local applicability and cheapness make ultrasound attractive for specific drug delivery purposes. Microbubbles are gas-filled micron-sized structures which were originally implemented to obtain a better contrast in ultrasound imaging techniques. Some of them have been FDA approved and are clinically used in ultrasound imaging. They recently became of interest to the drug delivery community as they may enhance the efficiency of ultrasound guided drug delivery by lowering the threshold for acoustic cavitation. Furthermore, microbubbles can be loaded with drugs which can be locally delivered upon ultrasound application.

In this chapter we give a short introduction on the onset of cancer and summarize some of the most important chemotherapeutics and genetic drugs that are currently used or under development to treat cancer. The most important viral and non-viral gene carriers are briefly discussed. Also the basic physics of ultrasound waves, their biological implications and therapeutic applications are described. Finally, we introduce the concept of microbubble-based ultrasound guided drug delivery and review some of the recent attempts made in the design of drug loaded microbubbles.

Chapter 1

Introduction

CANCER

Cancer is the transformation of normal cells into malignant cells as a result of mutations in the genome. A majority of these mutations are not inherited but arise spontaneously as a consequence of chemical damage to the DNA, resulting in an altered function of crucial genes¹. The continuous renewal of cells in the human body is controlled by a network of molecular mechanisms which govern cell proliferation and apoptosis. Mutations in the genes that control cell proliferation and apoptosis are responsible for the onset of cancer. These genes can be broadly divided into two classes: pro-oncogenes are responsible for the upregulation of their encoding proteins after mutation and oncogene formation, while the proteins encoded by tumor suppressor genes are inactivated or suppressed after mutation. Oncogenes are involved in signaling pathways which stimulate cell proliferation, while most human suppressor genes code for proteins controlling cell proliferation or cell death. In general five different pathways must be activated or inactivated in the genesis of a cancer cell¹:

- The cell must become independent of growth stimulatory signals.
- The cell must develop a refractory state to growth inhibitory signals.
- The cell must become resistant to apoptosis.
- The cell must overcome cell senescence i.e. require infinite proliferation properties.
- The cell must develop the capacity to form new blood vessels for nutrient supply.

Several genes are identified to play a crucial role in the development of cancers. An example of a crucial oncogene is ras, which is the most widely activated oncogene in human cancers. This gene codes for signal transduction molecules and mutations can result in a growth factor independent cell proliferation². The p53 gene has been identified as an important tumor suppressor gene in many cancers. This gene manages cell cycle and apoptosis. As a result, mutations can prevent cell apoptosis as a response to cell stress. The same gene also plays a role in regulating cell senescence³.

CANCER THERAPEUTICS

CHEMOTHERAPEUTICS

The majority of chemotherapeutic drugs can be divided into alkylating agents, antimetabolites, antibiotics and topoisomerase inhibitors. All of these drugs affect cell division or DNA synthesis and function in some way. Some newer agents do not directly interfere with DNA. These include monoclonal antibodies and the tyrosine kinase inhibitors which directly target a molecular abnormality in certain types of cancer. A very short overview of the most common anticancer drugs is given below.

Alkylating agents. This group of anticancer agents includes the nitrogen mustard derivatives and platinum anticancer agents. Alkylating agents are highly reactive drugs, alkylating several cellular components like proteins, RNA and DNA. Their main mechanism of action is their interaction with DNA, thereby blocking vital aspects of DNA metabolism⁴. This results in a transcriptional arrest and the activation of DNA damage pathways resulting in apoptosis⁴. Because of their cell cycle phase independence, alkylating agents are effective against a wide variety of cancers, although they are mainly used to treat slowly dividing tumors. Cisplatin and carboplatin have been widely used for many years to treat several forms of cancer. Cisplatin can form covalent crosslinks between the guanine bases of two DNA strands⁵. However, their activity remains limited due to side effects and the inherent and acquired resistance to these drugs. For this reason, several new platinum derivatives are currently investigated⁶.

Antimetabolites. The structure of antimetabolites is similar to certain compounds such as vitamins, amino acids, and precursors of DNA or RNA, found naturally in the human body. Antimetabolites interfere with cancer cell division and hinder the growth of tumor cells as they get incorporated in DNA, RNA or prevent the formation of new nucleotides. The toxicities associated with these drugs are seen in cells that are growing and dividing quickly. Examples of antimetabolites include purine antagonists, pyrimidine antagonists, and folate antagonists⁷⁻⁹.

Antitumor antibiotics. These antibiotics interfere with DNA and can prevent transcription, which makes them cell cycle nonspecific¹⁰⁻¹². The most well known antibiotic is doxorubicin. Three different working mechanisms have been identified, including DNA intercalation, lipid peroxidation

and inhibition of topoisomerase II¹³. Other antitumor antibiotics are daunorubicin, epirubicin and bleomycin.

Topoisomerase inhibitors. Topoisomerases are essential enzymes that maintain the topology of DNA. Inhibition of type I or II isomerases interferes with both DNA transcription and replication by preventing DNA supercoiling. Examples of topoisomerase inhibitors are doxorubicin, genistein and topotecan¹⁴.

Microtubule-targeted anticancer drugs (anti-mitotic drugs). Microtubules are key components of the cytoskeleton that are responsible for the transport of vesicles through the cell and play an important role in cell signalling and cell division. Microtubule-targeted drugs, including taxanes (paclitaxel, docetaxel) and *Vinca* alkaloids (vinblastine, vincristine), can suppress microtubule dynamics leading to mitotic block and apoptosis¹⁵.

Monoclonal antibodies. Monoclonal antibodies work by attaching to certain parts of the tumor-specific antigens and make them easily recognizable by the host's immune system. They also prevent growth of cancer cells by blocking the cell receptors to which chemicals called 'growth factors' attach promoting cell growth. Several antibodies have been approved for cancer treatment and most of these agents are combined with conventional chemotherapeutics or radiotherapy¹⁶.

CANCER GENE THERAPY

The discovery that the transformation of normal cells into malignant ones is associated with multi-mutational alterations on the genetic level of these cells, makes cancer cells an important target for gene therapy. The first approach in gene therapy is the introduction of a therapeutic gene, either transient or by inserting it into a non-specific place in the genome. This results in the expression of a therapeutic protein that was previously absent or malfunctioning. Another approach is to regulate the expression of a disease causing protein by degrading its mRNA. This can be accomplished by using antisense oligonucleotides, ribozymes or small interfering RNA¹⁷⁻¹⁹.

DNA-based therapeutics

Plasmid DNA. Plasmids are high molecular weight, double-stranded DNA constructs containing transgenes, which encode specific proteins. Gene therapy involves the use of plasmid DNA to introduce transgenes into cells that inherently lack the ability to produce a certain protein, encoded by the transgene²⁰. After cellular entry, the plasmid DNA should be able to enter the cell nucleus, to become transcribed by the cellular transcription machinery. Both the cellular entry and especially the nuclear entry are difficult processes and a good plasmid DNA carrier is essential for intracellular delivery of plasmid DNA. The mRNA, obtained after transcription, is subsequently transported to the cytoplasm of the cell, where it is translated into a functional protein (Figure 1)²⁰.

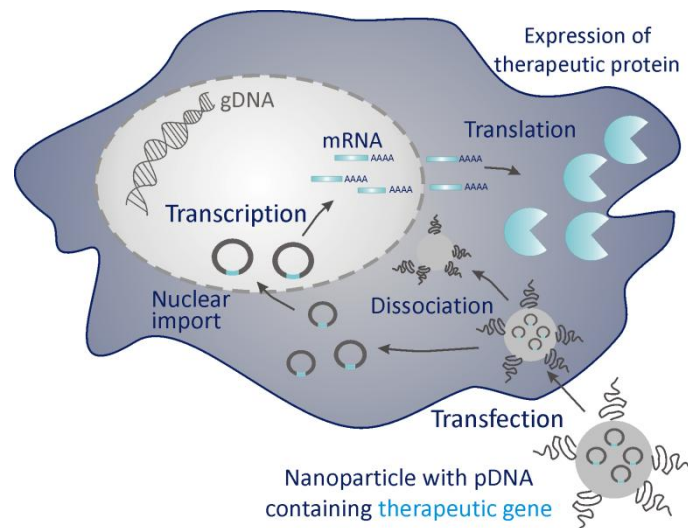


Figure 1 Mechanism of plasmid DNA transfection resulting in the expression of a therapeutic protein.

Antisense Oligonucleotides (ONs). ONs are short single stranded DNA molecules that selectively bind to their target mRNA in the cytoplasm. The duplex formation between ONs and mRNA blocks the translation process. Several mechanisms have been proposed to explain their antisense action. One theory suggests that binding of the ONs to the mRNA prevents interaction with the cellular machinery required for protein synthesis. Alternatively, ONs can function by activation of RNase H, an enzyme that degrades the targeted mRNA^{20,21}. Because of their rapid degradation by circulating nucleases in the body, ONs with several backbone modifications have been designed to withstand this degradation²².

Ribozymes and DNAzymes. A problem with the use of ONs is that their ability to impede DNA translation is concentration dependent and therefore tumour cells often continue to express low levels of the oncoprotein. This has led to the development of ribozymes. Ribozymes are RNA molecules that bind and cleave mRNA molecules with a specific sequence. After binding to the target mRNA, the formed duplex is easily hydrolyzed^{20,23}. An important disadvantage of ribozymes is their low *in vivo* stability, as they are quickly destroyed by circulating RNases. For this reason, DNAzymes have been developed, which are analogs of ribozymes with greater biological stability. The RNA backbone is replaced by a DNA backbone, thereby improving biological stability^{20,24}. They are also easier to modify synthetically, thereby generating even more stable second-generation analogs²⁵.

Short Interfering RNA (siRNA). RNA interference (RNAi) is a naturally occurring gene silencing mechanism initiated by double stranded RNA (dsRNA). When long dsRNA is introduced into a cell, it is processed by a dsRNA-specific enzyme, Dicer. This enzymatic cleavage degrades the RNA into a 19-23 basepair duplex, also called short interfering RNA (siRNA). The siRNA then binds to the RNA-induced gene silencing complex (RISC), which retains only the antisense strand of the siRNA. Subsequently, this activated RISC binds to the mRNA molecule of interest and stimulates mRNA degradation by the enzyme Slicer, leading to specific gene silencing (Figure 2)²⁶⁻³⁰. Because long dsRNA molecules can induce severe interferon responses in mammalian cells³¹, inducing RNAi is mostly accomplished by the addition of chemically synthesized 21mer siRNAs, mimicking Dicer cleavage products, or by the intracellular production of siRNAs from short hairpin RNA (shRNA) precursors that can be continuously expressed from RNA polymerase III driven expression cassettes³². Important advantages of siRNAs are their higher resistance to degradation and their higher specificity compared to ONs or ribozymes²⁰.

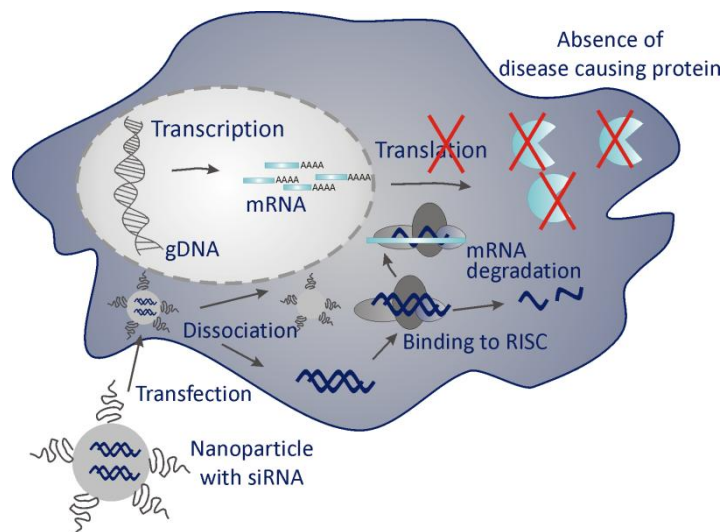


Figure 2 Mechanism of antisense therapy with siRNA molecules.

Strategies in cancer gene therapy

Cancer gene therapy can be used to compensate the genetic malfunctions by replacing the defective genes with their wild-type counterpart or to silence oncogenes. A second strategy is to make the cancer cells more visible for the immune system and employ the host's physiological immune response to selectively kill the cancer cells³³. A schematic overview of the different strategies is shown in Figure 3.

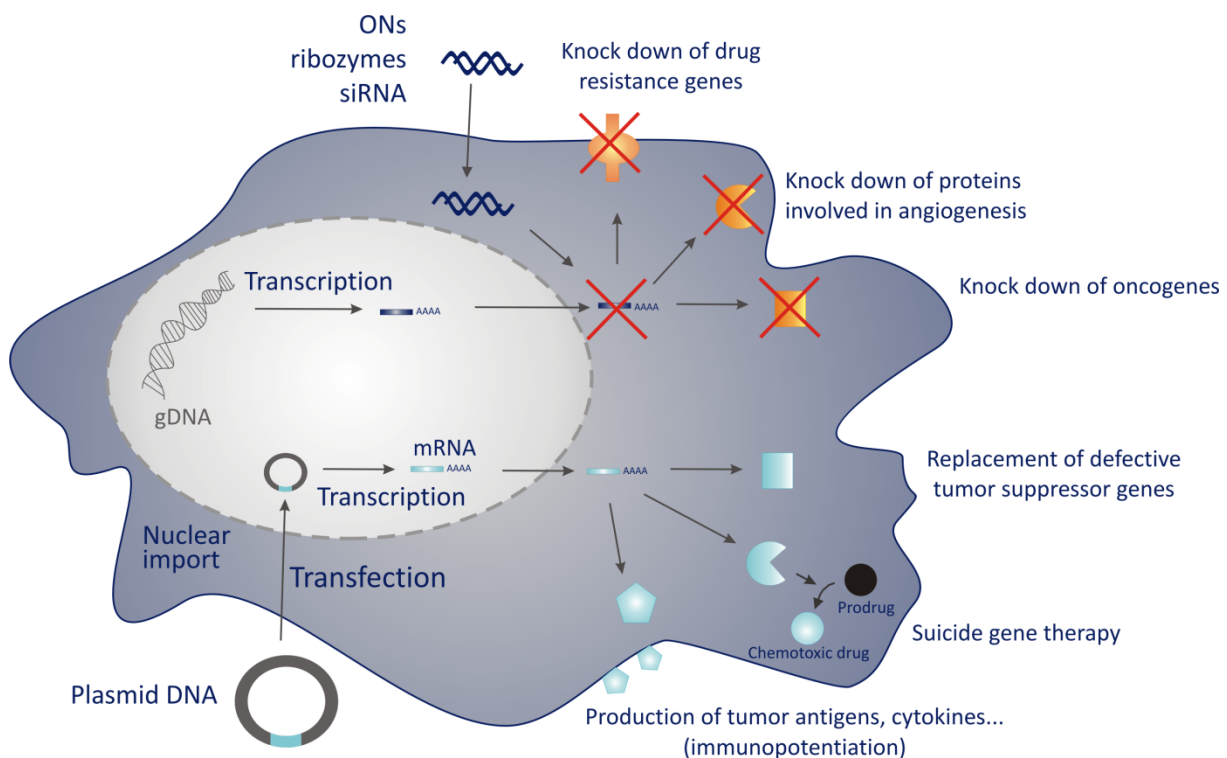


Figure 3 Schematic overview of different strategies in cancer gene therapy.

Oncogene inactivation. Mutations in proto-oncogenes can lead to the formation of oncogenes. The enhanced transcription of these genes makes unlimited division of the cancer cells possible. One form of cancer gene therapy is the silencing of these oncogenes. Antisense oligonucleotides, ribozymes and siRNAs can be used to degrade the mRNA, thereby preventing the translation of the oncogene mRNA into oncoproteins^{34,35}.

Tumor suppressor gene replacement. Tumor suppressor genes like p53³⁶, are responsible for repair or elimination of cells with DNA damage. By inhibiting the expression of tumor suppressor genes, cancer cells can continue to proliferate and avoid apoptosis. One strategy in cancer gene therapy is to replace the damaged tumor suppressor gene by plasmid DNA transfection. A successful

transfection of the cancer cell with the tumor suppressor gene will result in the production of proteins arranging growth arrest and apoptosis³⁷.

Immunologic therapies. Immunopotential is the enhancement of the immune system's ability to destroy cancer cells. Passive immunopotential involves boosting of the natural immune response to make it more effective³⁸. One of the frequently encountered genetic immunotherapy strategies involves the *ex vivo* transfection of immunologic blood cells (macrophages, dendritic cells, cytotoxic T-cells) with a transgene encoding cytokines and growth factors³⁹⁻⁴¹. Another possibility is the *in vitro* manipulation of antigen presenting cells to enable them of active tumor antigen presentation. Transfection of these antigen presenting cells with a plasmid DNA containing the genetic code of a tumor antigen results in antigen presentation, triggering the immune system⁴².

Active immunopotential is used to initiate an immune response against an unrecognized or poorly antigenic tumor³⁸. Tumor cells can be genetically modified to express a variety of factors including tumor antigens, cytokines or antigen presenting molecules⁴³. The transfected tumor cells are then irradiated both to minimize malignant potential and to improve immunogenicity before being introduced by vaccination into the patient³⁸. Another possibility is to inject the plasmid DNA, containing the antigen-encoding genes, subcutaneously or intramuscularly resulting in a genetic vaccination against the tumor cells⁴⁴.

Suicide gene therapy. This is the transfection of cancer cells with genes encoding enzymes able to activate non-toxic pro-drugs *in situ* to form cytotoxic drugs. After insertion of the suicide gene constructs into cancer cells, treatment with high dose of a relatively non-toxic pro-drug results in a local conversion of these prodrugs into cytotoxic drugs, leading to cancer cell death^{45,46}. An important advantage of suicide gene therapy is that only a fraction of the cancer cells has to be transfected to initiate tumor regression, as the cytotoxic drugs diffuse out of the transfected cells and are also capable of killing neighboring cells (bystander effect)³⁸.

Drug resistance genes. One major obstacle to a successful treatment with chemotherapy is the multidrug resistance of several tumor cells. Expression of the P-glycoprotein in cancer cells leads to the detection and the efflux of several drugs, resulting in a decreased sensitivity of the tumor cells for these drugs⁴⁷⁻⁴⁹. Gene silencing therapies like siRNA and ONs are implemented to prevent the expression of these drug transporters thereby lowering the chemotherapeutic drug doses (chemosensitization)⁵⁰⁻⁵³. Alternatively, hematopoietic stem and progenitor cells can be transfected with plasmid DNA encoding drug resistance genes. This is an important strategy to protect normal

cells from the toxic side-effect of therapeutic agents, thereby preventing myelosuppression (chemoprotection)⁵⁴.

Inhibition of angiogenesis, tumor invasion and metastasis. Recently, remarkable progress has been made in understanding the molecular mechanisms of angiogenesis, tumor invasion and metastasis. Several genes involved in these mechanisms are either deficient or overexpressed in tumor cells⁵⁴. Molecules such as vascular growth factor (VEGF) are known to enhance angiogenesis⁵⁵ and can be targeted by ONs, ribozymes and siRNA^{56,57}. Alternatively, tumor cells can also be transfected with plasmids encoding proteins involved in controlling tumor metastasis and invasion like TIMP-1 and others⁵⁸.

Viral Gene Delivery systems

Over several years, viruses have evolved to very infectious agents that are able to efficiently transfer their DNA to target cells. Despite their high transfection efficiency, there are several concerns over the use of viruses as gene delivery systems in humans. The chief concern is the toxicity and the potential of generating a strong immune response. Ad random genomic integration of the viral genome, can generate insertional mutagenesis, that may inhibit expression of normal cellular genes or activate oncogenes. A more practical limitation of viral gene carriers is their limitation on the size of the incorporated expression plasmid²⁰.

Retroviruses. Retroviruses are single-stranded RNA viruses surrounded by a protein capsid and a lipid bilayer²⁰. The virus attaches to cell-surface receptors via an envelope surface protein, followed by receptor-mediated endocytosis. After removal of the envelop, the viral genome undergoes reverse transcription to form a double-stranded DNA intermediate. The newly synthesized DNA enters the cell nucleus and integrates randomly in the host genome, at which point the retroviral vector is referred to as a provirus⁵⁹. The stably integrated viral genome can be transmitted to daughter cells, making stable and long-term gene expression possible. Important drawbacks of retroviral gene therapy are the requirement of cell division for the provirus integration, which limits their use to dividing cells and the limitation of the incorporated DNA to 8kb⁵⁴.

Adenoviruses. Adenoviruses are DNA containing, non-enveloped viruses. Adenoviruses enter the cell by receptor mediated endocytosis. Once the virus genome is released into the nucleus, the viral early genes are transcribed, leading to DNA replication, late transcription, synthesis of viral structural proteins and virus assembly. Because of their large packaging capacity (up to 35kb)

adenoviruses can be used to transfer larger genes⁵⁴. Adenoviruses produce high levels of gene expression in a large variety of dividing and non-dividing cells. However, the use of adenoviruses as vectors is limited by the fact that they do not integrate into the host chromosomes and the severe immune responses they can cause⁴⁴.

Adeno-associated viruses (AAV). Adeno-associated viruses are small, single-stranded DNA viruses, which need a helper-virus like adeno- or herpesvirus for productive virus replication. Similar to adenoviruses, AAV vectors can infect both dividing and non-dividing cells. However they integrate their DNA into the host cell genome specifically. In chromosome 19 of the human genome. Such specificity reduces the risk of insertional mutagenesis encountered in retroviral gene therapy^{44,54}. Disadvantages are the need for helper viruses during AAV production, which can result in contaminated AAV vectors during production and their limited DNA capacity (less than 5kb)⁴⁴.

Herpes simplex viruses (HSV). Herpes simplex viruses are large enveloped viruses with double stranded DNA. Features of HSV vectors are the possibility to incorporate very large genes (up to 150kb) and their ability to transfect dividing and non-dividing cells⁶⁰. Problems associated with the use of HSV vectors are the vector induced cytotoxicity and the transient nature of gene expression^{38,54,59}.

Non-viral Gene Delivery Systems

As explained above, viral gene delivery systems can cause some severe side-effects, such as cytotoxicity, immunogenicity and insertional mutagenesis. Therefore, several non-viral vectors have been developed. An ideal vector should be able to (1) protect the genetic material from degradation, (2) bring it into the cell cytoplasm (ONs, ribozymes, siRNA) or in the nucleus of the target cells and (3) limit cytotoxic side-effects. In general, non viral gene delivery systems are classified into chemical delivery systems, including polymers and lipids, and physical delivery systems, comprising electroporation, hydrodynamic gene delivery, laser beam transduction, magnetofection and ultrasound-based delivery systems.

Liposomes. Liposomes are vesicles that arise spontaneously when phospholipids are dispersed in an aqueous medium. Due to their polar head group and hydrophobic hydrocarbon tail, bilayered structures are formed with the tails pointing to each other and the polar head groups protruding in the aqueous environment⁶¹. Liposomes are used as versatile drug carriers, as both hydrophilic and hydrophobic drugs can be incorporated. For gene delivery purposes, they mostly contain a positive

charged lipid and a helper lipid⁶¹. Mixing of the cationic liposomes and nucleic acids results in the formation of lipoplexes, in which nucleic acids are sandwiched between lipid bilayers. Due to their net positive charge, they are easily taken up by endocytosis after electrostatic interaction with the cell membrane. The helper lipid, like DOPE (1,2-dioleoyl-*sn*-glycero-3-phosphatidylethanolamine), is believed to increase membrane fluidity and facilitate lipid exchange and membrane fusion between lipoplexes and the endosomal membrane, resulting in a good endosomal escape⁶². To prevent any unwanted interactions with serum proteins or reduce complement activation, a third PEGylated lipid has to be incorporated in the liposomes. The resulting PEG corona around the lipoplexes shields their positive charge, providing longer circulation times⁶³. However, an important drawback is the reduced transfection efficiency after PEGylation, resulting from a limited endosomal uptake and endosomal release^{64,65}. Several research groups are investigating the possibility of using acid-cleavable PEGylated lipids⁶⁶. These lipids lose their PEG-chain after endosomal uptake, promoting endosomal escape. Figure 4 shows the general structure of a PEGylated lipoplex together with the chemical structure of three commonly used lipids: the cationic lipid DOTAP (N-(1-(2,3-dioleoyloxy)propyl)-N,N,N-trimethylammoniumchloride), the helper-lipid DOPE and the PEGylated lipid DSPE-PEG (1,2-distearoyl-*sn*-glycero-phosphoethanolamine-N-[(polyethyleneglycol)-2000].

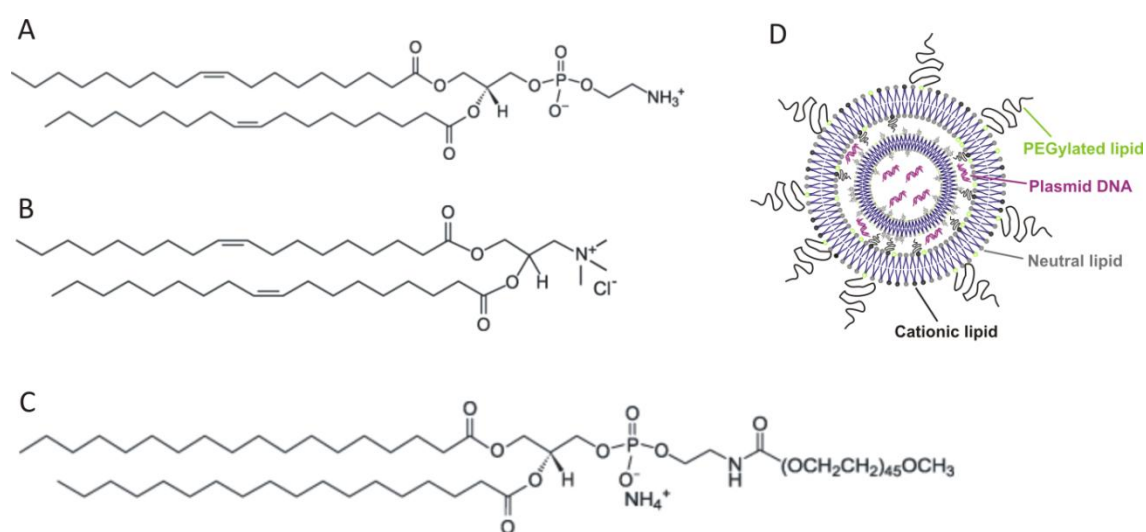


Figure 4 Chemical structure of the helper lipid DOPE (A), cationic lipid DOTAP (B) and PEGylated lipid DSPE-PEG-biotin (C). Figure D shows a PEGylated lipoplex.

Polymers. Several natural or synthetic cationic polymers have been evaluated as DNA carriers, including poly-(L-lysine) (pLL), Poly(ethylenimine) (pEI), chitosan, cationic proteins and cationic peptides. Most of these polymers condense the DNA into small particles (polyplexes) and facilitate intracellular uptake via endocytosis through electrostatic interactions with anionic sites on cell

surfaces⁶⁷. Large differences exist in the transfection efficiency and cytotoxicity among the different polymers⁶². Several synthetic biodegradable polymers are synthesized to reduce the cytotoxic side-effects and enhance transfection⁶⁸.

Electroporation. This technique comprises the direct application of electric pulses on tissues or cells. The electric field causes a transient permeabilization of the cell membrane and allows the entrance of nucleic acids⁶⁹. When the applied external field exceeds the capacity of the cell membrane, hydrophilic pores are formed through which water enters the cell. The degree of pore formation can be controlled by changing the intensity of the electric field, pulse duration and pulse number⁷⁰. Advantages of this technique are the simplicity, efficiency and safety. However, applications are limited to tissues where the electrodes can be inserted. Electroporation has been used in cancer gene therapy for genetic vaccination against melanoma antigens. In 2004 several clinical trials have been performed for the IL-12 transfection of melanoma cells finding encouraging results^{71,72}.

Hydrodynamic Delivery. Hydrodynamic gene delivery is a simple method that introduces naked plasmid DNA in highly perfused organs⁷³. Hydrodynamic gene delivery has been mainly applied for hepatic gene delivery. Tail vein injection of mice with an extremely large DNA containing volume, causes a transient overflow at the vena cava that exceeds the cardiac output. As a result, the injection induces a flow of DNA solution in retrograde into the liver and causes a rapid rise of intrahepatic pressure, resulting in liver expansion and reversible disruption of the liver fenestrae^{62,74}.

Gene Gun. In this delivery method, the DNA is deposited on the surface of gold particles, which are then accelerated by pressurized gas and expelled onto tissue. In this way, the particles are able to penetrate a few millimeters deep into the tissue and release the DNA. The major application of this technology is genetic immunization, although it has also been used for cancer pro-drug therapy⁷⁵.

Magnetofection. In this method, the nucleic acid is reversibly attached to magnetic particles, which are then focused to the target site via a high-energy magnetic field⁷². This technique allows delivery of the genetic particles into the target cells and can even cause extravasation⁷⁵. The genetic material dissociates from the magnetic particles after cellular entry. Magnetofection has shown *in vitro* to promote rapid and high gene expression levels and has also been applied to achieve genetic vaccination⁷².

ULTRASOUND AND MICROBUBBLES

ULTRASOUND

What is ultrasound?

Sound is a longitudinal compressional wave as depicted in Figure 5. When the frequency of the sound wave is above the typical human audible range (> 20 kHz), it is called ultrasound⁷⁶. Ultrasonic waves are generated by transducers which are piezoelectric elements producing elastic vibrations⁷⁷. The ultrasound wave consists of high pressure and low pressure areas. As the ultrasound wave is passing through a medium, the radiated material vibrates. Figure 5 shows the displacement of the different particles in a certain medium as the ultrasound wave is passing through. In the high pressure areas (*compression*), the particles are squeezed together, whereas at the low pressure areas (*rarefaction*) they are spread apart.

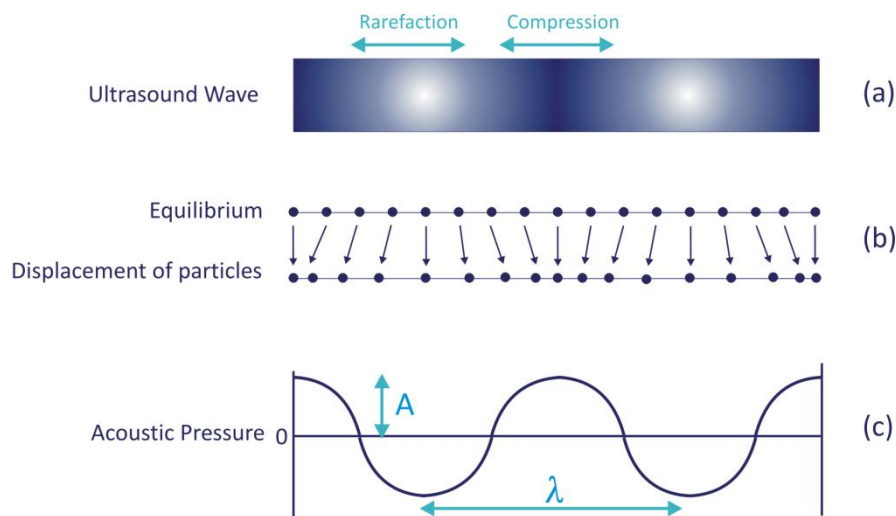


Figure 5 Schematic representation of a single-frequency ultrasonic wave (a). The ultrasound wave consists of low pressure (rarefaction) and high pressure (compression) phases. Part (b) shows the displacement of particles in a material as the ultrasonic wave is passing through. Part (c) displays the acoustic pressure of the ultrasound beam as a function of distance, and shows the amplitude (A) and wavelength (λ) of the wave. Adapted from reference⁷⁶.

The ultrasound wave is characterized by a specific frequency (f). While the frequency is unaltered when the ultrasound travels through different media, this is not the case for the wavelength (λ). The relation between the velocity (v), wavelength (λ) and frequency (f) is given by the following equation.

$$v = \lambda \times f$$

As the ultrasound is travelling through a more denser medium, its velocity and wavelength will increase. The intensity of the ultrasound is given by the amplitude (A) of the wave and is expressed as pressure (Pa). A summary can be found in Table 1.

Frequency (f)	f	Number of times a particle experiences a complete compression/rarefaction cycle in 1 second. ($\frac{1}{s}$) (Hz)
Wavelength	λ	The distance between two equivalent points on the waveform in a particular medium. (nm)
Period	T	Duration of 1 cycle ($\frac{1}{f}$). (s)
Amplitude	A	Peak pressure. (Pa)

Table 1 Different parameters characterizing an ultrasonic wave, passing through a particular medium.

Besides continuous ultrasound, ultrasound can also be repeatedly turned on and off. This is called pulsed wave ultrasound (PW). This generation mode is accomplished by exciting or shocking the ultrasonic transducer with very short electrical signals, waiting for some time and then repeating the electrical shocking. Figure 6 represents a pulsed ultrasonic wave, and indicates the pulse duration (τ) and Pulse Repetition Period (PRP). The different parameters characterizing a pulsed ultrasound wave are explained in Table 2.

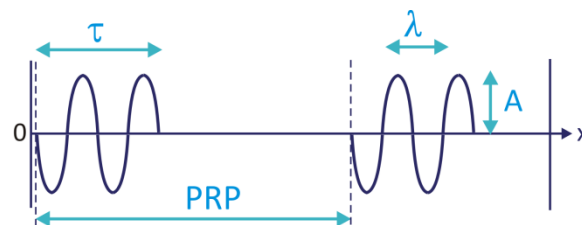


Figure 6 Schematic representation of a pulsed ultrasound wave with indication of the wavelength (λ), amplitude (A), pulse duration (τ) and Pulse Repetition Period (PRP).

Pulse duration	τ	Duration of one ultrasound pulse. (s)
Pulse repetition period	PRP	Time between the beginning of an ultrasound pulse and the beginning of a second one. (s)
Duty Factor	DF	Fraction of the time the ultrasound is “on” ($\frac{\tau}{PRP}$).
Pulse Repetition frequency	PRF	Number of pulses occurring during 1 second ($\frac{1}{PRP}$). ($\frac{1}{s}$) (Hz)

Table 2 Different parameters characterizing a pulsed ultrasound wave.

The velocity of an ultrasound wave is independent of the frequency, but depends on the material and is listed for several media in Table 3⁷⁶. The mass and spacing of the molecules of the material and the attracting force between the particles of the material all have an effect on the speed of the ultrasound as it passes through. Ultrasound travels faster in dense materials and slower in compressible materials. For medical applications the propagation speed in tissue is typically assumed to be constant at 1540 m/s.

Medium	Propagation Speed (m/s)
Air	330
Water	1520
Soft tissue	1540
Bone	3800

Table 3 Speed of sound in different media. Adapted from reference⁷⁷.

When ultrasound waves pass through tissue, their intensity decreases as a result of reflection, refraction and absorption of the ultrasound⁷⁶. The decrease in ultrasound intensity is called *attenuation* and depends on the type of tissue through which the ultrasound is passing. At the boundaries between tissues with different acoustic properties, the ultrasound wave will be partially reflected. This reflection becomes larger as the difference in acoustic properties of the tissues increases. So, for example, the reflection will be very high at the boundary of bone and soft tissue. As explained further in this introduction, this principle forms the basis of acoustic imaging. Another phenomenon that takes place is absorption of the ultrasound energy by the material. Because of the movement of the different particles in a tissue (Figure 5), part of the acoustic energy is converted

into heat. This absorption increases with rising frequency and can be used to ablate tumor tissue, as will be explained later on.

Biophysical effects of ultrasound

A tissue subjected to ultrasound can experience several biological effects. Generally these effects can be classified into primary physical effects and secondary effects. The most important primary physical effect of ultrasound is the direct deposition of acoustic energy as heat in the tissue. This phenomenon is used in High Intensity Focused Ultrasound (HIFU) to ablate tumor tissue. Ultrasound might also interact with pre-existing gas bubbles in tissue, resulting in cavitation of these “microbubbles”. However, little evidence is available that cavitation indeed develops *in vivo*, without previously injecting microbubbles⁷⁸. To enhance acoustic cavitation, microbubbles are injected into the bloodstream. The cellular effects associated with acoustic cavitation will be described in the microbubble section.

Other non-thermal, secondary effects are directly related to the *non linear propagation* of an ultrasonic wave⁷⁹. When the intensity of the ultrasound wave is high enough, the ultrasound starts to propagate non-linearly in the tissue. When a fluid or tissue is compressed in the high pressure phase, its stiffness and density increases. As a result, the high pressure peaks will travel faster than the low pressure phases⁷⁶ (Figure 7a). This non linear propagation leads to the distortion of the initially sinusoidal waves and can ultimately result in the generation of a *shock wave* (Figure 7b). As a consequence of the distortion of the wave in time, additional frequencies are generated, also called “harmonics” of the initial frequency⁸⁰. Pressure gradients coming directly from the ultrasonic wave normally have a rather long wavelength, which means that a broad distance exists between a high and low pressure phase (Figure 7a: D). However, when non linear propagation occurs, this distance is drastically shortened (Figure 7b: D’). Due to the sudden changes in pressure occurring at short distance, biological tissues are subjected to very high shear forces, which can damage the tissue⁸¹.

Other secondary physical effects are the formation of radiation pressure when the ultrasonic wave is reflected at a boundary. Due to the partial reflection of the ultrasound wave, the intensity is lowered and a difference in mean pressure on the boundary and behind arises. As a result particles in the medium can experience an *acoustic radiation force*, which can result in the displacement of particles. A second effect, called *acoustic streaming*, arises directly from the attenuation of the ultrasonic wave. During its passage through the tissue, the intensity of the ultrasonic wave decreases as energy is absorbed from the beam. A pressure gradient is formed and when this acts upon a liquid, a fluid stream develops that is directed away from the ultrasonic transducer^{76,76,80}.

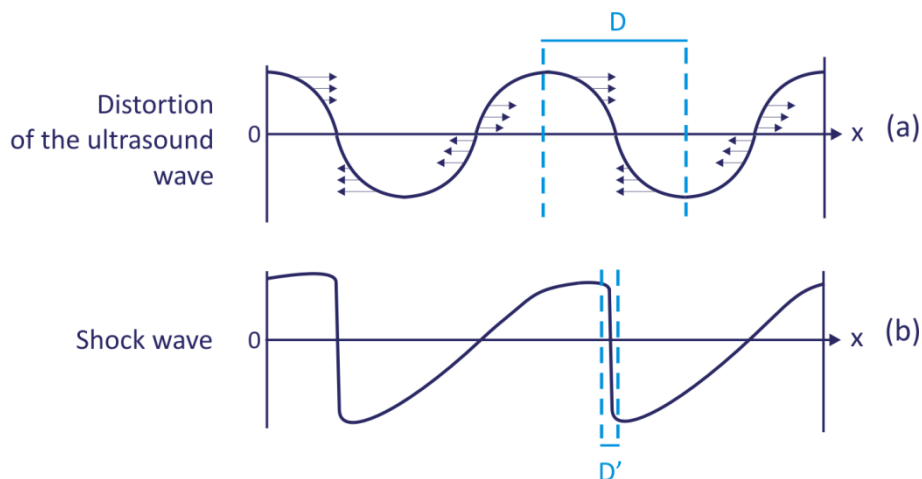


Figure 7 Schematic representation of *shock wave* formation (b) due to non linear propagation of the ultrasound (a). D and D' show the distance between the area of maximal compression and maximal decompression in a normal ultrasound wave and shock wave respectively. Adapted from reference⁷⁶.

Medical applications

The biophysical effects of ultrasonic radiation can provoke several biological responses. Whereas diagnostic ultrasound preferably should be free of medically significant bio-effects, the objective of therapeutic ultrasound is to provoke a specific biological response^{82,83}. Which biophysical effect will dominate mainly depends on the frequency and intensity of the applied ultrasound. High frequency ultrasound is more readily absorbed by tissue and is therefore extremely suited for HIFU applications. On the other hand, when cavitation should occur, low frequency ultrasound is more appropriate and pulsed ultrasound can be used to decrease heat formation^{78,83} (figure 8). Ultrasound therapy can be broadly divided into two subcategories: “high” power and “low” power therapies. High power acoustic therapies include HIFU and lithotripsy, whereas low power therapies comprises sonophoresis and physiotherapy.

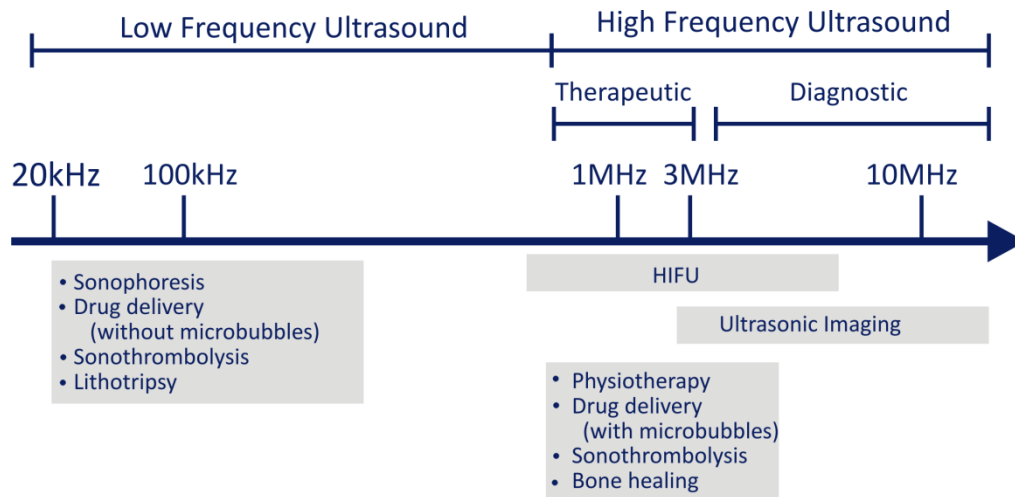


Figure 8 Overview of different ultrasound frequencies used for medical applications.

Ultrasound imaging. As mentioned above, part of the ultrasound becomes reflected at tissue interfaces. Image formation depends entirely on the returning echoes, which are converted into an electric signal by the transducer. The intensity or amplitude of the reflected wave, as well as the time between emission and receiving the signal are registered. An image is then constructed based on this information. Early imaging modalities displayed the amplitude of the signal as a function of time (A-mode: Amplitude)⁸⁴. Current imaging modalities build up a grayscale image, in which higher intensities can be seen as brighter areas and lower intensities as darker areas (B-mode: Brightness). As explained above, a shift to higher frequencies is observed as a result of the non linear propagation of the ultrasound wave. This principle is used in harmonic imaging^{80,84}. In this case, only harmonics of the initial frequency are registered to improve the signal-to-noise ratio and enhance the contrast.

Also Doppler imaging is widely used to image blood flow patterns. This imaging technique is based on the Doppler principle. Imaging of the moving blood flow results in a change in frequency of the reflected ultrasound. Higher frequencies are received from blood cells moving towards the transducer, while lower frequencies are received when blood cell move away. From the shift in frequency the direction and rate of the blood flow can be deducted⁷⁷. Compared to other imaging modalities, ultrasound has several advantages. Only minor side effects exist due to its non-invasive character and the fact that no ionizing radiation is used. Furthermore, ultrasound is a non-expensive and portable technique that is therefore widely used in pregnancy follow-up and diagnosis. However, it cannot be used to image air-containing media like lungs or bowel and imaging of deeper lying structures is sometimes impossible.

High Intensity Focused Ultrasound (HIFU). HIFU is more and more established as a full-fledged tumor ablation technique. In contrast to surgery it is a non-invasive technique and toxicity can be seriously reduced⁸⁵. Unlike other ablation techniques like radiotherapy or cryotherapy, areas located deeper in the body can be reached and HIFU lesions are well defined with no surrounding cellular damage. This makes HIFU extremely suited for ablation of tumors close to sensitive tissues that must be spared like prostate or oesophagus. When the ultrasound beam is passing through a tissue, a certain amount of the acoustic energy is absorbed by this tissue and converted into heat⁸⁶. If the ultrasound beam is brought into focus, the energy within the focal volume can cause a local rise in temperature that is high enough to induce tissue necrosis. In HIFU treatment, the temperature of an isolated tumor volume is raised above 55°C for longer than 1 second. This leads to necrosis and immediate cell death⁸⁵⁻⁸⁷.

Another phenomenon that enhances tissue necrosis is the appearance of cavitation^{88,89}. Cavitation can damage cells directly, but the strong scattering of the microbubbles also leads to the entrapment of the acoustic energy in the cavitating region. This increases the heat deposition in the immediate surroundings of the cavitating microbubble. Lesion dimensions depend on frequency and device geometry, but are in the mm range. If larger tumor volumes are treated, the transducer is moved in discrete steps until the whole tumor volume is ablated or the active transducer can be moved in a pre-determined track. Ultrasound frequencies used in HIFU treatment largely depend on the target region. As attenuation increases with higher ultrasound frequencies, frequencies up to 8MHz are used to treat shallow tumors, while lower frequencies (0.5 or 1MHz) at higher intensities are used to reach tumors more deeply within the body⁹⁰. Despite the above mentioned advantages, some limitations exist for HIFU treatment. Ultrasound is not able to propagate through air-filled organs like lungs or bowel and also other structures like bone can absorb or reflect the ultrasound beam⁹¹.

Several clinical trials have been established using HIFU for the treatment of breast^{92,93}, prostate⁹⁴ and liver cancer⁹⁵. The results look very promising and further clinical research is required to verify whether HIFU can become an alternative to surgery in these different applications.

Lithotripsy. Low frequency ultrasound can be applied extracorporally to induce fragmentation of bile and urine stones. After fragmentation, the small remainders can pass spontaneously through the urinary tract^{96,96,97,97}. Short pulses with high intensity are focused on the stones. As the ultrasound wave propagates non linear, a shock wave is focused in the stone. Due to the high pressure gradients in the stone, shear stress and finally tensile stress and strain are created resulting in the erosion of the surface⁹⁸. If the waves are less sharply focused, the ultrasound beam becomes reflected at the water-stone interface, which leads to the splitting of stone material.

Sonophoresis. Ultrasound can be used to locally enhance the transport of low and high molecular weight drugs through the skin⁹⁹⁻¹⁰⁴. The stratum corneum is the main barrier for drug delivery through the skin¹⁰⁵. Corneocytes are embedded in a continuous matrix of lipid bilayers, which effectively prevent the diffusion of drug molecules. Recent publications have shown that the stratum corneum becomes disrupted after ultrasound treatment and that localized regions of high permeability appear because of the creation of aqueous channels¹⁰⁶⁻¹¹³. Cavitation is thought to be the main mechanism of this enhanced drug transport¹¹⁴. Inertial cavitation (see microbubble chapter) of the gas bubbles present in the coupling medium between transducer and skin layer can cause the formation of shock waves and microjets that are able to disrupt the stratum corneum. Both high frequency and low frequency ultrasound have been used, although low frequency ultrasound has proven to be more effective, due to the higher level of cavitation. The passage of several low and high molecular weight drugs like insulin, NSAID, oligonucleotides and local anesthetics¹¹⁵⁻¹²⁰ has been demonstrated and the recent development of easy-to-use devices could lead to the application of sonophoresis in clinical medicine¹⁰⁵.

Physiotherapy. Therapeutic ultrasound has been addressed to treat soft tissue injuries, accelerate wound healing, reduce pain and soften scar tissue^{83,121-124}. The mechanisms involved are very complex and include thermal aspects, as well as non-thermal aspects¹²⁵⁻¹²⁷. Ultrasound has been shown to promote inflammation and stimulate tissue healing and wound repair, mainly *in vitro*¹²⁸. However, most *in vivo* trials have not succeeded in finding a beneficial effect of therapeutic ultrasound in physiotherapy¹²⁸.

Bone healing. The use of low frequency ultrasound for the stimulation of bone growth, has been approved by several *in vitro* and *in vivo* studies¹²⁹⁻¹³². Bone formation is a very complex process involving inflammation, proliferation (angiogenesis, callus formation and hardening) and remodeling of the bone tissue¹²⁷. Ultrasound exposure of the fracture promotes inflammation and angiogenesis. Also, the proliferation of stem cells and ossification of the matrix have been reported^{129,133}. In 2000 a commercial available ultrasound device became available, especially for fracture healing (EXOGEN™, Smith and Nephew).

Sonodynamic therapy. The term “sonodynamic therapy” was originally introduced to describe the phenomenon of sonochemical activation of photosensitive materials for cancer therapy. Ultrasound exposure of certain prodrugs like porphyrines causes the creation of reactive oxygen species which are able to destruct cancer tissue¹³⁴⁻¹³⁷. The prodrug itself has a very low cytotoxicity

and can be locally activated, so that only the tumor tissue will be affected¹³⁸. The same term is sometimes used to describe more generally the use of ultrasound to enhance drug delivery. These applications are described in the next paragraph.

Drug delivery. Ultrasound can be used to disrupt micelles and encourage drug release in the desired region. The physical entrapment of several anticancer drugs like doxorubicin and paclitaxel has been achieved and ultrasound has shown to promote their release from the micelles¹³⁹. Besides increasing the local concentration of anticancer drugs, a synergistic effect between ultrasound and chemotherapeutics has been described^{138,140-144}. After ultrasonic treatment, tissues can become more sensitive to lower chemotherapeutic drug concentrations.

MICROBUBBLES

Microbubble composition

Microbubbles are gas-filled structures consisting of a gaseous core surrounded by a stabilizing shell (Figure 9).

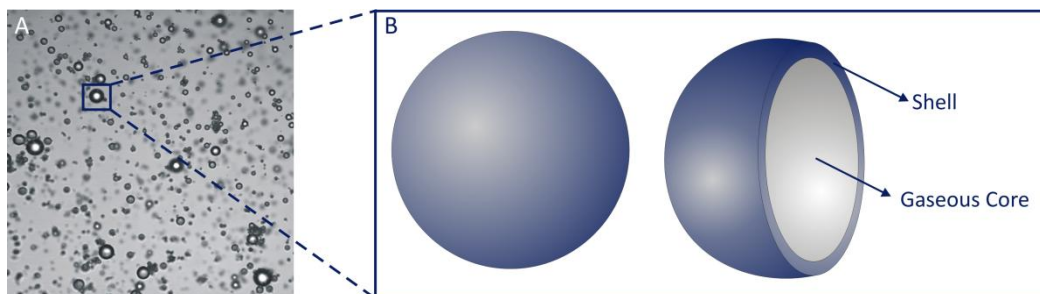


Figure 9 Transmission image of lipid coated microbubbles (A). Schematic and 3D representation of a microbubble with indication of the gas core and microbubble shell (B).

Core. First generation contrast agents were filled with air. Due to the relative high water solubility of air, these microbubbles quickly dissolve in the bloodstream¹⁴⁵. For this reason, second generation microbubbles are prepared with perfluorocarbon gases (C_nF_{n+2}) or sulfur hexafluoride (SF_6)¹⁴⁶. These gases are hydrophobic and prevent premature gas loss from the microbubble^{145,147-149}. Perfluorocarbons are extremely stable, biologically inert molecules that are not metabolized in the body, but exhaled within a few minutes¹⁴⁵.

Shell. The shell of a microbubble is essential to prevent or lower gas diffusion from the microbubble and hence, prevent microbubble dissolution. A disadvantage of this coating is the reduction of the microbubble oscillations in the ultrasonic field. Microbubbles can be divided into soft-shelled and hard-shelled contrast agents¹⁵⁰. First generation microbubbles were prepared with cross-linked albumin, which forms a stiff shell. A disadvantage of this shell type is the fact that the high stiffness reduces the extent of cavitation. Recently, also polymer-shelled microbubbles have been introduced. Polymer microbubbles have a thicker and even stiffer shell than albumin microbubbles¹⁵¹. This leads to a reduced scattering efficiency, which makes these microbubbles less suited for diagnostic applications. However, they have an improved stability and above a certain threshold the polymer shell fractures¹⁵¹ making these microbubble types very appropriate for drug delivery applications.

Lipid microbubble shells are more flexible and constrain the microbubble oscillations to a lesser extent¹⁴⁷. These shells are also more resistant to rupture, due to their higher flexibility¹⁵². The lipids are able to reseal and this leads to a longer lifetime, before and during cavitation¹⁵³. Another advantage of lipid shelled microbubbles is the easy modification of the shell by including different lipids. By increasing the chain length of the lipids more robust microbubbles are formed¹⁵⁴. Also, the inclusion of PEGylated lipids prevents any unwanted immune responses *in vivo*.

Name	Manufacturer	Stabilizing Coat	Gas Core	Availability
Sonovue	Bracco Diagnostics	Phospholipid	SF ₆	EU, China, South America
Definity	Lantheus Medical Imaging	Phospholipid	C ₃ F ₈	USA, Canada
Optison	GE Healthcare	Albumin	C ₃ F ₈	EU, USA
Sonazoid	Amersham Health	Lipids	C ₄ F ₁₀	Japan

Table 4 Commercially available microbubble agents.

Microbubbles normally have a size distribution between 0.5 and 10 µm. As microbubbles become larger, they become more echogenic. However, a compromise must be made between this echogenicity and the maximum size of bubbles for intravascular use, as the passage through the pulmonary capillary bed is restricted to particles with a size of 10µm.

Safety and clearance of microbubbles

The safety of approved microbubble contrast agents has been reviewed in 2005¹⁵⁵. Guidelines for their clinical use in humans were published by the European Federation of Societies for Ultrasound in Medicine and Biology¹⁵⁶. In general, ultrasound contrast agents are extremely safe and well tolerated. In humans, the incidence of side effects is low, predominantly minor in nature (headache, nausea) and self-limiting. Hypersensitivity or allergic events occur rarely. There is no evidence of nephrotoxicity, cardiotoxicity, cerebral or liver toxicity¹⁵⁷.

After intravenous injection microbubble-based contrast agents present a pure intravascular distribution in the peripheral circle and are defined blood pool agents. Some agents like Levovist, Sonavist and Sonazoid present a late hepatosplenic-specific phase¹⁵⁸⁻¹⁶⁰. This has been explained by the adherence and selective pooling of the micobubbles in the hepatic sinusoids or by the selective uptake from the circulation by phagocytic cells of the reticuloendothelial system in the liver and spleen^{158,159,161}. Removal of the microbubbles by the reticuloendothelial systems largely depends on the materials present on the microbubble shell¹⁶². Microbubbles that are not quickly taken by phagocytic cells, gradually dissolve in the blood stream^{145,162}. The gas content of the microbubbles is eliminated through the lungs. Perfluorocarbons and sulphur hexafluoride are inert gases which do not undergo metabolism in the human body but are exhaled via the lungs after a few minutes¹⁴⁵. The microbubble shell components are filtered by the kidney, eliminated by the liver or enter normal metabolism¹⁵⁷.

Response of microbubbles to ultrasound

Microbubbles are highly compressible, gas-filled structures surrounded by a stabilizing shell. The behaviour of microbubbles in an ultrasonic field mainly depends on the frequency, and intensity of the applied ultrasound.

At very low acoustic pressures (< 100kPa for 1MHz), the microbubbles oscillate in a symmetrical, linear way. This means that their expansion and compression is inversely proportional to the pressure phases in the ultrasound field^{151,163}. As a result, the microbubbles produce a backscatter with the same frequency of the transmitted ultrasound (linear backscatter). The intensity of this backscatter depends on the microbubble size, as the response of the microbubbles is higher when the frequency is closer to their natural resonant frequency. The higher the microbubble radius, the lower the resonant frequency¹⁶³.

At higher ultrasound intensities (0.1-1 MPa; 1MHz), the microbubbles behave non-linearly. Then the expansion phase of the microbubbles lengthens, as the microbubbles are more

resistant to compression than to expansion^{150,154}. This phenomenon is also known as *stable cavitation* or *non-inertial cavitation*¹⁵¹. During cavitation of the microbubble, there is gas influx (during rarefaction) and gas efflux (during compression). In the case of symmetrical oscillations, the netto gas influx over one expansion/compression cycle is zero. However, when the expansion phase prolongates, there is a netto gas influx into the microbubble. For this reason, the microbubble grows until it reaches its resonant size, whereupon it demonstrates stable, low amplitude oscillation (Figure 10b). Such stable oscillations create a strong liquid flow around the microbubbles, the so-called microstreams. Microstreams can apply a shear stress on cell membranes which may result in a transient opening of the membranes^{154,164-166}.

At even higher ultrasound intensities (> 1MPa; 1MHz), the oscillation amplitude of the microbubbles grows rapidly during the rarefaction phase, until the microbubble collapses due to the inertia of the intruding fluid. This results in the fragmentation of the microbubbles into many smaller microbubbles. This type of cavitation is called *inertial cavitation* (Figure 10). During the collapse of the microbubbles, shock waves are generated in the fluid near the microbubble. Finally, also jet formation can occur when a collapsing microbubble is located close to a surface like a cell wall. In this case an asymmetrical collapse takes place, which results in the formation of a liquid jet towards the surface. The shock waves and microjets create very high forces that can perforate cell membranes and even permeabilize blood vessels.

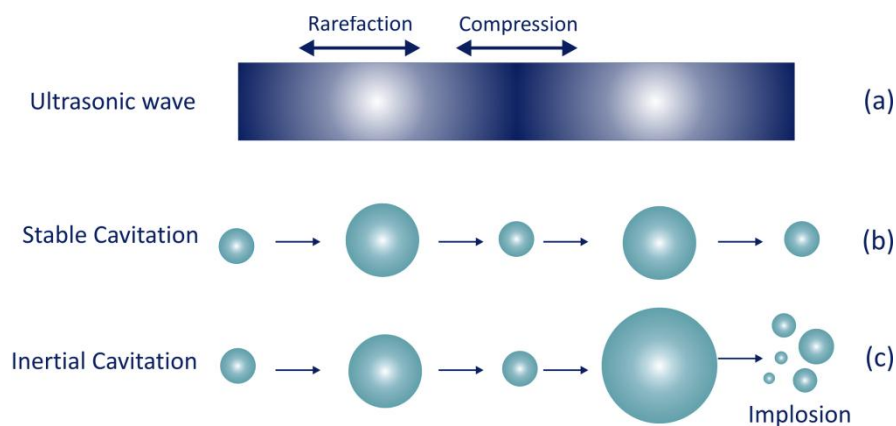


Figure 10 Schematic representation of microbubbles undergoing stable (b) or inertial cavitation (c) under the influence of an ultrasonic field (a). Adapted from reference⁷⁶.

Bio-effects of cavitating and imploding microbubbles

The gentle (microstreaming) or strong (shock waves and microjets) forces that develop in the neighbourhood of cavitating microbubbles can affect biological tissues¹⁶⁷.

Microstreams around a cavitating microbubble are much more powerful than acoustic streaming, arising from ultrasound treatment of tissue without microbubbles⁷⁸. The intensity of the microstreams quickly drops with increasing distance from the microbubble. As a result, cells or surfaces closely located to cavitating microbubbles are subjected to high shear stresses. This can temporarily permeabilize cell membranes and stimulate drug transport in the cell¹⁶⁸.

In the case of an imploding microbubble, even more powerful forces develop. Several *in vitro* and *in vivo* studies have reported capillary rupture, microvascular leakages and hemolysis¹⁶⁹⁻¹⁷³. This offers great potential for drug delivery applications as several pharmaceutical carriers are not able to cross the endothelial cell barrier. A schematic overview of different bio-effects is represented in Figure 11.

In addition, several papers have describe the formation of reactive oxygen species during cavitation. These can put a chemical stress on cell membranes and in turn permeabilize cell membranes¹⁷⁴⁻¹⁷⁶. Most likely, a combination of mechanical and chemical phenomenons is responsible for the creation of cell membrane pores and vascular defects. Depending on the frequency and intensity of the applied ultrasound, different bio-effects may become more important.

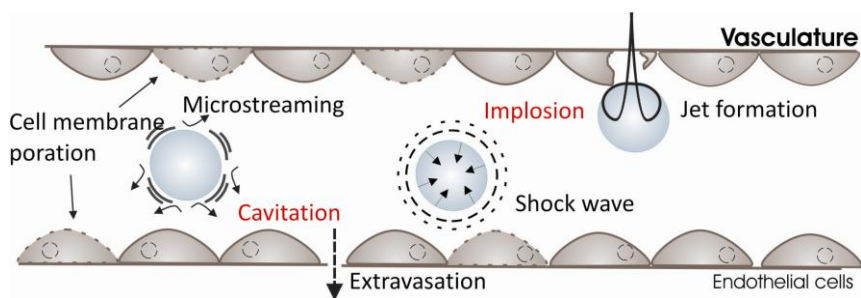


Figure 11 Bio-effects caused by a stably cavitating microbubble (left side) or imploding microbubble (right side). Adapted from reference¹⁷⁷.

Medical applications of microbubbles

Microbubbles were originally implemented in ultrasound imaging, as they increase the ultrasound reflection and are therefore also called “ultrasound contrast agents”. Several of these agents are now FDA approved and are already in use in daily clinic. Besides their diagnostic value, microbubbles are investigated as versatile therapeutic tools.

Enhanced ultrasound imaging. Because of their high compressibility, microbubbles can increase the reflection of the transmitted ultrasound wave and are therefore used to obtain a better

resolution in conventional imaging techniques¹⁷⁸. As microbubbles are not able to leave the blood stream, their use remains restricted to the imaging of myocardium and vasculature of different organs¹⁵⁴. While conventional ultrasound transmits and receives the same ultrasound frequency, harmonic imaging is based on the detection of harmonics of the transmitted frequency. Because of the non-linear behaviour of the microbubbles, subharmonics of the original frequency are returned to the transducer. This significantly improves the signal-to-noise ratio and refines the image. Microbubbles are particularly useful in myocardial imaging to diagnose infarction and identify coronary artery stenosis¹⁷⁹. Microbubbles also have an important role in imaging blood-flow and neovascularization¹⁸⁰. Another application is the diagnosis of breast tumors. Determination of the tumor vasculature can be extremely important in differentiating between benign and malignant tumors¹⁴². Also, some specific liver contrast agents exist like Levovist, Sonavist and Sonazoid. These agents are easily taken up by the reticulo endothelial system (RES) of the liver^{161,181,182}. This can be employed to improve the detection of liver malignancies and to study the condition of patients undergoing metastasis resection¹⁸³.

Ultrasound imaging aims to detect diseases or any abnormalities without causing bio-effects. Therefore, the ultrasound intensity is often low. In this case, inertial cavitation of the microbubbles is prevented, which contributes to a longer enhanced contrast of the image.

Sonothrombolysis. Ultrasound is used in the treatment of acute myocardial infarctions and ischemic stroke¹⁸⁴⁻¹⁸⁸. Both diseases originate from the presence of a thrombus in the coronary arteries or brain vasculature respectively, which blocks the blood circulation and leads to tissue necrosis. Dissolution of the clot within three hours after appearance of the first symptoms can drastically reduce mortality and reduce disability. Ultrasonic radiation of the thrombus results in the dissolution of the thrombus and reperfusion of the tissue. Low frequency ultrasound with a high intensity is delivered via a catheter, to minimize tissue damage, and can mechanically disrupt the clot¹⁸⁹. This has the advantage that also old thrombi and calcified clots can be destroyed. Another option is to treat the clot with high frequency ultrasound after the intravenous injection of thrombolytic agents like tissue Plasminogen Activator (tPA)^{190,191}. Several papers have reported an enhanced thrombolytic effect of tPA after ultrasound application. The acoustic streaming increases the permeability of the clot and rearranges the fibrin strands, which makes them more accessible for enzymatic degradation¹⁹². Another promising approach is the injection of ultrasound contrast agents in combination with low or high frequency ultrasound^{189,193-195}. The microstreamings, shock waves and microjets developed during inertial cavitation of the microbubbles, mechanically disrupt the clot^{189,190,190}. Several clinical trials already reported the beneficial effect of sonothrombolysis, and further randomized controlled clinical trials are currently going on to confirm these results¹⁹⁰.

Disruption of the brain-blood barrier. A new and very exciting application of microbubbles and ultrasound is their use as blood-brain barrier (BBB) disrupters¹⁹⁶. Drug transport to the brain is restricted by the impermeable BBB¹⁹⁷. The endothelial cells of the central nerve system are tightly attached to each other by intercellular attachments known as adherens junctions and tight junctions, the latter preventing intermixing of apical and basolateral surface components¹⁹⁸. Low frequency, as well as high frequency ultrasound with low intensity can be used to temporarily open the BBB. Although disruption with ultrasound alone has been demonstrated, BBB opening after the intravenous injection of microbubbles is the only method to produce reversible BBB disruption without brain tissue damage¹⁹⁹. Again, cavitation of the microbubbles with the corresponding microstreams, shock waves and microjets are responsible for this reversible opening²⁰⁰. Three different mechanisms have been identified that allow drug transport across the BBB after exposure to microbubbles and ultrasound. First, micro-disruptions of the brain capillaries were observed together with the extravasation of red blood cells²⁰¹. This effect is probably the result of powerful microjets that perforate vessel walls. Due to the risk of brain hemorrhages, extravasation should be limited, which can be done by restricting the ultrasound intensity²⁰². Second, dye leakage was observed through intact endothelium, in which the tight junctions were widened^{201,203}. Enhanced drug transport maintained for 1 or 2 hours after ultrasound exposure, and tight junctions completely recovered within 4 hours¹⁹⁹. Third, vacuoles were detected transporting marker molecules through the endothelial cells²⁰³. These effects have been observed *in vitro*^{201,204}, as well as *in vivo*^{205,206} and further research is required to optimize ultrasound settings, necessary to obtain a suitable ultrasound intensity through the skull^{199,203}.

DRUG AND GENE DELIVERY WITH MICROBUBBLES AND ULTRASOUND

WORKING PRINCIPLE

As explained earlier, microbubbles can undergo stable or inertial cavitation when exposed to ultrasound. While stable cavitation results in the formation of rather “gentle” microstreams, imploding microbubbles can induce very high forces like shock waves. Also, when an imploding microbubble is located close to a boundary like a cell layer, a microjet is formed directed towards the cell surface. These phenomena can result in the formation of transient pores in the cell membranes. The size and duration of the cell membrane pores depends on the ultrasound conditions, microbubbles and cell types used (Figure 11). In some studies 30 to 100 nm pores were reported²⁰⁷⁻²⁰⁹, while in other studies cell membrane perforations of a few micrometers in size were observed²¹⁰⁻²¹². Most cells are able to reseal these cell membrane wounds after several seconds to minutes^{208,209,212}. Recent publications have demonstrated that this recovery process is energy dependent²¹². Cell membrane wounds are resealed by the exocytosis of intracellular vesicles²¹². Lysosomes fuse with each other and are then transported to the cell membrane where they fuse with the cell membrane lipids²¹³, a process which is also seen when cells are subjected to other physical stress, like cell scraping²¹². Macromolecular drugs are able to reach the cytoplasm of the cell through these cell membrane pores. The intracellular uptake of several drugs like proteins, plasmid DNA, siRNA has been demonstrated after exposure to microbubbles and ultrasound. The microjets and shock waves may also permeabilize blood vessels which can promote the extravasation of high molecular weight drugs and drug containing nanoparticles.

Ultrasonic drug delivery offers many advantages. Ultrasound exposure of microbubbles can locally release drugs, assist in intracellular drug delivery and induce extravasation of drugs. Other advantages of ultrasound are related to the fact that it is a cheap, portable technique which is applicable to a major part of the body. As it is a non-invasive method, ultrasound could be particularly interesting for these applications where repeated treatment is required.

MICROBUBBLE DESIGN

Why designing a drug loaded microbubble?

Early drug delivery studies involved the systemic co-injection of a drug (being in solution or incorporated in a particle) and microbubbles followed by the local application of ultrasound.

Although these studies were often successful in enhancing drug delivery, it would be even more advantageous to bind the drug molecules to the microbubbles. There are different reasons why drug loaded microbubbles are so interesting. First, a drug carrying microbubble can locally release its content and simultaneously increase the drug uptake in the ultrasound treated area. In this way, drug release and uptake in untreated (and unwanted) body parts can be drastically reduced. This is particularly useful in cases where the cytotoxicity of the drug is an issue.

Second, the concurrent drug release during the implosion of the drug carrying microbubbles will result in a very high drug concentration close to the cell or blood vessel perforations. This is very important as drug transport through the sonoporated pores may significantly improve when the drug concentration near these pores is high.

Third, a closer contact between microbubbles and drug will increase the chance that the drugs are taken by the microstreams and shock waves that develop around a cavitating microbubble. As these fluid streams are causing cell membrane perforations, drugs that are taken by these streams might be more easily pushed through the cell membrane disruptions. Also, many biological drugs under development, like nucleic acids and proteins, rapidly degrade in blood after systemic injection. Binding of such labile biologicals to microbubbles may protect them from degradation, which is another interesting feature. Especially as it may lower the required dose and thus the therapy costs.

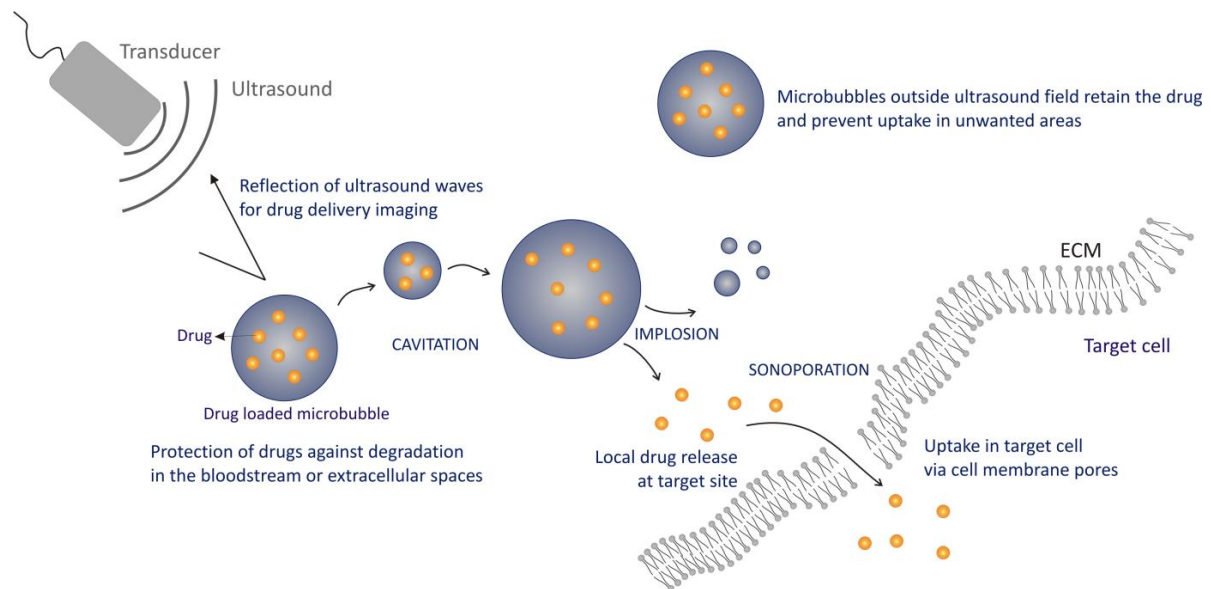


Figure 12 Schematic overview showing the advantages of targeted drug delivery with drug loaded microbubbles and ultrasound.

Finally, binding drug molecules to microbubbles will allow to „visualize“ drug delivery. In this case, a low acoustic pressure can be applied to image the target site followed by a higher acoustic pressure to rupture the microbubbles and deliver the therapeutic agents in the target region. Clearly, drug loaded microbubbles show potential to reduce the required dose of a drug and hence toxic side effects, which is particularly useful for drugs with a low therapeutic index.

Drug loaded microbubbles

Generally speaking, as illustrated in Figure 13, drugs can be either (a) incorporated in the gaseous core, (b) incorporated in the microbubble shell or (c), (d) attached to the surface of the microbubbles.

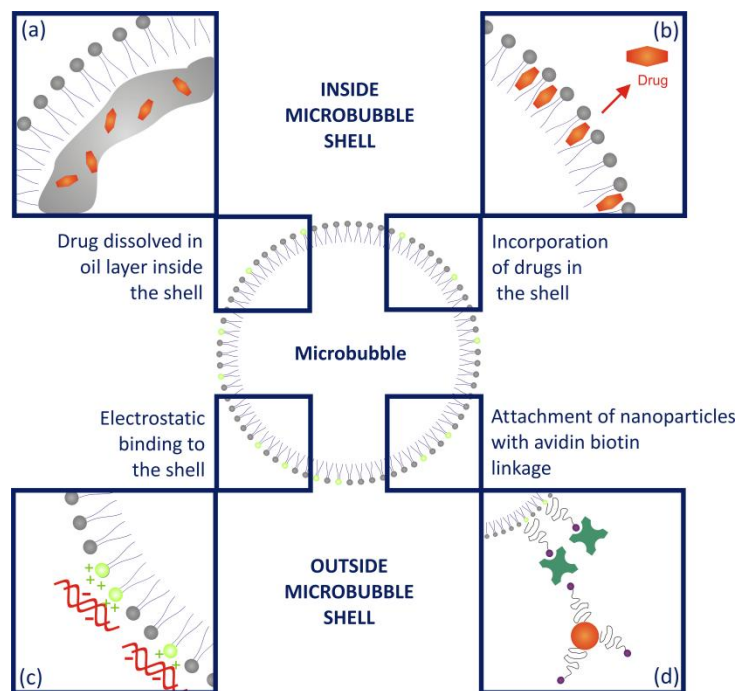


Figure 13 Schematic representation of possible drug cargo spaces in microbubbles. Drugs can be encapsulated within the perfluorocarbon core (a) or incorporated in the shell of the microbubble (b). Drug loading outside the microbubble shell can be accomplished through electrostatic interaction (c) or avidin-biotin linkage (d). Instead of a lipid microbubble shell, albumin or polymer shells can be used.

Drugs incorporated in the gaseous core of the microbubble. Incorporating drugs in the interior of the microbubbles has the advantage that it assures complete protection of the drug and that it lowers the chance of premature release i.e. drug release before applying ultrasound.

Acoustically Active Liposomes (AALS) are microbubbles encapsulating an oil layer between the gaseous core and lipid shell in which hydrophobic drugs can be dissolved (Figure 14A). High drug

loading capacities have been reported with paclitaxel loaded AALS²¹⁴. However, very high ultrasound intensities are required to obtain sufficient drug release, as the oil layer inside retards wall velocity associated with cavitation^{214,215}. Recently also polymer-shelled, oil-filled microbubbles were reported encapsulating sudan black as model drug²¹⁶.

Echogenic Liposomes (ELIP) are another microbubble type, enabling the incorporation of hydrophilic drugs inside the microbubble²¹⁷⁻²¹⁹(Figure 14B). Drug loading and gas encapsulation is obtained after different freeze and thaw cycles in the presence of mannitol. This results in the rupture of the lipid bilayer which increases gas inclusion and makes drug loading possible^{153,219-221}. Drug release from ELIPs is expected to occur relatively easy. Drugs are able to leak out when the expansion of the microbubble exceeds the elastic limit of the lipid shell. Furthermore, successive expansion cycles can be used to increase drug release, as the microbubble shell is able to reseal due to the flexibility of the lipid monolayer²²¹.

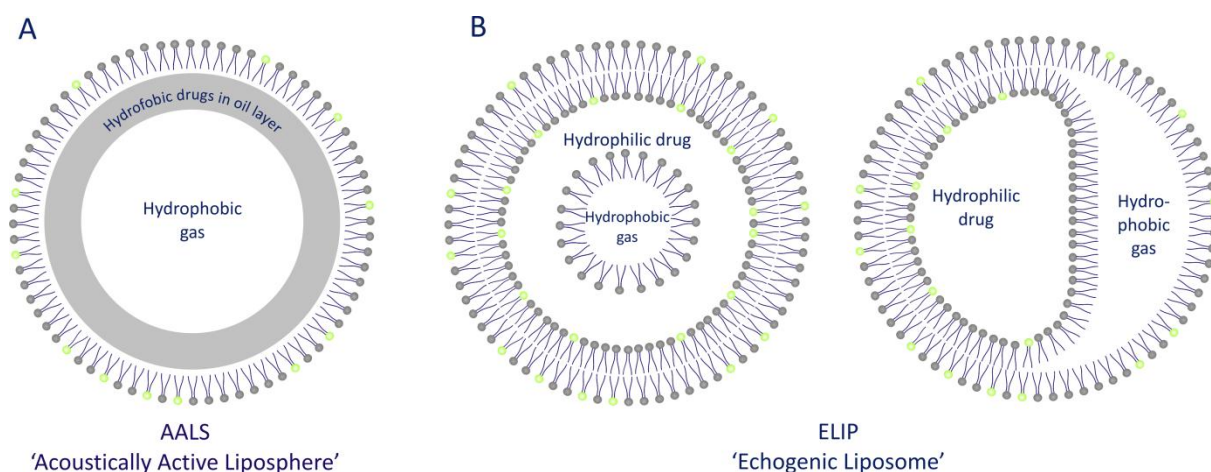


Figure 14 Schematic presentation of an acoustically active liposphere (AALS) encapsulating hydrophobic drugs and hydrophobic gas (A). Two possible presentations of an echogenic liposome encapsulating hydrophilic drugs and hydrophobic gas (B).

An alternative strategy to enclose hydrophilic compounds is the formation of pLGA (poly-(D,L-lactide-coglycolide)) microparticles²²². This echogenic microcapsule has been loaded with pDNA and pDNA-polymer complexes. However, important drawbacks are the large size (3-7 μ m), the low loading efficiency and the fact that drugs are able to leak out before ultrasound exposure, due to the high porosity of this capsule.

Drugs incorporated in the shell of a microbubble. Drug loading inside the microbubble shell has been demonstrated with pDNA loaded albumin microbubbles. In this case, the genetic material is

added during microbubble preparation^{223,224}. Experiments revealed that the DNA was still intact after sonication of the albumin solution. After intravenous injection of the microbubbles there might be a risk of premature release due to interaction of the microbubble shell with several blood components. Also, shell-loaded ELIP containing hirudin, a small (7kDa) thrombin inhibiting peptide, were prepared²²⁵. Therefore, the hirudin was added to the ELIPs after successive freeze-drying steps of the liposome mixture. Important remarks are the fact that drug loading is rather limited and will depend mainly on the polarity of the drug, as lipid microbubbles are surrounded by a mono-layer of phospholipids²²⁶. One can assume that only the hydrophobic parts of the peptide are present in the lipid shell, while the hydrophilic parts protrude in the aqueous phase. This saves place in the microbubble shell and might be a possible explanation for the high loading efficiency reported (30-50%).

Adenoviral (Ad) loaded microbubbles were prepared by reconstitution of commercially available Imagent™ microbubbles in the presence of Ad²²⁷. Exposure of the Ad containing microbubbles to human complement deactivated uncomplexed Ad. Exposure of the viral microbubble to ultrasound resulted in an ultrasound targeted viral gene expression.

Another very interesting approach is the preparation of liquid perfluorocarbon (C₅F₁₂) nanoparticles encapsulating doxorubicin (DOX) in their shell^{228,229}. After intravenous injection in mice, the nanodroplets accumulated in the tumor tissue as the high permeability of the tumor endothelium enabled the nanoparticles to extravasate from the tumor vasculature. The most innovative part of this work was that nanodroplets converted into microbubbles at body temperature. Microbubbles appeared in the tumor and remarkably enhanced echo contrast. Furthermore, DOX was released from the microbubbles and selectively taken up by the tumor cells after application of ultrasound with a higher intensity.

Drugs electrostatically attached to the microbubble shell. The loading of drugs onto the surface of microbubbles through electrostatic interactions has especially been evaluated for the ultrasound mediated delivery of nucleic acids. Electrostatic loading of pDNA onto microbubbles was first demonstrated onto cationically charged lipid microbubbles^{230,231}. pDNA loading can be achieved by simply mixing cationic microbubbles and pDNA, which avoids sonication in the presence of pDNA. Consequently, the risk of pDNA degradation is substantially lower. The reported loading efficiencies are rather low (6700 plasmids/microbubble), which might be due to the relatively low amount of cationic lipids in the microbubble shell. Although the loading of the microbubbles can be improved by increasing the amount of positive charges, too many charged lipids in the microbubble shell can disrupt lipid packing, resulting in a higher surface tension and subsequent lower microbubble stability¹⁵⁴.

Also envelop-deficient (lacking envelop proteins), retroviruses were electrostatically coupled onto cationic lipid microbubbles²³². After exposure to ultrasound, the viral particles were able to reach the cytoplasm of the target cells, where they could unpack and proceed to the nucleus for viral transcription. A very interesting feature of these microbubbles, is the fact that they will only be able to transfect ultrasound treated regions, thereby achieving a localized viral gene transfer. Viral particles that dissociate from the microbubbles outside the ultrasound will not be able to enter target cells. Also cationically charged AAV particles were loaded onto anionic lipid microbubbles²³³. However, in this case, transduction was also achieved in organs outside the ultrasound beam, as the AAVs were not made deficient.

Drug loaded nanoparticles linked to the microbubble shell. A more advanced drug carrying microbubble was obtained by attaching nanoparticles to lipid microbubbles via avidin-biotin interactions. This concept was first demonstrated using avidinylated polystyrene beads²³⁴. Biotinylated lipid microbubbles are prepared by the inclusion of a biotinylated lipid in the microbubble shell. Also, biotinylated liposomes were attached after avidinylation of these microbubbles²³⁵. Liposomes are versatile drug delivery systems, able to encapsulate hydrophilic and hydrophobic drugs, their attachment onto the microbubble shell can drastically increase the drug loading capacity of the microbubbles.

References

- (1) Bertram J.S. The molecular biology of cancer. *Molecular aspects of medicine* **2000** 21(6) 167-223.
- (2) Chiaradonna F., Balestrieri C., Gaglio D., & Vanoni M. RAS and PKA pathways in cancer: new insight from transcriptional analysis. *Frontiers in bioscience : a journal and virtual library* **2008** 1(13) 5257-7852.
- (3) Vazquez A., Bond E.E., Levine A.J., & Bond G.L. The genetics of the p53 pathway, apoptosis and cancer therapy. *Nature reviews* **2008** 7(12) 979-987.
- (4) Scharer O.D. DNA interstrand crosslinks: Natural and drug-induced DNA adducts that induce unique cellular responses. *ChemBiochem* **2005** 6(1) 27-32.
- (5) Ahmad S., Isab A.A., & Ali S. Structural and mechanistic aspects of platinum anticancer agents. *Transition Metal Chemistry* **2006** 31(8) 1003-1016.
- (6) Wang D. & Lippard S.J. Cellular processing of platinum anticancer drugs. *Nature Reviews Drug Discovery* **2005** 4(4) 307-320.

- (7) Genestier L., Paillot R., Quemeneur L., Izeradjene K., & Revillard J.P. Mechanisms of action of methotrexate. *Immunopharmacology* **2000** 47(2-3) 247-257.
- (8) McGuire J.J. Anticancer antifolates: Current status and future directions. *Current Pharmaceutical Design* **2003** 9(31) 2593-2613.
- (9) Sigmond J. & Peters G.J. Pyrimidine and purine analogues, effects on cell cycle regulation and the role of cell cycle inhibitors to enhance their cytotoxicity. *Nucleosides Nucleotides & Nucleic Acids* **2005** 24(10-12) 1997-2022.
- (10) Abdella B.R.J. & Fisher J. A Chemical Perspective on the Anthracycline Antitumor Antibiotics. *Environmental Health Perspectives* **1985** 643-18.
- (11) Hecht S.M. Bleomycin: New perspectives on the mechanism of action. *Journal of Natural Products* **2000** 63(1) 158-168.
- (12) Zunino F. & Capranico G. DNA Topoisomerase-II As the Primary Target of Antitumor Anthracyclines. *Anti-Cancer Drug Design* **1990** 5(4) 307-317.
- (13) Patil R.R., Guhagarkar S.A., & Devarajan P.V. Engineered nanocarriers of doxorubicin: A current update. *Critical Reviews in Therapeutic Drug Carrier Systems* **2008** 25(1) 1-61.
- (14) Malonne H. & Atassi G. DNA topoisomerase targeting drugs: mechanisms of action and perspectives. *Anti-Cancer Drugs* **1997** 8(9) 811-822.
- (15) Jordan M.A. & Wilson L. Microtubules as a target for anticancer drugs. *Nature Reviews Cancer* **2004** 4(4) 253-265.
- (16) Carter P. Improving the efficacy of antibody-based cancer therapies. *Nature Reviews Cancer* **2001** 1(2) 118-129.
- (17) Karthikeyan B.V. & Pradeep A.R. Gene therapy in periodontics: a review and future implications. *The journal of contemporary dental practice* **2006** 7(3) 83-91.
- (18) Pai S.I., Lin Y.Y., Macaes B., Meneshian A., Hung C.F., & Wu T.C. Prospects of RNA interference therapy for cancer. *Gene Therapy* **2006** 13(6) 464-477.
- (19) Tong A.W., Zhang Y.A., & Nemunaitis J. Small interfering RNA for experimental cancer therapy. *Current Opinion in Molecular Therapeutics* **2005** 7(2) 114-124.
- (20) Patil S.D., Rhodes D.G., & Burgess D.J. DNA-based therapeutics and DNA delivery systems: a comprehensive review. *AAPS Journal* **2005** 7(1) E61-E77.
- (21) Crooke S.T. Molecular mechanisms of action of antisense drugs. *Biochimica et Biophysica Acta-Gene Structure and Expression* **1999** 1489(1) 31-44.
- (22) Kurreck J. Antisense technologies - Improvement through novel chemical modifications. *European Journal of Biochemistry* **2003** 270(8) 1628-1644.
- (23) Stull R.A. & Szoka F.C. Antigene, Ribozyme and Aptamer Nucleic-Acid Drugs - Progress and Prospects. *Pharmaceutical Research* **1995** 12(4) 465-483.

- (24) Isaka Y., Imai E., Takahara S., & Rakugi H. Oligonucleotidic therapeutics. *Expert Opinion on Drug Discovery* **2008** 3(9) 991-996.
- (25) Achenbach J.C., Chiuman W., Cruz R.P.G., & Li Y. DNAzymes: From creation in vitro to application in vivo. *Current Pharmaceutical Biotechnology* **2004** 5(4) 321-336.
- (26) Agrawal N., Dasaradhi P.V.N., Mohmmmed A., Malhotra P., Bhatnagar R.K., & Mukherjee S.K. RNA interference: Biology, mechanism, and applications. *Microbiology and Molecular Biology Reviews* **2003** 67(4) 657-+.
- (27) Carthew R.W. Gene silencing by double-stranded RNA. *Current Opinion in Cell Biology* **2001** 13(2) 244-248.
- (28) Devi G.R. siRNA-based approaches in cancer therapy. *Cancer gene therapy* **2006** 13(9) 819-829.
- (29) Matzke M.A. & Birchler J.A. RNAi-mediated pathways in the nucleus. *Nature Reviews Genetics* **2005** 6(1) 24-35.
- (30) Rayburn E.R. & Zhang R.W. Antisense, RNAi, and gene silencing strategies for therapy: Mission possible or impossible? *Drug Discovery Today* **2008** 13(11-12) 513-521.
- (31) Bridge A.J., Pebernard S., Ducraux A., Nicoulaz A.L., & Iggo R. Induction of an interferon response by RNAi vectors in mammalian cells. *Nature Genetics* **2003** 34(3) 263-264.
- (32) Paddison P.J., Caudy A.A., Bernstein E., Hannon G.J., & Conklin D.S. Short hairpin RNAs (shRNAs) induce sequence-specific silencing in mammalian cells. *Genes & Development* **2002** 16(8) 948-958.
- (33) El-Aneed A. Current strategies in cancer gene therapy. *European journal of pharmacology* **2004** 498(1-3) 1-8.
- (34) Rejiba S., Wack S., Aprahamian M., & Hajri A. K-ras oncogene silencing strategy reduces tumor growth and enhances gemcitabine chemotherapy efficacy for pancreatic cancer treatment. *Cancer Science* **2007** 98(7) 1128-1136.
- (35) Butz K., Ristriani T., Hengstermann A., Denk C., Scheffner M., & Hoppe-Seyler F. siRNA targeting of the viral E6 oncogene efficiently kills human papillomavirus-positive cancer cells. *Oncogene* **2003** 22(38) 5938-5945.
- (36) Almazov V.P., Kochetkov D.V., & Chumakov P.M. Use of p53 for therapy of human cancer. *Molecular Biology* **2007** 41(6) 863-877.
- (37) Bouvet M., Ellis L.M., Nishizaki M. *et al.* Adenovirus-mediated wild-type p53 gene transfer down-regulates vascular endothelial growth factor expression and inhibits angiogenesis in human colon cancer. *Cancer Research* **1998** 58(11) 2288-2292.
- (38) Hughes R.M. Strategies for cancer gene therapy. *Journal of Surgical Oncology* **2004** 85(1) 28-35.
- (39) Weiss J.M., Subleski J.J., Wigginton J.M., & Wiltout R.H. Immunotherapy of cancer by IL-12-based cytokine combinations. *Expert Opinion on Biological Therapy* **2007** 7(11) 1705-1721.

- (40) Hoshino T., Jiang Y.Z., Dunn D. *et al.* Transfection of interleukin-12 cDNAs into tumor cells induces cytotoxic immune responses against native tumor: implications for tumor vaccination. *Cancer gene therapy* **1998** 5(3) 150-157.
- (41) Melero I., Duarte M., Ruiz J. *et al.* Intratumoral injection of bone-marrow derived dendritic cells engineered to produce interleukin-12 induces complete regression of established murine transplantable colon adenocarcinomas. *Gene Therapy* **1999** 6(10) 1779-1784.
- (42) Gilboa E. & Vieweg J. Cancer immunotherapy with mRNA-transfected dendritic cells. *Immunological Reviews* **2004** 199(1) 251-263.
- (43) Kimura T., Ohashi T., Kikuchi T., Kiyota H., Eto Y., & Ohishi Y. Antitumor immunity against bladder cancer induced by ex vivo expression of CD40 ligand gene using retrovirus vector. *Cancer gene therapy* **2003** 10(11) 833-839.
- (44) El-Aneed A. An overview of current delivery systems in cancer gene therapy. *Journal of Controlled Release* **2004** 94(1) 1-14.
- (45) Springer C.J. & Niculescu-Duvaz I. Prodrug-activating systems in suicide gene therapy. *Journal of Clinical Investigation* **2000** 105(9) 1161-1167.
- (46) Moolten F.L. Drug-Sensitivity (Suicide) Genes for Selective Cancer-Chemotherapy. *Cancer gene therapy* **1994** 1(4) 279-287.
- (47) Gottesman M.M. Mechanisms of cancer drug resistance. *Annual Review of Medicine* **2002** 53:615-627.
- (48) Bellamy W.T. P-glycoproteins and multidrug resistance. *Annual Review of Pharmacology and Toxicology* **1996** 36 161-183.
- (49) Chan H.S.L., Haddad G., Thorner P.S. *et al.* P-Glycoprotein Expression As A Predictor of the Outcome of Therapy for Neuroblastoma. *New England Journal of Medicine* **1991** 325(23) 1608-1614.
- (50) Yague E., Higgins C.F., & Raguz S. Complete reversal of multidrug resistance by stable expression of small interfering RNAs targeting MDR1. *Gene Therapy* **2004** 11(14) 1170-1174.
- (51) Nieth C., Priebisch A., Stege A., & Lage H. Modulation of the classical multidrug resistance (MDR) phenotype by RNA interference (RNAi). *Febs Letters* **2003** 545(2-3) 144-150.
- (52) Alahari S.K., Dean N.M., Fisher M.H. *et al.* Inhibition of expression of the multidrug resistance-associated P-glycoprotein by phosphorothioate and 5' cholesterol-conjugated phosphorothioate antisense oligonucleotides. *Molecular Pharmacology* **1996** 50(4) 808-819.
- (53) Cucco C. & Calabretta B. In vitro and in vivo reversal of multidrug resistance in a human leukemia-resistant cell line by mdr1 antisense oligodeoxynucleotides. *Cancer Research* **1996** 56(19) 4332-4337.
- (54) Seth P. Vector-mediated cancer gene therapy - An overview. *Cancer Biology & Therapy* **2005** 4(5) 512-517.
- (55) Hicklin D.J. & Ellis L.M. Role of the vascular endothelial growth factor pathway in tumor growth and angiogenesis. *Journal of Clinical Oncology* **2005** 23(5) 1011-1027.

- (56) Schifflers R.M., Ansari A., Xu J. *et al.* Cancer siRNA therapy by tumor selective delivery with ligand-targeted sterically stabilized nanoparticle. *Nucleic Acids Research* **2004** 32(19) e149.
- (57) Filleur S., Courtin A., it-Si-Ali S. *et al.* SiRNA-mediated inhibition of vascular endothelial growth factor severely limits tumor resistance to Antiangiogenic thrombospondin-1 and slows tumor vascularization and growth. *Cancer Research* **2003** 63(14) 3919-3922.
- (58) Miyagi M., Aoyagi K., Kato S., & Shirouzu K. The TIMP-1 gene transferred through adenovirus mediation shows a suppressive effect on peritoneal metastases from gastric cancer. *International Journal of Clinical Oncology* **2007** 12(1) 17-24.
- (59) Robbins P.D. & Ghivizzani S.C. Viral vectors for gene therapy. *Pharmacology & Therapeutics* **1998** 80(1) 35-47.
- (60) Shen Y. & Nemunaitis J. Herpes simplex virus 1 (HSV-1) for cancer treatment. *Cancer gene therapy* **2006** 13(11) 975-992.
- (61) Karmali P.P. & Chaudhuri A. Cationic Liposomes as non-viral carriers of gene medicines: Resolved issues, open questions, and future promises. *Medicinal Research Reviews* **2007** 27(5) 696-722.
- (62) Gao X., Kim K.S., & Liu D.X. Nonviral gene delivery: What we know and what is next. *AAPS Journal* **2007** 9(1) E92-E104.
- (63) Zaldumbide A. & Hoeben R.C. How not to be seen: immune-evasion strategies in gene therapy. *Gene Therapy* **2008** 15(4) 239-246.
- (64) Deshpande M.C., Davies M.C., Garnett M.C. *et al.* The effect of poly(ethylene glycol) molecular architecture on cellular interaction and uptake of DNA complexes. *Journal of Controlled Release* **2004** 97(1) 143-156.
- (65) Mishra S., Webster P., & Davis M.E. PEGylation significantly affects cellular uptake and intracellular trafficking of non-viral gene delivery particles. *European Journal of Cell Biology* **2004** 83(3) 97-111.
- (66) Wong J.B., Grosse S., Tabor A.B., Hart S.L., & Hailes H.C. Acid cleavable PEG-lipids for applications in a ternary gene delivery vector. *Molecular bioSystems* **2008** 4(6) 532-541.
- (67) Conwell C.C. & Huang L. Recent advances in non-viral gene delivery. *Advances in genetics* **2005** 533-18.
- (68) Schaffert D. & Wagner E. Gene therapy progress and prospects: synthetic polymer-based systems. *Gene Therapy* **2008** 15(16) 1131-1138.
- (69) Cemazar M., Golzio M., Sersa G., Rols M.P., & Teissie J. Electrically-assisted nucleic acids delivery to tissues in vivo: Where do we stand? *Current Pharmaceutical Design* **2006** 12(29) 3817-3825.
- (70) Gehl J. Electroporation: theory and methods, perspectives for drug delivery, gene therapy and research. *Acta Physiologica Scandinavica* **2003** 177(4) 437-447.

- (71) Prud'homme G.J., Glinka Y., Khan A.S., & Draghia-Akli R. Electroporation-enhanced nonviral gene transfer for the prevention or treatment of immunological, endocrine and neoplastic diseases. *Current Gene Therapy* **2006** 6(2) 243-273.
- (72) Russ V. & Wagner E. Cell and tissue targeting of nucleic acids for cancer gene therapy. *Pharmaceutical Research* **2007** 24(6) 1047-1057.
- (73) Herweijer H. & Wolff J.A. Progress and prospects: naked DNA gene transfer and therapy. *Gene Therapy* **2003** 10(6) 453-458.
- (74) Suda T. & Liu D. Hydrodynamic gene delivery: Its principles and applications. *Molecular Therapy* **2007** 15(12) 2063-2069.
- (75) Mehier-Humbert S. & Guy R.H. Physical methods for gene transfer: Improving the kinetics of gene delivery into cells. *Advanced Drug Delivery Reviews* **2005** 57(5) 733-753.
- (76) Leighton T.G. What is ultrasound? *Prog. Biophys. Mol. Biol.* **2007** 93(1-3) 3-83.
- (77) Hauff P., Reinhardt M., & Foster S. Ultrasound basics. *Handbook of experimental pharmacology* **2008** 185(1) 91-107.
- (78) Baker K.G., Robertson V.J., & Duck F.A. A review of therapeutic ultrasound: Biophysical effects. *Physical Therapy* **2001** 81(7) 1351-1358.
- (79) O'Brien W.D., Jr. Ultrasound-biophysics mechanisms. *Progress in biophysics and molecular biology* **2007** 93(1-3) 212-255.
- (80) Humphrey V.F. Ultrasound and matter--physical interactions. *Progress in biophysics and molecular biology* **2007** 93(1-3) 195-211.
- (81) Kuznetsova L.A. & Coakley W.T. Applications of ultrasound streaming and radiation force in biosensors. *Biosensors & bioelectronics* **2007** 22(8) 1567-1577.
- (82) Miller D.L. Overview of experimental studies of biological effects of medical ultrasound caused by gas body activation and inertial cavitation. *Progress in biophysics and molecular biology* **2007** 93(1-3) 314-330.
- (83) Ter Haar G. Therapeutic applications of ultrasound. *Prog. Biophys. Mol. Biol.* **2007** 93(1-3) 111-129.
- (84) Santoro G.A. Fundamental Principles of Ultrasound Imaging. *Benign Anorectal Diseases* **2006** , 3-9 .
- (85) Dubinsky T.J., Cuevas C., Dighe M.K., Kolokythas O., & Hwang J.H. High-intensity focused ultrasound: Current potential and oncologic applications. *American Journal of Roentgenology* **2008** 190191-199.
- (86) Ter Haar G. & Coussios C. High intensity focused ultrasound: physical principles and devices. *Int J Hyperthermia* **2007** 23(2) 89-104.
- (87) Dewhurst M.W., Viglianti B.L., Lora-Michiels M., Hanson M., & Hoopes P.J. Basic principles of thermal dosimetry and thermal thresholds for tissue damage from hyperthermia. *International Journal of Hyperthermia* **2003** 19(3) 267-294.

- (88) Coussios C.C., Farny C.H., Ter Haar G., & Roy R.A. Role of acoustic cavitation in the delivery and monitoring of cancer treatment by high-intensity focused ultrasound (HIFU). *International Journal of Hyperthermia* **2007** 23(2) 105-120.
- (89) Khokhlova V.A., Bailey M.R., Reed J.A., Cunitz B.W., Kaczkowski P.J., & Crum L.A. Effects of nonlinear propagation, cavitation, and boiling in lesion formation by high intensity focused ultrasound in a gel phantom. *Journal of the Acoustical Society of America* **2006** 119(3) 1834-1848.
- (90) Ter Haar G. & Coussios C. High intensity focused ultrasound: Physical principles and devices. *International Journal of Hyperthermia* **2007** 23(2) 89-104.
- (91) Kennedy J.E., ter Haar G.R., & Cranston D. High intensity focused ultrasound: surgery of the future? *British Journal of Radiology* **2003** 76(909) 590-599.
- (92) Wu F., Wang Z.B., Cao Y.D. *et al.* A randomised clinical trial of high-intensity focused ultrasound ablation for the treatment of patients with localised breast cancer. *British Journal of Cancer* **2003** 89(12) 2227-2233.
- (93) Wu F., Wang Z.B., Zhu H. *et al.* Extracorporeal high intensity focused ultrasound treatment for patients with breast cancer. *Breast Cancer Research and Treatment* **2005** 92(1) 51-60.
- (94) Thuroff S., Chaussy C., Vallancien G. *et al.* High-intensity focused ultrasound and localized prostate cancer: Efficacy results from the European multicentric study. *Journal of Endourology* **2003** 17(8) 673-677.
- (95) Illing R.O., Kennedy J.E., Wu F. *et al.* The safety and feasibility of extracorporeal high-intensity focused ultrasound (HIFU) for the treatment of liver and kidney tumours in a Western population. *British Journal of Cancer* **2005** 93(8) 890-895.
- (96) Auge B.K. & Preminger G.M. Update on shock wave lithotripsy technology. *Current opinion in urology* **2002** 12(4) 287-290.
- (97) Bailey M.R., Khokhlova V.A., Sapozhnikov O.A., Kargl S.G., & Crum L.A. Physical mechanisms of the therapeutic effect of ultrasound - A review. *Acoustical Physics* **2003** 49(4) 369-388.
- (98) Eisenmenger W. The mechanisms of stone fragmentation in ESWL. *Ultrasound in medicine & biology* **2001** 27(5) 683-693.
- (99) Merino G., Kalia Y.N., & Guy R.H. Ultrasound-enhanced transdermal transport. *Journal of Pharmaceutical Sciences* **2003** 92(6) 1125-1137.
- (100) Mitragotri S. & Kost J. Low-frequency sonophoresis - A review. *Advanced Drug Delivery Reviews* **2004** 56(5) 589-601.
- (101) Mitragotri S. Innovation - Healing sound: the use of ultrasound in drug delivery and other therapeutic applications. *Nature Reviews Drug Discovery* **2005** 4(3) 255-260.
- (102) Joshi A. & Raje J. Sonicated transdermal drug transport. *Journal of Controlled Release* **2002** 83(1) 13-22.
- (103) Lavon A. & Kost J. Ultrasound and transdermal drug delivery. *Drug Discovery Today* **2004** 9(15) 670-676.

- ⁽¹⁰⁴⁾ Smith N.B. Perspectives on transdermal ultrasound mediated drug delivery. *International Journal of Nanomedicine* **2007** 2(4) 585-594.
- ⁽¹⁰⁵⁾ Ogura M., Pahwal S., & Mitragotri S. Low-frequency sonophoresis: Current status and future prospects. *Advanced Drug Delivery Reviews* **2008** 60(10) 1218-1223.
- ⁽¹⁰⁶⁾ Kushner J., Blankschtein D., & Langer R. Experimental demonstration of the existence of highly permeable localized transport regions in low-frequency sonophoresis. *Journal of Pharmaceutical Sciences* **2004** 93(11) 2733-2745.
- ⁽¹⁰⁷⁾ Kushner J., Blankschtein D., & Langer R. Heterogeneity in skin treated with low-frequency ultrasound. *Journal of Pharmaceutical Sciences* **2008** 97(10) 4119-4128.
- ⁽¹⁰⁸⁾ Morimoto Y., Mutoh M., Ueda H. *et al.* Elucidation of the transport pathway in hairless rat skin enhanced by low-frequency sonophoresis based on the solute-water transport relationship and confocal microscopy. *Journal of Controlled Release* **2005** 103(3) 587-597.
- ⁽¹⁰⁹⁾ Paliwal S., Menon G.K., & Mitragotri S. Low-frequency sonophoresis: Ultrastructural basis for stratum corneum permeability assessed using quantum dots. *Journal of Investigative Dermatology* **2006** 126:1095-1101.
- ⁽¹¹⁰⁾ Tezel A., Sens A., & Mitragotri S. Description of transdermal transport of hydrophilic solutes during low-frequency sonophoresis based on a modified porous pathway model. *Journal of Pharmaceutical Sciences* **2003** 92(2) 381-393.
- ⁽¹¹¹⁾ Varez-Roman R., Merino G., Kalia Y.N., Naik A., & Guy R.H. Skin permeability enhancement by low frequency sonophoresis: Lipid extraction and transport pathways. *Journal of Pharmaceutical Sciences* **2003** 92(6) 1138-1146.
- ⁽¹¹²⁾ Varez-Roman R., Naik A., Kalia Y.N., Fessi H., & Guy R.H. Visualization of skin penetration using confocal laser scanning microscopy. *European Journal of Pharmaceutics and Biopharmaceutics* **2004** 58(2) 301-316.
- ⁽¹¹³⁾ Ghosh S., Kim D., So P., & Blankschtein D. Visualization and quantification of skin barrier perturbation induced by surfactant-humectant systems using two-photon fluorescence microscopy. *Journal of Cosmetic Science* **2008** 59(4) 263-289.
- ⁽¹¹⁴⁾ Tezel A. & Mitragotri S. Interactions of inertial cavitation bubbles with stratum corneum lipid bilayers during low-frequency sonophoresis. *Biophysical Journal* **2003** 85(6) 3502-3512.
- ⁽¹¹⁵⁾ Meshali M.M., Abdel-Aleem H.M., Sakr F.M., Nazzal S., & El-Malah Y. In vitro sonophoresis: effect of ultrasound intensity and mode at high frequency on NSAIDs transport across cellulose and rabbit skin membranes. *Pharmazie* **2008** 63(1) 49-53.
- ⁽¹¹⁶⁾ Smith N.B., Lee S., Maione E., Roy R.B., McElligott S., & Shung K.K. Ultrasound-mediated transdermal transport of insulin in vitro through human skin using novel transducer designs. *Ultrasound in Medicine and Biology* **2003** 29(2) 311-317.
- ⁽¹¹⁷⁾ Tezel A., Dokka S., Kelly S., Hardee G.E., & Mitragotri S. Topical delivery of anti-sense oligonucleotides using low-frequency sonophoresis. *Pharmaceutical Research* **2004** 21(12) 2219-2225.

- (118) Boucaud A., Garrigue M.A., Machet L., Vaillant L., & Patat F. Effect of sonication parameters on transdermal delivery of insulin to hairless rats. *Journal of Controlled Release* **2002** 81(1-2) 113-119.
- (119) Spierings E.L.H., Brevard J.A., & Katz N.P. Two-minute skin anesthesia through ultrasound pretreatment and iontophoretic delivery of a topical anesthetic: A feasibility study. *Pain Medicine* **2008** 9(1) 55-59.
- (120) Tachibana K. & Tachibana S. Use of Ultrasound to Enhance the Local-Anesthetic Effect of Topically Applied Aqueous Lidocaine. *Anesthesiology* **1993** 78(6) 1091-1096.
- (121) Ainsworth R., Dziedzic K., Hiller L., Daniels J., Bruton A., & Broadfield J. Comment on: A prospective double blind placebo-controlled randomized trial of ultrasound in the physiotherapy treatment of shoulder pain: reply. *Rheumatology* **2008** 47(2) 230-231.
- (122) Hurley M.V. The contribution of physiotherapy to the management of osteoarthritis. *British Journal of Hospital Medicine* **2008** 69(1) 31-34.
- (123) Byl N.N., McKenzie A.L., West J.M., Whitney J.D., Hunt T.K., & Scheuenstuhl H.A. Low-dose ultrasound effects on wound healing: a controlled study with Yucatan pigs. *Archives of physical medicine and rehabilitation* **1992** 73(7) 656-664.
- (124) Young S.R. & Dyson M. Effect of therapeutic ultrasound on the healing of full-thickness excised skin lesions. *Ultrasonics* **1990** 28(3) 175-80.
- (125) Dyson M. & Suckling J. Stimulation of tissue repair by ultrasound: a survey of the mechanisms involved. *Physiotherapy* **1978** 64(4) 105-108.
- (126) Watson T. Ultrasound in contemporary physiotherapy practice. *Ultrasonics* **2008** 48(4) 321-329.
- (127) Paliwal S. & Mitragotri S. Therapeutic opportunities in biological responses of ultrasound. *Ultrasonics* **2008** 48(4) 271-278.
- (128) Speed C.A. Therapeutic ultrasound in soft tissue lesions. *Rheumatology* **2001** 40(12) 1331-1336.
- (129) Pounder N.M. & Harrison A.J. Low intensity pulsed ultrasound for fracture healing: A review of the clinical evidence and the associated biological mechanism of action. *Ultrasonics* **2008** 48(4) 330-338.
- (130) Pilla A.A., Mont M.A., Nasser P.R. *et al.* Non-invasive low-intensity pulsed ultrasound accelerates bone healing in the rabbit. *Journal of orthopaedic trauma* **1990** 4(3) 246-253.
- (131) Wang S.J., Lewallen D.G., Bolander M.E., Chao E.Y., Ilstrup D.M., & Greenleaf J.F. Low intensity ultrasound treatment increases strength in a rat femoral fracture model. *Journal of orthopaedic research* **1994** 12(1) 40-47.
- (132) Tam K.F., Cheung W.H., Lee K.M., Qin L., & Leung K.S. Osteogenic effects of low-intensity pulsed ultrasound, extracorporeal shockwaves and their combination - an in vitro comparative study on human periosteal cells. *Ultrasound in medicine & biology* **2008** 34(12) 1957-1965.

- (133) Rubin C., Bolander M., Ryaby J.P., & Hadjiargyrou M. The use of low-intensity ultrasound to accelerate the healing of fractures. *Journal of Bone and Joint Surgery-American Volume* **2001** 83A(2) 259-270.
- (134) Yumita N., Okuyama N., Sasaki K., & Umemura S. Sonodynamic therapy on chemically induced mammary tumor: pharmacokinetics, tissue distribution and sonodynamically induced antitumor effect of gallium-porphyrin complex ATX-70. *Cancer Chemotherapy and Pharmacology* **2007** 60(6) 891-897.
- (135) Yumita N., Okuyama N., Sasaki K., & Umemura S. Sonodynamic therapy on chemically induced mammary tumor: Pharmacokinetics, tissue distribution and sonodynamically induced antitumor effect of porfimer sodium. *Cancer Science* **2004** 95(9) 765-769.
- (136) Yumita N. & Umemura S. Sonodynamic antitumor effect of chloroaluminum phthalocyanine tetrasulfonate on murine solid tumour. *Journal of Pharmacy and Pharmacology* **2004** 56(1) 85-90.
- (137) Yumita N., Sakata I., Nakajima S., & Umemura S. Ultrasonically induced cell damage and active oxygen generation by 4-formyloximeethylidene-3-hydroxyl-2-vinyl-deuterio-porphynyl(IX)-6-7-dia spartic acid: on the mechanism of sonodynamic activation. *Biochimica et Biophysica Acta-General Subjects* **2003** 1620(1-3) 179-184.
- (138) Tachibana K., Feril L.B., & Ikeda-Dantsuji Y. Sonodynamic therapy. *Ultrasonics* **2008** 48(4) 253-259.
- (139) Hussein G.A. & Pitt W.G. Micelles and nanoparticles for ultrasonic drug and gene delivery. *Advanced Drug Delivery Reviews* **2008** 60(10) 1137-1152.
- (140) Saad A.H. & Hahn G.M. Ultrasound-Enhanced Effects of Adriamycin Against Murine Tumors. *Ultrasound in Medicine and Biology* **1992** 18(8) 715-723.
- (141) Loverock P., Ter Haar G., Ormerod M.G., & Imrie P.R. The Effect of Ultrasound on the Cytotoxicity of Adriamycin. *British Journal of Radiology* **1990** 63(751) 542-546.
- (142) Feril L.B., Jr. & Kondo T. Biological effects of low intensity ultrasound: the mechanism involved, and its implications on therapy and on biosafety of ultrasound. *J Radiat. Res. (Tokyo)* **2004** 45(4) 479-489.
- (143) Rosenthal I., Sostaric J.Z., & Riesz P. Sonodynamic therapy - a review of the synergistic effects of drugs and ultrasound. *Ultrasonics Sonochemistry* **2004** 11(6) 349-363.
- (144) Myhr G. & Moan J. Synergistic and tumour selective effects of chemotherapy and ultrasound treatment. *Cancer Letters* **2006** 232(2) 206-213.
- (145) Schutt E.G., Klein D.H., Mattrey R.M., & Riess J.G. Injectable microbubbles as contrast agents for diagnostic ultrasound imaging: The key role of perfluorochemicals. *Angewandte Chemie-International Edition* **2003** 42(28) 3218-3235.
- (146) Skyba D.M. & Kaul S. Advances in microbubble technology. *Coronary artery disease* **2000** 11(3) 211-219.
- (147) Grayburn P.A. Current and future contrast agents. *Echocardiography - A Journal of Cardiovascular Ultrasound and Allied Techniques* **2002** 19(3) 259-265.

- (148) Riess J.G. Fluorocarbon-based injectable gaseous microbubbles for diagnosis and therapy. *Current Opinion in Colloid & Interface Science* **2003** 8(3) 259-266.
- (149) Stride E. & Edirisinghe M.J. Novel microbubble preparation technologies. *soft matter* **8 A.D.** 4(12), 2350-2359 .
- (150) Sboros V. Response of contrast agents to ultrasound. *Advanced Drug Delivery Reviews* **2008** 60(10) 1117-1136.
- (151) Hernot S. & Klibanov A.L. Microbubbles in ultrasound-triggered drug and gene delivery. *Advanced Drug Delivery Reviews* **2008** 60(10) 1153-1166.
- (152) Borden M.A., Kruse D.E., Caskey C.F., Zhao S.K., Dayton P.A., & Ferrara K.W. Influence of lipid shell physicochemical properties on ultrasound-induced microbubble destruction. *Ieee Transactions on Ultrasonics Ferroelectrics and Frequency Control* **2005** 52(11) 1992-2002.
- (153) Huang S.L., McPherson D.B., & MacDonald R.C. A method to co-encapsulate gas and drugs in liposomes for ultrasound-controlled drug delivery. *Ultrasound in Medicine and Biology* **2008** 34(8) 1272-1280.
- (154) Ferrara K., Pollard R., & Borden M. Ultrasound microbubble contrast agents: fundamentals and application to gene and drug delivery. *Annual review of biomedical engineering* **2007** 9415-447.
- (155) Jakobsen J.A., Oyen R., Thomsen H.S., & Morcos S.K. Safety of ultrasound contrast agents. *European radiology* **2005** 15(5) 941-945.
- (156) Albrecht T., Blomley M., Bolondi L. *et al.* Guidelines for the use of contrast agents in ultrasound. *Ultraschall in der Medizin* **2004** 25(4) 249-256.
- (157) Quaia E. Classification and Safety of Microbubble-Based Contrast Agents. *Contrast Media in ultrasonography* **2005** , 3-14 .
- (158) Forsberg F., Goldberg B.B., Liu J.B., Merton D.A., Rawool N.M., & Shi W.T. Tissue-specific US contrast agent for evaluation of hepatic and splenic parenchyma. *Radiology* **1999** 210(1) 125-132.
- (159) Quaia E., Blomley M.J.K., Patel S. *et al.* Initial observations on the effect of irradiation on the liver-specific uptake of Levovist. *European Journal of Radiology* **2002** 41(3) 192-199.
- (160) Blomley M., Albrecht T., Cosgrove D., Jayaram V., Butler-Barnes J., & Eckersley R. Stimulated acoustic emission in liver parenchyma with Levovist. *Lancet* **1998** 351(9102) 568.
- (161) Yanagisawa K., Moriyasu F., Miyahara T., Yuki M., & Iijima H. Phagocytosis of ultrasound contrast agent microbubbles by Kupffer cells. *Ultrasound in medicine & biology* **2007** 33(2) 318-325.
- (162) Kabalnov A., Bradley J., Flaim S. *et al.* Dissolution of multicomponent microbubbles in the bloodstream: 2. Experiment. *Ultrasound in Medicine and Biology* **1998** 24(5) 751-760.
- (163) Quaia E. Physical Basis and Principles of Action of Microbubble-based contrast agents. *Contrast Media in ultrasonography* **2005** , 15-30.

- (164) VanBavel E. Effects of shear stress on endothelial cells: possible relevance for ultrasound applications. *Progress in biophysics and molecular biology* **2007** 91(1-3) 374-383.
- (165) Wu J. & Nyborg W.L. Ultrasound, cavitation bubbles and their interaction with cells. *Advanced Drug Delivery Reviews* **2008** 60(10) 1103-1116.
- (166) Wu J.R., Ross J.P., & Chiu J.F. Reparable sonoporation generated by microstreaming. *Journal of the Acoustical Society of America* **2002** 111(3) 1460-1464.
- (167) Miller D.L., Averkiou M.A., Brayman A.A. *et al.* Bioeffects considerations for diagnostic ultrasound contrast agents. *Journal of ultrasound in medicine* **2008** 27(4) 611-632.
- (168) Pitt W.G., Hussein G.A., & Staples B.J. Ultrasonic drug delivery--a general review. *Expert Opinion on Drug Delivery* **2004** 1(1) 37-56.
- (169) Chappell J.C. & Price R.J. Targeted therapeutic applications of acoustically active microspheres in the microcirculation. *Microcirculation* **2006** 13(1) 57-70.
- (170) Price R.J., Skyba D.M., Kaul S., & Skalak T.C. Delivery of colloidal, particles and red blood cells to tissue through microvessel ruptures created by targeted microbubble destruction with ultrasound. *Circulation* **1998** 98(13) 1264-1267.
- (171) Vancraeynest D., Havaux X., Pouleur A.C. *et al.* Myocardial delivery of colloid nanoparticles using ultrasound-targeted microbubble destruction. *European heart journal* **2006** 27(2) 237-245.
- (172) Wible J.H., Jr., Galen K.P., Wojdyla J.K., Hughes M.S., Klibanov A.L., & Brandenburger G.H. Microbubbles induce renal hemorrhage when exposed to diagnostic ultrasound in anesthetized rats. *Ultrasound in medicine & biology* **2002** 28(11-12) 1535-1546.
- (173) Li P., Armstrong W.F., & Miller D.L. Impact of myocardial contrast echocardiography on vascular permeability: comparison of three different contrast agents. *Ultrasound in medicine & biology* **2004** 30(1) 83-91.
- (174) Kondo T., Misik V., & Riesz P. Effect of gas-containing microspheres and echo contrast agents on free radical formation by ultrasound. *Free radical biology & medicine* **1998** 25(4-5) 605-612.
- (175) Misik V. & Riesz P. Free radical intermediates in sonodynamic therapy. *Annals of the New York Academy of Sciences* **2000** 899 335-348.
- (176) Juffermans L.J., Dijkmans P.A., Musters R.J., Visser C.A., & Kamp O. Transient permeabilization of cell membranes by ultrasound-exposed microbubbles is related to formation of hydrogen peroxide. *American journal of physiology* **2006** 291(4) 1595-1601.
- (177) Pitt W.G., Hussein G.A., & Staples B.J. Ultrasonic drug delivery--a general review. *Expert Opinion on Drug Delivery* **2004** 1(1) 37-56.
- (178) Ohlerth S. & O'Brien R.T. Contrast ultrasound: General principles and veterinary clinical applications. *Veterinary Journal* **2007** 174501-512.
- (179) Harvey C.J., Pilcher J.M., Eckersley R.J., Blomley M.J.K., & Cosgrove D.O. Advances in ultrasound. *Clinical Radiology* **2002** 57(3) 157-177.

- (180) Feinstein S.B. The powerful microbubble: from bench to bedside, from intravascular indicator to therapeutic delivery system, and beyond. *American Journal of Physiology-Heart and Circulatory Physiology* **2004** 287(2) H450-H457.
- (181) Blomley M.J.K., Cooke J.C., Unger E.C., Monaghan M.J., & Cosgrove D.O. Science, medicine, and the future - Microbubble contrast agents: a new era in ultrasound. *British Medical Journal* **2001** 322(7296) 1222-1225.
- (182) Kono Y., Steinbach G.C., Peterson T., Schmid-Schonbein G.W., & Mattrey R.F. Mechanism of parenchymal enhancement of the liver with a microbubble-based US contrast medium: An intravital microscopy study in rats. *Radiology* **2002** 224(1) 253-257.
- (183) Stewart V.R. & Sidhu P.S. New directions in ultrasound: microbubble contrast. *The British journal of radiology* **2006** 79(939) 188-194.
- (184) Alexandrov A.V. Ultrasound enhanced thrombolysis for stroke. *International Journal of Stroke* **2006** 1(1) 26-29.
- (185) Alexandrov A.V. - Ultrasound Enhancement of Fibrinolysis. *Stroke* **2009** 40(3) 107-110.
- (186) Daffertshofer M., Huang Z., Fatar M. *et al.* Efficacy of sonothrombolysis in a rat model of embolic ischemic stroke. *Neuroscience Letters* **2004** 361(1-3) 115-119.
- (187) Kawata H., Naya N., Takemoto Y. *et al.* Ultrasound accelerates thrombolysis of acutely induced platelet-rich thrombi similar to those in acute myocardial infarction. *Circulation Journal* **2007** 71:1643-1648.
- (188) White H.D. & Van De Werf F.J.J. Thrombolysis for Acute Myocardial Infarction. *Circulation* **1998** 97(16), 1632-1646 .
- (189) Hajri Z., Boukadoum M., Hamam H., & Fontaine R. An investigation of the physical forces leading to thrombosis disruption by cavitation. *Journal of Thrombosis and Thrombolysis* **2005** 20(1) 27-32.
- (190) Pfaffenberger S., Vcic-Kuhar B., Kastl S.P. *et al.* Ultrasound thrombolysis. *Thrombosis and Haemostasis* **2005** 94(1) 26-36.
- (191) Stone M.J., Frenkel V., Dromi S. *et al.* Pulsed-high intensity focused ultrasound enhanced tPA mediated thrombolysis in a novel in vivo clot model, a pilot study. *Thrombosis Research* **2007** 121(2) 193-202.
- (192) Vcic-Kuhar B., Pfaffenberger S., Gherardini L. *et al.* Ultrasound affects distribution of plasminogen and tissue-type plasminogen activator in whole blood clots in vitro. *Thrombosis and Haemostasis* **2004** 92(5) 980-985.
- (193) Wang B., Wang L., Zhou X.B. *et al.* Thrombolysis effect of a novel targeted microbubble with low-frequency ultrasound in vivo. *Thrombosis and Haemostasis* **2008** 100(2) 356-361.
- (194) Wu Y.Q., Unger E.C., McCreery T.P. *et al.* Binding and lysing of blood clots using MRX-408. *Investigative radiology* **1998** 33(12) 880-885.
- (195) Xie F., Tsutsui J.M., Lof J. *et al.* Effectiveness of lipid microbubbles and ultrasound in declotting thrombosis. *Ultrasound in Medicine and Biology* **2005** 31(7) 979-985.

- (196) Hynynen K. Focused ultrasound for blood-brain disruption and delivery of therapeutic molecules into the brain. *Expert Opinion on Drug Delivery* **2007** 427-35.
- (197) Abbott N.J. & Romero I.A. Transporting therapeutics across the blood-brain barrier. *Molecular medicine today* **1996** 9(1) 73-83.
- (198) Johansson B.B. The physiology of the blood-brain barrier. *Advances in experimental medicine and biology* **1990** 274 25-39.
- (199) Hynynen K. Ultrasound for drug and gene delivery to the brain. *Advanced Drug Delivery Reviews* **2008** 60(10) 1209-1217.
- (200) McDannold N., Vykhodtseva N., & Hynynen K. Targeted disruption of the blood-brain barrier with focused ultrasound: association with cavitation activity. *Physics in Medicine and Biology* **2006** 51(4) 793-807.
- (201) Sheikov N., McDannold N., Vykhodtseva N., Jolesz F., & Hynynen K. Cellular mechanisms of the blood-brain barrier opening induced by ultrasound in presence of microbubbles. *Ultrasound in Medicine and Biology* **2004** 30(7) 979-989.
- (202) McDannold N., Vykhodtseva N., & Hynynen K. Blood-brain barrier disruption induced by focused ultrasound and circulating preformed microbubbles appears to be characterized by the mechanical index. *Ultrasound in Medicine and Biology* **2008** 34(5) 834-840.
- (203) Hynynen K., McDannold N., Sheikov N.A., Jolesz F.A., & Vykhodtseva N. Local and reversible blood-brain barrier disruption by noninvasive focused ultrasound at frequencies suitable for trans-skull sonications. *Neuroimage* **2005** 24(1) 12-20.
- (204) Reinhard M., Hetzel A., Kruger S. *et al.* Blood-brain barrier disruption by low-frequency ultrasound. *Stroke* **2006** 37(6) 1546-1548.
- (205) Choi J.J., Pernet M., Small S.A., & Konofagou E.E. Noninvasive, transcranial and localized opening of the blood-brain barrier using focused ultrasound in mice. *Ultrasound in Medicine and Biology* **2007** 33(1) 95-104.
- (206) Hynynen K., McDannold N., Martin H., Jolesz F.A., & Vykhodtseva N. The threshold for brain damage in rabbits induced by bursts of ultrasound in the presence of an ultrasound contrast agent (Optison (R)). *Ultrasound in Medicine and Biology* **2003** 29(3) 473-481.
- (207) Ross J.P., Cai X., Chiu J.F., Yang J., & Wu J.R. Optical and atomic force microscopic studies on sonoporation. *Journal of the Acoustical Society of America* **2002** 111(3) 1161-1164.
- (208) Mehier-Humbert S., Bettinger T., Yan F., & Guy R.H. Plasma membrane poration induced by ultrasound exposure: Implication for drug delivery. *Journal of Controlled Release* **2005** 104(1) 213-222.
- (209) Van Wamel A., Kooiman K., Hartevelde M. *et al.* Vibrating microbubbles poking individual cells: Drug transfer into cells via sonoporation. *Journal of Controlled Release* **2006** 112(2) 149-155.
- (210) Ohl C.D., Arora M., Ikink R. *et al.* Sonoporation from jetting cavitation bubbles. *Biophysical journal* **2006** 91(11) 4285-4295.

- (211) Prentice P., Cuschierp A., Dholakia K., Prausnitz M., & Campbell P. Membrane disruption by optically controlled microbubble cavitation. *Nature Physics* **2005** 1(2) 107-110.
- (212) Schlicher R.K., Radhakrishna H., Tolentino T.P., Apkarian R.P., Zarnitsyn V., & Prausnitz M.R. Mechanism of intracellular delivery by acoustic cavitation. *Ultrasound in Medicine and Biology* **2006** 32(6) 915-924.
- (213) Yang F., Gu N., Chen D. *et al.* Experimental study on cell self-sealing during sonoporation. *Journal of Controlled Release* **2008** 131(3) 205-210.
- (214) Unger E.C., McCreery T.P., Sweitzer R.H., Caldwell V.E., & Wu Y.Q. Acoustically active lipospheres containing paclitaxel - A new therapeutic ultrasound contrast agent. *Investigative radiology* **1998** 33(12) 886-892.
- (215) Shortencarier M.J., Dayton P.A., Bloch S.H., Schumann P.A., Matsunaga T.O., & Ferrara K.W. A method for radiation-force localized drug delivery using gas-filled lipospheres. *Ieee Transactions on Ultrasonics Ferroelectrics and Frequency Control* **2004** 51(7) 822-831.
- (216) Kooiman K., böhmer M, Emmer M. *et al.* oil-filled polymer microcapsules for ultrasound-mediated delivery of lipophilic drugs. *Journal of Controlled Release* **2009** 133(2) 109-118.
- (217) Tiukinhoy-Laing S., Huang S.L., Parikh D.S. *et al.* Ultrasound-facilitated clot lysis using tPA-loaded echogenic liposomes. *Circulation* **2005** 112(17) U696.
- (218) Tiukinhoy-Laing S.D., Huang S.L., Klegerman M., Holland C.K., & McPherson D.D. Ultrasound-facilitated thrombolysis using tissue-plasminogen activator-loaded echogenic liposomes. *Thrombosis Research* **2007** 119(6) 777-784.
- (219) Tiukinhoy S.D., Khan A.A., Huang S.L., Klegerman M.E., MacDonald R.C., & McPherson D.D. Novel echogenic drug-immunoliposomes for drug delivery. *Investigative radiology* **2004** 39(2) 104-110.
- (220) Huang S.L. & MacDonald R.C. Acoustically active liposomes for drug encapsulation and ultrasound-triggered release. *Biochimica et Biophysica Acta-Biomembranes* **2004** 1665(1-2) 134-141.
- (221) Huang S.L. Liposomes in ultrasonic drug and gene delivery. *Advanced Drug Delivery Reviews* **2008** 60(10) 1167-1176.
- (222) Seemann S., Hauff P., Schultze-Mosgau M., Lehmann C., & Reszka R. Pharmaceutical evaluation of gas-filled microparticles as gene delivery system. *Pharmaceutical Research* **2002** 19(3) 250-257.
- (223) Teupe C., Richter S., Fisslthaler B. *et al.* Vascular gene transfer of phosphomimetic endothelial nitric oxide synthase (S1177D) using ultrasound-enhanced destruction of plasmid-loaded microbubbles improves vasoreactivity. *Circulation* **2002** 105(9) 1104-1109.
- (224) Teupe C., Richter S., Fisslthaler B. *et al.* Efficient endothelial gene transfer with preserved vascular integrity by ultrasound-enhanced destruction of plasmid-loaded albumin microbubbles. *European heart journal* **2002** 23 381.

- (225) Zhao Y.Z., Liang H.D., Mei X.G., & Halliwell M. Preparation, characterization and in vivo observation of phospholipid-based gas-filled microbubbles containing hirudin. *Ultrasound in Medicine and Biology* **2005** 31(9) 1237-1243.
- (226) Borden M.A., Martinez G.V., Ricker J. *et al.* Lateral phase separation in lipid-coated microbubbles. *Langmuir* **2006** 22(9) 4291-4297.
- (227) Howard C.M., Forsberg F., Minimo C., Liu J.B., Merton D.A., & Claudio P.P. Ultrasound guided site specific gene delivery system using adenoviral vectors and commercial ultrasound contrast agents. *Journal of Cellular Physiology* **2006** 209(2) 413-421.
- (228) Gao Z., Kennedy A.M., Christensen D.A., & Rapoport N.Y. Drug-loaded nano/microbubbles for combining ultrasonography and targeted chemotherapy. *Ultrasonics* **2008** 48(4) 260-270.
- (229) Rapoport N., Gao Z.G., & Kennedy A. Multifunctional nanoparticles for combining ultrasonic tumor imaging and targeted chemotherapy. *Journal of the National Cancer Institute* **2007** 99(14) 1095-1106.
- (230) Christiansen J.P., French B.A., Klivanov A.L., Kaul S., & Lindner J.R. Targeted tissue transfection with ultrasound destruction of plasmid-bearing cationic microbubbles. *Ultrasound in Medicine and Biology* **2003** 29(12) 1759-1767.
- (231) Vannan M., McCreery T., Li P. *et al.* Ultrasound-mediated transfection of canine myocardium by intravenous administration of cationic microbubble-linked plasmid DNA. *Journal of the American Society of Echocardiography* **2002** 15(3) 214-218.
- (232) Taylor S.L., Rahim A.A., Bush N.L., Barnber J.C., & Porter C.D. Targeted retroviral gene delivery using ultrasound. *Journal of Gene Medicine* **2007** 9(2) 77-87.
- (233) Muller O.J., Schinkel S., Kleinschmidt J.A., Katus H.A., & Bekeredjian R. Augmentation of AAV-mediated cardiac gene transfer after systemic administration in adult rats. *Gene Ther.* **2008** 15(23) 1558-1565.
- (234) Lum A.F.H., Borden M.A., Dayton P.A., Kruse D.E., Simon S.I., & Ferrara K.W. Ultrasound radiation force enables targeted deposition of model drug carriers loaded on microbubbles. *Journal of Controlled Release* **2006** 111(1-2) 128-134.
- (235) Kheiriloom A., Dayton P.A., Lum A.F.H. *et al.* Acoustically-active microbubbles conjugated to liposomes: Characterization of a proposed drug delivery vehicle. *Journal of Controlled Release* **2007** 118(3) 275-284.

Chapter 2

Polymer-coated albumin microbubbles that bind and protect plasmid DNA

This chapter is published.

Lentacker I.¹, De Geest B.G.¹, Vandenbroucke R.E.¹, Peeters L.¹, Demeester J.¹, De Smedt S.C.¹, Sanders N.N.¹
Langmuir **2006** 22(17) 7273-7278.

¹ Laboratory of General Biochemistry and Physical Pharmacy, Department of Pharmaceutics, Ghent University, Ghent, Belgium.

ABSTRACT

Ultrasound in combination with microbubbles has recently been considered by gene delivery scientists to be an interesting approach to enhance gene transfer into cells. Its low toxicity and simplicity to apply *in vivo* without major complications make this technology (sonoporation) especially attractive. Sonoporation of DNA has been evaluated *in vivo* by the injection of free plasmid DNA (pDNA) together with microbubbles (as used in diagnostic imaging) in the bloodstream. However, the *in vivo* gene-transfer efficiency in these experiments remained rather low. Both the enzymatic degradation of the injected pDNA as well as the low pDNA concentration in the neighborhood of sonoporated cell membranes may explain this low efficiency. Therefore, we developed polymer-coated microbubbles that can bind and protect the pDNA. Coating albumin-shelled microbubbles with poly(allylamine hydrochloride) (PAH) makes the surface charge of the microbubbles positive without drastically affecting the size distribution of the microbubbles, thereby not affecting the ultrasound responsiveness and injectability. The cationic coating allowed both to bind up to 0.1 pg of DNA per microbubble as well as to protect the bound DNA against nucleases. Finally, the PAH coating significantly increased the lifetime of the microbubbles (half-life \pm 7 h), making them more convenient for *in vivo* applications because more microbubbles are expected to reach the target organ. Binding and nuclease protection of DNA by polymer-coated diagnostic microbubbles has, to our knowledge, never been demonstrated. We conclude that these LbL-coated microbubbles might be significant in the further development of ultrasound-mediated gene delivery.

Chapter 2

Polymer-coated albumin microbubbles that bind and protect plasmid DNA

INTRODUCTION

Gene therapy was put forward in the late 1980s as the most promising therapy for genetic diseases. However, gene therapy is currently caught in a bottleneck because of the lack of efficient and safe gene carriers. DNA molecules are large, negatively charged molecules and have major difficulties in entering the cell or cell nucleus. On top, DNA becomes rapidly degraded by extra- and intracellular nucleases¹. Therefore, suitable DNA delivery systems are under development. The first system makes use of replication-deficient viruses that accommodate the therapeutic DNA in their genome¹. These viral gene carriers transfect very efficiently because they have an ingenious system for the nuclear delivery of exogenous DNA. However, viral gene carriers have some important disadvantages: they often provoke an immune response and severe inflammation reactions². Additionally, the risk for insertional mutagenesis and the size limitation of the DNA that they can accommodate are other drawbacks of viral gene carriers¹. Therefore, nonviral transfection systems based on cationic lipids or cationic polymers have gained more and more attention.¹ Although non-viral carriers may be safer and cheaper, they have, especially *in vivo*, a much lower transfection efficiency than viral gene carriers.

As outlined above, the *in vivo* application of viral and non-viral DNA delivery systems is currently hampered by safety concerns and low efficiency, respectively. To overcome the limitations of nonviral gene therapy, ultrasound energy, alone or in combination with gas-filled microbubbles, has recently been proposed to enhance the intracellular delivery of DNA, siRNA, and proteins³⁻¹¹. Because ultrasound energy in combination with gas-filled microbubbles has been used for several years in medical imaging, it can be considered to be very safe¹². The mechanism by which ultrasound mediates intracellular drug delivery has been ascribed as cavitation, which is the alternate growing and shrinking of gas-filled microbubbles as a result of the high- and low-pressure waves generated by

ultrasound energy. Finally, these “cavitating” (oscillating) microbubbles implode. The cavitation and especially the implosion of the microbubbles generate local shock waves and microjets that can temporarily perforate the cell membrane, allowing macromolecules to enter the cells^{8,13-16}. This ultrasound-assisted delivery of macromolecules, often called sonoporation, has been proved to be effective both *in vitro* and *in vivo*^{3-11,17}. However, a major limitation of the currently available microbubbles is that they have a short lifetime and neither bind nor protect the therapeutic DNA against nucleases. Binding of the DNA on the microbubbles will ensure that the DNA is present at the site of cell membrane poration, enhancing the chance that the DNA is dragged inside the cell or even inside the nucleus by the generated microjets.

The aim of this work is to develop ultrasound-responsive microbubbles that (a) can bind the DNA, (b) protect the DNA against nucleases, and (c) remain stable for several hours. Therefore, we coated, to our knowledge for the first time, perfluorocarbon gas-filled microbubbles with a cationic polymer via the layer-by-layer (LbL) technique¹⁸. We characterized the physical properties, ultrasound responsiveness, DNA binding, and DNA protection toward nucleases of this new type of microbubble.

MATERIALS & METHODS

Preparation of microbubbles and PAH-coated microbubbles

Microbubbles were prepared following the procedure developed by Porter *et al.*¹⁹ Briefly, one part of a 5% bovine serum albumin (Sigma Aldrich, St Louis, MO) solution in HEPES buffer (20 mM, pH 7.4) was mixed with two parts of a 5 % dextrose (Sigma Aldrich, St Louis, MO) solution in HEPES buffer. Subsequently, the mixture was drawn into a 30 mL syringe and blended with 10 mL of perfluorobutane (MW 238 g/mol, F2 chemicals, Preston, Lancashire, U.K.) through a three-way valve. After mixing by hand, the solution was sonicated with a 20 kHz probe (Branson 250 sonifier, Branson Ultrasonics Corp., Danbury, CT). Following sonication, the microbubbles were centrifuged at 118g for 1 min. The supernatants were discarded, and the microbubbles were washed three times with sterile HEPES buffer. Finally, the microbubbles were suspended in 5 mL of sterile HEPES buffer.

The PAH-coated microbubbles were prepared by the layer-by layer (LbL) coating of the microbubbles obtained above. Five milliliters of a microbubble dispersion was incubated with 5 mL of a poly(allylamine hydrochloride) (PAH, MW 70 000 g/mol, Sigma- Aldrich) solution (2 mg/mL, HEPES buffer). Subsequently, the PAH was removed by washing (three times) the microbubbles with sterile

HEPES buffer. Therefore, after each wash step the microbubbles were centrifuged at 118g for 1 min. Finally, the LbL-coated microbubbles were suspended in 5 mL of sterile HEPES buffer.

Characterization of the microbubbles

The concentration of the microbubble dispersions was determined immediately after their preparation with the aid of a Burkert chamber and a light microscope. The concentrations of the uncoated and coated microbubble dispersions were $9.57 \pm 0.65 \times 10^8$ and $1.99 \pm 0.10 \times 10^8$ microbubbles/mL, respectively. To visualize the microbubbles, they were brought into a μ -slide VI flow chamber (Ibidi Integrated BioDiagnostics, Munchen, Germany) and studied via light (Nikon TS100-F, Melville, NY) or confocal laser scanning microscopy (CLSM) using a 40x lens. The size distribution of the microbubbles was determined within 10 min after preparation by laser diffraction (Mastersizer S, Malvern, Worcestershire, U.K.). The zeta potential of the microbubbles was measured by particle electrophoresis (Zetasizer 2000, Malvern, Worcestershire, U.K.). All the experiments were performed on microbubbles dispersed in HEPES buffer (20 mM, pH 7.4).

Plasmid DNA preparation

The plasmid DNA (pDNA; pGL3, Promega, Leiden, The Netherlands) used in this study contained as a reporter gene luciferase from *Photinus pyralis* under the control of a simian virus 40 promoter. After amplification of the pDNA in *Escherichia coli*, the pDNA was extracted and purified from the bacterial cells using the Qiagen giga kit (Valencia, CA). The pDNA concentration was set at 1.0 mg/mL HEPES buffer assuming that the absorption at 260 nm of a 50 μ g/mL DNA solution equals 1. The pDNA showed a high purity because the ratio of the absorptions at 260 and 280 nm was between 1.8 and 2.0.

Fluorescent labeling of albumin, PAH and pDNA

Bovine serum albumin (BSA, Sigma-Aldrich) was labeled with fluoresceine isothiocyanate (FITC; Sigma-Aldrich) by vigorous mixing of 60 mL of FITC solution (0.2 mg/mL 0.1 M borate buffer at pH 8.5) with 60 mL of BSA (5 mg/mL 0.1 M borate buffer at pH 8.5). The labeling of PAH with rhodamine isothiocyanate (RITC) occurred in a similar way. Twelve milligrams of RITC and 300 mg of PAH were separately dissolved in 60 mL of borate buffer (0.1 M, pH 8.5) and subsequently mixed under vigorous stirring. After overnight incubation, the reaction mixtures were dialyzed (MW cutoff

of the membrane was 25 kDa) against pure water for several days. Finally, the dialyzed FITC-BSA and RITC-PAH were freeze dried, and the resulting fluffy solids were stored at 4 °C.

Intercalating dyes YOYO-1 and TOTO-3 were used to label the pDNA. Therefore, 111 µg of pDNA was mixed with 57 µL of a 1/100 diluted YOYO-1 or TOTO-3 solution (Molecular Probes, Eugene, OR) and diluted in TE buffer (10 mM tris-HCl; 1 mM EDTA; pH 7.4) until a final pDNA concentration of 1 mg/mL was obtained. The dye/base pair ratio was 1:30 for both the YOYO-1 and TOTO-3 labeled pDNA. For the FCS measurements, the pDNA was labeled with cy-5, using the Mirus labeling kit (Mirus Bio Corporation, Madison, WI). The dye/base pair ratio was 1:2.

Confocal laser scanning microscopy

The microbubbles, put in µ-slide VI-flow chambers, were visualized by a confocal laser scanning microscope (CLSM, BioRad MRC1024, Hemel Hempstadt, U.K.) equipped with a krypton-argon laser and a dichroic mirror that reflects the laser light in a 40x objective. The 488 nm line of this laser was used to excite YOYO-1 and FITC, and the 568 nm line was used to excite RITC. To ensure a proper spectral separation, appropriate emission filters were used before the green and red detector.

Electron microscopy

Five microliters of a coated microbubble dispersion was applied on a silicon wafer and air dried. The remains of the microbubbles were then examined with a scanning electron microscope (Quanta 200 FEG, FEI Company, Hillsboro, Oregon).

Picogreen assay and fluorescence fluctuation spectroscopy

To determine the maximal pDNA loading capacity of the microbubbles, we mixed 150 µL of the uncoated or coated microbubble dispersions with increasing amounts of pDNA. After 10 min of incubation, the microbubbles (with pDNA) were centrifuged at 118g, and the concentration of unbound pDNA in the supernatants was determined using PicoGreen (Invitrogen, Merelbeke, Belgium) and fluorescence correlation spectroscopy (FCS).

For the PicoGreen assay, 50 µL of the supernatants was incubated with 1 mL of diluted (200-fold in TE buffer) PicoGreen reagent for 5 min, and subsequently the fluorescence was determined ($\lambda_{\text{excitation}} = 480 \text{ nm}$ and $\lambda_{\text{emission}} = 520 \text{ nm}$).

We also determined the maximal pDNA loading capacity in another way, making use of fluorescence fluctuation spectroscopy (FFS) to measure the fluorescence of the unbound pDNA in the subnanoliters. FFS monitors the fluorescence fluctuations in the excitation volume of the microscope. The fluorescence signal is fluctuating because of the diffusion of fluorescent molecules in and out of the excitation volume. From the fluorescence fluctuations, an autocorrelation curve can be derived that allows one to calculate both the diffusion coefficient of the fluorescent molecules as well as the number of fluorescent molecules in the excitation volume²⁰. Details of the FFS setup used are explained in our earlier reports²¹. For these experiments, Cy5-labeled pDNA was used, and samples were excited with 6% laser intensity (647 nm). First, a diluted solution of Cy5-pDNA was measured. Afterwards, 50 μL of a coated bubble suspension was incubated with 2 μg of pDNA. After 5 min of incubation, the sample was diluted to the same Cy5-pDNA concentration, and the amount of free pDNA was determined via FCS.

Ultrasound responsiveness of the microbubbles

The ultrasound responsiveness of pDNA-loaded, PAH-coated microbubbles was determined by comparing their (number) concentration before and after exposure to ultrasound. pDNA-loaded microbubbles were prepared by mixing 100 μL of a PAH-coated microbubble dispersion with 2 μg of pDNA. After 10 min of incubation, the concentration of the pDNA-loaded microbubbles was determined in a Burkert chamber. Subsequently, the pDNA loaded microbubbles were sonicated (1 MHz, 1 W/cm²; 50% duty cycle) for 30 s using a Sonitron 2000 (RichMar, Inola, Oklahoma) and again counted in a Burkert chamber.

Gel electrophoresis to evaluate the stability of microbubble-bound pDNA to rhDNase I

To determine whether the microbubbles were able to protect the pDNA against rhDNase I (Pulmozyme, Roche, Belgium), gel electrophoresis experiments were performed. Two micrograms of pDNA were mixed with 50 μL of a PAH-coated microbubble dispersion. After 5 min of incubation, the pDNA/microbubble mixtures were diluted in HEPES buffer supplied with 110 mM potassium acetate and 2 mM magnesium acetate (pH 7.4), which is necessary to activate the rhDNase I. Subsequently, rhDNase I was incubated with the pDNA/microbubbles mixtures for 15 min at room temperature. The rhDNase I activity in the microbubble dispersions was 200 U/L. Microbubble dispersions “incubated with inhibited rhDNase I” received 8 μL of Na₂EDTA (50 mM) before the addition of the rhDNase I to the pDNA/ microbubble mixtures. Na₂EDTA inhibits rhDNase I by complexing the

divalent cations, which are required for activating rhDNase I. Other samples were supplemented with Na₂EDTA after incubation with rhDNase I.

After the incubation period with rhDNase I, the pDNA was released from the microbubbles to investigate whether it survived the exposure to rhDNase I. Therefore, NaCl was added to the pDNA/microbubbles dispersions at a final concentration of 5M. Subsequently, the pDNA/microbubbles dispersions were centrifuged for 1 min at 118g. Fifty microliters of the supernatants was mixed with 10 μ L of a 30% glycerol solution and loaded onto a 1.5% agarose gel prepared in TBE (10.8 g/L tris base, 5.5 g/L boric acid, and 0.58 g/L EDTA). The samples were subjected to electrophoresis at 100 V for 60-90 min, and the pDNA was visualized by ethidium bromide (0.5 μ g/mL) staining prior to UV photography.

RESULTS & DISCUSSION

Preparation and characterization of uncoated and PAH-coated microbubbles

After the preparation of perfluorocarbon microbubbles stabilized with (FITC-labeled) albumin, CLSM experiments revealed the existence of micrometer-sized spherical structures covered with green-labeled albumin (Figure 1) that floated atop the liquid. Because the size of the microbubbles determines their ability to serve as cavitation nuclei, we subsequently studied the size distribution of freshly made microbubbles by laser diffraction²². Most of the albumin-stabilized microbubbles (about 90%) were between 1 and 5 μ m diameter (Figure 2), which is a size known to favor cavitation upon exposure to clinically used ultrasound frequencies (such as 1 MHz)²².

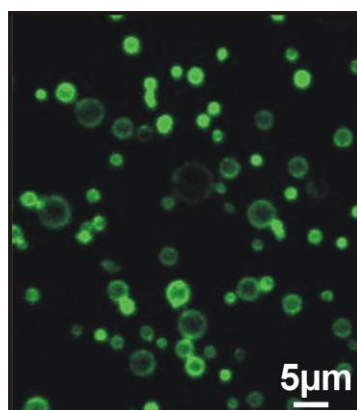


Figure 1 Confocal fluorescence microscopy image of perfluorocarbon microbubbles stabilized with FITC-labeled albumin. Depending on the position of the confocal plane in the microbubbles, we observed fluorescent rings (confocal plane in the middle of the microbubbles) or filled circles (confocal plane at the top or bottom of the microbubbles).

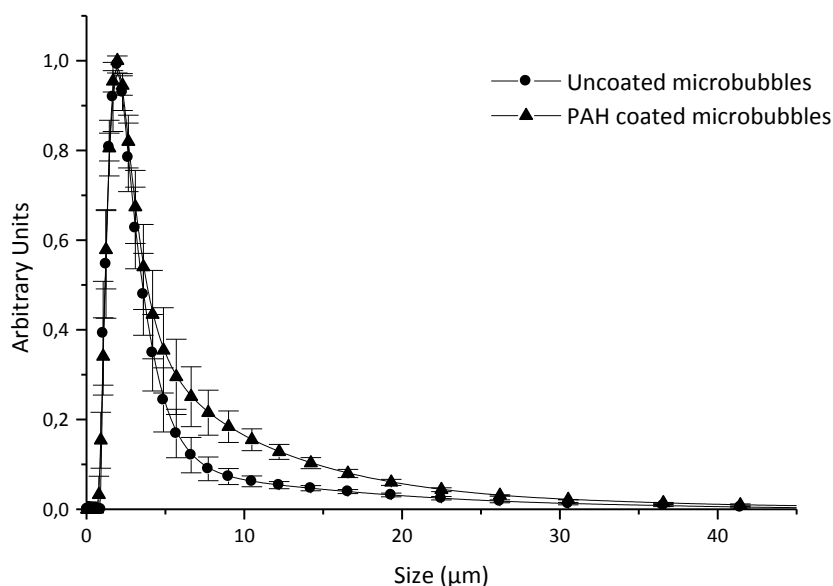


Figure 2 Size distribution of uncoated and PAH-coated albumin/ perfluorocarbon microbubbles as measured by laser diffraction. The y axis shows to what extent a certain class of microbubbles is present, normalized to the most abundant fraction of microbubbles ($y = 1$) (number fraction). Data are the means of three independent measurements.

The albumin chains, which cover the gaseous cores, stabilize the microbubbles because they reduce the diffusion of the perfluorocarbon gas out of the microbubbles in the surrounding water. The shell-forming properties of albumin most likely originate from its amphiphilic nature. The presence of negative charges at the surface of the albumin-stabilized microbubbles was indeed confirmed from zeta potential (ζ) measurements: the average ζ equalled -45 mV (Figure 3).

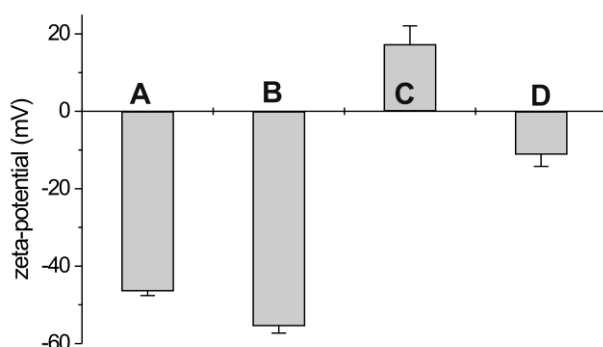


Figure 3 Zeta potential of uncoated microbubbles (A), uncoated microbubbles (50 μ L) incubated with 1 μ g of pDNA (B), PAH coated microbubbles (C), and PAH-coated bubbles (50 μ L) incubated with 1 μ g of pDNA (D). The data are the means of three independent measurements.

One can expect that the negative charges at the microbubbles' surface would enable them to be coated with cationic polymers. Therefore, we tried to apply a positively charged layer around the albumin shell using PAH, a polycation that is widely used in the LbL coating of planar substrates and colloidal templates²³⁻²⁵. Figure 4 shows CLSM images of microbubbles prepared with (non fluorescently labeled) albumin and coated with RITC-labeled PAH. Clearly, the PAH chains cover the outer surface of the microbubbles and are not incorporated into the perfluorocarbon gas core. Also, after the PAH coating, the zeta potential of the microbubbles became positive (15 mV; Figure 3), which further confirms the presence of PAH at the surface of the microbubbles. Apart from a slightly elevated fraction in the 5-20 μm range, which is probably due to the aggregation of smaller microbubbles after coating, the PAH coating changed the size distribution of the microbubbles only moderately (Figure 2). In the remainder of this article, we use the terms “uncoated: and “PAH-coated” microbubbles to refer to albumin/perfluorocarbon microbubbles without and with a PAH coating, respectively.

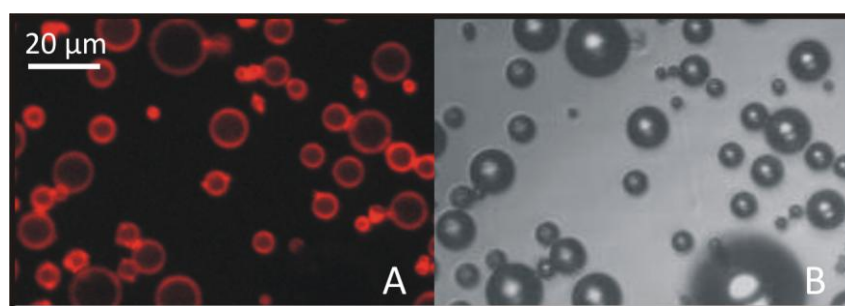


Figure 4 Confocal fluorescence microscopy image (A) and transmission image (B) of PAH-coated microbubbles made with unlabeled albumin and RITC-labeled PAH.

Stability of uncoated and PAH-coated microbubbles

It is well known that the lifetime of *air*-filled albumin-stabilized microbubbles is very short because the air diffuses rapidly out of the microbubbles²⁶. The use of perfluorocarbon gas, which has a lower water solubility than air, effectively delays gas diffusion²⁷. Nevertheless, their lifetime remains very short. Coating microbubbles with PAH should offer a solution to this problem because polyelectrolyte multilayers have been reported to prevent or drastically decrease gas diffusion²⁸. Therefore, we evaluated the stability of the microbubbles at room temperature by following the concentration of the microbubbles as a function of time. Figure 5A shows the percentage of remaining uncoated and PAH-coated microbubbles as a function of time. Uncoated microbubbles

seem to destabilize very rapidly: after 75 min, 50% of the uncoated microbubbles have already disappeared. In contrast, PAH-coated microbubbles clearly existed for much longer times: half of the PAH-coated microbubbles had disappeared after 6 h.

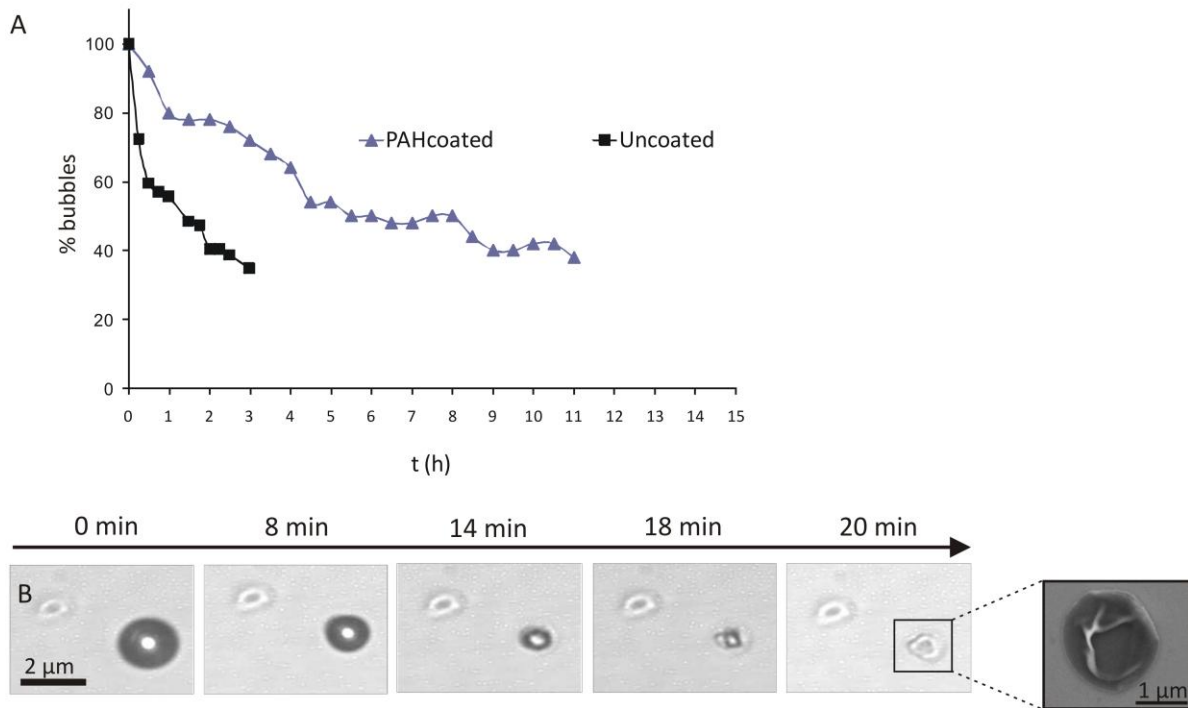


Figure 5 (A) Stability of uncoated and PAH-coated microbubbles. The concentration of the microbubbles was measured as a function of time and normalized to the concentration just after preparation. The dispersions were placed at room temperature under continuous stirring at 750 rpm, and the concentration of microbubbles was determined microscopically using a Burkert chamber. (B) Light microscopy images of a destabilizing PAH-coated microbubble. The inset is a SEM image of the remaining polymer coating. Gradual shrinking was also observed on uncoated microbubbles, although it occurred faster.

DNA binding properties of the microbubbles

The pDNA binding properties of the microbubbles were first evaluated by CSLM. To enable the visualization of the binding of pDNA to the microbubbles, YOYO-1-labeled pDNA (green) and RITC labeled PAH (red) were used. Uncoated and PAH-coated albumin microbubbles were incubated with pDNA for 2 min, transferred to a μ -slide VI flow chamber, and studied via CLSM. Figure 6 shows the results. Clearly, the green-labeled pDNA does not bind to the uncoated albumin microbubbles but remains in solution (Figure 6A). However, the green-labeled pDNA does bind to the RITC-PAH-coated microbubbles (Figure 6B) because yellow rings are present around the microbubbles, indicating the

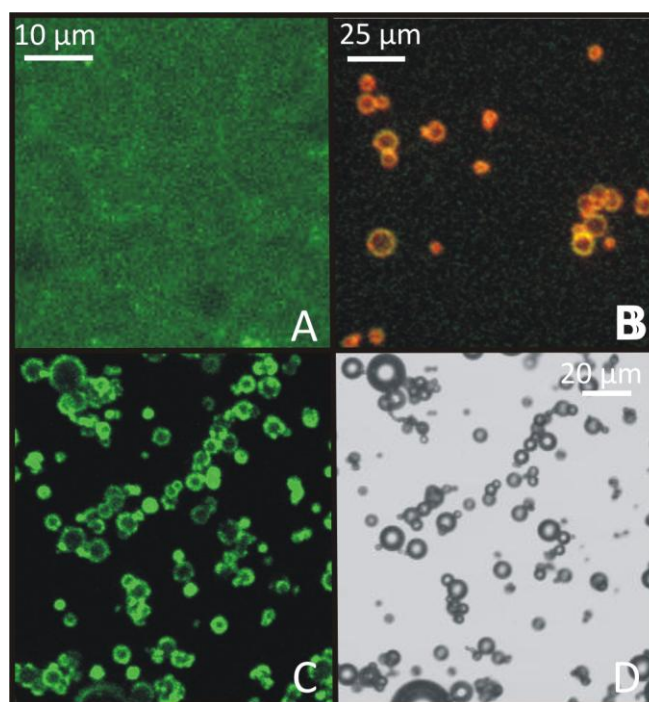


Figure 6 (A) Confocal fluorescence images of uncoated microbubbles (50 μ L) incubated with 1 μ g of YOYO-1-labeled DNA, (B) RITC-labeled PAH-coated microbubbles (50 μ L) incubated with 2.6 μ g of YOYO-1-labeled pDNA, and (C) unlabeled AH-coated microbubbles (50 μ L) incubated with 1 μ g of YOYO-1-labeled pDNA. (D) Transmission image corresponding to image C.

co-localization of pDNA and PAH. Between the microbubbles in Figure 6B, some green fluorescence (i.e., unbound pDNA) is still detected. This could be expected because the maximal pDNA loading capacity of the microbubbles was exceeded (see below). When the microbubbles (in this experiment, unlabeled) were incubated with lower amounts of YOYO-1-labeled pDNA, green fluorescence between the microbubbles was no longer observed (Figure 6C). Successful loading of the PAH-coated microbubbles with pDNA could also be observed from zeta potential measurements because the addition of pDNA turned the zeta potential of the PAH-coated microbubbles negative (Figure 3). This most likely indicates that pDNA is bound to the surface of the PAH-coated microbubbles. In contrast, the addition of pDNA to the uncoated albumin microbubbles did not drastically alter the zeta potential of the uncoated microbubbles (Figure 3), which is in line with the observations above. Previously, Porter *et al.* reported that oligonucleotides do bind to albumin microbubbles¹⁹. However, these authors used phosphorothioate-modified oligonucleotides, which are known to interact nonspecifically with proteins²⁹. To estimate the maximal pDNA binding capacity of the PAH-coated microbubbles, they were incubated (for 5 min) with increasing amounts of pDNA, and the amount of unbound (i.e., free) pDNA in the supernatants (obtained after centrifugation) was determined via both

the PicoGreen assay and FCS. Both tests revealed that 50 μL of the PAH-coated microbubble dispersion could maximally bind 1 μg of pDNA (data not shown). Taking into account that 50 μL of microbubble dispersion contains about 9.95×10^6 microbubbles, one can estimate that the PAH coating of the microbubbles enables them to carry 0.1 μg of pDNA or about 20 000 pDNA molecules per microbubble. These experiments prove that coating the microbubbles with PAH enables a very efficient loading of albumin microbubbles with plasmid DNA. As mentioned above, pDNA-loaded microbubbles have also been developed by other groups. Christiansen et al. and Vannan et al. prepared cationic microbubbles using lipids as a shell-forming material^{11,13}. Compared to PAH-coated microbubbles, these microbubbles have a 2.5-fold lower pDNA loading capacity. However, we should take into account that in their studies the average microbubble size was smaller, which automatically implies a lower DNA loading. Also, cationic lipid based microbubbles are probably more expensive. Frenkel et al. showed that the sonication of a solution of dextrose, albumin, and pDNA with perfluoropropane gas leads to microbubbles that contain albumin and pDNA in their shell^{11,30}. However, a major drawback of this technique is that only a small fraction of the pDNA seems to become incorporated into the shell.

Ultrasound responsiveness and DNase protection

Microbubbles enhance the efficiency of ultrasound-assisted gene delivery as they generate microjets that, upon implosion, temporarily perforate the cell membranes^{8,13-16}. Given the importance of cavitation, the ultrasound responsiveness of the uncoated and pDNA-loaded PAH-coated microbubbles was studied by exposing them for 30 s to ultrasound energy (1 MHz, 1 W/cm², 50% duty cycle). After ultrasound radiation, 99% and 95% of the uncoated and PAH-coated microbubbles, respectively, were destroyed, which is in agreement with previous reports^{19,31}. Despite their higher stability (Figure 5), PAH-coated microbubbles are thus clearly ultrasound-responsive. Subsequently, the ability of the microbubbles to protect pDNA against nucleases was tested using gel electrophoresis. As described in the Materials and Methods section, the microbubble dispersions were exposed to 200 U/L rhDNase-I, which is about 20-fold higher than the DNase activity found in human blood³². Figure 7 shows the gel electrophoresis results on pDNA released from pDNA-loaded microbubbles (by NaCl) that were exposed to DNase-I. As shown in Figure 7A, DNase-I degrades both free pDNA (lane 3) and pDNA in the presence of uncoated microbubbles (lane 6). In contrast, the pDNA on PAH-coated microbubbles remains mainly protected (Figure 7B) because only a very small part of degraded pDNA seems to be present (arrow in lane 6). The latter can be explained by the fact that in this experiment a small amount of the pDNA remained in the solution as the maximal loading capacity of the microbubbles was exceeded. Clearly, in Figure 7B (lanes 5-7) a part of the pDNA

remained in the slots of the agarose gel. Most presumably, this is attributed to the fact that, besides free pDNA, (high molecular weight) pDNA-PAH complexes were also liberated from the microbubbles upon adding NaCl. This implies that the electrostatic binding between DNA and PAH is stronger than the interaction between the albumin and PAH. Thus, a second advantage of the PAH-coated microbubbles compared to the microbubbles of Frenkel's group is that they also protect DNA against DNase-I degradation. From Figure 7B (lanes 2 and 5), we can also conclude that no conformational change of the pDNA occurred upon binding to the microbubbles. Indeed, the released DNA (lane 5) is visible at the same height on the gel as the free pDNA (lane 2).

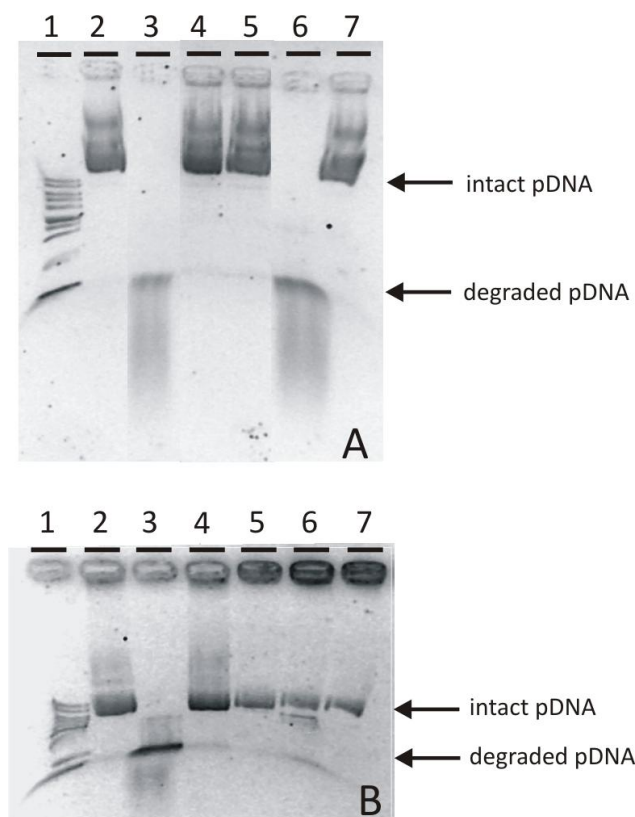


Figure 7 Gel electrophoresis of pDNA present in an uncoated and PAH-coated microbubble dispersion with or without DNase-I, respectively. The data obtained with uncoated microbubbles are shown by gel A, and those with PAH-coated microbubbles, by gel B. Each lane contains 1 μ g of pDNA. Lane 1, DNA molecular weight marker; lane 2, free pDNA; lane 3, free pDNA incubated with DNase-I; lane 4, free pDNA incubated with inhibited DNase-I; lane 5, microbubbles and pDNA; lane 6, microbubbles and pDNA incubated with DNase-I; lane 7, microbubbles and pDNA incubated with inhibited DNase-I. Smiling appeared because of the high salt concentrations used (5 M NaCl).

Conclusions

A major issue in ultrasound-assisted gene transfer is the development of microbubbles that both bind and protect pDNA against circulating DNases in the bloodstream. It is well known that binding pDNA with cationic polymers or lipids protects the pDNA against degradation by DNase I.¹ Therefore, we evaluated the possibility of coating the medically used albumin/perfluorocarbon contrast agents with a cationic polymer. A successful coating of the albumin-shelled perfluorocarbon microbubbles with PAH was evidenced from CLSM and zeta potential measurements. The positive charges on the surface of the PAH coated microbubbles allowed the binding of up to 0.1 pg of pDNA on the wall of a single microbubble. The pDNA bound on PAH-coated microbubbles was clearly protected against nucleases. The presence of pDNA on the microbubble may also enhance the number of pDNA molecules that can enter a cell during sonoporation. Indeed, small pores (up to 100 nm large) created by imploding microbubbles have a very short lifetime (millisecond range).¹⁶ To increase the number of pDNA molecules that pass through these quickly closing pores, it seems clear that it is important to co-localize DNA and pore-forming microbubbles. Furthermore, PAH coating of the microbubbles improved their stability, thereby increasing their (average) lifetime from 75 min to 6 h while they remained ultrasound-responsive. Their longer lifetime makes them more convenient for in vivo therapy because more microbubbles are expected to reach the target organ. In this study, we used PAH as a cationic polymer to coat the microbubbles. This polymer is not suitable for in vivo applications because, as a result of its high molecular weight and nonbiodegradability, it will not be efficiently cleared from the human body. However, it is obvious that other cationic polymers that are more biocompatible and biodegradable may also be used as coating material. Also, coating microbubbles with cationic polymers may be an attractive strategy to promote the targeting of microbubbles because it is rather straightforward to attach targeting ligands to the polymer coating. This could further enhance the site-specific delivery of pDNA and could provide an even higher pDNA concentration close to cell membrane perforations³³. However, to obtain good gene transfer it is also important that the pDNA dissociates from the microbubble upon ultrasound exposure. In our future work, we will tackle this issue and perform transfection experiments with our microbubbles.

Acknowledgments

Ine Lentacker is a doctoral fellow of FWO-Flanders. Niek N. Sanders is a postdoctoral fellow of FWO (Fund for Scientific Research-Flanders). The financial support of this institute is

acknowledged with gratitude. We thank Professor Vervaeet and Evy Corbany for the use of the laser diffractor. We thank Olivier Janssens and Philippe Smet for taking the SEM images.

References

- (1) Patil S.D., Rhodes D.G., & Burgess D.J. DNA-based therapeutics and DNA delivery systems: a comprehensive review. *AAPS. Journal* **2005** 7(1) E61-E77.
- (2) Marshall E. Gene Therapy Death Prompts Review of Adenovirus Vector. *Science* **1999** 286, 2244-2245 .
- (3) Bekeredjian R., Chen S.Y., Grayburn P.A., & Shohet R.V. Augmentation of cardiac protein delivery using ultrasound targeted microbubble destruction. *Ultrasound in Medicine and Biology* **2005** 31(5) 687-691.
- (4) Duvshani-Eshet M. & Machluf M. Therapeutic ultrasound optimization for gene delivery: A key factor achieving nuclear DNA localization. *Journal of Controlled Release* **2005** 108(2-3) 513-528.
- (5) Kinoshita M. & Hynynen K. Intracellular delivery of Bak BH3 peptide by microbubble-enhanced ultrasound. *Pharmaceutical Research* **2005** 22(5) 716-720.
- (6) Kinoshita M. & Hynynen K. Intracellular delivery of Bak BH3 peptide by microbubble-enhanced ultrasound. *Pharmaceutical Research* **2005** 22(5) 716-720.
- (7) Manome Y., Nakayama N., Nakayama K., & Furuhashi H. Insonation facilitates plasmid DNA transfection into the central nervous system and microbubbles enhance the effect. *Ultrasound in Medicine and Biology* **2005** 31(5) 693-702.
- (8) Mehier-Humbert S., Bettinger T., Yan F., & Guy R.H. Plasma membrane poration induced by ultrasound exposure: Implication for drug delivery. *Journal of Controlled Release* **2005** 104(1) 213-222.
- (9) Newman C.M., Lawrie A., Brisken A.F., & Cumberland D.C. Ultrasound gene therapy: On the road from concept to reality. *Echocardiography-A Journal of Cardiovascular Ultrasound and Allied Techniques* **2001** 18(4) 339-347.
- (10) Pislaru S.V., Pislaru C., Kinnick R.R. *et al.* Optimization of ultrasound-mediated gene transfer: comparison of contrast agents and ultrasound modalities. *European Heart Journal* **2003** 24(18) 1690-1698.
- (11) Vannan M., McCreery T., Li P. *et al.* Ultrasound-mediated transfection of canine myocardium by intravenous administration of cationic microbubble-linked plasmid DNA. *Journal of the American Society of Echocardiography* **2002** 15(3) 214-218.
- (12) Grayburn P.A. Current and future contrast agents. *Echocardiography-A Journal of Cardiovascular Ultrasound and Allied Techniques* **2002** 19(3) 259-265.

- (13) Christiansen J.P., French B.A., Klibanov A.L., Kaul S., & Lindner J.R. Targeted tissue transfection with ultrasound destruction of plasmid-bearing cationic microbubbles. *Ultrasound in Medicine and Biology* **2003** 29(12) 1759-1767.
- (14) Marmottant P. & Hilgenfeldt S. Controlled vesicle deformation and lysis by single oscillating bubbles. *Nature* **2003** 423(6936) 153-156.
- (15) Tachibana K., Uchida T., Ogawa K., Yamashita N., & Tamura K. Induction of cell-membrane porosity by ultrasound. *Lancet* **1999** 353(9162) 1409.
- (16) Van Wamel A., Bouakaz A., Versluis M., & De Jong N. Micromanipulation of endothelial cells: Ultrasound-microbubble-cell interaction. *Ultrasound in Medicine and Biology* **2004** 30(9) 1255-1258.
- (17) Chen S.Y., Shohet R.V., Bekeredjian R., Frenkel P., & Grayburn P.A. Optimization of ultrasound parameters for cardiac gene delivery of adenoviral or plasmid deoxyribonucleic acid by ultrasound-targeted microbubble destruction. *Journal of the American College of Cardiology* **2003** 42(2) 301-308.
- (18) Decher G. Fuzzy nanoassemblies: Toward layered polymeric multicomposites. *Science* **1997** 277(5330) 1232-1237.
- (19) Porter T.R., Iversen P.L., Li S., & Xie F. Interaction of diagnostic ultrasound with synthetic oligonucleotide-labeled perfluorocarbon-exposed sonicated dextrose albumin microbubbles. *J Ultrasound Med.* **1996** 15(8) 577-584.
- (20) Schwille P. & Haustein E. Fluorescence Correlation Spectroscopy: An introduction to its concepts and applications. *Biophysics Textbook online* **2006**
- (21) Lucas B., Van Rompaey E., De Smedt S.C., Demeester J., & Van Oostveldt P. Dual-color fluorescence fluctuation spectroscopy to study the complexation between poly-l-lysine and oligonucleotides. *Macromolecules* **2002** 35(21) 8152-8160.
- (22) Unger E.C., Porter T., Culp W., Labell R., Matsunaga T., & Zutshi R. Therapeutic applications of lipid-coated microbubbles. *Advanced Drug Delivery Reviews* **2004** 56(9) 1291-1314.
- (23) De Geest B.G., Dejugnat C., Sukhorukov G.B., Braeckmans K., De Smedt S.C., & Demeester J. Self-Rupturing Microcapsules. **2005** 17 2357-2361 .
- (24) Park M.K., Deng S.X., & Advincula R.C. Sustained release control via photo-cross-linking of polyelectrolyte layer-by-layer hollow capsules. *Langmuir* **2005** 21(12) 5272-5277.
- (25) Zahr A.S., de Villiers M., & Pishko M.V. Encapsulation of drug nanoparticles in self-assembled macromolecular nanoshells. *Langmuir* **2005** 21(1) 403-410.
- (26) Kabalnov A., Bradley J., Flaim S. *et al.* Dissolution of multicomponent microbubbles in the bloodstream: 2. Experiment. *Ultrasound Med. Biol.* **1998** 24(5) 751-760.
- (27) Riess J.G. Fluorocarbon-based injectable gaseous microbubbles for diagnosis and therapy. *Current Opinion in Colloid & Interface Science* **2003** 8(3) 259-266.
- (28) Shchukin D.G., Kohler K., Mohvald H., & Sukhorukov G.B. Gas-filled polyelectrolyte capsules. *Angewandte Chemie-International Edition* **2005** 44(21) 3310-3314.

- (29) Stein C.A. & Cheng Y.C. Antisense Oligonucleotides As Therapeutic Agents - Is the Bullet Really Magical. *Science* **1993** 261(5124) 1004-1012.
- (30) Frenkel P.A., Chen S.Y., Thai T., Shohet R.V., & Grayburn P.A. DNA-loaded albumin microbubbles enhance ultrasound-mediated transfection in vitro. *Ultrasound in Medicine and Biology* **2002** 28(6) 817-822.
- (31) Mehier-Humbert S., Bettinger T., Yan F., & Guy R.H. Ultrasound-mediated gene delivery: Kinetics of plasmid internalization and gene expression. *Journal of Controlled Release* **2005** 104(1) 203-211.
- (32) Kawai Y., Yoshida M., Arakawa K. *et al.* Diagnostic use of serum deoxyribonuclease I activity as a novel early-phase marker in acute myocardial infarction. *Circulation* **2004** 109(20) 2398-2400.
- (33) Klibanov A.L. Ligand-carrying gas-filled microbubbles: Ultrasound contrast agents for targeted molecular imaging. *Bioconjugate Chemistry* **2005** 16(1) 9-17.

Chapter 3

Transfection properties of uncoated and polymer-coated albumin microbubbles

ABSTRACT

Microbubbles in combination with ultrasound are currently considered as a very promising new gene delivery method. The use of a pDNA loaded microbubbles offers several advantages as the pDNA is protected against degradation and is only locally released in the ultrasound treated areas. This can reduce the required pDNA dose and prevent the uptake of pDNA in unwanted areas. Albumin microbubbles can be coated with a cationic polymer, enabling electrostatic pDNA loading onto the microbubble shell. In this study, we evaluated the transfection efficiency of uncoated and polymer-coated albumin microbubbles on primary Vascular Smooth Muscle Cells (VSMC) and melanoma cells. We showed that it is important to pre-incubate uncoated albumin microbubbles with pDNA to obtain a good transfection efficiency. Despite their high pDNA loading, the polymer-coated microbubbles failed to transfect primary VSMC and melanoma cells. Confocal images showed that this is most likely due to the presence of large aggregates consisting of microbubble shell fragments and pDNA, which arise upon ultrasound induced implosion of the microbubbles. Additionally, gel electrophoresis experiments indeed showed that the pDNA remained attached to microbubble shell fragments after ultrasound exposure. It was also shown that the unprotected pDNA became subjective to mechanical degradation in the presence of albumin microbubbles and exposure to ultrasound intensities of $2\text{W}/\text{cm}^2$.

Chapter 3

Transfection properties of uncoated and polymer-coated albumin microbubbles

INTRODUCTION

Due to the fact that ultrasound is a cheap, non-invasive and locally applicable technique, it is a very attractive drug delivery strategy¹⁻³. Ultrasonic drug delivery often requires the presence of microbubbles, also called echo contrast agents⁴. These microbubbles are intravenously injected and subsequently start to cavitate and implode when they enter an ultrasound field. This can result in the formation of cell membrane pores, which leads to drug uptake in the insonated areas⁵. Additionally, extravasation can occur, thereby reaching areas further away from the blood vessels. Because only the targeted region will be treated with ultrasound, it is possible to obtain an ultrasound controlled local drug delivery. The preparation of a gene loaded microbubble is advantageous for several reasons. First, the enclosed gene will be protected against enzymatic degradation during circulation in the bloodstream. Second, the gene will only be released in ultrasound treated regions upon microbubble implosion. This can prevent the gene transfection of undesired tissues and will limit therapy costs, as the genetic drug dose can be significantly lowered. Moreover, a local release of the pDNA can assure that more pDNA is locally available for uptake through the created cell membrane pores.

We previously succeeded in preparing polymer-coated albumin microbubbles⁶. Therefore albumin microbubbles were incubated with the cationic polymer poly-(allylamine hydrochloride) (PAH) and washed several times to remove the unbound polymer. Subsequently, the cationic microbubbles were mixed with plasmid DNA (pDNA), that electrostatically bound to the microbubble shell. This novel microbubble has the advantage that more pDNA can be bound to the surface of the microbubbles and the increased microbubble stability. In a next step we wanted to compare the transfection efficiencies of uncoated albumin microbubbles and polymer coated microbubbles. Here, we evaluate their transfection efficiency on primary Vascular Smooth Muscle Cells (VSMC) and

melanoma cells. Additionally, the ultrasound induced release of pDNA from polymer-coated microbubbles was evaluated and visualized with confocal microscopy. We also studied the influence of different ultrasound parameters on the stability of naked pDNA in the presence of uncoated microbubbles.

MATERIALS & METHODS

Preparation of microbubbles and PAH-coated microbubbles

Microbubbles were prepared following the procedure developed by Porter *et al.*⁷ Briefly, one part of a 5% bovine serum albumin (Sigma Aldrich, St Louis, MO) solution in HEPES buffer (20 mM, pH 7.4) was mixed with two parts of a 5 % dextrose (Sigma Aldrich, St Louis, MO) solution in HEPES buffer. Subsequently, the mixture was drawn into a 30 mL syringe and blended with 10 mL of perfluorobutane (MW 238 g/mol, F2 chemicals, Preston, Lancashire, U.K.) through a three-way valve. After mixing by hand, the solution was sonicated with a 20 kHz probe (Branson 250 sonifier, Branson Ultrasonics Corp., Danbury, CT). Following sonication, the microbubbles were centrifuged at 118g for 1 min. The supernatants were discarded, and the microbubbles were washed three times with sterile HEPES buffer. Finally, the microbubbles were suspended in 5 mL of sterile HEPES buffer.

The PAH-coated microbubbles were prepared by layer-by-layer (LbL) coating of the abovementioned microbubbles. Five milliliters of a microbubble dispersion was incubated with 5 mL of a poly(allylamine hydrochloride) (PAH, MW 70 000 g/mol, Sigma- Aldrich) solution (2 mg/mL, HEPES buffer). Subsequently, the PAH was removed by washing (three times) the microbubbles with sterile HEPES buffer. Therefore, after each wash step the microbubbles were centrifuged at 118g for 1 min. Finally, the LbL-coated microbubbles were suspended in 5 mL of sterile HEPES buffer.

Plasmid DNA preparation

The plasmid DNA (pDNA; pGL3, Promega, Leiden, The Netherlands) used in this study contained as a reporter gene luciferase from *Photinus pyralis* under the control of a simian virus 40 promoter. After amplification of the pDNA in *Escherichia coli*, the pDNA was extracted and purified from the bacterial cells using the Qiagen giga kit (Valencia, CA). The pDNA concentration was set at 1.0 mg/mL HEPES buffer assuming that the absorption at 260 nm of a 50 µg/mL DNA solution equals 1. The pDNA showed a high purity because the ratio of the absorptions at 260 and 280 nm was between 1.8 and 2.0.

Cell culture and transfection experiments

The experiments performed on primary cells were done in the lab of Prof. Newman (Cardiovascular Division, Northern General Hospital, Sheffield University). Vascular smooth muscle cells (VSMCs) from the thoracic aorta of Yorkshire White cross pigs aged <6 months were cultured in DMEM containing 10% porcine serum. The transfections were performed for 3 hours at 37°C in 24-well plates with cells at 60% to 70% confluence and were stopped by dilution with 1 mL of fresh culture medium. Transfection was performed with 300 μ L transfection medium per well. This contained 10% microbubbles (either the Bracco microbubbles, albumin microbubbles or polymer coated microbubbles) and 0.75 μ g of pGL-3 diluted in Optimem (Gibco, Merelbeke, Belgium). Microbubbles and plasmid DNA were mixed according to the different protocols (Figure 1) and subsequently diluted in optimem. Secreted alkaline phosphatase (SEAP) expression plasmid (pMet7 h β SEAP) was used to presaturate the albumin microbubbles with DNA (5 μ g). Lipofection was done with Lipofectin. The transfection medium was prepared in a similar way for transfection experiments with naked pDNA, except that the microbubble solution was replaced by an equal volume of HEPES. Immediately after addition of the microbubbles to the well plates, ultrasound exposure (USE) was performed for 60 seconds with a custom-built, 10mm diameter, 1-MHz piezoelectric ceramic transducer within the transfection medium 2 mm above the cell monolayer and the 24-well plates suspended in a polystyrene water bath at 37°C to minimize acoustic reflections (<5%) and standing wave formation. The transducer was calibrated to produce continuous-wave 1-MHz ultrasound at a spatial average temporal average intensity of 0.4 W/cm². USE caused only minor acute damage to the cell monolayer.

BLM cells (melanoma cells)⁸ were cultured in Dulbecco's modified Eagle's medium (DMEM) with the growth factor F12 and phenol red containing 2 mM glutamine, 10% heat-deactivated fetal bovine serum (FBS), 1% penicillin–streptomycin (Gibco, Merelbeke, Belgium), and HEPES buffer (100 mM, pH7.4). The cells were grown to 90% confluency in Opticell units (Biocrystal, Westerville, OH, USA) inside a humidified incubator at 37 °C under 5% CO₂. Subsequently, the cells were washed with 10 mL of phosphate buffered saline (PBS, Gibco) and the transfection medium was added. The transfection was performed in the same way as described above. The pDNA concentration was the same as in the experiments described above. The microbubbles were mixed with the pDNA according to the different protocols (Figure 1) and diluted in optimem. For the ultrasound treatment, the Opticells were placed in a water bath at 37 °C with an absorbing rubber substrate at the bottom and immediately subjected to ultrasound radiation. The ultrasound radiation was performed for 10 s with a Sonitron 2000 instrument (RichMar, Inola, OK, USA) equipped with a 22 mm probe. In all these

ultrasound-assisted experiments, the following ultrasound settings were used: 1 MHz, 10% duty cycle, and an ultrasound intensity of 2 W/cm². The areas treated with ultrasound were marked and after radiation the Opticells were incubated for an additional 2h at 37 °C. At the end of this incubation period, the transfection medium was removed and the cells were washed two times with PBS, before adding fresh culture medium. Each transfection experiment was performed three times.

Assays for Luciferase Activity, Adherent Cell Number, and Viability

Analysis of the VSMC

For each condition, four wells were used. Three wells were analysed for luciferase expression and one well was used to measure the cell concentration. Luciferase activity in cell lysates 48 hours after transfection was measured with the GenGlow kit (Labtech International) and 1253 Luminometer (BioOrbit) and expressed as relative light units (RLU) per 10⁴ cells. Background luminescence was zero in untransfected cell lysates. Cell counts were assayed by a Beckman Coulter Counter.

Analysis of the BLM cells

Luciferase expression by the cells was analyzed 24 h after transfection. The culture medium was removed and the cells were washed with PBS. The areas exposed to ultrasound (20 mm diameter) were cut from the Opticell membrane and placed in a 24 well plate. A 80 µL solution of cell culture lyse reagent (CCLR, Promega, Leiden, The Netherlands) buffer was added to each well and incubated at room temperature for at least 20 min to allow cell lysis. 20 µL of the cell lysate was transferred to a 96 well plate and the luciferase activity was measured using a Glomax 96 Microplate Luminometer (Promega), as described previously in the literature⁹. An aliquot (20 µL) of each cell lysate was also analyzed for protein concentration using the bichinonic acid (BCA) protein assay (Pierce, Rockford, IL, USA). The transfection results are expressed as relative light units (RLU) per milligram of protein.

Gel electrophoresis

Two micrograms of pDNA were mixed with 50 µL of an uncoated or PAH-coated microbubble dispersion. After 5 min of incubation, the pDNA/microbubble mixtures were exposed to different ultrasound parameters. Ten microliters of the subnatants was mixed with 10 µL of a 30% glycerol solution and loaded onto a 1.5% agarose gel prepared in TBE (10.8 g/L tris base, 5.5 g/L boric acid,

and 0.58 g/L EDTA). The samples were subjected to electrophoresis at 100 V for 60-90 min, and the pDNA was visualized by ethidium bromide (0.5 $\mu\text{g}/\text{mL}$) staining prior to UV photography.

Fluorescent labeling of pDNA and PAH.

PAH labelling with Rhodamine IsoThioCyanate (RITC) occurred in a similar way. Twelve milligrams of RITC and 300 mg of PAH were separately dissolved in 60 mL of borate buffer (0.1 M, pH 8.5) and subsequently mixed under vigorous stirring. After overnight incubation, the reaction mixtures were dialyzed (MW cutoff of the membrane was 25 kDa) against pure water for several days. Finally, the dialyzed RITC-PAH was freeze dried, and the resulting fluffy solid was stored at 4 °C. The intercalating dye YOYO-1 was used to label the pDNA. Therefore, 111 μg of pDNA was mixed with 57 μL of a 1/100 diluted YOYO-1 (Molecular Probes, Eugene, OR) and diluted in TE buffer (10 mM tris-HCl; 1 mM EDTA; pH 7.4) until a final pDNA concentration of 1 mg/mL was obtained. The dye/base pair ratio was 1:30.

Confocal Laser Scanning Microscopy

The microbubble remainders were put on a glass slide and visualized by a confocal laser scanning microscope (CLSM, BioRadMRC1024, Hemel Hempstadt, U.K.) equipped with a krypton-argon laser and a dichroic mirror that reflects the laser light in a 60x objective. The 488 nm line of this laser was used to excite YOYO-1 and the 568 nm line was used to excite RITC. To ensure a proper spectral separation, appropriate emission filters were used before the green and red detector.

RESULTS & DISCUSSION

Figure 1 gives an overview of the different protocols used in our experimental setup. In protocol 1 we pre-incubated the cells for 30 minutes with plasmid DNA. The microbubbles were added to the transfection medium after this pre-incubation period, immediately followed by ultrasound exposure. We also pre-incubated microbubbles and pDNA (protocol 2 and 3), followed by ultrasound exposure of the cells and a further incubation period at 37°C for 90 minutes (protocol 2) or 2 hours (protocol 3). Protocol 2' and 3' are exactly the same protocols as protocol 2 and 3 respectively, except that the microbubbles were pre-saturated with SEAP plasmid DNA. In this case, all possible pDNA binding places are occupied, preventing any interaction between the microbubbles and the pGL-3.

Transfection efficiency in Vascular Smooth Muscle Cells (VSMCs) and melanoma cells

Figure 2 displays the transfection results obtained in primary VSMCs with uncoated and PAH-coated albumin microbubbles, following the different protocols explained in Figure 1. Lipofectin and BR-14 bubbles (Bracco) were used as a positive control. We used protocol 3 to evaluate the transfection efficiency of the BR-14 bubbles. We will first focus on the results from the uncoated microbubbles. It is clear from figure 2 that pre-incubation of the microbubbles and plasmid DNA (protocol 2 and 3) results in a higher transfection efficiency. Although we previously did not observe any binding of the plasmid DNA to the uncoated microbubbles⁶, there should be a (weak) interaction resulting in an enhanced transfection. Adherence of the plasmid DNA to the microbubbles assures that more pDNA is closely located to the cell membrane poration site, resulting in an increased uptake of the pDNA through these pores^{10,11}. Saturation of the microbubbles with the SEAP plasmid drastically reduced gene transfer (protocol 2' and 3'). There are two different hypotheses to explain this drop in transfection efficiency. First, the SEAP DNA will occupy all possible binding places on the microbubble shell, hampering any association between the pGL-3 plasmid and the microbubbles. As explained above, this will limit the chance that pGL-3 plasmids are taken by the fluid streams, reducing their ability to enter cell membrane pores. A second explanation is that the presence of such a huge amount of SEAP pDNA gets in competition with the pGL-3 pDNA for cellular uptake. Because the concentration of SEAP plasmid is more than 6 times higher than pGL-3 concentration, more SEAP molecules will be able to passively diffuse through the cell membrane pores. Moreover,

after cellular entry, the SEAP pDNA will also get in competition for nuclear transcription with the pGL-3.

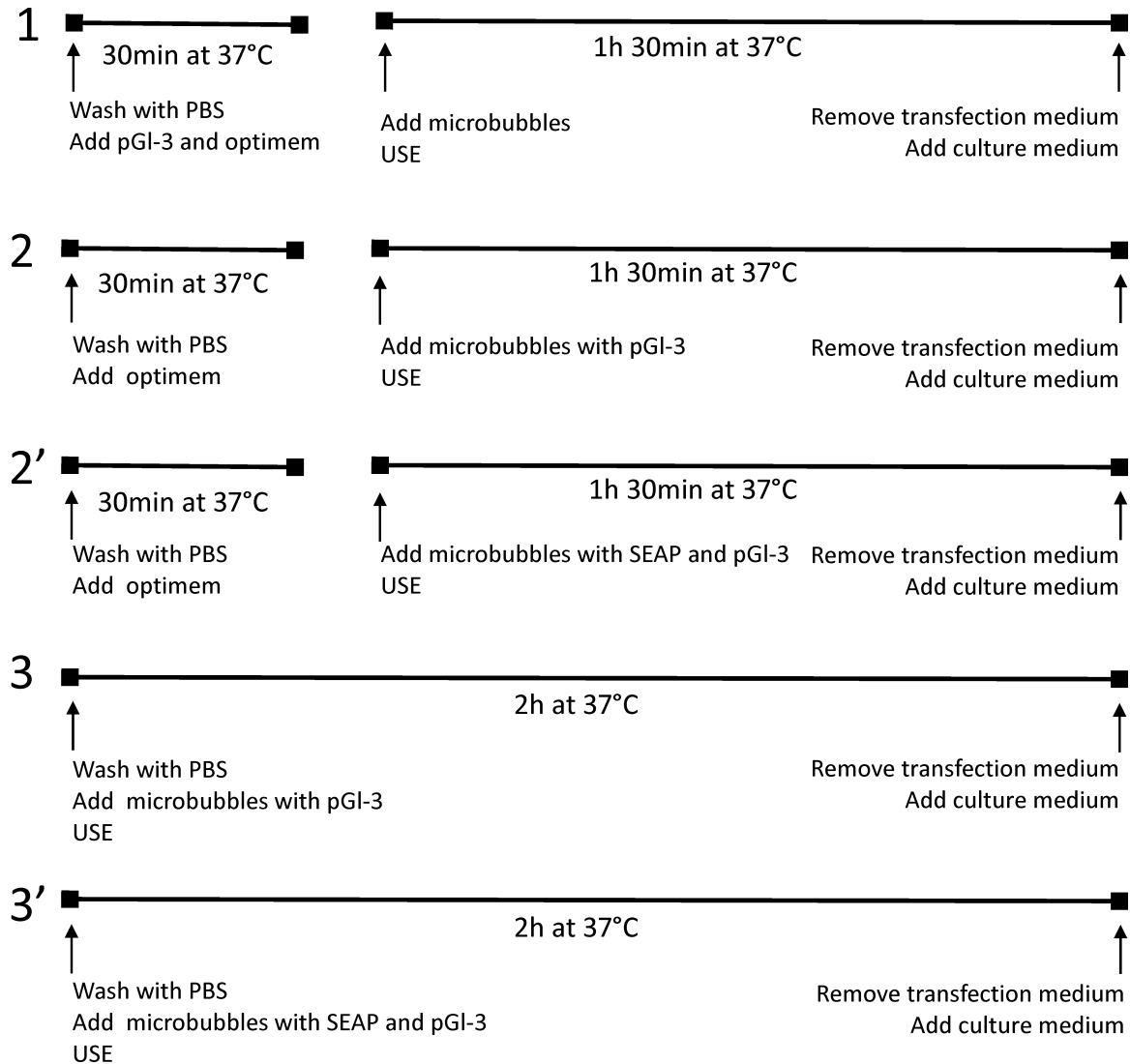


Figure 1 Schematic overview of the used protocols in the transfection experiments. *Protocol 1:* Cells were first incubated with the pGL-3 and after 30 minutes of incubation the microbubbles were added and the cells were irradiated. *Protocol 2:* After incubating the cells for 30 minutes with Optimem only, the microbubbles were added together with the pGL-3. Microbubbles and pDNA were first incubated together and subsequently added to the Optimem medium, immediately after addition of the microbubbles and pDNA ultrasound was applied. *Protocol 3:* Microbubbles and pDNA were incubated for 5 minutes and diluted in Optimem. The transfection medium was added to the cells and ultrasound exposure was performed. Cells were incubated for an additional 2 hours at 37°C with the transfection medium. *Protocol 2' and 3'* are the same as protocol 2 and 3 respectively, except that the microbubbles were first incubated with SEAP pDNA to saturate the possible pDNA binding places on the microbubbles.

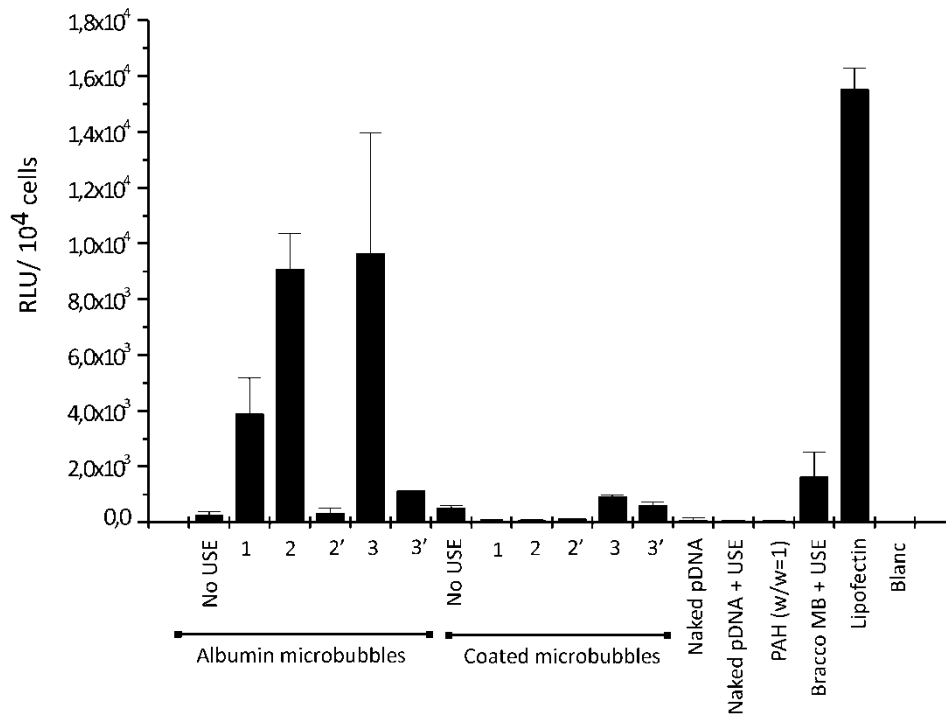


Figure 2 Transfection efficiencies of uncoated and polymer coated albumin microbubbles in primary VSMCs. The different protocols shown in figure 1 were used.

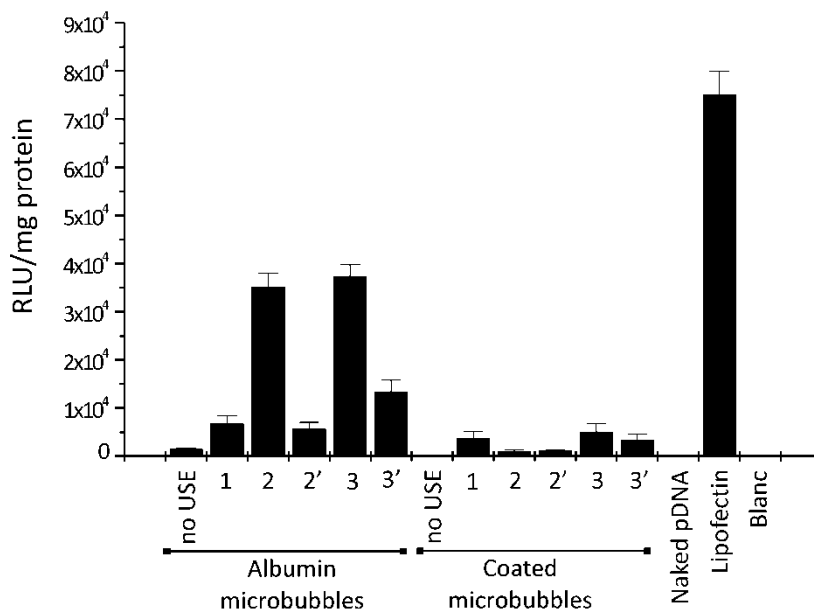


Figure 3 Transfection efficiencies of uncoated and polymer-coated albumin microbubbles in melanoma cells. The different protocols shown in figure 1 were used.

Unfortunately the transfection efficiencies obtained with the polymer-coated microbubbles were very low. The highest transfection efficiency was obtained with protocol 3 (premixing of DNA and microbubbles and 2 hours incubation time). However, gene transfer was only slightly higher as the transfection obtained with naked pDNA.

We repeated these experiments on melanoma cells. Figure 3 shows the transfection results obtained in a melanoma cell line. We obtained the same results in this cell line as with the primary VSMCs.

Stability and ultrasound induced release of pDNA from uncoated albumin microbubbles and polymer-coated microbubbles.

To explain the poor transfection results from the PAH-coated albumin microbubbles, we studied the pDNA release from the microbubbles upon ultrasound radiation. Figure 4A shows a gel electrophoresis experiment in which pDNA-loaded polymer coated microbubbles were exposed to different ultrasound intensities and subsequently loaded onto an agarose gel. Lane 2 displays the migration of the free pDNA in the agarose gel. After addition of the microbubbles there was no free pDNA detected anymore (Lane 3). Although the intention of our experiment was to release the pDNA from the microbubbles after ultrasound exposure, we did not succeed in releasing any pDNA with the different ultrasound parameters used (Lane 4-12). We visually observed that > 90% of the microbubbles imploded under the highest ultrasound intensities used ($2\text{W}/\text{cm}^2$). The fact that there was no pDNA detected inside the agarose gel means that the pDNA is still complexed to the fragments of the cationic microbubble shell, preventing any diffusion of the pDNA into the gel. To verify this hypothesis we performed a confocal laser scanning microscopy experiment in which we exposed pDNA loaded, fluorescently labelled polymer coated microbubbles to ultrasound. The polymer was labelled in red, and subsequently incubated with green labelled pDNA. After ultrasound exposure we saw the appearance of very large (μm in size) and heterogeneous complexes consisting of microbubble shell fragments (red) and plasmid DNA (green) (figure 5). Due to their huge size, it is very unlikely that these complexes are taken up by the target cells, as cell membrane pores are reported to be between 100 and $1\mu\text{m}$ in size¹²⁻¹⁵.

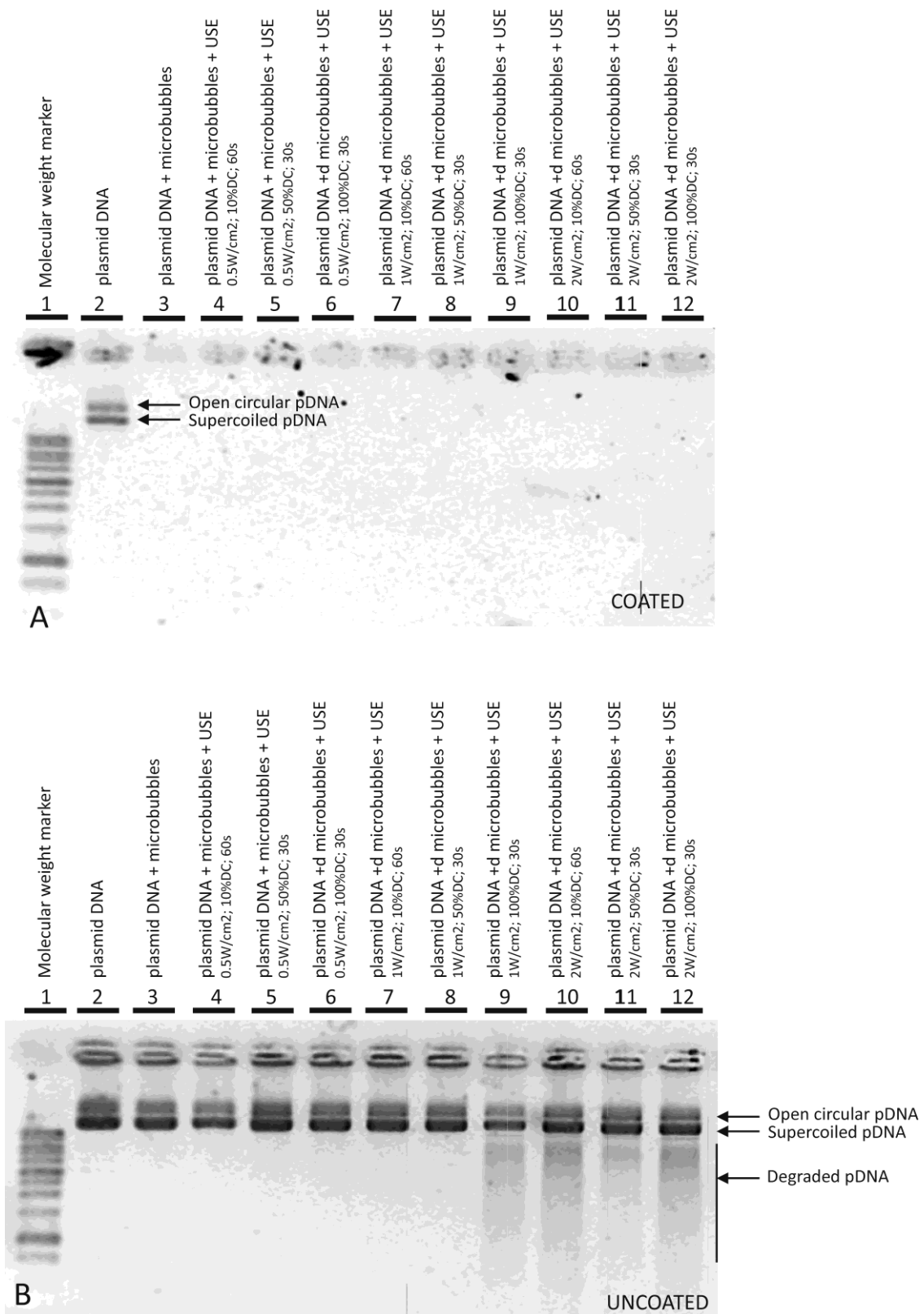


Figure 4 Gel electrophoresis of naked pDNA (lane 2) and pDNA present in a PAH-coated microbubble (A) or uncoated (B) microbubble dispersion (Lane 3). The effect of different ultrasound parameters on the release and stability of pDNA was evaluated (lane 4-12).

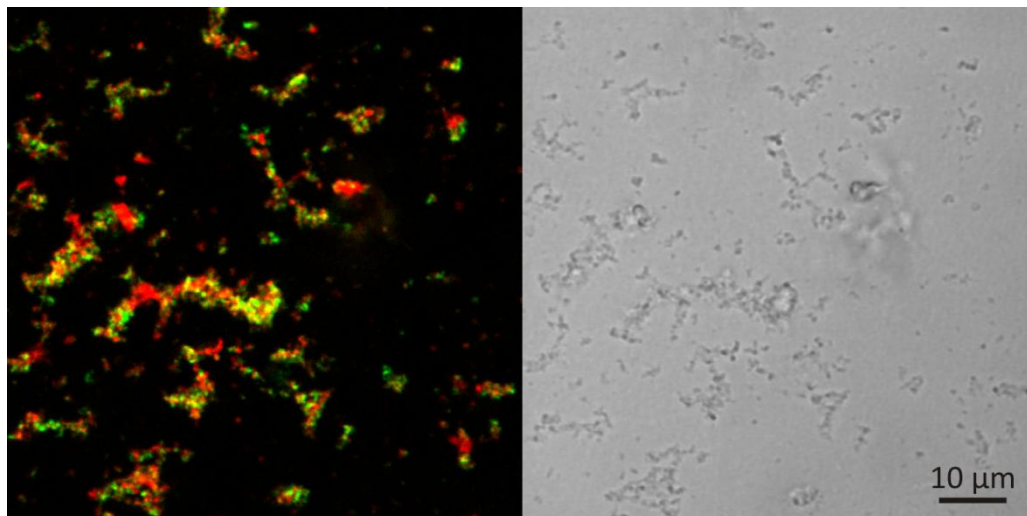


Figure 5 Confocal laser scanning microscopy image and corresponding transmission image of aggregates obtained after ultrasound induced implosion of PAH-coated microbubbles loaded with pDNA. Microbubble shell fragments are visible in red and pDNA is visible in green.

We also performed the same electrophoresis experiment with uncoated albumin microbubbles (Figure 3B). In contrast to the polymer-coated microbubbles, we did not see any retardation of the pDNA after incubation with the albumin microbubbles (Lane 3). This implies that only a very small fraction of the pDNA is indeed bound to the albumin shell, or that the interaction between the microbubbles and the pDNA is too low to prevent pDNA migration under the influence of the electric field. Exposure of pDNA to higher ultrasound intensities ($2\text{W}/\text{cm}^2$) in the presence of albumin microbubbles resulted in a partial degradation of the pDNA (lane 9-12). Because the pDNA is not complexed, it is more sensitive to the very high mechanical forces occurring during microbubble cavitation and implosion. This can result in a mechanical break-down of the pDNA¹⁶. This implies that the pDNA should be encapsulated or complexed to prevent mechanical degradation¹⁷. For this reason, pDNA should be bound to the microbubble shell or condensed into electrostatic complexes.

Two possible solutions exist for preparing a pDNA loaded microbubble, capable of releasing pDNA or small pDNA complexes. A first solution can be found in coating the albumin microbubbles with another cationic polymer, possessing less cationic charges. This would reduce the interactions between microbubble and pDNA. Electrostatic interaction might be lowered to such an extent that the pDNA is released during microbubble implosion. However, this increases the chance that the pDNA will become released in the blood circulation after interaction of the microbubbles with charged serum components. A second solution can be the attachment of well-defined pre-formed

pDNA complexes to the microbubble shell. In this case, the pDNA is protected inside the complexes during extracellular circulation. When the microbubbles enter the ultrasonic field, these small complexes can then be released and are available for uptake through the created cell membrane pores. Several papers have shown that at least part of these complexes are able to dissociate intracellularly, after which the pDNA can be transported to the nucleus for transcription^{18,19}. In chapter 4 we will focus on the creation of a novel particle loaded microbubble.

CONCLUSION

In conclusion, we showed that the pre-incubation of uncoated albumin microbubbles and pDNA drastically increases ultrasound mediated gene transfer. Although the PAH-coated albumin microbubbles enable high pDNA loading efficiencies and a good pDNA protection, they are not capable of transfecting primary endothelial cells or melanoma cells. Our confocal microscopy experiments revealed that this is due to the formation of large aggregates, arising upon microbubble implosion. These aggregates might be too large to reach cellular cytoplasm through cell membrane pores. Gel electrophoresis experiments confirmed that the pDNA is still associated with the microbubble shell fragments, which can also hamper intracellular dissociation. Exposure of pDNA in the presence of albumin microbubbles to ultrasound intensities of $2\text{W}/\text{cm}^2$ resulted in a partial degradation of the plasmid DNA, indicating that the pDNA should be complexed or encapsulated to prevent this degradation. In the next chapter we will focus on the attachment of small, pre-formed pDNA complexes to the microbubble shell and evaluate whether this will solve the different problems encountered in this study.

ACKNOWLEDGMENTS

Ine Lentacker is supported by the Fund for Scientific Research-Flanders (FWO). The financial support of this institute is acknowledged with gratitude. Prof. Newman is thanked for the discussions. Dr. Su is thanked for practical help with the VSMC experiments.

REFERENCES

- (1) Mitragotri S. Innovation - Healing sound: the use of ultrasound in drug delivery and other therapeutic applications. *Nature Reviews Drug Discovery* **2005** 4(3) 255-260.

- (2) Newman C.M.H. & Bettinger T. Gene therapy progress and prospects: Ultrasound for gene transfer. *Gene Therapy* **2007** 14(6) 465-475.
- (3) Tachibana K. & Tachibana S. The use of ultrasound for drug delivery. *Echocardiography-A Journal of Cardiovascular Ultrasound and Allied Techniques* **2001** 18(4) 323-328.
- (4) Ferrara K., Pollard R., & Borden M. Ultrasound microbubble contrast agents: fundamentals and application to gene and drug delivery. *Annual review of biomedical engineering* **2007** 9 415-447.
- (5) Feril L.B., Jr. & Kondo T. Biological effects of low intensity ultrasound: the mechanism involved, and its implications on therapy and on biosafety of ultrasound. *Journal of Radiation Research* **2004** 45(4) 479-489.
- (6) Lentacker I., De Geest B.G., Vandenbroucke R.E. *et al.* Ultrasound-responsive polymer-coated microbubbles that bind and protect DNA. *Langmuir* **2006** 22(17) 7273-7278.
- (7) Porter T.R., Iversen P.L., Li S., & Xie F. Interaction of diagnostic ultrasound with synthetic oligonucleotide-labeled perfluorocarbon-exposed sonicated dextrose albumin microbubbles. *Journal of ultrasound in medicine and biology* **1996** 15(8) 577-584.
- (8) Quax P.H.A., Vanmuijen G.N.P., Weeningverhoeff E.J.D. *et al.* Metastatic Behavior of Human-Melanoma Cell-Lines in Nude-Mice Correlates with Urokinase-Type Plasminogen-Activator, Its Type-1 Inhibitor, and Urokinase-Mediated Matrix Degradation. *Journal of Cell Biology* **1991** 115(1) 191-199.
- (9) von Gersdorff K., Sanders N.N., Vandenbroucke R., De Smedt S.C., Wagner E., & Ogris M. The internalization route resulting in successful gene expression depends on polyethylenimine both cell line and polyplex type. *Molecular Therapy* **2006** 14(5) 745-753.
- (10) Ferrara K.W. Driving delivery vehicles with ultrasound. *Advanced Drug Delivery Reviews* **2008** 60(10) 1097-1102.
- (11) Sboros V. Response of contrast agents to ultrasound. *Advanced Drug Delivery Reviews* **2008** 60(10) 1117-1136.
- (12) Mehier-Humbert S., Bettinger T., Yan F., & Guy R.H. Plasma membrane poration induced by ultrasound exposure: Implication for drug delivery. *Journal of Controlled Release* **2005** 104(1) 213-222.
- (13) Prentice P., Cuschierp A., Dholakia K., Prausnitz M., & Campbell P. Membrane disruption by optically controlled microbubble cavitation. *Nature Physics* **2005** 1(2) 107-110.
- (14) Schlicher R.K., Radhakrishna H., Tolentino T.P., Apkarian R.P., Zarnitsyn V., & Prausnitz M.R. Mechanism of intracellular delivery by acoustic cavitation. *Ultrasound in Medicine and Biology* **2006** 32(6) 915-924.
- (15) Van Wamel A., Kooiman K., Hartevelde M. *et al.* Vibrating microbubbles poking individual cells: Drug transfer into cells via sonoporation. *Journal of Controlled Release* **2006** 112(2) 149-155.
- (16) Coakley W.T. & Dunn F. Degradation of Dna in High-Intensity Focused Ultrasonic Fields at 1 Mhz. *Journal of the Acoustical Society of America* **1971** 50(6) 1539-&.

- (17) Kuo J.H.S., Jan M.S., & Sung K.C. Evaluation of the stability of polymer-based plasmid DNA delivery systems after ultrasound exposure. *International Journal of Pharmaceutics* **2003** 257(1-2) 75-84.
- (18) Miyata K., Kakizawa Y., Nishiyama N. *et al.* Block cationic polyplexes with regulated densities of charge and disulfide cross-linking directed to enhance gene expression. *Journal of the American Chemical Society* **2004** 126(8) 2355-2361.
- (19) Zuhorn I.S., Kalicharan R., & Hoekstra D. Lipoplex-mediated transfection of mammalian cells occurs through the cholesterol-dependent clathrin-mediated pathway of endocytosis. *Journal of Biological Chemistry* **2002** 277(20) 18021-18028.

Chapter 4

Lipoplex loaded microbubbles for ultrasound targeted gene delivery

This chapter is published.

Lentacker I.¹, De Smedt S.C.¹, Demeester J.¹, Van Marck V.², Bracke M.² and Sanders N.N.¹ *Advanced Functional Materials* **2007** 17(12) 1910-1916.

¹ Laboratory of General Biochemistry and Physical Pharmacy, Department of Pharmaceutics, Ghent University, Ghent, Belgium.

² Laboratory of Experimental Cancerology , Department of Radiotherapy and nuclear medicine, Ghent University Hospital, Ghent, Belgium.

ABSTRACT

Cationic poly(ethylene glycol)ylated (PEGylated) liposomes are one of the most important gene transfer reagents in non-viral gene therapy. However, the low transfection efficiencies of highly PEGylated lipoplexes currently hamper their clinical use. Recently, ultrasound has been used in combination with microbubbles to enhance the uptake of genes in different cell types. However, the gene transfer efficiency still remains low in these experiments. To overcome the limitations of both techniques, we present the attachment of PEGylated lipoplexes to microbubbles via biotin–avidin–biotin linkages. Exposure of these lipoplex-loaded microbubbles to ultrasound results in the release of unaltered lipoplexes. Furthermore, these lipoplex-loaded microbubbles exhibit much higher transfection efficiencies than “free” PEGylated lipoplexes or naked plasmid DNA (pDNA) when combined with microbubbles and ultrasound. Interestingly, the lipoplex-loaded microbubbles only transfect cells when exposed to ultrasound, which is promising for space- and time-controlled gene transfer. Finally, this novel Trojan-horse-like concept can also be exploited to achieve the ultrasound-triggered release of nanoparticles containing other therapeutic agents such as anticancer drugs.

Chapter 4

Lipoplex loaded microbubbles for ultrasound targeted gene delivery

INTRODUCTION

The use of nucleic acids to replace defective genes or silence aberrant ones is an attractive strategy for the treatment of genetic disorders. However, the development of efficient and safe materials that can deliver therapeutic nucleic acids to the target cells of a patient is an enormous challenge. Both viral and non-viral nucleic acid delivery systems, such as cationic liposomes and cationic polymers, which electrostatically bind to negatively charged nucleic acids, are currently being investigated¹. Unfortunately, the former system is plagued by safety issues², whereas the latter systems are vulnerable to non-specific interactions with blood compounds due to their positive surface charge, resulting in the formation of life-threatening aggregates and suffering from rapid clearance by the mononuclear phagocyte system^{3,4}. These unwanted interactions have been prevented by coating the non-viral gene delivery systems with non-fouling polymers like poly(ethylene glycol) (PEG)⁵. However, 'PEGylation' drastically reduces the transfection efficacy of non-viral gene delivery systems, which has been attributed to reduced cellular uptake and/or limited endosomal escape^{6,7}. To overcome these limitations, the use of ultrasound energy in combination with gas-filled microbubbles has recently been proposed⁸⁻¹⁴. Ultrasound may mediate the intracellular delivery of nucleic acids by the formation of transient pores in cell membranes. These cell perforations are caused by shockwaves and microjets that are generated by the ultrasound-induced implosion of microbubbles in the vicinity of the cell membranes. The lifetimes of the cell membrane perforations have been reported to be very short, in the millisecond to seconds range¹⁵⁻¹⁷. Therefore, we believe that the binding of nanoparticles to microbubbles will allow the particles to be present at the site of cell membrane perforation, which may enhance the number of nanoparticles that can enter the cell. In this study, we have attempted to load PEGylated lipoplexes onto microbubbles to overcome their low transfection efficiency. Furthermore, the coupling of liposomes

to microbubbles could be an interesting approach for the ultrasound-induced release of different types of therapeutic molecules.

MATERIALS & METHODS

Preparation and characterization of lipid microbubbles containing DSPE–PEG–Biotin

Liposomes containing DPPC/DSPE–PEG–biotin in a 95:5 molar ratio were prepared as previously described¹⁸. Briefly, the lipids dissolved in chloroform were placed in a round-bottomed flask and the solvent was removed by evaporation followed by flushing with nitrogen. The obtained lipid film was subsequently hydrated in a 4-(2-hydroxyethyl)piperazine-1-ethanesulfonic acid (HEPES) buffer solution (20 mM HEPES, pH7.4) at a final lipid concentration of 5 mg/mL; the film was incubated overnight in this solution at 4 °C to allow the formation of liposomes. The resulting liposomes were first extruded through a polycarbonate membrane (pore size of 0.2 μm) using a mini-extruder (Avanti Polar Lipids, Alabaster, AL, USA). Subsequently, the extruded liposomes were sonicated with a 20 kHz probe (Branson 250 sonicator, Branson Ultrasonics, Danbury, CT, USA) in the presence of perfluorobutane gas (C₄F₁₀, molecular weight (MW) 238 g/mol, F2 Chemicals, Preston, Lancashire, UK). After sonication, the microbubbles were washed (to remove excess lipids) with 3 mL fresh HEPES buffer, and finally resuspended in 5 mL of a fresh HEPES buffer solution. To allow the attachment of biotinylated lipoplexes, the biotinylated microbubbles were incubated with 500 μL avidin (10 mg/mL) for 10 min at room temperature. Subsequently, the microbubbles were centrifuged and washed again with 3 mL fresh HEPES buffer. Finally, the microbubbles were resuspended in a 5 mL HEPES buffer solution. The concentration of the avidinylated microbubbles in the dispersions was determined with the aid of a Burkert chamber and a light microscope, and was found to be 4×10⁸ microbubbles/mL. The size distribution of the microbubbles was determined within 10 min of preparation by laser diffraction (Mastersizer S, Malvern, Worcestershire, UK). To measure the size distribution of the lipoplex-loaded microbubbles, 130 μL of the 15 mol% DSPE–PEG–biotin-containing lipoplexes was incubated for 5 min with 1 mL of the microbubble suspension and the measurement was performed again. The results are expressed as number percentages normalized to the most abundant fraction of microbubbles. All these experiments were performed using microbubbles dispersed in HEPES buffer. For the visualization of avidin on the surface of the biotinylated microbubbles, we incubated the microbubbles with 50 μL of Cy5-labeled streptavidin (1 mg/mL).

Preparation and characterization of PEGylated cationic liposomes and lipoplexes

The phospholipids, *N*-(1-(2,3-dioleoyloxy)propyl)-*N,N,N*-trimethylammonium chloride (DOTAP), dioleoyl phosphatidyl ethanolamine (DOPE), DSPE-PEG, DSPE-PEG-biotin, and cholesteryl 4,4-difluoro-5,7-dimethyl-4-bora-3a,4a-diaza-s-indacene-3-dodecanoate (cholesteryl Bodipy FLC12) were purchased from Avanti Polar Lipids. Cationic liposomes containing DOTAP/DOPE in a 1:1 molar ratio with 0.1 mol% cholesteryl Bodipy FLC12 and 0 to 15 mol% DSPE-PEG or DSPE-PEG-biotin were prepared as described above. For the preparation of lipoplexes, we used pDNA (pGL3, Promega, Leiden, The Netherlands) containing the luciferase gene from *Photinus pyralis* as the reporter. The pDNA was amplified in *Escherichia coli* and purified as described elsewhere¹⁸. The pDNA concentration was set at 1.0 mg/mL in HEPES buffer taking into account that the absorption of a 50 µg/mL DNA solution at 260 nm equals 1. The pDNA was of high purity as evidenced by the ratios of the optical absorptions at 260 and 280 nm varying from 1.8 to 2.0. Lipoplexes (with different percentages of DSPE-PEG or DSPE-PEG-biotin) were prepared with a charge ratio of 4. The charge ratio is defined as the ratio of the number of the positive charges (originating from DOTAP) to the number of the negative charges (originating from the pDNA). pDNA was first diluted in HEPES buffer to a concentration of 0.41 mg/mL. Subsequently, the diluted pDNA was added to an equal volume of cationic liposomes (5 mM DOTAP), resulting in a final +/- charge ratio of 4. Immediately after the addition of pDNA to the cationic liposomes, HEPES buffer was added until the final concentration of pDNA in the system was 0.126 mg/mL. This mixture was then vortexed and incubated at room temperature for 30 min. To obtain green labeled lipoplexes, liposomes prepared with 0.5 mol% of cholesteryl Bodipy FLC12 were used. The average hydrodynamic diameter of the PEGylated lipoplexes was determined by DLS (Autosizer 4700, Malvern). The data were analyzed using the automatic data analysis mode, i.e., a monomodal fit was used when the polydispersity (PD) was < 0.05 and a continuous fit was used when the PD was > 0.05. The zeta potential (ζ) was determined using electrophoretic mobility measurements (Malvern Zetasizer Nano ZS, Malvern). For these experiments, the lipoplexes were dispersed in HEPES buffer. The size and zeta potential of lipoplexes released from the lipoplex-loaded microbubbles after exposure to ultrasound (1 MHz, 10% duty cycle) for 10 s were determined in a similar way. Gel electrophoresis experiments were performed following previously described protocols¹⁸ to determine the presence of free pDNA in the lipoplexes before binding to the microbubbles and after ultrasound-assisted release from the microbubbles.

Attachment of biotinylated PEG-lipoplexes to avidinylated microbubbles

130 μL of a solution of biotinylated PEG-lipoplexes was mixed with a 1 mL solution of avidinylated microbubbles and incubated at room temperature for 5 min. The attachment of fluorescent-labeled lipoplexes to the microbubbles was visualized by CLSM using a Nikon EZC1-si microscope (Nikon, Brussels, Belgium) equipped with a 40 \times objective. The 491 nm line of this microscope was used to excite the Bodipy label.

Transfection Experiments

BLM cells (melanoma cells)¹⁹ were cultured in Dulbecco's modified Eagle's medium (DMEM) with the growth factor F12 and phenol red containing 2 mM glutamine, 10% heat-deactivated fetal bovine serum (FBS), 1% penicillin–streptomycin (Gibco, Merelbeke, Belgium), and HEPES buffer (100 mM, pH7.4). The cells were grown to 90% confluency in Opticell units (Biocrystal, Westerville, OH, USA) inside a humidified incubator at 37 °C under 5% CO₂. Subsequently, the cells were washed with 10 mL of phosphate buffered saline (PBS, Gibco) and the transfection medium was added. The transfection media were prepared by first mixing 130 μL PEGylated lipoplexes with 1 mL of the microbubble suspension (containing 4×10^8 microbubbles). After incubation for 5 min at room temperature, Optimem (Gibco) was added to a final volume of 10 mL. The transfection medium was prepared in a similar way for transfection experiments with naked pDNA, except that the 130 μL solution of the PEGylated lipoplexes was replaced by an equal volume of HEPES buffer containing 16.5 μg pDNA, the same amount as present in the lipoplexes. 10 mL of the transfection medium was added to the Opticell units (surface area of 50 cm²). Subsequently, the cells were placed in a water bath at 37 °C with an absorbing rubber substrate at the bottom and immediately subjected to ultrasound radiation. The ultrasound irradiation was performed for 10 s with a Sonitron 2000 instrument (RichMar, Inola, OK, USA) equipped with a 22 mm probe. In all the ultrasound-assisted experiments, the following ultrasound settings were used: 1 MHz, 10% duty cycle, and an ultrasound intensity of 2 W/cm². The areas treated with ultrasound were marked and after radiation the Opticells were incubated for an additional 2 h at 37 °C. At the end of this incubation period, the transfection medium was removed and the cells were washed two times with PBS, before adding fresh culture medium. Each transfection experiment was performed three times. Luciferase expression by the cells was analyzed 24 h after transfection. The culture medium was removed and the cells were washed with PBS. The areas exposed to ultrasound (20 mm diameter) were cut from the Opticell membrane and placed in a 24 well plate. A 80 μL solution of cell culture lysis reagent (CCLR, Promega, Leiden, The Netherlands) buffer was added to each well and incubated at room

temperature for at least 20 min to allow cell lysis. 20 μ L of the cell lysate was transferred to a 96 well plate and the luciferase activity was measured using a Glomax 96 Microplate Luminometer (Promega), as described previously in the literature²⁰. An aliquot (20 μ L) of each cell lysate was also analyzed for protein concentration using the bichinonic acid (BCA) protein assay (Pierce, Rockford, IL, USA). The transfection results are expressed as relative light units (RLU) per milligram of protein.

Cellular uptake of green-labeled 15 mol% DSPE–PEG–biotin-containing lipoplexes

Bodipy-labeled lipoplexes containing 15 mol% DSPE–PEG–biotin were prepared and attached to the microbubbles as described above. BLM cells present in Opticell units were exposed to the lipoplex-loaded microbubbles and ultrasound using the same conditions as in the transfection experiments. The areas treated with ultrasound were immediately visualized by CLSM using a Nikon EZC1-si microscope equipped with a 60 \times objective. The 491 nm line of this microscope was used to excite the Bodipy label in the lipoplexes.

Statistical Analysis

All the data in this report are expressed as mean \pm standard deviation (SD). For the transfection results, the student's t-test was used to determine whether the data groups differed significantly from each other. A *p*-value lower than 0.05 was considered statistically significant.

RESULTS AND DISCUSSION

Preparation and characterization of lipoplex-loaded microbubbles

As schematically illustrated in Figure 1A, PEGylated lipoplexes, i.e., complexes of DNA with cationic PEGylated liposomes (Fig. 1B), have been attached to microbubbles via biotin–avidin–biotin bridges. To prepare these lipoplex-loaded microbubbles, we have used lipid-based microbubbles that contain 1,2-distearoyl-*sn*-glycero-3-phosphoethanolamine-*N*-[biotinyl-PEG-2000] (DSPE–PEG–biotin) in their lipid shell. To evaluate whether the biotin molecules are present on the outer surface of the microbubbles, we have incubated them with Cy5-labeled streptavidin. After removal of the free Cy5–streptavidin, confocal laser scanning microscopy (CLSM) clearly reveals the presence of red fluorescence around the microbubbles, indicating the formation of a biotin–avidin linkage (Fig. 2). This confirms that the DSPE–PEG–biotin molecules in the shell of the microbubbles are oriented with

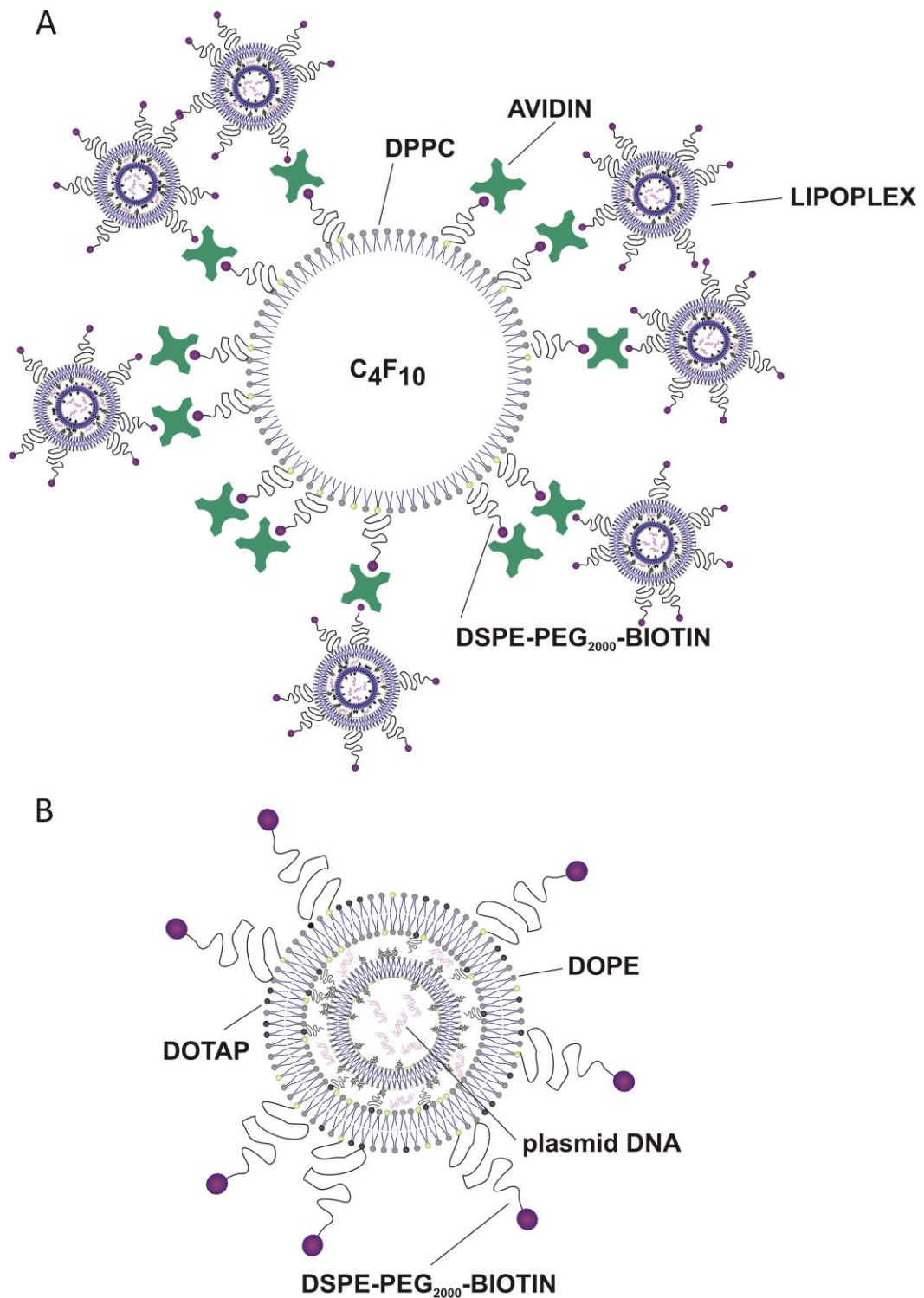


Figure 1 A) Schematic depiction of a lipoplex-loaded microbubble. The white disk surrounded by the lipids, dipalmitoylphosphatidylcholine (DPPC) and 1,2-distearoyl-*sn*-glycero-3-phosphoethanolamine-*N*-[biotinyl-PEG-2000] (DSPE-PEG-biotin), represents an avidinylated lipid microbubble with a perfluorobutane (C₄F₁₀) gas core. Lipoplexes with increasing amounts of DSPE-PEG-biotin are attached to these avidinylated microbubbles via biotin-avidin-biotin bridges. B) Detailed illustration of a single biotinylated lipoplex.

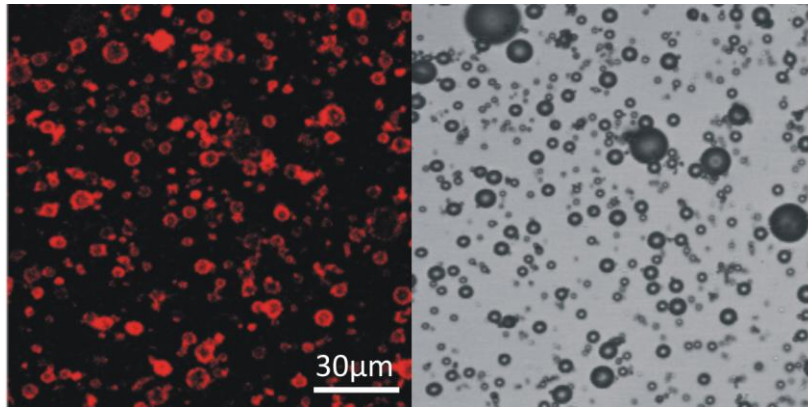


Figure 2 CLSM (left) and transmission (right) image of biotinylated microbubbles after incubation with Cy5-labeled streptavidin.

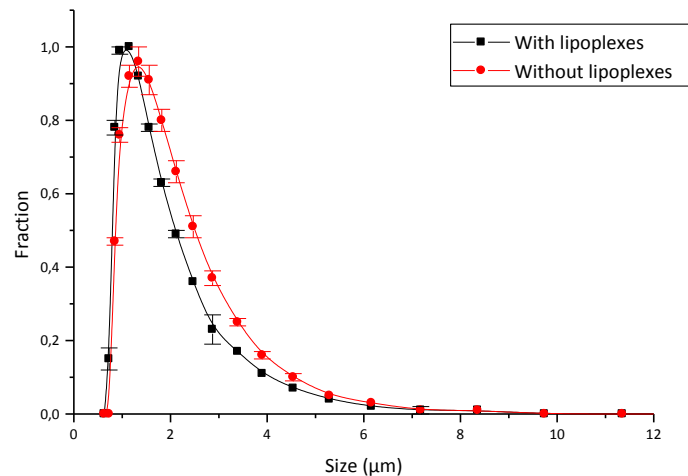


Figure 3 Size distribution of DPPC/DSPE-PEG-biotin microbubbles before and after the addition of 15 mol% PEGylated lipoplexes, as measured by laser diffraction. The y-axis shows the abundance of a certain class of microbubbles normalized to the most abundant fraction of microbubbles ($y = 1$). The data represent the mean of three independent measurements.

their hydrophobic tails pointing to the perfluorobutane gas core and with their hydrophilic head groups in the aqueous medium, as previously suggested by Unger et al²¹. To determine whether the biotinylated microbubbles have an optimal size distribution for cavitation, we have studied their size distribution by laser diffraction (Figure 3, red circles). As shown in Figure 3, the microbubbles are between 0.5 and 10 μm in size, which is indeed optimal for cavitation upon exposure to clinically relevant ultrasound irradiation²¹. To enable the binding of the PEGylated lipoplexes to the biotin-containing microbubbles, we have first incubated the microbubbles with an excess of avidin. After removing the unbound avidin, PEGylated lipoplexes containing increasing amounts of DSPE-PEG-

biotin (2, 5, and 15 mol%) are added to the microbubbles. Figure 4 demonstrates the binding of fluorescently-labeled PEGylated lipoplexes to the microbubbles. We observe that all the microbubbles have attached lipoplexes on their surface independent of the percentage of DSPE–PEG–biotin in the lipoplexes, indicating that the number of lipoplexes greatly exceeds the number of microbubbles. The amount of DSPE–PEG–biotin in the PEGylated lipoplexes clearly effects on the number of lipoplexes bound per microbubble. Lipoplexes containing 2 mol% DSPE–PEG–biotin do not completely cover the surface of the microbubbles, likely because of the limited degree of biotinylation of the lipoplexes. The surfaces of most microbubbles are fully covered with PEGylated lipoplexes when 5 mol% DSPE–PEG–biotin is incorporated in the lipoplexes, whereas all the microbubbles are completely covered with PEGylated lipoplexes when lipoplexes containing 15 mol% DSPE–PEG–biotin are used. The inset to Figure 4B shows a high-magnification image of a single lipoplex-loaded microbubble.

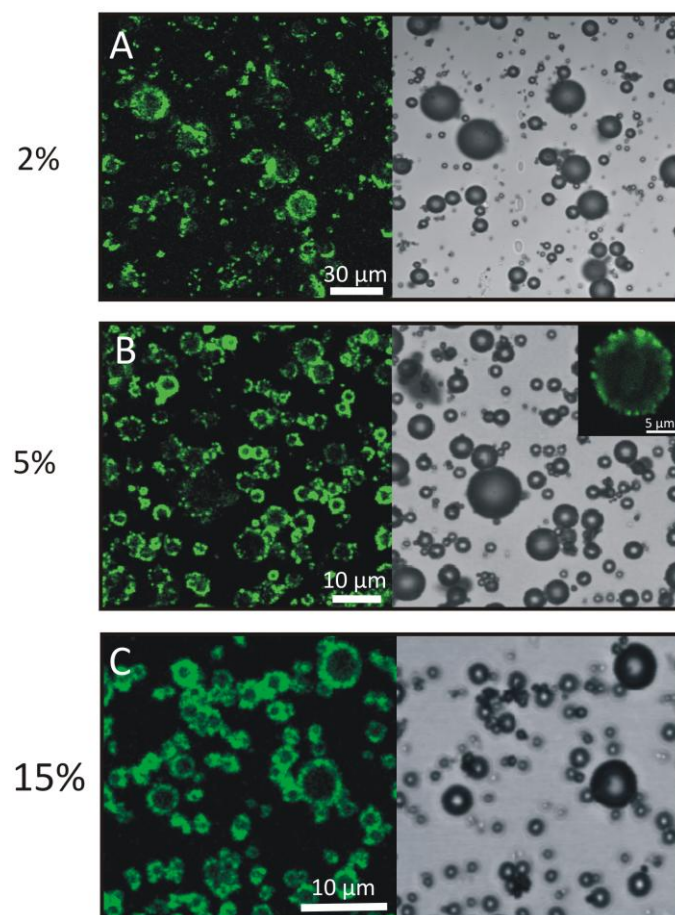


Figure 4 CLSM and corresponding transmission images of avidinylated microbubbles incubated with fluorescently labeled (green) PEGylated lipoplexes. The PEGylated lipoplexes contain A) 2 mol %, B) 5 mol %, and C) 15 mol% DSPE–PEG–biotin. The inset to (B) shows a microbubble with single lipoplexes on its surface.

To determine the effect of lipoplex binding on the size of the microbubbles, we have also measured the size distribution of the microbubbles after incubation with the biotinylated lipoplexes (Figure 3, solid squares). Compared to the unloaded microbubbles, the lipoplex loaded microbubbles are slightly smaller, which is probably due to experimental variations such as localization of the sonication probe and removal of the supernatant during successive washing steps. To confirm that the lipoplexes are specifically bound to the microbubbles through avidin–biotin interactions, we have tested the binding of PEGylated lipoplexes lacking biotin. The lipoplexes used in this control experiment contain 5 mol% DSPE–PEG instead of DSPE–PEG–biotin. The moderate binding of these non-biotinylated lipoplexes to the microbubbles is observed (data not shown). Since avidin is a glycosylated protein, non-specific interactions with different types of molecules and particulate matter can be expected.

Ultrasound-induced release of PEGylated lipoplexes from microbubbles

As mentioned in Section 1, the exposure of microbubbles to ultrasound causes the implosion and hence destruction of the microbubbles. Consequently, nanoparticles that are attached to the lipid-based microbubbles can be released from the microbubbles by ultrasound. Lum et al.²² have succeeded in attaching latex beads to lipid microbubbles, and have demonstrated the release of these beads under ultrasonic treatment. However, in contrast to inert beads, lipoplexes, which arise from the self-assembly of cationic liposomes and DNA, may undergo physicochemical alterations (which can possibly reduce their biological performance) during ultrasound-triggered release from the microbubbles.

Therefore, some physicochemical properties of the lipoplexes have been measured before attachment to the microbubbles and after ultrasound-triggered release from the microbubbles. The size of the free lipoplexes has been measured using dynamic light scattering (DLS). The lipoplexes decrease in size (from ca. 325 to 125 nm) with increasing degree of PEGylation. No significant difference in size is observed after the ultrasound-induced release of the lipoplexes from the microbubbles, except that the lipoplexes prepared with 15 mol% DPPC–PEG–biotin become slightly larger (Figure 5). The zeta potential before attachment to the microbubbles is around 25 mV for lipoplexes containing 2 mol% DSPE–PEG–biotin, around 22 mV for lipoplexes with 5 mol% DSPE–PEG–biotin, and ca. 14mV for lipoplexes containing 15 mol% DSPE–PEG–biotin. The zeta potential of the lipoplexes is not significantly altered after release from the microbubbles by ultrasound treatment (Figure 6). Apart from the retention of the size and zeta potential of the lipoplexes, it is

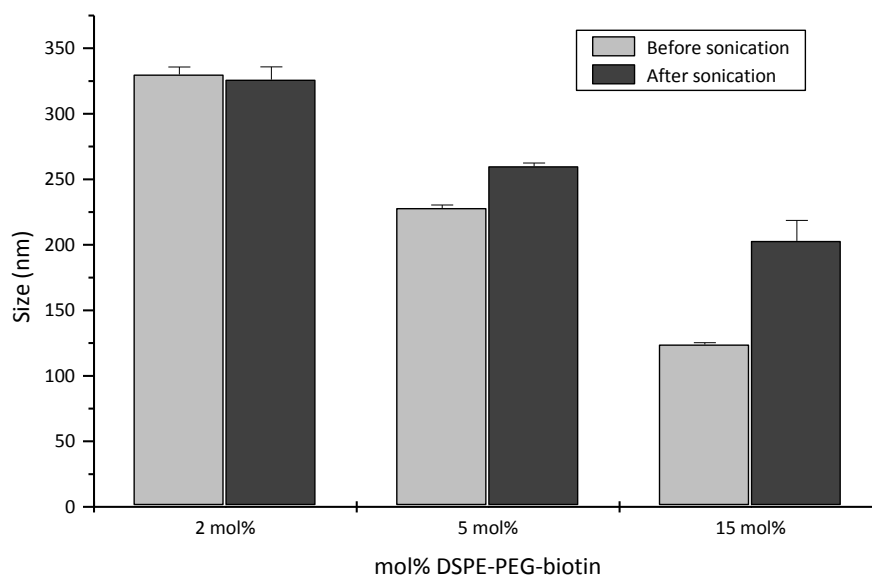


Figure 5 Sizes of PEGylated lipoplexes containing 2, 5, and 15 mol% DSPE–PEG–biotin before attachment to the microbubbles (white bars) and after ultrasound-mediated release from the microbubbles (black bars). The data represent the mean of three independent measurements and the error bars indicate the standard deviation.

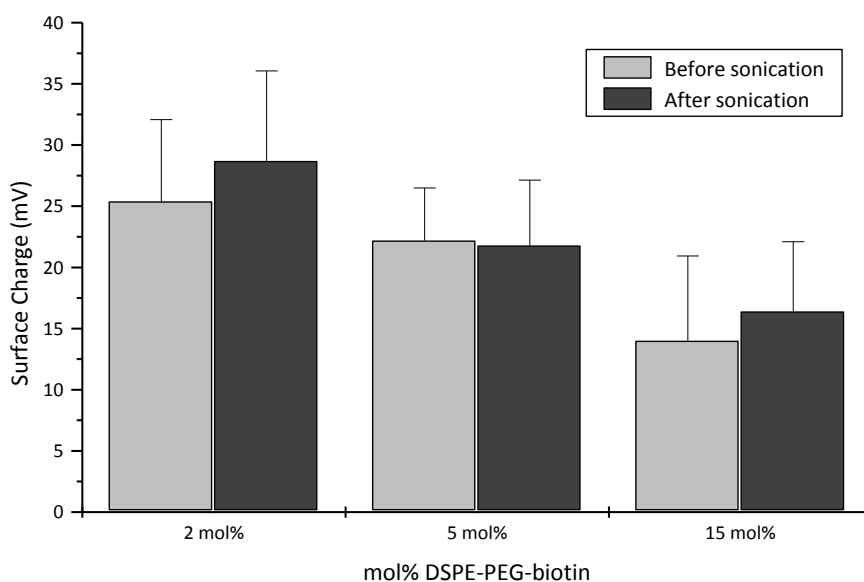


Figure 6 Zeta potential of PEGylated lipoplexes containing 2, 5, and 15 mol% DSPE–PEG–biotin before attachment to the microbubbles (white bars) and after ultrasound-mediated release from the microbubbles (black bars). The data represent the mean of three independent measurements and the error bars indicate the standard deviation.

also important that they do not dissociate upon exposure to ultrasound. Therefore, gel electrophoresis has been used to evaluate whether the ultrasound-assisted release of lipoplexes from the microbubbles leads to the release of plasmid DNA (pDNA). Free pDNA is not detected before the attachment of the lipoplexes or after the ultrasound-induced release of the lipoplexes from the microbubbles (Figure 7). This means that the ultrasound-mediated implosion of the microbubbles and the induced microjets do not influence the complexation properties of the cationic liposomes.

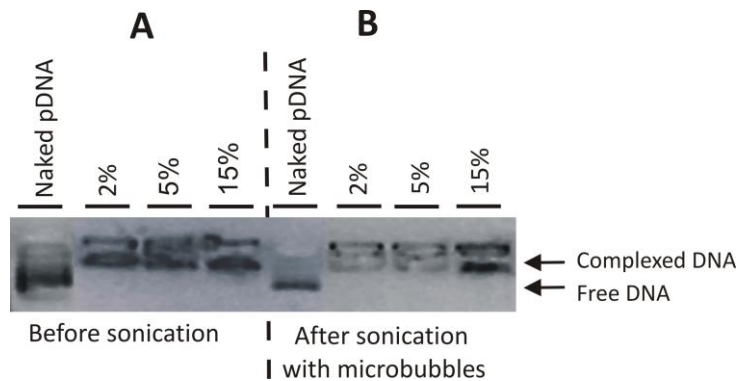


Figure 7 Gel electrophoresis of PEGylated lipoplexes containing 2, 5 and 15 mol% DSPE-PEG-biotin before attachment to the microbubbles (A) and after ultrasound mediated release from the microbubbles (B). **A:** Lane 1: free pDNA; Lane 2-4: PEGylated lipoplexes prepared with increasing amounts of DSPE-PEG-biotin: 2 mol%, 5 mol% and 15 mol%. **B:** Lane 5: free pDNA; Lane 6-8: PEGylated lipoplexes prepared with an increasing amount of DSPE-PEG-biotin subsequently 2mol%, 5mol% and 15mol%.

Gene transfer efficiency of lipoplex-bearing microbubbles

The gene transfer efficacies of PEGylated lipoplexes, a (physical) mixture of PEGylated lipoplexes and microbubbles, and the lipoplex-loaded microbubbles have been evaluated. As shown in Figure 8 (white bars, part B), the higher the degree of PEGylation of the lipoplexes, the lower their transfection capacity. Lipoplexes with a degree of PEGylation of 5 mol% are only slightly better than naked DNA (part A in Figure 8), whereas lipoplexes with a degree of PEGylation of 15 mol% show almost no transfection. The failure of highly PEGylated lipoplexes to transfect cells is in agreement with results of other research groups, and has been ascribed to both a reduced cellular uptake²³ and an inhibition of the endosomal release of DNA into the cytoplasm by the PEG lipids in the lipoplexes²³⁻²⁸. Figure 8 (grey bars, part B) also shows data for the transfection of cells when they are exposed to a (physical) mixture of PEGylated lipoplexes using microbubbles and ultrasound. Since the

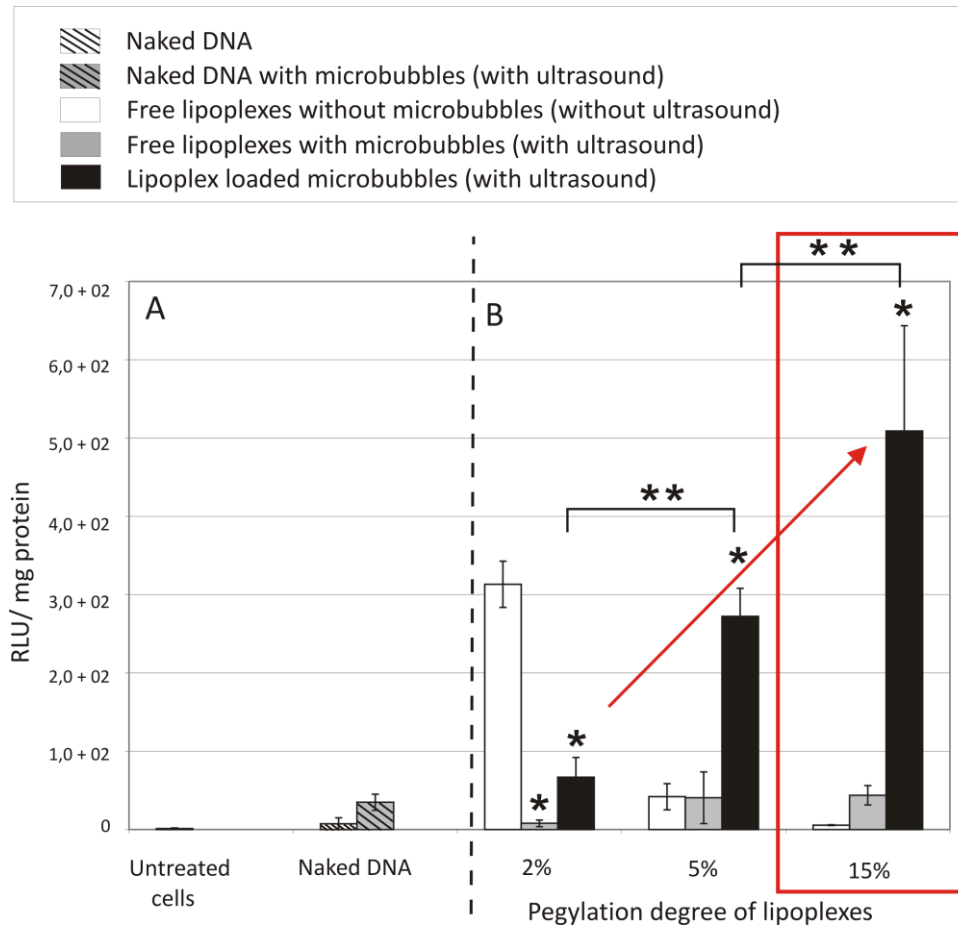


Figure 8 A) The transfection efficiency of naked DNA in the absence and presence of microbubbles and ultrasound, and the background luciferase signal in untreated cells. B) The transfection efficiency of free PEGylated lipoplexes in the absence and presence of microbubbles and ultrasound, and that of lipoplex-loaded microbubbles in the presence of ultrasound. The transfection results, i.e., the extent of luciferase expression, are expressed as RLU/mg-1 (RLU: relative light units) protein. * $p < 0.05$, compared to lipoplexes or naked DNA without microbubbles and ultrasound. ** $p < 0.05$.

ultrasound energy itself does not alter the physicochemical properties of the PEGylated lipoplexes (see discussion above), it is reasonable to expect that the transfection of the cells should at least be similar to that observed when only free PEGylated lipoplexes are used (white bars, part B of Fig. 8). However, we hypothesize that the strong decrease in gene transfer observed for the 2 mol% PEGylated lipoplexes arises from an ultrasound-induced blockage of endocytosis, which is line with previous observations by Schlicher et al.¹⁶ They have shown that ultrasound treatment in the presence of microbubbles removes patches of the plasma membrane; these are subsequently resealed by lipid vesicles transported from the inside of the cell to the plasma membrane (exocytosis). The endocytosis of the cells, which is the major mechanism for the uptake of the lipoplexes, may be significantly altered upon exposure to ultrasound. Such repair mechanisms of the cell membrane may prevent the endocytic uptake of the lipoplexes²⁹. Figure 8 (grey bars, part B)

shows that the presence of microbubbles and the application of ultrasound does not really reduce the transfection properties of 5 and 15 mol% PEGylated lipoplexes. Since the 5 and 15 mol% PEGylated lipoplexes are much less endocytosed by the cells, it is reasonable to expect that the (negative) influence of ultrasound and microbubbles will be much less pronounced. Importantly, Figure 8 (black bars, part B) clearly shows that the attachment of the lipoplexes to the microbubbles tremendously increases the transfection efficiency of the 5 mol %, and especially the 15 mol %, PEGylated lipoplexes. As noted above, free PEGylated lipoplexes encounter difficulties in entering the cells and/ or in escaping from endosomes, especially when they are highly PEGylated^{23,25-28}. We hypothesize that most of the PEGylated lipoplexes released from the microbubbles do not enter the cells by endocytosis, and consequently do not have to escape from the endosomes. To verify this hypothesis, we have studied the cellular uptake of the 15 mol% PEGylated lipoplexes after exposure to ultrasound. Figure 9 shows a massive internalization of the fluorescently labeled 15 mol% PEGylated lipoplexes immediately after exposure of the melanoma cells to lipoplex-loaded microbubbles and ultrasound. As mentioned above, several groups have reported the formation of transient cell membrane perforations upon the implosion of microbubbles at or near cell membranes^{15-17,30,31}. Consequently, it is reasonable to expect that the PEGylated lipoplexes released from the microbubbles enter the cells through these perforations, explaining their rapid internalization in Figure 9. Since the lifetime of the cell membrane perforations is very short,¹⁵ it is important that the lipoplexes are closely located to the cell membrane perforations, which is indeed the case when they are attached to the microbubbles. This phenomenon most likely also explains why the physical mixing of the PEGylated lipoplexes with the microbubbles does not dramatically enhance gene transfer (grey bars, part B), since most of the PEGylated lipoplexes are not located close to the microbubbles. As indicated by the arrow in Figure 8, the transfection efficiency of the lipoplex-loaded microbubbles increases as a function of the amount of DSPE-PEG-biotin in the lipoplexes. This can be explained as follows: firstly, more PEGylated lipoplexes are attached to the microbubbles when the lipoplexes contain more DSPE-PEG-biotin, which results in an increased concentration of PEGylated lipoplexes at the cell membrane perforations. Secondly, we note that the higher the degree of PEGylation, the smaller the size of the lipoplexes released from the microbubbles, which increases the chances of more PEGylated lipoplexes passing through the cell perforations. Finally, when no ultrasound is applied, the cell transfection by lipoplex-loaded microbubbles is negligible, and even lower than the transfection by free PEGylated lipoplexes (data not shown). This is again reasonable since without ultrasound the lipoplexes remain attached to the micrometer- sized bubbles that are too large to enter the cells. Interestingly, this may enable the microbubbles to transfect only those cells that are exposed to ultrasound energy, which may be promising for targeted *in vivo* gene delivery.

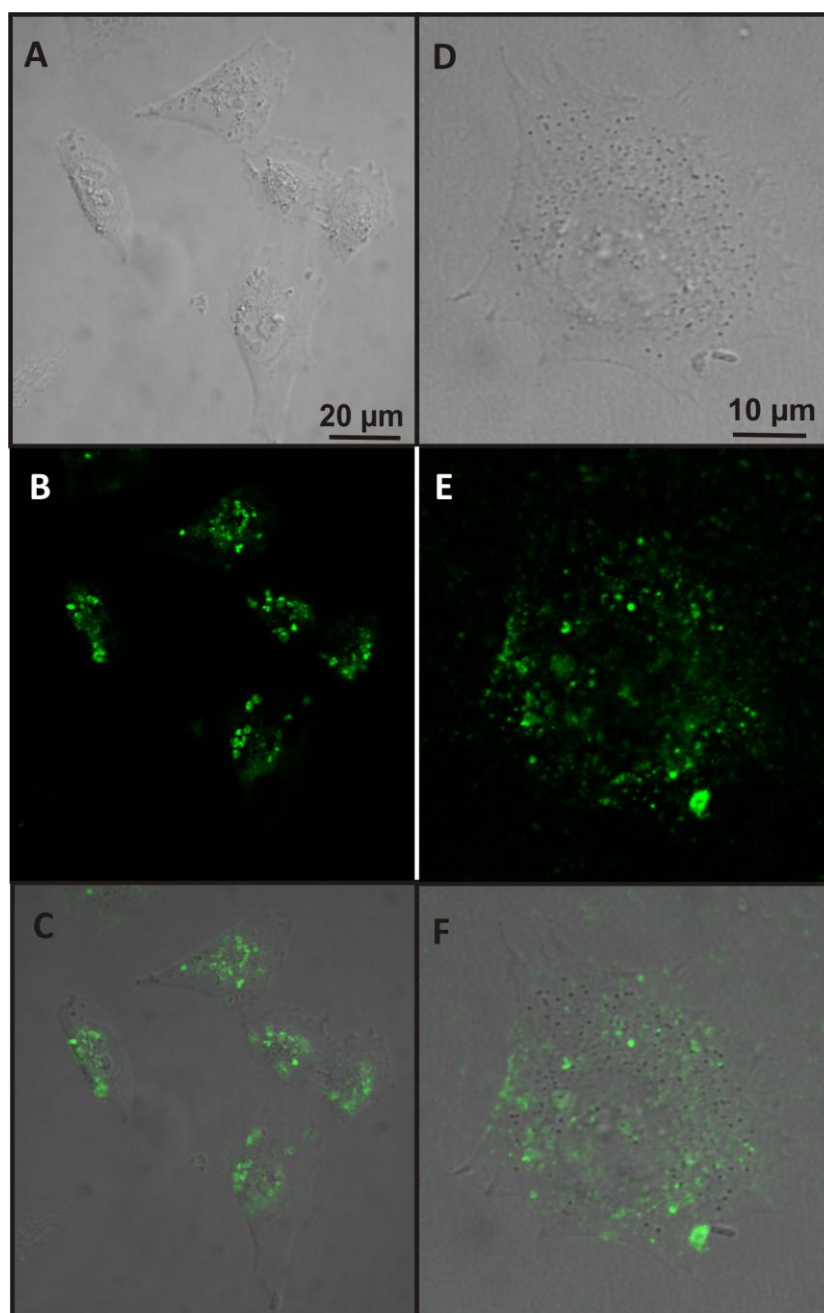


Figure 9 Cellular uptake of green-labeled 15 mol% PEGylated lipoplexes in BLM cells immediately after exposure of the cells with lipoplex-loaded microbubbles and ultrasound. Transmission images (A-D) and CLSM images (B-E) of green-labeled lipoplexes; overlays of the transmission and the green fluorescent confocal images (C-F). High-magnification images of a single cell (D-F).

Conclusions

We have designed a novel lipid microbubble to which PEGylated lipoplexes are attached via biotin–avidin–biotin linkages. Upon exposure to ultrasound, unaltered lipoplexes are released from these lipoplex-loaded microbubbles. This is in contrast to previously developed layer-by-layer coated microbubbles, which lead to the release of undefined DNA-containing clusters that are too large to pass through the small cell perforations³². The lipoplex-loaded microbubbles have a much higher gene transfer capacity than “free” PEGylated lipoplexes and naked pDNA used in combination with microbubbles and ultrasound. Interestingly, the lipoplex-loaded microbubbles only transfect cells when exposed to ultrasound, which is promising for space- and time-controlled gene transfer^{33,34}. Thus far, the lack of gene transfer has impeded the clinical evaluation of PEGylated lipoplexes. To the best of our knowledge, we have demonstrated for the first time that gene transfer by lipoplexes containing > 5 mol% PEG–lipid can be strongly improved by attaching them to microbubbles and exposing them to ultrasound energy. The microbubbles presented in this study are also expected to be suitable for systemic applications. Indeed, microbubbles are already routinely injected in the clinic to enhance the ultrasound- mediated visualization of blood vessels, whereas highly PEGylated lipoplexes are known not to aggregate in blood and have been shown to be harmless^{4,5}. Moreover, this novel Trojan-horse-like concept can be used to achieve the ultrasound- controlled delivery of drug-loaded liposomes by simply attaching the drug-loaded liposomes or nanoparticles to the microbubbles. In this way, a more targeted delivery of drugloaded nanoparticles can be achieved, resulting in an increase of the therapeutic index of the drugs.

ACKNOWLEDGMENTS

Katharzyna Smigielska is thanked for practical assistance. Ine Lentacker is a doctoral fellow supported by the Fund for Scientific Research—Flanders (Belgium). Niek N. Sanders is a Postdoctoral Fellow supported by the Fund for Scientific Research—Flanders (Belgium). Financial support from FWO and BOF-Ghent are acknowledged.

REFERENCES

- (1) Patil S.D., Rhodes D.G., & Burgess D.J. DNA-based therapeutics and DNA delivery systems: a comprehensive review. *AAPS Journal* **2005** 7(1) E61-E77.
- (2) Marshall E. Gene Therapy Death Prompts Review of Adenovirus Vector. *Science* **1999** 286, 2244-2245 .
- (3) Eliyahu H., Serval N., Domb A.J., & Barenholz Y. Lipoplex-induced hemagglutination: potential involvement in intravenous gene delivery. *Gene Therapy* **2002** 9(13) 850-858.
- (4) Sakurai F., Nishioka T., Yamashita F., Takakura Y., & Hashida M. Effects of erythrocytes and serum proteins on lung accumulation of lipoplexes containing cholesterol or DOPE as a helper lipid in the single-pass rat lung perfusion system. *European Journal of Pharmaceutics and Biopharmaceutics* **2001** 52(2) 165-172.
- (5) Moghimi S.M. & Szebeni J. Stealth liposomes and long circulating nanoparticles: critical issues in pharmacokinetics, opsonization and protein-binding properties. *Progress in Lipid Research* **2003** 42(6) 463-478.
- (6) Wasungu L. & Hoekstra D. Cationic lipids, lipoplexes and intracellular delivery of genes. *J. Control Release* **2006** 116(2) 255-264.
- (7) Zuhorn I.S., Engberts J.B., & Hoekstra D. Gene delivery by cationic lipid vectors: overcoming cellular barriers. *European Biophysical Journal* **2007** 36(4-5) 349-362.
- (8) Bekeredjian R., Chen S.Y., Frenkel P.A., Grayburn P.A., & Shohet R.V. Ultrasound-targeted microbubble destruction can repeatedly direct highly specific plasmid expression to the heart. *Circulation* **2003** 108(8) 1022-1026.
- (9) Duvshani-Eshet M. & Machluf M. Therapeutic ultrasound optimization for gene delivery: A key factor achieving nuclear DNA localization. *Journal of Controlled Release* **2005** 108(2-3) 513-528.
- (10) Kinoshita M. & Hynynen K. A novel method for the intracellular delivery of siRNA using microbubble-enhanced focused ultrasound. *Biochemical and Biophysical Research Communications* **2005** 335(2) 393-399.
- (11) Manome Y., Nakayama N., Nakayama K., & Furuhashi H. Insonation facilitates plasmid DNA transfection into the central nervous system and microbubbles enhance the effect. *Ultrasound in Medicine and Biology* **2005** 31(5) 693-702.
- (12) Newman C.M., Lawrie A., Brisken A.F., & Cumberland D.C. Ultrasound gene therapy: On the road from concept to reality. *Echocardiography - A Journal of Cardiovascular Ultrasound and Allied Techniques* **2001** 18(4) 339-347.
- (13) Pislaru S.V., Pislaru C., Kinnick R.R. *et al.* Optimization of ultrasound-mediated gene transfer: comparison of contrast agents and ultrasound modalities. *European Heart Journal* **2003** 24(18) 1690-1698.

- (14) Vannan M., McCreery T., Li P. *et al.* Ultrasound-mediated transfection of canine myocardium by intravenous administration of cationic microbubble-linked plasmid DNA. *Journal of the American Society of Echocardiography* **2002** 15(3) 214-218.
- (15) Mehier-Humbert S., Bettinger T., Yan F., & Guy R.H. Plasma membrane poration induced by ultrasound exposure: Implication for drug delivery. *Journal of Controlled Release* **2005** 104(1) 213-222.
- (16) Schlicher R.K., Radhakrishna H., Tolentino T.P., Apkarian R.P., Zarnitsyn V., & Prausnitz M.R. Mechanism of intracellular delivery by acoustic cavitation. *Ultrasound in Medicine and Biology* **2006** 32(6) 915-924.
- (17) Van Wamel A., Kooiman K., Hartevelde M. *et al.* Vibrating microbubbles poking individual cells: Drug transfer into cells via sonoporation. *Journal of Controlled Release* **2006** 112(2) 149-155.
- (18) Sanders N.N., Van Rompaey E., De Smedt S.C., & Demeester J. Structural alterations of gene complexes by cystic fibrosis sputum. *American Journal of Respiratory and Critical Care Medicine* **2001** 164(3) 486-493.
- (19) Quax P.H.A., Vanmuijen G.N.P., Weeningverhoeff E.J.D. *et al.* Metastatic Behavior of Human-Melanoma Cell-Lines in Nude-Mice Correlates with Urokinase-Type Plasminogen-Activator, Its Type-1 Inhibitor, and Urokinase-Mediated Matrix Degradation. *Journal of Cell Biology* **1991** 115(1) 191-199.
- (20) Von Gersdorff K., Sanders N.N., Vandenbroucke R., De Smedt S.C., Wagner E., & Ogris M. The internalization route resulting in successful gene expression depends on polyethylenimine both cell line and polyplex type. *Molecular Therapy* **2006** 14(5) 745-753.
- (21) Unger E.C., Porter T., Culp W., Labell R., Matsunaga T., & Zutshi R. Therapeutic applications of lipid-coated microbubbles. *Advanced Drug Delivery Reviews* **2004** 56(9) 1291-1314.
- (22) Lum A.F.H., Borden M.A., Dayton P.A., Kruse D.E., Simon S.I., & Ferrara K.W. Ultrasound radiation force enables targeted deposition of model drug carriers loaded on microbubbles. *Journal of Controlled Release* **2006** 111(1-2) 128-134.
- (23) Deshpande M.C., Davies M.C., Garnett M.C. *et al.* The effect of poly(ethylene glycol) molecular architecture on cellular interaction and uptake of DNA complexes. *Journal of Controlled Release* **2004** 97(1) 143-156.
- (24) Audouy S. & Hoekstra D. Cationic lipid-mediated transfection in vitro and in vivo. *Molecular Membrane Biology* **2001** 18(2) 129-143.
- (25) Meyer O., Kirpotin D., Hong K.L. *et al.* Cationic liposomes coated with polyethylene glycol as carriers for oligonucleotides. *Journal of Biological Chemistry* **1998** 273(25) 15621-15627.
- (26) Mishra S., Webster P., & Davis M.E. PEGylation significantly affects cellular uptake and intracellular trafficking of non-viral gene delivery particles. *European Journal of Cell Biology* **2004** 83(3) 97-111.
- (27) Shi F.X., Wasungu L., Nomden A. *et al.* Interference of poly(ethylene glycol)-lipid analogues with cationic-lipid-mediated delivery of oligonucleotides; role of lipid exchangeability and non-lamellar transitions. *Biochemical Journal* **2002** 366 333-341.

- (28) Song L.Y., Ahkong Q.F., Rong Q. *et al.* Characterization of the inhibitory effect of PEG-lipid conjugates on the intracellular delivery of plasmid and antisense DNA mediated by cationic lipid liposomes. *Biochimica et Biophysica Acta-Biomembranes* **2002** 1558(1) 1-13.
- (29) Andrews N.W. Regulated secretion of conventional lysosomes. *Trends in Cell Biology* **2000** 10(8) 316-321.
- (30) Tachibana K., Uchida T., Ogawa K., Yamashita N., & Tamura K. Induction of cell-membrane porosity by ultrasound. *Lancet* **1999** 353(9162) 1409.
- (31) Van Wamel A., Bouakaz A., Versluis M., & De Jong N. Micromanipulation of endothelial cells: Ultrasound-microbubble-cell interaction. *Ultrasound in Medicine and Biology* **2004** 30(9) 1255-1258.
- (32) Lentacker I., De Geest B.G., Vandenbroucke R.E. *et al.* Ultrasound-responsive polymer-coated microbubbles that bind and protect DNA. *Langmuir* **2006** 22(17) 7273-7278.
- (33) Klibanov A.L. Microbubble contrast agents - Targeted ultrasound imaging and ultrasound-assisted drug-delivery applications. *Investigative Radiology* **2006** 41(3) 354-362.
- (34) Liu Y.Y., Miyoshi H., & Nakamura M. Encapsulated ultrasound microbubbles: Therapeutic application in drug/gene delivery. *Journal of Controlled Release* **2006** 114(1) 89-99.

Chapter 5

Ultrasound exposure of lipoplex loaded microbubbles facilitates direct cytoplasmic entry of the lipoplexes

This chapter is published.

Lentacker I.¹, Wang N.¹, Vandenbroucke R.E.¹, Demeester J.¹, De Smedt S.C.¹, Sanders N.N.² *Molecular Pharmaceutics* **2009** 6(2) 457-467.

¹ Laboratory of General Biochemistry and Physical Pharmacy, Ghent University, Harelbekestraat 72, B-9000 Ghent, Belgium.

² Laboratory of Gene Therapy, Department of Nutrition, Genetics and Ethology, Ghent University, Heidedstraat 19, B-9820 Merelbeke, Belgium

ABSTRACT

Recently we reported that the transfection of cells by PEGylated lipoplexes becomes significantly better by binding the PEGylated lipoplexes to the surface of microbubbles and applying ultrasound. To further optimize this gene delivery system it is important to understand the working mechanism. This paper elucidates the cellular entry path of these lipoplexes. The results clearly show that the PEGylated lipoplexes, released from the microbubbles upon applying ultrasound, are not taken up by endocytosis, being the most common route for nanoparticles to enter cells. Our data demonstrate that upon implosion of the microbubbles, the PEGylated lipoplexes are released and are most probably able to passively diffuse through the cell membrane pores or become ejected in the cytoplasm of the target cells. This is attractive as the *in vivo* use of PEGylated nanoparticles remains currently limited due to a decreased cellular uptake and inefficient escape of the PEGylated nanoparticles from the endosomes.

Chapter 5

Ultrasound exposure of lipoplex loaded microbubbles facilitates direct cytoplasmic entry of the lipoplexes

INTRODUCTION

The development of safe and efficient gene delivery systems is crucial for *in vivo* gene therapy. Viral delivery systems are the most efficient gene delivery systems. However, their *in vivo* use has been limited after the death of several patients during clinical trials with both adenoviral and adenoassociated viral (AAV) vectors¹. Furthermore, viral delivery systems are expensive while, especially, AAV vector cannot host (very) large transgenes. Also the risk of insertional mutagenesis and severe immune responses limit their *in vivo* use. In contrast, non-viral gene delivery systems have several advantages: easy and cheap production and the possibility of incorporating large plasmids². Furthermore they cause a relatively lower immune response². To improve the efficiency of non-viral delivery systems researchers have upgraded them with different functionalities like targeting ligands and fusogenic peptides to enable their endosomal escape. The latter is important as almost all non-viral vectors are taken up via endocytosis. Additionally, to avoid (a) aggregation in blood and (b) interaction with blood compounds like albumin, the surface of many types of non-viral delivery systems has been covered with polymers like poly-ethylene-glycol (PEG)³⁻⁵. However, PEGylation drastically lowers the transfection efficiency of non-viral vectors by hampering their cellular uptake and endosomal release. Therefore, PEG chains have been attached to lipids and polymers via chemical bonds that become cleaved in the acidic environment of the late endosomes. However, the synthesis of such so-called 'bioresponsive' carriers remains rather difficult^{6,7}.

Recently, the use of ultrasound and microbubbles has gained more and more attention to deliver drugs, especially nucleic acids⁸. Although microbubbles are currently used as contrast agent in ultrasound imaging⁹, they can also provoke several cellular effects. At low ultrasound intensities,

the microbubbles oscillate linearly in the acoustic pressure waves, a phenomenon called stable cavitation. This results in micro-streaming which affects the cellular membrane when the microbubbles are located close enough to the cells¹⁰. At higher ultrasound intensities, the expansions of the microbubbles become larger followed by a violent collapse of the microbubbles that results in shock waves that can temporarily perforate cell membranes (this phenomenon is called sonoporation). This collapse is due to the inertia of the intruding fluid and is therefore called inertial cavitation¹¹. Ultrasound assisted drug delivery has many advantages and one of the most attractive properties is the potential for time and space controlled delivery of drugs. On top, microbubbles and ultrasound energy are considered relative safe as both are applied in medical imaging for several years¹².

Ultrasound in combination with microbubbles has been intensively evaluated to enhance the delivery of *naked* DNA (genes and antisense oligonucleotides) and siRNA¹³⁻²¹. However, to obtain a significant higher biological effect large amounts of DNA and siRNA are required. This is due to the fact that naked DNA and siRNA are sensitive to degradation by nucleases, which are widely distributed in the body. Also, as the ultrasound induced pores in the cell membranes are short living, large amounts of DNA and siRNA are required near the pores to ensure a sufficient influx inside the cells. To overcome the limitations of (a) naked DNA combined with ultrasound and microbubbles, and (b) PEGylated lipoplexes (which suffer from an inefficient cellular uptake and endosomal escape), we previously coupled PEGylated lipoplexes onto ultrasound responsive microbubbles (Figure 1)^{22,23}. The idea being that the lipoplexes will be released upon ultrasound treatment and that they will be more easily transported inside the cell. Applying ultrasound to PEGylated lipoplexes bound to microbubbles resulted in much higher transfection when compared to the transfection obtained with free PEGylated lipoplexes with or without the use of microbubbles and ultrasound (Figure 2B). To further optimize this new delivery system it is necessary to understand the mechanism which explains this higher transfection efficiency. Therefore, the aim of this work was to elucidate the cellular pathway by which PEGylated lipoplexes, upon release from the microbubbles by ultrasound, enter the cells.

MATERIALS & METHODS

Preparation and characterization of lipid microbubbles containing DSPE-PEG-biotin

Liposomes containing DPPC (dipalmitoylphosphatidylcholine) and DSPE-PEG-biotin (1,2-distearoyl-sn-glycero-3-phosphoethanolamine-N-(biotinyl(polyethyleneglycol)2000)) in a 95:5 molar ratio were prepared as previously described²⁴. Briefly, the lipids were put in a round-bottomed flask, dissolved in chloroform. Subsequently, the solvent was removed via evaporation followed by flushing with nitrogen. The obtained lipid film was hydrated in HEPES buffer (20 mM HEPES, pH 7.4) at a final lipid concentration of 5 mg/mL and incubated overnight at 4°C to allow the formation of liposomes. The resulting liposomes were first extruded through a polycarbonate membrane (pore size of 0.2 µm) using a mini-extruder (Avanti Polar Lipids, Alabaster, AL, USA). Subsequently, the extruded liposomes were sonicated with a 20 kHz probe (Branson 250 sonifier, Branson Ultrasonics Corp., Danbury, CT, USA) in the presence of perfluorobutane gas (C₄F₁₀, MW 238 g/mol, F2 chemicals, Preston, Lancashire, UK). After sonication the microbubbles were washed (to remove the excess of lipids) with 3 mL fresh HEPES buffer and finally resuspended in 5 mL. To enable the attachment of biotinylated lipoplexes, the biotinylated microbubbles were incubated with 500 µL avidin (10 mg/mL) and incubated for 10 min at room temperature. Subsequently, the microbubbles were centrifuged and washed again with 3 mL fresh HEPES buffer. Finally the microbubbles were resuspended in 5 mL HEPES buffer. The concentration of the avidinylated microbubbles in the dispersions was determined with the aid of a Burker chamber and a light microscope and equalled 4 x 10⁸ microbubbles/mL.

Preparation and characterization of PEGylated cationic liposomes and lipoplexes

The cationic lipid DOTAP (N-(1-(2,3-dioleoyloxy)propyl)-N,N,N-trimethylammonium chloride), the phospholipid DOPE (dioleoyl phosphatidyl ethanolamine), DSPE-PEG, DSPE-PEG-biotin and cholesteryl Bodipy FLC12 (cholesteryl 4,4-difluoro-5,7-dimethyl-4-bora-3a,4a-diaza-s-indacene-3dodecanoate) were purchased from Avanti Polar Lipids. Cationic liposomes containing DOTAP and DOPE in a 1:1 molar ratio with 0 to 15 mol% DSPE-PEG or DSPE-PEG-biotin were prepared as described above.

For the preparation of lipoplexes we used plasmid DNA (pDNA; pGL3, Promega, Leiden, The Netherlands) containing the luciferase gene from *Photinus pyralis* as reporter (i.e. *firefly* luciferase). The pDNA was amplified in *Escherichia coli* and purified as described elsewhere²⁴. The pDNA was dissolved in HEPES buffer and the concentration was set at 1.0 mg/mL taking into account that the

absorption at 260 nm of a 50 µg/mL DNA solution equals 1. The pDNA showed a high purity as the ratio of the absorption at respectively 260 and 280 nm was between 1.8 and 2.0.

Lipoplexes were prepared at a charge ratio of 4. The charge ratio is defined as the ratio of the number of the positive charges (originating from DOTAP) to the number of the negative charges (originating from the pDNA). pDNA was first diluted in HEPES buffer to a concentration of 0.41 mg/ml. Subsequently, the diluted pDNA was added to an equal volume of cationic liposomes (5 mM DOTAP) resulting in a final +/- charge ratio of 4. Immediately after the addition of pDNA to the cationic liposomes, HEPES buffer was added until the final concentration of pDNA in the system was 0.126 mg/ml. This mixture was then vortexed and incubated at room temperature for 30 min. To fluorescently label the liposomes cholesteryl Bodipy FLC12 (cholesteryl 4,4-difluoro-5,7-dimethyl-4-bora-3a,4a-diaza-s-indacene-3-dodecanoate) was used (Molecular probes, Eugene Oregon, USA).

Melanoma cells stably expressing renilla luciferase (rLuc)

BLM_rLuc cells stably expressing renilla luciferase were generated by transfecting BLM-cells (melanoma cells)²⁵ with the pGL4.76_CMV plasmid. The pGL4.76_CMV plasmid was generated by ligating the PCR amplified (forward primer AATAGTCGACTAGTTATTAATAGTAATCAA and reversed primer AATAGGATCCGATCTGACGGTTCCTAAAC) and *Sall/BamHI* double digested CMV promoter into the *XhoI/BglII* double digested pGL4.76 plasmid (Promega, Leiden, The Netherlands). The resulting pGL4.76_CMV plasmid was linearized with the *BamHI* restriction enzyme and complexed with linear polyethylenimine (pEI; 22 kDa) to transfect the BLM cells. Transfected cells were incubated in fresh medium for 48 h and then selected with 250 µg/mL hygromycin. After two weeks, clones were isolated and expanded. Subsequently, the generated clones were analyzed and a renilla luciferase positive clone was selected.

Transfection experiments

BLM-cells were cultured in Dulbecco's modified Eagle's medium (DMEM) with the growth factor F12 and phenol red containing 2 mM glutamine, 10% heat deactivated foetal bovine serum (FBS), 1% penicillin-streptomycin (Gibco, Merelbeke, Belgium) and HEPES buffer (100 mM, pH 7.4). Cells were grown to 90% confluency in OptiCell units (Biocrystal, Westerville, OH , USA) in a humidified incubator at 37°C and 5% CO₂. Subsequently, cells were washed with 10 mL of phosphate buffered saline (PBS, Gibco) and the transfection medium was added.

A first transfection medium was prepared by mixing 130 µl PEGylated lipoplexes with 1 mL of the microbubble suspension (containing 4 x 10⁸ microbubbles). After 5 min of incubation at room

temperature, Optimem(Gibco, Merelbeke, Belgium) was added to a final volume of 10 mL. A second transfection medium was prepared in a similar way except that the 130 μ l PEGylated lipoplexes were replaced by an equal volume of HEPES buffer containing 16.5 μ g pDNA, the same amount as present in the lipoplexes.

The 10 mL transfection medium was completely added to the OptiCell units (surface 50 cm²). Subsequently, the cells were placed in a water bath at 37°C with an absorbing rubber at the bottom and immediately subjected to ultrasound radiation. The ultrasound radiation was performed for 10 s with a sonitron 2000 (RichMar, Inola, OK, USA) equipped with a 22 mm probe. A schematic representation of the experimental setup used is displayed in Figure 2A. In all ultrasound experiments the following ultrasound settings were applied: 1 MHz, 10% duty cycle and an ultrasound intensity of 2 W/cm². The areas treated with ultrasound were marked and after radiation, the OptiCells were incubated for an additional 2 h at 37°C. At the end of this incubation period, the transfection medium was removed and the cells were washed two times with PBS, before adding fresh culture medium. Each transfection was performed in threefold. Twenty four hours after transfection the firefly luciferase expression by the cells was analysed. Therefore, the culture medium was removed and cells were washed with PBS. The areas exposed to ultrasound (20 mm diameter) were cut from the optiCell membrane and brought into a 24-well plate. 80 μ L of CCLR (Cell Culture Lyse Reagent, Promega, Leiden, The Netherlands) buffer was added to each well and incubated at room temperature for at least 20 min to allow cell lysis. Twenty μ L of the cell lysate was transferred to a 96-well plate and the luciferase activity was measured using the GlomaxTM 96 Microplate Luminometer (Promega) as described elsewhere²⁶. An aliquot (20 μ l) of each cell lysate was also analysed for protein concentration using the BCA protein Assay (Pierce, Rockford, IL). Transfection results are expressed as relative light units (RLU) per mg protein.

In the transfection experiment with methyl- β -cyclodextrin (M β CD), the BLM cell line stably expressing *renilla* luciferase (BLM_rLuc) was used. The cells were preincubated for two hours with M β CD before the addition of the lipoplexes or lipoplex loaded microbubbles. Ultrasound radiation was carried out as described above. Both, *firefly* and *renilla* luciferase were measured with the Dual-Luciferase Reporter Assay System[®] (Promega, Leiden, The Netherlands) in the GlomaxTM 96 Microplate Luminometer (Promega). Results were expressed as *firefly* RLU/ *renilla* RLU.

Photochemical Internalization experiments

The photosensitizer (PS) TPPS2a, meso-tetraphenylporphine with two sulfonate groups on adjacent phenyl rings, was kindly provided by Dr. Anders Høgset (PCI Biotech AS, Oslo, Norway). The PS was light protected and stored at 4°C until use. Cells were exposed to blue light from the

LumiSource[®], a bank of four light tubes emitting light in the region of 375–450 nm, with 13 mW/cm² irradiance (PCI Biotech AS, Oslo, Norway). Cells were incubated overnight with 0.8 µg/mL PS. The day after, the PS was removed and cells were incubated with lipoplexes or transfected with lipoplex loaded microbubbles and exposed to ultrasound. After 2 h incubation time, the transfection medium was removed and cells were incubated at 37°C for an additional 2 h with culture medium. Subsequently the cells were exposed to the Lumisource for 40s and again placed at 37°C. Cells were analysed 24 h later.

Confocal Experiments

BLM-cells were seeded into culture dishes or Opticell plates one day before the confocal experiment. The cell membrane was labelled with concanavalin A-Alexa647 (Molecular Probes). The concanavalin A stock solution was diluted 10 fold in Optimem and added to the cells immediately before visualization. Cells were incubated with the free PEGylated lipoplexes for respectively 30 min and 150 min at 37°C and 5% CO₂. Ultrasound exposure of BLM-cells was performed immediately after addition of the lipoplex loaded microbubbles and cells were incubated then at 37°C for respectively 30 and 150 min. After the incubation time, cells were visualized using a Nikon EZC1-si confocal laser scanning microscope (Nikon, Brussels, Belgium) equipped with a 40x objective. The 491 nm line of this microscope was used to excite the Bodipy label. The 639 nm line was used to excite concanavalin A-Alexa647.

Propidium Iodide (PI) uptake

PI was added to the cells in a concentration of 25 µg/mL in Optimem. The PI was added either before the exposure of the cells to lipoplex loaded microbubbles and ultrasound or afterwards. The uptake of PI resulted in the appearance of red fluorescent nuclei, that were visualized with the 639 nm laser of the Nikon EZC1-si confocal microscope.

Statistical analysis

All the data in this report are expressed as mean ± standard deviation (SD). For the transfection results, the Student's t-test was used to determine whether data groups differed significantly from each other. A p-value lower than 0.05 was considered statistically significant.

RESULTS & DISCUSSION

Design and transfection efficiency of lipoplex loaded microbubbles

As schematically presented in Figure 1, we earlier succeeded in coupling highly PEGylated lipoplexes onto lipid microbubbles with the aid of an avidin-biotin link²². Biotinylated lipid microbubbles consisting of DPPC and DSPE-PEG-biotin were prepared next to DOTAP/DOPE based lipoplexes with 15 mol% DSPE-PEG-biotin. Subsequently, avidin was bound to the biotinylated microbubbles and mixed with the biotinylated lipoplexes. As published previously²², exposure of these lipoplex loaded microbubbles to ultrasound caused a massive release of intact lipoplexes and drastically increased the transfection efficiency of the PEGylated lipoplexes. Figure 2B shows the transfection of cells by respectively free PEGylated lipoplexes (light grey bars), PEGylated lipoplexes physically mixed with microbubbles (dark grey bars) and lipoplex loaded microbubbles after exposure to ultrasound (black bars). Only the PEGylated lipoplexes that were coupled to the microbubbles were able to transfect the cells after ultrasound radiation (black bars). It has been postulated that sonication of free lipoplexes could increase their transfection efficiency, but this was not confirmed in our experiments²⁷⁻²⁹ in agreement with the observations by Mehier-Humbert and colleagues¹⁸. Considering the giant increase in transfection efficiency after coupling the PEGylated lipoplexes to the microbubbles, we wanted to elucidate the differences in cellular uptake between respectively “free” PEGylated lipoplexes and PEGylated lipoplexes released from the lipoplex loaded microbubbles by ultrasound.

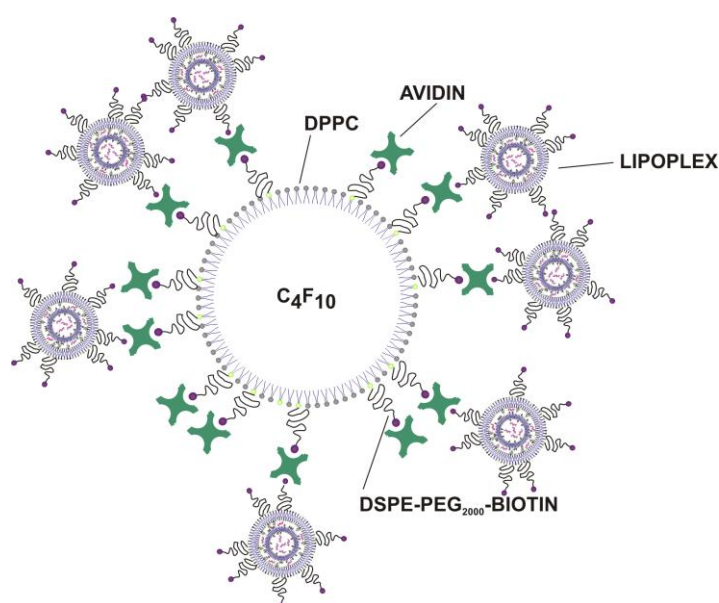


Figure 1 Schematic presentation of a lipoplex loaded microbubble.

Which mechanism do lipoplexes use to enter cells after exposure of lipoplex loaded microbubbles to ultrasound?

Influence of the endocytic inhibitor methyl- β -cyclodextrine (M β CD)

The intracellular uptake of lipoplexes has been intensively studied and has been ascribed to endocytosis³⁰. It is believed that the main reasons for the low transfection efficiency of highly PEGylated lipoplexes are their limited endocytic uptake (as the PEG chains prevent association of the lipoplexes with the cellular membrane) and, especially, their difficulties to escape from the endosome³¹⁻³⁵. As lipoplex loaded microbubbles are able to transfect BLM cells efficiently after ultrasound exposure (Figure 2B), we hypothesize that the PEGylated lipoplexes released from microbubbles by ultrasound do not enter the cell through an endocytic pathway. To evaluate this hypothesis, we first investigated the effect of inhibitors on the cellular uptake and transfection efficiency of respectively free lipoplexes and lipoplex loaded microbubbles exposed to ultrasound. We tested the effect of different endocytosis-interfering drugs (chlorpromazin, filipin, genistein, methyl- β -cyclodextrin, nystatin) on the transfection efficiency of free DOTAP/DOPE lipoplexes without or with 5 mol% DSPE-PEG. The 15 mol% PEGylated lipoplexes were excluded in this experiment, as the transfection efficiency of these lipoplexes (in the absence of microbubbles and ultrasound) is too low to observe any influence of an endocytic inhibitor. We found that M β CD, which depletes cholesterol from the cell membrane, caused the strongest inhibition of the gene expression of these lipoplexes (data not shown). This suggests a cholesterol-dependent uptake pathway in the BLM-cells for the free DOTAP/DOPE lipoplexes. This is in agreement with the work of Zuhorn et al.³⁶ who showed that cholesterol depletion of cells can extensively decrease the internalization of SAINT-2/DOPE lipoplexes. To assure that the decrease in gene expression caused by M β CD is really due to reduced endosomal uptake and not due to toxic effects on the cells, we evaluated the cytotoxicity of M β CD. As depicted in Figure 3, M β CD was not toxic for the BLM cells up to a concentration of 1500 μ M, i.e. the highest concentration used in our experiments.

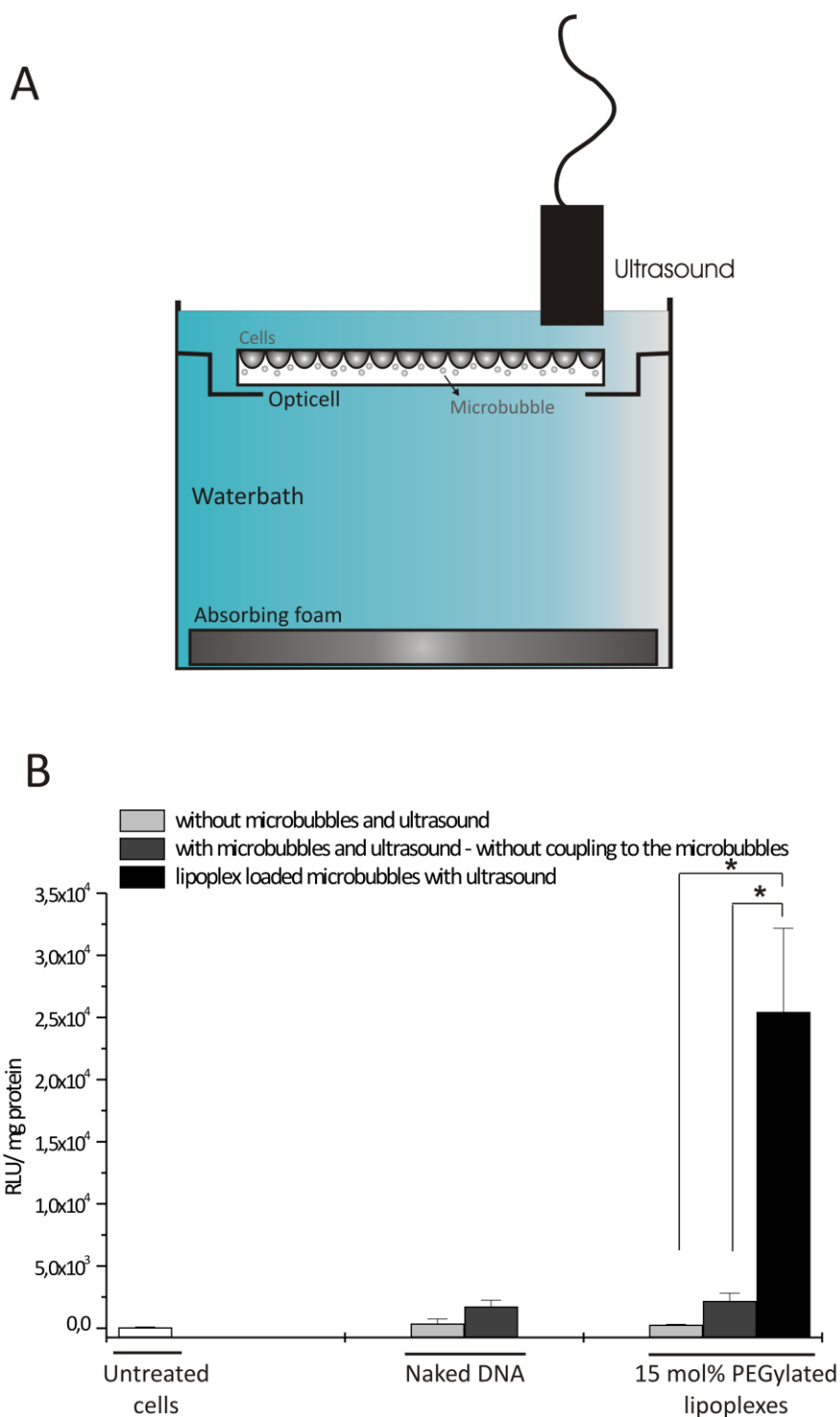


Figure 2A Schematic representation of the experimental set-up. Cells were grown on one side of an Opticell unit. For ultrasound exposure, Opticell plates were turned upside down. In this way, microbubbles were able to rise against the cell layer. **Figure 2B** The transfection efficiency of lipoplex loaded microbubbles in the presence of ultrasound (black bars) compared to the transfection efficiency of naked DNA and free 15 mol% PEGylated lipoplexes in the absence (light grey bars) and presence of microbubbles and ultrasound (dark grey bars). The background luciferase signal in untreated cells is also shown (white bars). The transfection results, i.e., the extent of luciferase expression, are expressed as RLU (RLU: relative light units) per mg protein. * $p < 0.05$

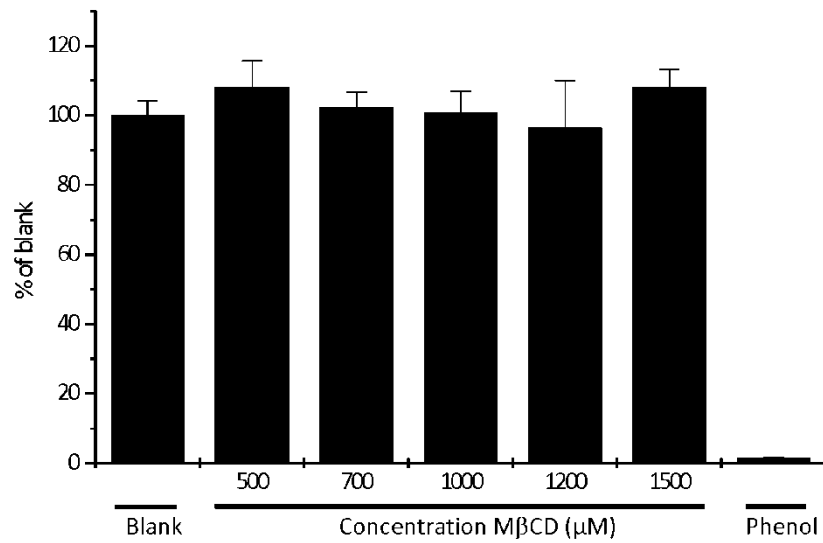


Figure 3 Cell viability of the BLM cells after incubation with different MβCD concentrations. Results are expressed as a percentage of the viability of untreated cells (blank). Phenol (10mg/mL) was used as a positive control.

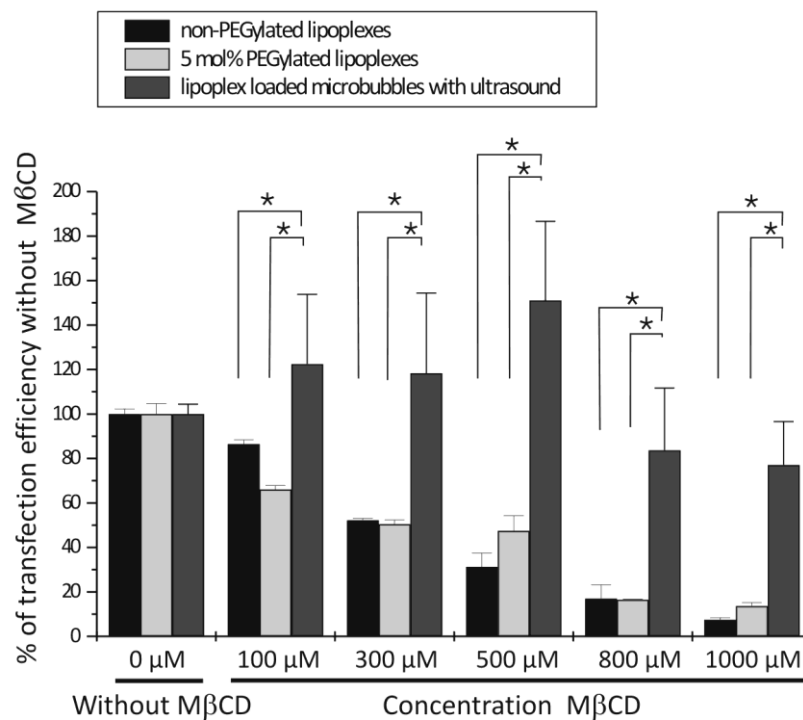


Figure 4 Effect of increasing MβCD concentrations on the transfection efficiency of non-PEGylated (black bars), 5 mol% PEGylated lipoplexes (light grey bars) and lipoplex loaded microbubbles (dark grey bars) exposed to ultrasound. Results are expressed as a percentage of the transfection efficiency obtained in cells in the absence of MβCD. * $p < 0.05$

Subsequently we studied the effect of M β CD on the transfection efficiency of (a) non-pegylated lipoplexes, (b) 5 mol% PEGylated lipoplexes and (c) microbubbles loaded with PEGylated lipoplexes exposed to ultrasound. As demonstrated in Figure 4, even the lowest M β CD concentrations had an influence on the transfection efficiency of the non-PEGylated (black bars) and PEGylated lipoplexes (light grey bars). Increasing the concentration of M β CD clearly diminished their transfection efficiency further. Via confocal microscopy we confirmed that M β CD reduced the gene expression of the lipoplexes by lowering the cellular uptake of the lipoplexes. Figure 5A-B shows the uptake of the non-PEGylated lipoplexes by BLM-cells in the absence of M β CD. A major part of the lipoplexes can be detected in the intracellular space. Incubation of the cells with 500 μ M M β CD (Figure 5C-D), and especially 1000 μ M M β CD (Figure 5E-F), almost completely blocked the cellular uptake of non-PEGylated lipoplexes. Similar images were obtained with the PEGylated lipoplexes.

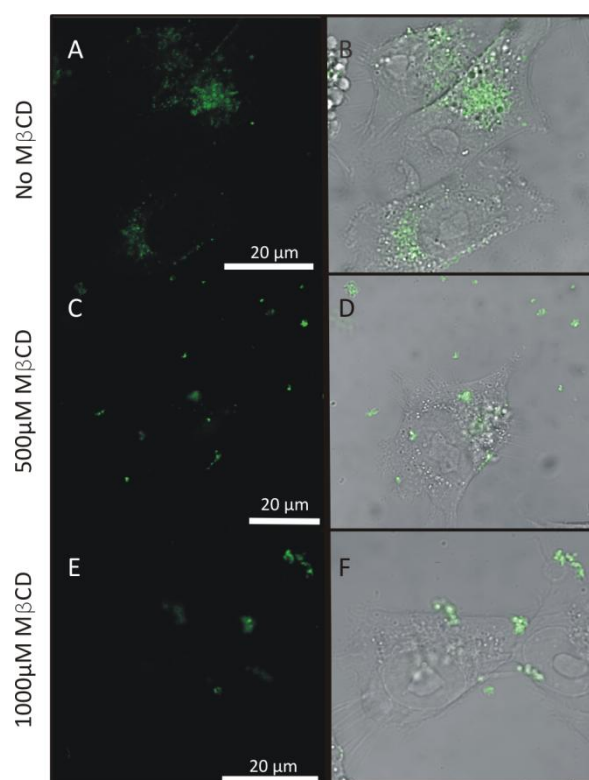


Figure 5 Effect of increasing M β CD concentrations on the uptake of non-PEGylated lipoplexes. Panels A, C and E are confocal fluorescence microscopy images and B, D and F are overlays of the confocal images with the corresponding transmission images. Fig. 5A and B. Uptake of non-PEGylated lipoplexes in the absence M β CD. Fig. 5C and D. Uptake of non-PEGylated lipoplexes in the presence of 500 μ M M β CD. Fig. 5E and F. Uptake of non-PEGylated lipoplexes in the presence of 1000 μ M M β CD. Cells were pre-incubated with the inhibitor 2 hours before addition of the non-PEGylated lipoplexes.

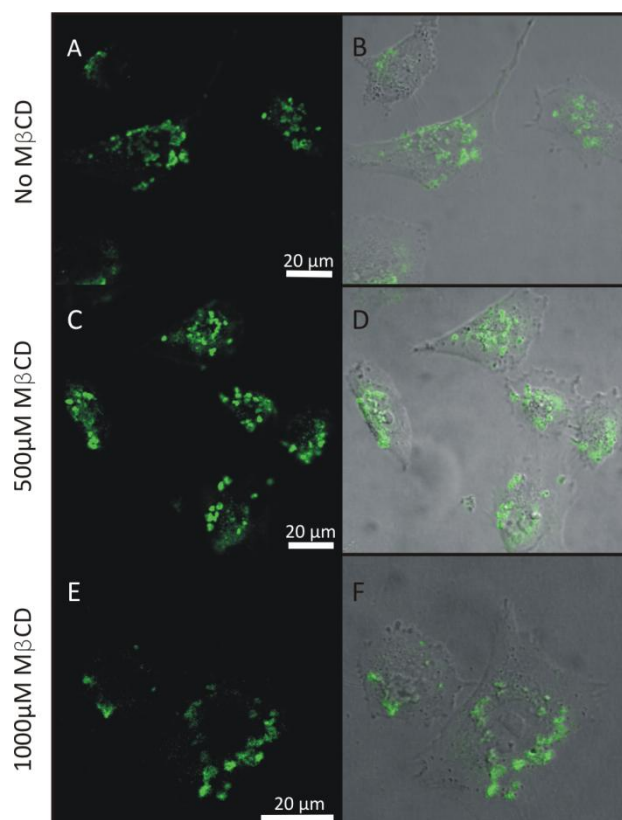


Figure 6 Effect of increasing M β CD concentrations on the uptake of PEGylated lipoplexes (originating from lipoplex loaded microbubbles exposed to ultrasound). Panels A, C and E are confocal fluorescence microscopy images and B, D and F are overlays of the confocal images with the corresponding transmission images. Fig. 6A and B: Uptake of PEGylated lipoplexes in the absence M β CD. Fig. 6 C and D: Uptake of PEGylated lipoplexes in the presence of 500 μ M M β CD. Fig. 6 E and F: Uptake of PEGylated lipoplexes in the presence of 1000 μ M M β CD. Cells were pre-incubated with the inhibitor two hours before treatment with lipoplex loaded microbubbles and ultrasound.

In contrast to the free lipoplexes, the transfection efficiency of the PEGylated lipoplexes loaded on the microbubbles and exposed to ultrasound was by far less sensitive to M β CD treatment, as depicted in Figure 4 (dark grey bars). The lowest concentrations (100 to 500 μ M) did not affect the transfection values at all. However, the transfection efficiency slightly dropped starting from 800 μ M M β CD onwards. We previously found that the ultrasound conditions used in these experiments had only minor effect on the cell viability (results not shown). However, it might be possible that an extensive depletion of cholesterol may make cells more vulnerable to ultrasound. This may explain the drop in gene expression at higher M β CD concentrations (Figure 4, dark grey bars). Alternatively, depletion of cholesterol may change the fluidity of the plasma membrane³⁷. As a result this may hamper the capability of ultrasound to cause cell perforations. Indeed, Brayman et al. suggested that the cell fluidity may influence the extent of membrane poration³⁷. Finally, we also evaluated the effect of M β CD on the cellular uptake of lipoplex loaded microbubbles after exposure to ultrasound

(Figure 6): image A-B, C-D and E-F present the uptake of the lipoplexes in the presence of 0, 500 and 1000 μM M β CD, respectively. In contrast to the free lipoplexes, M β CD was not able to prevent the cellular uptake of lipoplexes that were released from the lipoplex loaded microbubbles after exposure to ultrasound. These results clearly prove that the PEGylated lipoplexes released from the microbubbles, do not enter the cell by endocytosis after ultrasound radiation, this in contrast to the free lipoplexes.

Influence of photochemical internalization (PCI) on the transfection efficiency of free PEGylated lipoplexes and lipoplex loaded microbubbles exposed to ultrasound

We evaluated the effect of PCI on the transfection efficiency of free 15 mol% PEGylated lipoplexes (which are poorly transfecting) and lipoplex loaded microbubbles in the presence of ultrasound. PCI was first presented in 1999 as a novel technology for the delivery of a variety of therapeutic molecules into the cytosol³⁸. PCI technology employs amphiphilic, photosensitizing compounds which accumulate in the membranes of the vesicles. Upon illumination, such photosensitizers (PS) become excited, and subsequently induce the formation of reactive oxygen species, primarily singlet oxygens. These highly reactive intermediates can damage cellular components, but the short life-time and thus the short range of action, confines the damaging effect to the production site. This localized effect induces the disruption of the vesicles, thereby releasing the entrapped therapeutic molecules into the cytosol³⁹.

Figure 7 demonstrates that the transfection efficiency of free 15 mol% PEGylated lipoplexes became three times higher when PCI was used. In contrast, the transfection efficiency of the lipoplex loaded microbubbles was not enhanced by PCI. Figure 7 proves that the endosomal release is indeed a barrier, though not the only one, in the gene transfection process with highly PEGylated lipoplexes. The fact that the gene transfer by the same lipoplexes but loaded onto microbubbles and treated with ultrasound was not altered upon PCI implies that the lipoplexes released from the microbubbles are not present in the endosomes. These observations suggests that they transfect cells through a non-endocytic uptake mechanism that delivers the lipoplexes directly in the cytoplasm of the cells.

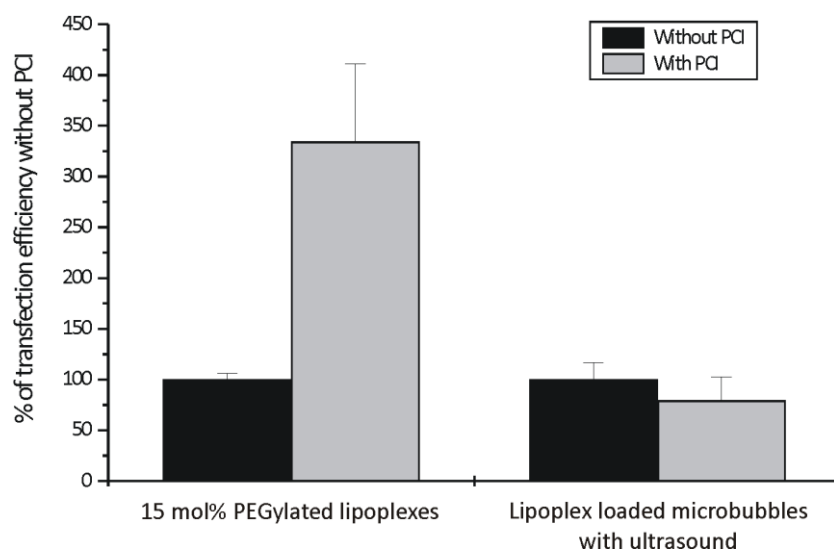


Figure 7 Effect of photochemical internalization (PCI) on the transfection efficiency of respectively 15 mol% PEGylated lipoplexes and lipoplex loaded microbubbles in the presence of ultrasound.

What happens at the cellular membrane during exposure of lipoplex loaded microbubbles to ultrasound?

First we studied the uptake of green labelled 15 mol% PEGylated lipoplexes into BLM-cells (at 37 °C) by confocal microscopy (Figure 8). Image 8A presents the cellular uptake of free lipoplexes 30 minutes after addition to the cells, while 8B and C present the cellular uptake of the same lipoplexes 150 minutes after addition to the cells. Free lipoplexes started to stick on the cell membranes shortly after their addition to the cells (Figure 8A). As indicated in image 8A, lipoplexes were not internalized 30 minutes after addition to the cells. Only after 150 minutes the lipoplexes were internalized by the BLM-cells: a punctuate pattern was observed which indeed suggests an endocytic uptake for the free PEGylated lipoplexes (Figure 8B and C). In contrast, we saw a completely different pattern 30 minutes after sonication of the cells in the presence of the lipoplex loaded microbubbles (Figure 8D). Lipoplexes were present near the cellular membrane and inside the cell. Similar images were obtained 150 minutes after treatment of the cells with lipoplex loaded microbubbles and ultrasound (Figure 8E and F); these images indicate that the uptake of the lipoplexes released from the microbubbles occurs during or immediately after ultrasound treatment.

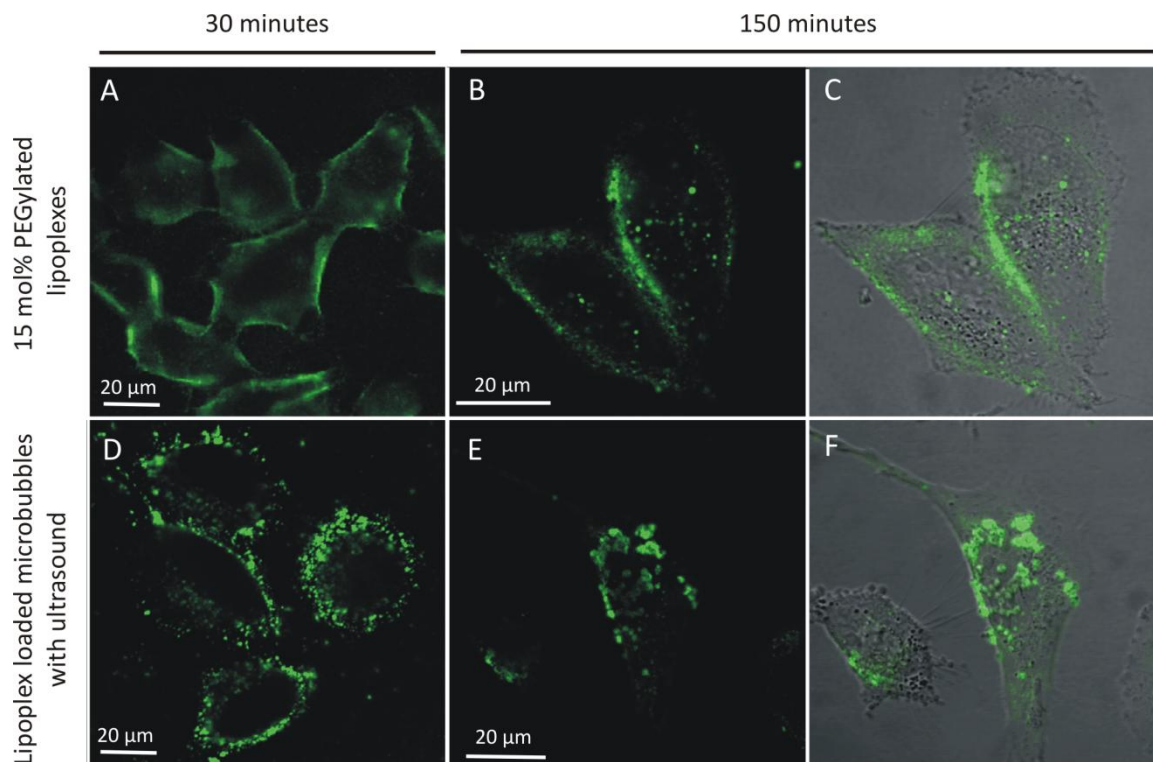


Figure 8A Uptake of free 15 mol% PEGylated lipoplexes in BLM cells a 30 minutes incubation after addition to the cells. **Figure 8B and C** Uptake of free 15 mol% PEGylated lipoplexes in BLM cells after 150 minutes incubation time. **Figure 8D** Uptake of lipoplexes in BLM cells 30 minutes after treatment with lipoplex loaded microbubbles and ultrasound. **Figure 8E and F** Uptake of lipoplexes in BLM cells 30 minutes after treatment with lipoplex loaded microbubbles and ultrasound. Lipoplexes were labelled with Bodipy FIC12 cholesteryl. **Figure 8A, B, C and D** are confocal fluorescence microscopy images and figures 8C and F are the overlays of the confocal images B and E with the corresponding transmission image.

To get further insight into the effect on the cell membrane we stained the cell membrane and took z-stacks of the BLM cells after incubating them with respectively free PEGylated lipoplexes (Figure 9A and C) and lipoplex loaded microbubbles exposed to ultrasound (Figure 9B and D). The first important difference between image 9A and 9B is the irregular shape of the BLM cells after sonication. This was also observed by several other groups^{18,37,40-42}. Although the shape of the cells was different after exposure to ultrasound and microbubbles, our propidium iodide uptake experiments proved that the cells were still viable (see Figure 10). In image 9A, a smooth, undisturbed cell membrane is visible (red) with PEGylated lipoplexes (green) lying on top of it, while a small part of the lipoplexes seems present in endocytic vesicles. Figure 9C displays the intensity

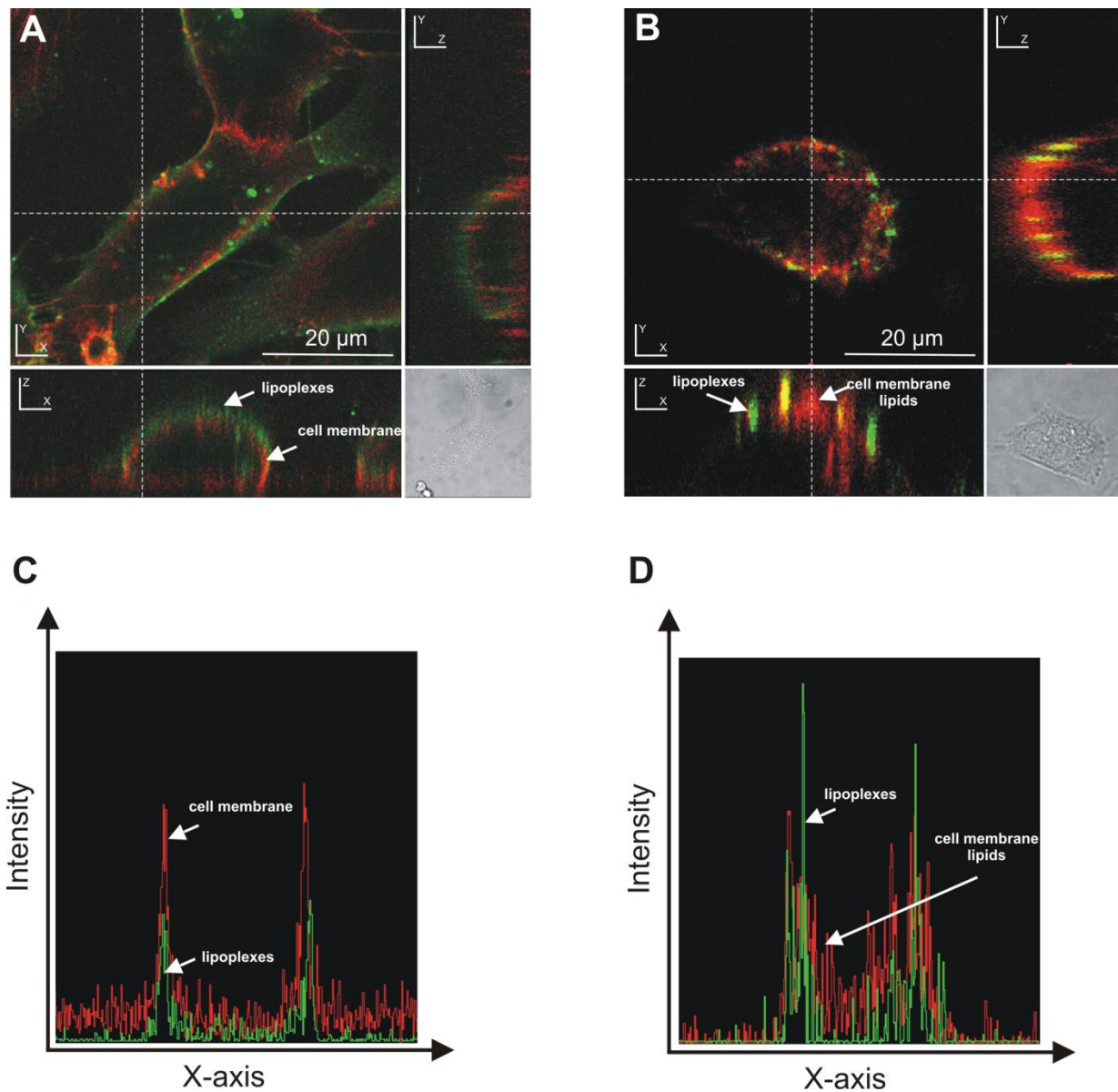


Figure 9A displays a confocal fluorescence microscopy image and z-scans (at the position indicated by the white dotted line) of a BLM cell that was incubated during 30 minutes with free PEGylated lipoplexes. **Figure 9B** displays a confocal fluorescence microscopy image and z-stacks, at the position indicated by the white dotted line, of BLM cells 30 minutes after treatment with lipoplex loaded microbubbles and ultrasound. The cell membrane was labelled red with concanavale A-Alexa637 and PEGylated lipoplexes are visible in green. Figure 9C and D present the according intensity profiles of respectively image A and B following the X-axis (white dotted line) through the cell.

profile of the green and red fluorescence following an X-axis (being the dotted line in Figure 9A) through the cell. This intensity profile in Figure 9C confirms that the lipoplexes are attached to the cell membrane as the green fluorescence of the lipoplexes colocalizes with the red fluorescence of the cell membrane. In image 9B the PEGylated lipoplexes appear as bright green structures pinching through the cell membrane. Furthermore the cell membrane seems disturbed and lipids seem to be relocated, resulting in lipid enhanced areas and areas lacking cell membrane lipids. Lipoplexes and membrane lipids seemed partially colocalized, visible as the yellow parts. Earlier, Schlicher et al. also reported on the displacement of large lipid areas from the cell membrane upon ultrasound treatment⁴¹. Also the intensity profile (Figure 9D) of this cell looks completely different: green lipoplexes are visible within the cell. The green spots in 8E and 9B most likely originate from intact lipoplexes as we recently showed that intact lipoplexes are released from the microbubbles after sonication of the lipoplex loaded microbubbles²². To be effective these lipoplexes must dissociate intracellularly, so that the DNA can enter the cell nucleus for transcription. Zuhorn and colleagues demonstrated that after endosome rupture by osmotic shock, lipoplexes still showed the same transfection efficiency, indicating that intact lipoplexes can dissociate in the cytosol⁴³. This is most likely also the case for the lipoplexes present in the BLM cells after their release from the lipoplex loaded microbubbles, as they have a very high transfection efficiency.

Why is the coupling of the lipoplexes to the microbubbles so important?

Figure 2B shows that the transfection efficiency of free PEGylated lipoplexes does not improve upon (physically) mixing them with microbubbles and applying ultrasound (dark grey bars). Therefore, we wondered whether the cells were perforated under our ultrasound conditions. To demonstrate the presence of pores in the cell membrane we determined whether propidium iodide (PI) was able to enter the cells during ultrasound exposure. Figure 10A presents the uptake of PI during incubation of the BLM cells with lipoplexes: as expected none of the BLM cells was able to take up PI. Figure 10B is an image of BLM cells to which PI, PEGylated lipoplexes and microbubbles were added and which were exposed to ultrasound. Almost all the cells had a bright red fluorescent nucleus, due to PI, which indicates that upon sonication pores are indeed created in the cell membranes which allow the passage of small molecules like PI. To exclude the possibility that all the red coloured cells were dead cells, we added PI 15 minutes after the exposure of the cells to ultrasound as only dead cells would then be able to take up PI; living cells are expected to quickly reseal their (transient) pores after applying ultrasound. As demonstrated in image 10C, only a small

fraction of the cells took up PI, which proves that the uptake of PI in Figure 10B can be ascribed to short-living pores in the cell membrane caused by ultrasound in the presence of microbubbles.

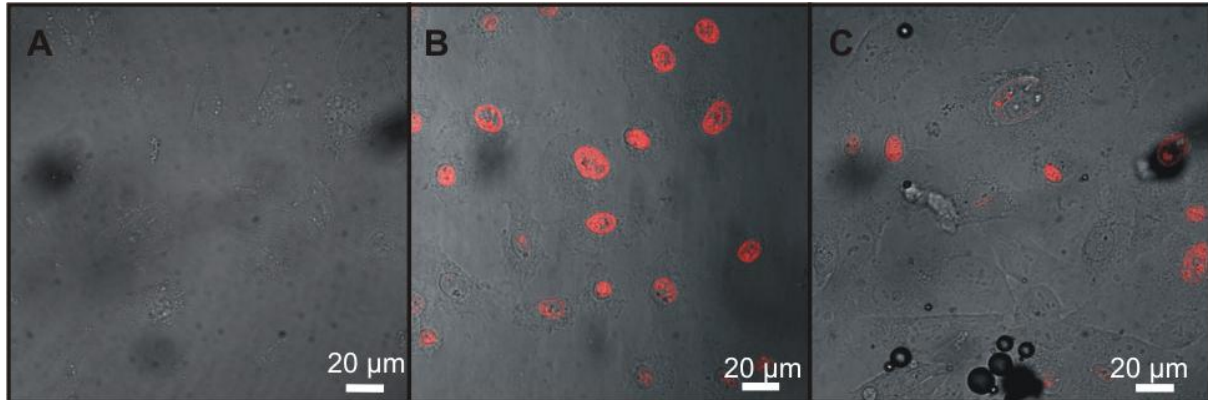


Figure 10 Cellular uptake of propidium iodide (PI) in BLM cells. **Figure 10A** PI uptake during incubation of the cells with free PEGylated lipoplexes. **Figure 10B** PI uptake in cells simultaneously exposed to PI, free PEGylated lipoplexes, microbubbles and ultrasound. **Figure 10C** Confocal image of cells that were first treated with free PEGylated lipoplexes, microbubbles and ultrasound and subsequently, after 15 minutes, exposed to PI.

Our data show that the attachment of the PEGylated lipoplexes to microbubbles is required to obtain a good gene transfer in the presence of ultrasound. We would like to present two hypothesis that may explain why the lipoplexes should be attached to the microbubbles. First, as the microbubbles rise against the cell surface, it is possible that the massive release of lipoplexes upon ultrasound radiation results in a higher lipoplex concentration near the cell perforations, which might increase the amount of lipoplexes that is able to passively diffuse through these pores. We estimated the concentration of lipoplexes released near the cells after exposure of the lipoplex loaded microbubbles to ultrasound. Therefore, we first determined how much of the lipoplexes are bound to the microbubbles after mixing the biotinylated lipoplexes and avidinylated microbubbles. Half of the lipoplexes is able to bind to the microbubbles. As presented in Figure 1B, the Opticells were incubated with the cell monolayer on top, so that microbubbles could rise against the cell surface. Let us assume that, after exposure of the lipoplex loaded microbubbles to ultrasound, all the lipoplexes are released in a 20 µm thick plane just beneath the cells present on the Opticell unit. The volume then equals 100µL (an Opticell unit has a surface of 50cm²). Taking into account that half of the lipoplexes are attached to the microbubbles, we can calculate that the local concentration of lipoplexes near the cell membrane (i.e. the concentration near the cell perforations) is 50 times higher than the lipoplex concentration near the cells when uncoupled lipoplexes are mixed with

microbubbles and exposed to ultrasound. Thus, the first hypothesis makes sense if the lipoplexes are small enough to pass through the cell perforations. This might be the case as pores of up to 1 μm have been reported^{41,44}.

The second hypothesis is that the microjets that occur when the microbubbles collapse drag along the released lipoplexes and inject them in and through the cell membrane. Ohl et al. and Dijkink et al. previously described the appearance of a jetting flow after the collapse of microbubbles in an ultrasonic field^{10,45}. These flow is directed towards the cell layer and causes shear stress on the cells which results in pore formation. During the implosion of the microbubbles, the lipoplexes are released and can be taken by this jetting flow towards the cell surface. In this way it might be possible that lipoplexes become ejected into the cell layer when the streaming forces are high enough. Our data obtained via confocal microscopy support this hypothesis (Figure 9). Additionally, Marmottant and Hilgenfeldt⁴⁶ visualized the behaviour of a lipid vesicle in the presence of a stable cavitating microbubble. This vesicle was expelled away from the cavitating microbubbles. It is possible that lipoplexes are taken by these fluid streams around the microbubble and in this way propelled, so that they are deposited in the adjacent cell layer. Especially as most of our microbubbles are cavitating transiently and are able to implode, which will cause even stronger streaming forces. The actual lipoplex uptake will most presumably be a combination of the two described hypothesis, as an increased local lipoplex concentration will make it more plausible that a lipoplex is taken by these fluid streams and increases the chance that it is deposited near or in the cell membrane (pores).

As earlier mentioned, the aim of this work was to elucidate how the transfection efficiency of PEGylated lipoplexes can be increased by loading them onto lipid microbubbles and expose them to ultrasound. Our results clearly show that endocytosis of the lipoplexes is circumvented and that lipoplexes are able to reach the cytoplasm of the radiated cells. However, direct microscopic observations of the lipoplex loaded microbubbles during ultrasound exposure are required to elucidate the exact uptake mechanisms.

CONCLUSION

In this study we elucidate the cellular mechanism responsible for the high gene transfection efficiency of lipoplex loaded microbubbles in the presence of ultrasound. Inhibition of the endocytotic activity of the cells demonstrated that the cellular uptake of the lipoplexes released from the lipoplex loaded microbubbles by ultrasound must be governed by a non-endocytotic pathway.

Indeed, blockage of the endocytotic activity or stimulation of the endosomal release via PCI did not affect the gene expression of the lipoplex loaded microbubbles after exposure to ultrasound. Confocal images demonstrated that shortly after exposure of the BLM cells to lipoplex loaded microbubbles and ultrasound, lipoplexes are present in the cell membrane and in the intracellular space. In contrast, classic “free” PEGylated lipoplexes mainly adhere on top of the cell membranes. We also observed that the cell membranes became disturbed after applying ultrasound and lipoplex loaded microbubbles. The addition of propidium iodide during the sonication step proved that there were short-living pores formed. As ultrasound could not improve the gene transfer of PEGylated lipoplexes that were physically mixed (and thus not chemically bound) to microbubbles, it seems that coupling of lipoplexes and microbubbles is necessary to obtain a high transfection value. Loading of the lipoplexes onto the microbubbles leads to an increase in local lipoplex concentration near the cell membrane. Because we have shown that cell membrane porations are formed during our ultrasound exposure, it is possible that more lipoplexes are able to passively diffuse through these pores. Moreover, lipoplexes might be propelled by the fluid streams that develop around a cavitating and imploding microbubble and propelled inside the adjacent cell layer. However, real time fluorescence imaging of the lipoplexes during the ultrasound step will be required to completely understand their cellular entrance. In summary, we have proven that the endocytotic uptake of PEGylated particles can be avoided by loading these particles onto microbubbles and applying ultrasound. In this manner the lipoplexes become directly delivered into the cytoplasm of the cell. So far the lack of gene transfer hampered the clinical use of PEGylated lipoplexes. We believe that lipoplex loaded microbubble may overcome this. Clearly, besides lipoplexes one can also attach other drugs or drug containing nanoparticles to the microbubbles which makes this material of special interest for time and space controlled delivery of drugs.

ACKNOWLEDGMENTS

Ine Lentacker is a doctoral fellow of Fund for Scientific Research-Flanders. Niek N. Sanders is a Postdoctoral Fellow of the Fund for Scientific Research—Flanders (Belgium). The financial support of FWO, BOF-Ghent and the European Union (via the FP7 Projects Arise and SonoDrugs) are acknowledged.

REFERENCES

- (1) Marshall E. Clinical trials –Gene Therapy Death Prompts Review of Adenovirus Vector. *Science* **1999** 286(5448) 2244-2245 .
- (2) Patil S.D., Rhodes D.G., & Burgess D.J. DNA-based therapeutics and DNA delivery systems: a comprehensive review. *AAPS Journal* **2005** 7(1) E61-E77.
- (3) Eliyahu H., Serval N., Domb A.J., & Barenholz Y. Lipoplex-induced hemagglutination: potential involvement in intravenous gene delivery. *Gene Therapy* **2002** 9(13) 850-858.
- (4) Moghimi S.M. & Szebeni J. Stealth liposomes and long circulating nanoparticles: critical issues in pharmacokinetics, opsonization and protein-binding properties. *Progress in Lipid Research* **2003** 42(6) 463-478.
- (5) Sakurai F., Nishioka T., Yamashita F., Takakura Y., & Hashida M. Effects of erythrocytes and serum proteins on lung accumulation of lipoplexes containing cholesterol or DOPE as a helper lipid in the single-pass rat lung perfusion system. *European Journal of Pharmaceutics and Biopharmaceutics* **2001** 52(2) 165-172.
- (6) Meyer M. & Wagner E. Recent developments in the application of plasmid DNA-based vectors and small interfering RNA therapeutics for cancer. *Human gene therapy* **2006** 17(11) 1062-1076.
- (7) Wong J.B., Grosse S., Tabor A.B., Hart S.L., & Hailes H.C. - Acid cleavable PEG-lipids for applications in a ternary gene delivery vector. *Molecular bioSystems* **2008** 4(6) 532-541.
- (8) Hernot S. & Klibanov A.L. Microbubbles in ultrasound-triggered drug and gene delivery. *Advanced Drug Delivery Reviews* **2008** 60(10) 1153-1166.
- (9) Riess J.G. Fluorocarbon-based injectable gaseous microbubbles for diagnosis and therapy. *Current Opinion in Colloid & Interface Science* **2003** 8(3) 259-266.
- (10) Ohl C.D., Arora M., Ikink R. *et al.* Sonoporation from jetting cavitation bubbles. *Biophysical journal* **2006** 91(11) 4285-4295.
- (11) Newman C.M.H. & Bettinger T. Gene therapy progress and prospects: Ultrasound for gene transfer. *Gene Therapy* **2007** 14(6) 465-475.
- (12) Grayburn P.A. Current and future contrast agents. *Echocardiography-A Journal of Cardiovascular Ultrasound and Allied Techniques* **2002** 19(3) 259-265.
- (13) Bekeradjian R., Chen S.Y., Grayburn P.A., & Shohet R.V. Augmentation of cardiac protein delivery using ultrasound targeted microbubble destruction. *Ultrasound in Medicine and Biology* **2005** 31(5) 687-691.
- (14) Duvshani-Eshet M. & Machluf M. Therapeutic ultrasound optimization for gene delivery: A key factor achieving nuclear DNA localization. *Journal of Controlled Release* **2005** 108(2-3) 513-528.

- (15) Kinoshita M & Hynynen K. A novel method for the intracellular delivery of siRNA using microbubbles-enhanced focused ultrasound. *Biomedical and Biophysical Research Communications* **2005** 335(2) 393-399.
- (16) Kinoshita M. & Hynynen K. Intracellular delivery of Bak BH3 peptide by microbubble-enhanced ultrasound. *Pharmaceutical Research* **2005** 22(5) 716-720.
- (17) Manome Y., Nakayama N., Nakayama K., & Furuhashi H. Insonation facilitates plasmid DNA transfection into the central nervous system and microbubbles enhance the effect. *Ultrasound in Medicine and Biology* **2005** 31(5) 693-702.
- (18) Mehier-Humbert S., Bettinger T., Yan F., & Guy R.H. Plasma membrane poration induced by ultrasound exposure: Implication for drug delivery. *Journal of Controlled Release* **2005** 104(1) 213-222.
- (19) Newman C.M., Lawrie A., Brisken A.F., & Cumberland D.C. Ultrasound gene therapy: On the road from concept to reality. *Echocardiography-A Journal of Cardiovascular Ultrasound and Allied Techniques* **2001** 18(4) 339-347.
- (20) Pislaru S.V., Pislaru C., Kinnick R.R. *et al.* Optimization of ultrasound-mediated gene transfer: comparison of contrast agents and ultrasound modalities. *European Heart Journal* **2003** 24(18) 1690-1698.
- (21) Vannan M., McCreery T., Li P. *et al.* Ultrasound-mediated transfection of canine myocardium by intravenous administration of cationic microbubble-linked plasmid DNA. *Journal of the American Society of Echocardiography* **2002** 15(3) 214-218.
- (22) Lentacker I., De Smedt S.C., Demeester J., Van Marck V., Bracke M., & Sanders N.N. Lipoplex-loaded microbubbles for gene delivery: A Trojan horse controlled by ultrasound. *Advanced Functional Materials* **2007** 17(12) 1910-1916.
- (23) Vandenbroucke R.E., Lentacker I., Demeester J., De Smedt S.C., & Sanders N.N. Ultrasound assisted siRNA delivery using PEG-siPlex loaded microbubbles. *Journal of controlled release* **2007** 126(3) 265-273.
- (24) Sanders N.N., Van Rompaey E., De Smedt S.C., & Demeester J. Structural alterations of gene complexes by cystic fibrosis sputum. *American Journal of Respiratory and Critical Care Medicine* **2001** 164(3) 486-493.
- (25) Quax P.H.A., Vanmuijen G.N.P., Weeningverhoeff E.J.D. *et al.* Metastatic Behavior of Human-Melanoma Cell-Lines in Nude-Mice Correlates with Urokinase-Type Plasminogen-Activator, Its Type-1 Inhibitor, and Urokinase-Mediated Matrix Degradation. *Journal of Cell Biology* **1991** 115(1) 191-199.
- (26) von Gersdorff K., Sanders N.N., Vandenbroucke R., De Smedt S.C., Wagner E., & Ogris M. The internalization route resulting in successful gene expression depends on polyethylenimine both cell line and polyplex type. *Molecular Therapy* **2006** 14(5) 745-753.
- (27) Koch S., Pohl P., Cobet U., & Rainov N.G. Ultrasound enhancement of liposome-mediated cell transfection is caused by cavitation effects. *Ultrasound in Medicine and Biology* **2000** 26(5) 897-903.

- (28) Lawrie A., Brisken A.F., Francis S.E., Cumberland D.C., Crossman D.C., & Newman C.M. Microbubble-enhanced ultrasound for vascular gene delivery. *Gene Therapy* **2000** 7(23) 2023-2027.
- (29) Unger E.C., McCreery T.P., & Sweitzer R.H. Ultrasound enhances gene expression of liposomal transfection. *Investigative Radiology* **1997** 32(12) 723-727.
- (30) Wasungu L. & Hoekstra D. Cationic lipids, lipoplexes and intracellular delivery of genes. *Journal of controlled release* **2006** 116(2) 255-264.
- (31) Audouy S. & Hoekstra D. Cationic lipid-mediated transfection in vitro and in vivo. *Molecular Membrane Biology* **2001** 18(2) 129-143.
- (32) Meyer O., Kirpotin D., Hong K.L. *et al.* Cationic liposomes coated with polyethylene glycol as carriers for oligonucleotides. *Journal of Biological Chemistry* **1998** 273(25) 15621-15627.
- (33) Mishra S., Webster P., & Davis M.E. PEGylation significantly affects cellular uptake and intracellular trafficking of non-viral gene delivery particles. *European Journal of Cell Biology* **2004** 83(3) 97-111.
- (34) Shi F.X., Wasungu L., Nomden A. *et al.* Interference of poly(ethylene glycol)-lipid analogues with cationic-lipid-mediated delivery of oligonucleotides; role of lipid exchangeability and non-lamellar transitions. *Biochemical Journal* **2002** 3(66) 333-341.
- (35) Song L.Y., Ahkong Q.F., Rong Q. *et al.* Characterization of the inhibitory effect of PEG-lipid conjugates on the intracellular delivery of plasmid and antisense DNA mediated by cationic lipid liposomes. *Biochimica et Biophysica Acta-Biomembranes* **2002** 1558(1) 1-13.
- (36) Zuhorn I.S., Kalicharan R., & Hoekstra D. Lipoplex-mediated transfection of mammalian cells occurs through the cholesterol-dependent clathrin-mediated pathway of endocytosis. *Journal of Biological Chemistry* **2002** 277(20) 18021-18028.
- (37) Brayman A.A., Coppage M.L., Vaidya S., & Miller M.W. Transient poration and cell surface receptor removal from human lymphocytes in vitro by 1 MHz ultrasound. *Ultrasound in Medicine and Biology* **1999** 25(6) 999-1008.
- (38) Berg K., Selbo P.K., Prasmickaite L. *et al.* Photochemical internalization: a novel technology for delivery of macromolecules into cytosol. *Cancer research* **1999** 59(6) 1180-1183.
- (39) Prasmickaite L., Hogset A., Tjelle T.E., Olsen V.M., & Berg K. Role of endosomes in gene transfection mediated by photochemical internalisation (PCI). *Journal of Gene Medicine* **2000** 2(6) 477-488.
- (40) Ross J.P., Cai X., Chiu J.F., Yang J., & Wu J.R. Optical and atomic force microscopic studies on sonoporation. *Journal of the Acoustical Society of America* **2002** 111(3) 1161-1164.
- (41) Schlicher R.K., Radhakrishna H., Tolentino T.P., Apkarian R.P., Zarnitsyn V., & Prausnitz M.R. Mechanism of intracellular delivery by acoustic cavitation. *Ultrasound in Medicine and Biology* **2006** 32(6) 915-924.
- (42) Zhao Y.Z., Luo Y.K., Lu C.T. *et al.* Phospholipids-based microbubbles sonoporation pore size and reseal of cell membrane cultured in vitro. *Journal of Drug Targeting* **2008** 16(1) 18-25.

- (43) Zuhorn I.S., Visser W.H., Bakowsky U., Engberts J.B.F.N., & Hoekstra D. Interference of serum with lipoplex-cell interaction: modulation of intracellular processing. *Biochimica et Biophysica Acta-Biomembranes* **2002** 1560(1-2) 25-36.
- (44) Prentice P., Cuschierp A., Dholakia K., Prausnitz M., & Campbell P. Membrane disruption by optically controlled microbubble cavitation. *Nature Physics* **2005** 1(2) 107-110.
- (45) Dijkink R., Le G.S., Nijhuis E. *et al.* Controlled cavitation-cell interaction: trans-membrane transport and viability studies. *Physics in medicine and biology* **2008** 53(2) 375-390.
- (46) Marmottant P. & Hilgenfeldt S. Controlled vesicle deformation and lysis by single oscillating bubbles. *Nature* **2003** 423(6936) 153-156.

Chapter 6

Ultrasound assisted siRNA delivery using PEG-siPlex loaded microbubbles

This chapter is published.

Vandenbroucke R.E.^{1*}, Lentacker I.^{1*}, Demeester J.¹, De Smedt S.C.¹ and Sanders N.N.¹; *Journal of Controlled Release* **2008** 126(3) 265-273.

¹ Laboratory of General Biochemistry and Physical Pharmacy, Department of Pharmaceutics Ghent University, Ghent, Belgium.

* Both authors contributed equally to this work.

ABSTRACT

Short interfering RNA (siRNA) attracts much attention for the treatment of various diseases. However, its delivery, especially via systemic routes, remains a challenge. Indeed, naked siRNAs are rapidly degraded, while complexed siRNAs massively aggregate in the blood or are captured by macrophages. Although this can be circumvented by PEGylation, we found that PEGylation had a strong negative effect on the gene silencing efficiency of siRNA-liposome complexes (siPlexes). Recently, ultrasound combined with microbubbles has been used to deliver naked siRNA but the gene silencing efficiency is rather low and very high amounts of siRNA are required. To overcome the negative effects of PEGylation and to enhance the efficiency of ultrasound assisted siRNA delivery, we coupled PEGylated siPlexes (PEG-siPlexes) to microbubbles. Ultrasound radiation of these microbubbles resulted in massive release of unaltered PEG-siPlexes. Interestingly, PEG-siPlexes loaded on microbubbles were able to enter cells after exposure to ultrasound, in contrast to free PEG-siPlexes, which were not able to enter cells rapidly. Furthermore, these PEG-siPlex loaded microbubbles induced, in the presence of ultrasound, much higher gene silencing than free PEG-siPlexes. Additionally, the PEG-siPlex loaded microbubbles only silenced the expression of genes in the presence of ultrasound, which allows space and time controlled gene silencing.

Chapter 6

Ultrasound assisted siRNA delivery using PEG-siPlex loaded microbubbles

INTRODUCTION

RNA interference (RNAi), a naturally occurring process of sequence-specific post-transcriptional gene silencing, is an important biological process for modulating gene expression. The silencing effect of RNAi is highly potent and requires only that the sequence of the target RNA is known. One approach to evoke RNAi in target cells is by the delivery of chemically synthesized siRNAs, which results in a sequence-specific, robust silencing of the targeted gene¹. The potential of siRNA molecules as therapeutic agent in the treatment of e.g. cancer, viral infections, arthritis, Huntington's disease and hypercholesterolemia has been widely studied². However, cells do not readily take up siRNAs. Therefore, clinical applications of siRNA largely depend on the development of delivery systems that can bring intact siRNA into the cytoplasm of the target cells of a patient.

Strategies that have been considered for *in vivo* delivery of synthetic siRNA in laboratory animals are hydrodynamic injection of naked siRNA³ or siRNA conjugates⁴, electroporation⁵⁻⁸ and the use of cationic carriers⁹⁻¹⁵. However, several aspects limit the applicability of these methods in humans. Indeed, hydrodynamic injection, which involves the intravascular injection of large volumes, generates high pressure in the vascular system and therefore often results in heart failure. Additionally, undesirable gene suppression may be induced in non-target organs. Electroporation allows targeting, but requires the insertion of electrodes into the target area, and hence invasive procedures that limit its range of application. Cationic siRNA delivery carriers, such as cationic lipids and polymers, are often cytotoxic and/or not very efficient. Furthermore, they are often not suited for systemic application since their positively charged surface makes them vulnerable to non-specific interactions with blood compounds, leading to life-threatening aggregates and a rapid clearance by the mononuclear phagocyte system^{10,16}. A common approach for reducing these undesired interactions is by masking the cationic surface of the nanoparticles with hydrophilic polymers, such as poly(ethylene glycol) (PEG). This prevents the aggregation of these nucleic acid containing

nanoparticles in blood and prolongs their circulation time¹⁷⁻²⁰. However, it has been observed by many groups that shielding the surface of non-viral gene delivery systems with polymers like PEG leads to a drastic reduction in gene transfer, due to a reduced cellular uptake or limited endosomal release^{21,22}.

The use of ultrasound energy has intensively been studied for pDNA delivery²³⁻³⁰. Recently, ultrasound in combination with microbubbles has also been used in two reports to deliver naked siRNA^{31,32}. However, the gene silencing efficiency in these studies was rather low and very high amounts of siRNA were required. Nevertheless, ultrasound assisted drug delivery is considered as rather safe as ultrasound, in combination with microbubbles, is routinely used in the clinic for diagnostic purposes. It is believed that ultrasound, especially when combined with microbubbles, causes small (100 to a few 100 nm large) transient pores in the cell membrane which allows large molecules to enter the cell cytoplasm³³. These perforations are caused by microjets that are generated by the ultrasound induced cavitation, i.e. alternate growing and shrinking of microbubbles, and implosion of microbubbles. The lifetime of these pores in the cell membranes is very short, i.e. milliseconds to seconds³⁴, making high concentrations of nucleic acids in the surrounding of the cells beneficial to ensure that a significant amount of nucleic acids can enter the cells through these short-living pores. Consequently, as recently shown by our group for pDNA, microbubbles that at the same time perforate cells and release massive amounts of nucleic acids containing nanoparticles near these perforations may drastically enhance the cellular uptake and hence the biological activity of nucleic acids²⁶.

Therefore, the aim of this study was to evaluate (a) the loading and release of PEGylated siRNA-liposome complexes (PEG-siPlexes) on/off ultrasound responsive microbubble, and (b) the cellular distribution and gene silencing efficiency of the PEG-siPlex loaded microbubbles after ultrasound radiation.

MATERIALS & METHODS

Cell culture

HuH-7 and HuH-7_eGFPLuc cells were cultured in Dulbecco's modified Eagle's medium supplemented with F12 (DMEM:F12) containing 2 mM L-glutamine (L-Gln), 10 % heat-inactivated fetal bovine serum (FBS) and 100 U/ml penicilline/streptomycine (P/S) at 37°C in a humidified atmosphere containing 5 % CO₂. All cell culture products were purchased from Invitrogen (Merelbeke, Belgium).

HuH-7_eGFP_{Luc} cells stably expressing eGFP-Luciferase were generated by transfecting HuH-7 cells with the vector pEGFP_{Luc} (Clontech, Palo Alto, USA). The vector was linearized using the restriction enzyme *Dra*III and transfected using linear poly(ethyleneimine) (PEI) 22 kDa. Transfected cells were incubated in fresh medium for 72 hrs and then selected with 60 to 400 µg/ml G418. After several days, surviving cells were seeded at low densities into 6-well plates in order to generate separate colonies. Single cell clones were then isolated and expanded. The generated clones were analyzed for the percentage of GFP-positive (eGFP_{Luc} stably transfected) cells. Clones with the highest number of GFP-positive cells were then further selectively grown up under the above described selective conditions and this procedure was repeated until all cells were positive for GFP.

SiRNA

Atto488-labeled and non labeled siRNA duplexes against firefly luciferase and control siRNA duplexes were purchased from Eurogentec (Seraing, Belgium) and dissolved in RNase free water at a final concentration of 20 µM.

Preparation and characterization of lipid microbubbles

1,2-Dipalmitoyl-sn-glycero-3-phosphocholine (DPPC) and 1,2-distearoyl-sn-glycero-3-phosphoethanolamine-N-[biotinyl(polyethylene glycol)2000] (ammonium salt) (DSPE-PEG₂₀₀₀-biotin) were purchased from Avanti Polar Lipids (Alabaster, AL).

Lipid microbubbles were prepared from liposomes composed of DPPC and DSPE-PEG₂₀₀₀-biotin with molar ratios of 95:5. Therefore, as described previously³⁵, appropriate amounts of lipids were dissolved in chloroform and mixed. The chloroform was subsequently removed by rotary evaporation at 37°C followed by flushing the obtained lipid film with nitrogen during 30 min at room temperature. The dried lipids were then hydrated by adding Hepes buffer (20 mM, pH 7.4) till a final lipid concentration of 5 mg/ml. After mixing in the presence of glass beads, liposome formation was allowed overnight at 4°C. Thereafter, the DPPC:DSPE-PEG₂₀₀₀-biotin liposomes were extruded through two stacked 0.200 µm polycarbonate membrane filters (Whatman; Brentfort, UK) at 55°C using an Avanti Mini-Extruder (Avanti Polar Lipids). Subsequently, the liposome suspension was sonicated with a 20 kHz probe (Branson 250 sonifier, Branson Ultrasonics Corp.; Danbury, CT) in the presence of perfluorobutane gas (MW 238 g/mol; F2 chemicals; Preston, Lancashire, UK). After sonication, the lipid microbubbles were washed with 3 ml Hepes buffer by 5 min centrifugation at 470 g. The amount of microbubbles per ml was determined by light microscopy and equalled 4×10^8

microbubbles/ml. The size distribution of the microbubbles was determined by laser diffraction (Mastersizer S, Malvern; Worcestershire, UK).

Preparation of avidin coated lipid microbubbles

Avidinylated microbubbles were prepared by incubating them at room temperature with 500 μ l avidin (10 mg/ml). After 10 min of incubation, the microbubbles were washed with 3 ml Hepes buffer by 5 min centrifugation at 470 g and finally resuspended in 10 ml. For the preparation of red labelled lipid microbubbles, the microbubbles were incubated with the unlabelled avidin supplemented with 50 μ l Cy5-labelled streptavidin (1 mg/ml) (Zymed Laboratories; San Francisco, CA).

Preparation and characterization of liposomes and PEG-siPlexes

The cationic lipid 1,2-dioleoyl-3-trimethylammonium-propane (chloride salt) (DOTAP) and the helper lipid 1,2-dioleoyl-sn-glycero-3-phosphoethanolamine (DOPE) were purchased from Avanti Polar Lipids. Cationic liposomes containing DOTAP and DOPE in a 1:1 molar ratio, supplemented with 0 to 15 mol% DSPE-PEG₂₀₀₀-biotin, were prepared at a final DOTAP concentration of 5 mM. All liposomes were prepared as described above for the DPPC:DSPE-PEG₂₀₀₀-biotin liposomes, however extrusion occurred through two stacked 0.100 μ m polycarbonate membrane filters at room temperature. To obtain (PEG-)siPlexes, equal volumes of siRNA solution and extruded liposomes were mixed in a N:P ratio of 20:1. Subsequently, the obtained mixture was vortexed for 5 sec and incubated at room temperature for 30 min.

The average particle size and the zeta potential (ζ) of the (PEGylated) liposomes and siPlexes were measured by photon correlation spectroscopy (PCS) (Malvern zetasizer nano ZS; Malvern) and by particle electrophoresis (Malvern zetasizer nano ZS; Malvern), respectively. Therefore, the liposome and PEG-siPlex dispersions were diluted 40-fold in 20 mM Hepes buffer. The size of the liposomes was independent of the degree of PEGylation and averaged 120 nm. In contrast, the zeta potential clearly dropped with increasing degree of PEGylation, varying from \sim 50 mV for the 0 mol% and \sim 20 mV for the 5 mol% DSPE-PEG₂₀₀₀-biotin containing DOTAP:DOPE liposomes. The size and zeta potential of the siPlexes are displayed in Fig. 5.

Preparation and characterization of siPlexes loaded microbubbles

130 μ l siPlex dispersion was mixed with 1 ml microbubbles, vortexed shortly and incubated at room temperature for 5 min. Subsequently, the size distribution of the siPlex loaded microbubbles was determined as described for the non-loaded microbubbles. The time-dependent stability of the (PEG-)siPlex loaded microbubbles was followed for 36 hrs at room temperature via light microscopy using a motorized Nikon TE2000-E inverted microscope (Nikon Benelux, Brussels, Belgium). The small microbubbles ($< 2 \mu$ m) were stable for at least 24 hrs and the larger ones for at least 36 hrs.

Gel electrophoresis

(PEG-)siPlexes, before binding to the microbubbles and after ultrasound induced release from the microbubbles, were loaded on a native 20 % polyacrylamide gel (PAGE). All samples were supplemented with 10 % glycerol and subjected to electrophoresis at 100 V for 2 hrs. Finally, the siRNA was stained with 1:10000 diluted SYBR-green II dye (Molecular Probes; Merelbeke, Belgium) and visualized by UV transillumination.

Confocal laser scanning microscopy

The Cy5-streptavidin coated microbubbles and Atto488-siRNA containing siPlexes were visualized using a Nikon C1si confocal laser scanning module attached to a motorized Nikon TE2000-E inverted microscope (Nikon Benelux; Brussels, Belgium). Images were captured with a 60 x objective lens using the 488 nm line from an Ar-ion laser for the excitation of Atto488-siRNA and the 639 nm laser line from a diode laser for the excitation of Cy5-streptavidin.

Cellular distribution of PEG-siPlexes in HuH-7 cells

Atto488-siRNA containing PEG-siPlexes (with 5 mol% DSPE-PEG₂₀₀₀-biotin) were prepared as described above. HuH-7 cells were grown in OptiCells and incubated for 20 min with the free PEG-siPlexes or with the PEG-siPlexes loaded microbubbles, immediately followed by ultrasound treatment. The ultrasound settings were the same as in the transfection experiments (see below). After one wash step with phosphate buffered saline (PBS; Invitrogen), cells were treated for 10 min with Draq5 (Biostatus Limited; Leicestershire, UK), to stain the nucleus, and TRITC-concanavalin A (Molecular Probes), to stain the cellular membrane. Subsequently, the cellular distribution of the Atto488-siRNA was visualized using a Nikon EZC1-si confocal laser scanning microscope equipped

with a 60 x objective. The 488 nm line of the Ar-ion laser was used to excite the Atto488 label and the 639 nm line from a diode laser to excite Draq5 and TRITC-concanavalin A.

Transfection experiments

HuH-7_eGFPLuc cells were seeded in OptiCell units (Biocrystal; Westerville, OH) at 4×10^4 cells/cm², and allowed to attach overnight in a humidified incubator at 37°C and 5 % CO₂. The culture medium was removed from the cells and after a washing step with PBS, the free siPlexes or siPlex loaded microbubbles, both dissolved in OptiMEM (Invitrogen) and containing 50 nM siRNA, were added to the OptiCell units. Subsequently, the OptiCell units were placed in a water bath at 37°C with an absorbing rubber at the bottom as shown in Fig. 1B and immediately subjected to ultrasound radiation for 10 sec with a sonitron 2000 (RichMar; Inola, OK) equipped with a 22 mm probe. It has been reported that standing waves can influence the ultrasound assisted transfection efficiency dramatically³⁶. In our ultrasound set up (Fig. 1B) standing waves are eliminated as much as possible by (1) using the ultrasound transparent OptiCell units, (2) placing an absorbing rubber at the bottom of the water bath and (3) degassing the water. In all experiments the same ultrasound settings were applied: 1 MHz, 10 % duty cycle (DC) and an ultrasound intensity of 2 W/cm² during 10 sec. After 2 hrs incubation of the cells (at 37°C) with the free siPlexes or siPlex loaded microbubbles, the transfection medium was removed, cells were washed twice with PBS and culture medium was added. After 48 hrs incubation, discs (22 mm in diameter) were cut from the OptiCell membrane, transferred to a 24-well plate and lysed with 80 µl 1x CCLR buffer (Promega; Leiden, The Netherlands) to measure both the luciferase activity and the total protein concentration.

Luciferase activity was determined with the Promega luciferase assay kit according to the manufacturer's instructions in relative light units (RLU). Briefly, 100 µl substrate was added to 20 µl cell lysate and after a 2 sec delay, the luminescence was measured during 10 sec with a GloMaxTM 96 luminometer. To correct for the amount of cells per well, the protein concentration was determined with the BCA kit (Pierce; Rockford, IL). Therefore, 200 µl mastermix, containing 50 parts reagent A to 1 part B, was mixed with 20 µl cell lysate or BSA (to make the standard curve). After 30 min incubation at 37°C, the absorbance at 590 nm was measured with a Wallac Victor² absorbance plate reader (Perkin Elmer; Waltham, MA).

RESULTS & DISCUSSION

Preparation and characterization of PEG-siPlex loaded microbubbles

As schematically depicted in Fig. 1A, the first goal of this work was to attach PEGylated siRNA-liposome complexes (PEG-siPlexes) to gas-filled microbubbles via a biotin-avidin-biotin bridge. Therefore, we first prepared perfluorobutane filled lipid microbubbles by sonication of a DPPC:DSPE-PEG₂₀₀₀-biotin liposome dispersion in the presence of perfluorobutane gas. The lipid coating prevents a rapid diffusion of the perfluorobutane gas out of the microbubbles. To assure that biotin molecules were present at the outer surface of the microbubbles, we incubated them with Cy5 labelled streptavidin. As shown by the confocal images in Fig. 2A and 2B, after removal of the unbound streptavidin, a thin fluorescent layer of streptavidin molecules surrounding the gas-filled microbubbles could be observed, which indicates the formation of biotin-avidin linkages. This suggests that the DSPE-PEG₂₀₀₀-biotin molecules in the lipid shell are oriented with their hydrophobic tails to the perfluorobutane gas core while their hydrophilic head groups are exposed to the surrounding aqueous medium, as previously suggested by Unger³⁷.

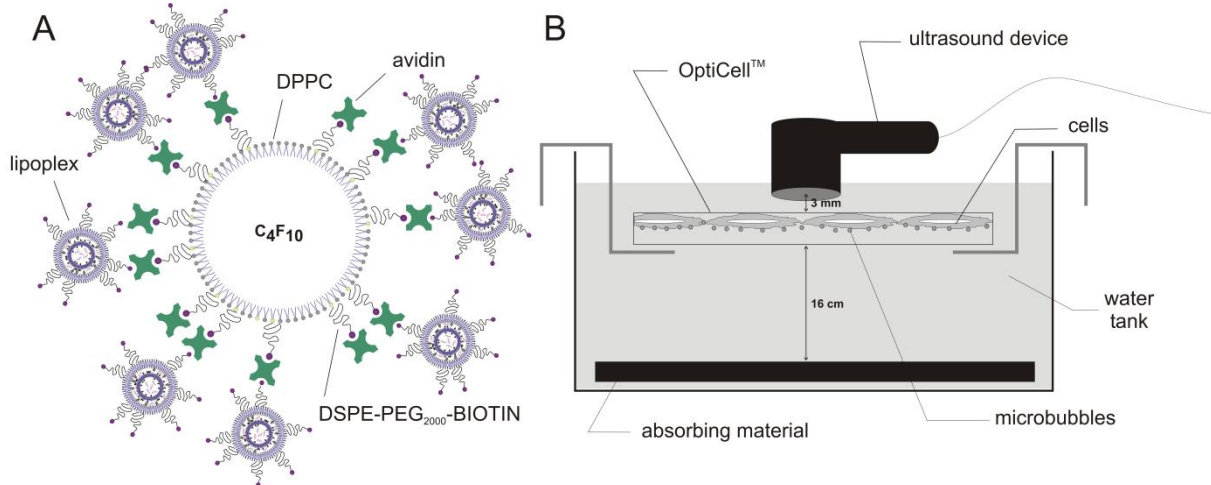


Figure 1A Schematic overview of a PEG-siPlex loaded microbubble. The white disk surrounded by lipids (95 mol% DPPC and 5 mol% DSPE-PEG₂₀₀₀-biotin) represents an avidinylated lipid microbubble with its perfluorobutane (C₄F₁₀) gas core. PEG-siPlexes with increasing amounts of DSPE-PEG₂₀₀₀-biotin were attached to these avidinylated microbubbles via a biotin-avidin-biotin bridge. **Figure 1B** Experimental setup used in the transfection experiments. An OptiCell unit containing a monolayer of HuH-7 cells on one of their membranes was placed in a water tank with a rubber plate, designed to minimize ultrasound reflection or scattering, at the bottom. In all experiments the same ultrasound settings were applied: 10 sec, 1 MHz, 10 % duty cycle and an ultrasound intensity of 2 W/cm². The ultrasound was delivered vertically to the cells which were present on the upper membrane of the OptiCell unit, closest to the ultrasound probe. Different regions of the OptiCell unit were sonicated separately by moving the ultrasound device.

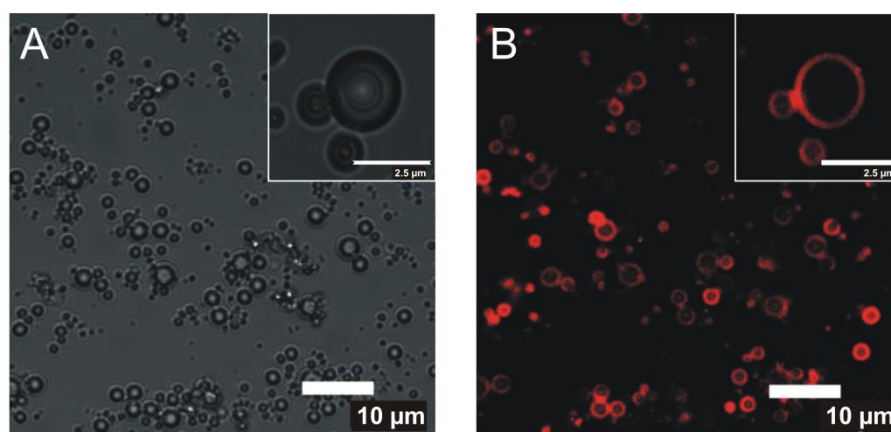


Figure 2 Transmission image (A) and confocal laser scanning microscopy image (B) of avidinylated microbubbles coated with Cy5-streptavidin (red). The inserts display a close-up of three microbubbles.

In a next step, we prepared DOTAP:DOPE based siPlexes containing increasing amounts of DSPE-PEG₂₀₀₀-biotin (0, 2, 5 and 15 mol%). In all cases, a N:P ratio of 20:1 was chosen as non-PEGylated siPlexes showed at this ratio the highest gene silencing effect in HuH-7 cells (data not shown). The ability of the siPlexes to bind siRNA was analyzed by PAGE (Figure 3A). In case of the 0, 2 and 5 mol% DSPE-PEG₂₀₀₀-biotin containing siPlexes, no free siRNA could be detected. This implies that all the siRNA is complexed with the liposomes, which are too large to migrate into the gel network. In contrast, a smear of siRNA was observed in case of the 15 mol% PEG-siPlexes, indicating only a partial siRNA complexation in these siPlexes.

Subsequently, the ability of the different siPlexes to bind to the surface of the biotinylated microbubbles was tested. Therefore, the biotinylated microbubbles were first incubated with avidin. An excess of avidin was used to avoid massive clustering of the microbubbles, due to avidin mediated bridging. After removal of the unbound avidin, siPlexes, containing Atto488 labelled siRNA, were added to the avidinylated microbubbles. The confocal images in Fig. 3B till 3E show that the amount of DSPE-PEG₂₀₀₀-biotin in the siPlexes clearly influences to which extent the microbubble surface becomes covered with siPlexes. Non-PEGylated siPlexes (Figure 3B), thus not containing DSPE-PEG₂₀₀₀-biotin, only showed some non-specific binding to the avidinylated microbubbles. In contrast, the PEGylated siPlexes, containing DSPE-PEG₂₀₀₀-biotin, clearly bound to the avidinylated surface of the microbubbles. The surface of the microbubbles became only partially covered with siPlexes containing 2 mol% DSPE-PEG₂₀₀₀-biotin (Figure 3C), probably due to the limited degree of biotinylation of the siPlexes. In contrast, the microbubble surface was almost completely coated with siPlexes when they contained 5 mol% DSPE-PEG₂₀₀₀-biotin (Figure 3D). The 15 mol% containing PEG-siPlexes also showed an efficient coating of the surface of the microbubbles. However, as these

siPlexes showed incomplete complexation of the siRNA, previously shown by gel electrophoresis experiments (Figure 3A, lane 5), these siPlexes were further excluded from the study.

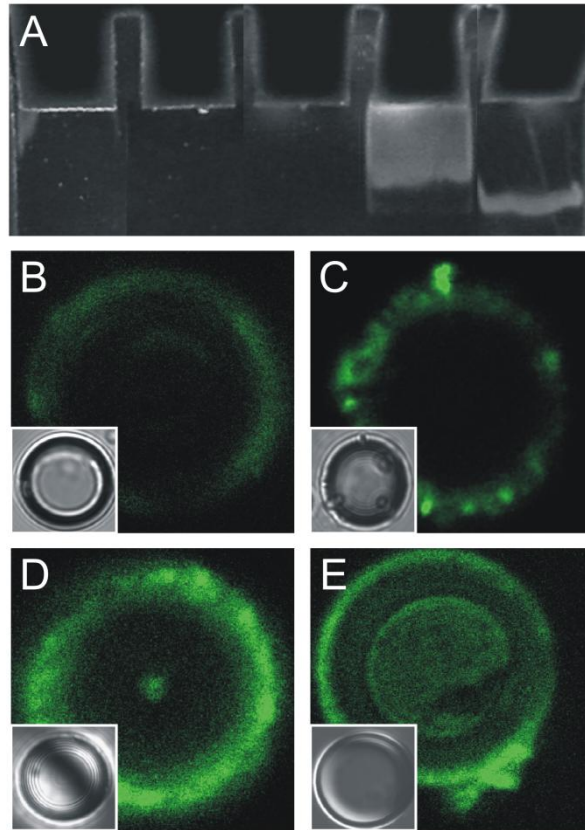


Figure 3 (A) Polyacrylamide gel after electrophoresis of siPlexes containing 0 mol% (lane 1), 2 mol% (lane 2), 5 mol% (lane 3) and 15 mol% DSPE-PEG₂₀₀₀-biotin (lane 4) before attachment to the microbubbles. As a reference, free siRNA was loaded in lane 5 and each lane contains 0.3 µg siRNA. (B-E) Confocal laser scanning microscopy images and corresponding transmission images (inserts) of avidinylated microbubbles incubated with siPlexes containing 0 mol% (B), 2 mol% (C), 5 mol% (D) and 15 mol% DSPE-PEG₂₀₀₀-biotin (E). The siPlexes were visualized by using Atto488-siRNA.

Subsequently we studied the size distribution of the siPlex coated microbubbles by laser diffraction to assure that the microbubbles had the optimal size distribution for cavitation. Figure 4 shows the size distribution of microbubbles incubated with non-PEGylated siPlexes and microbubbles loaded with PEGylated siPlexes. In both cases, the diameter of the microbubbles varied between 0,5 and 10 µm, which is an appropriate size to favour cavitation upon exposure to clinically relevant ultrasound energy. Figure 4 (arrow) also shows a significant amount of sub-micron particles in case of the non-PEGylated siPlexes, indicating the presence of non bound siPlexes. In contrast, this sub-micron peak was not visible in case of the microbubbles loaded with PEGylated siPlexes (Figure 4, grey circles). These results are in agreement with the confocal images shown in Figure 3B and 3D.

Similar size distributions were found for microbubbles that were loaded with 2 mol% DSPE-PEG₂₀₀₀-biotin containing siPlexes (data not shown).

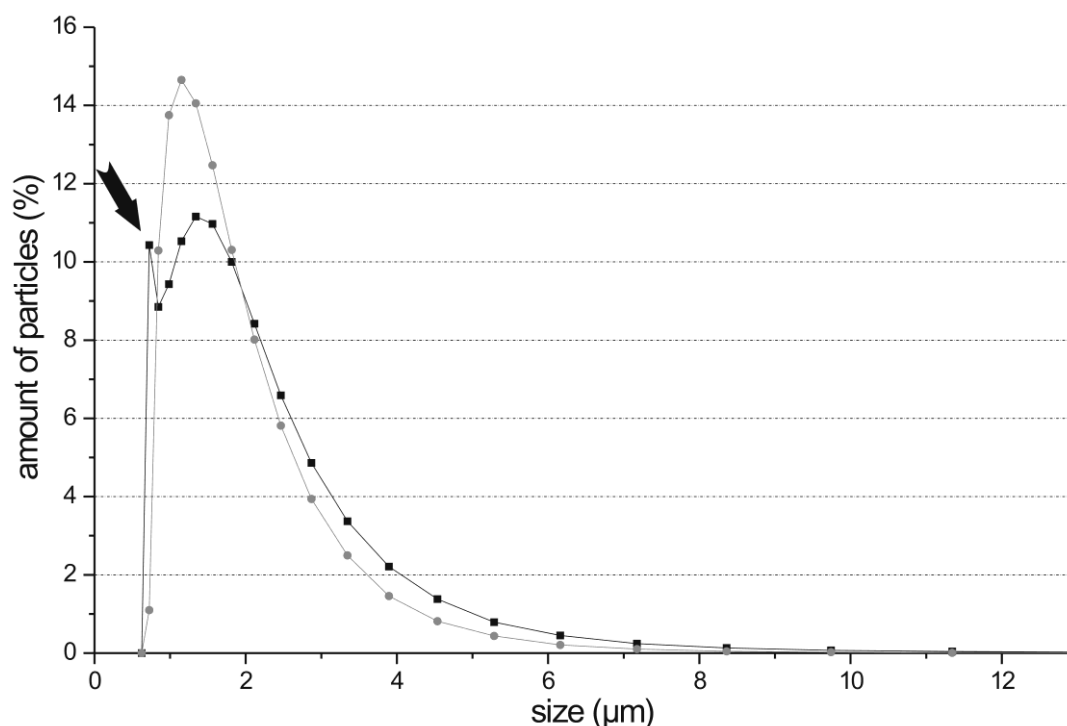


Figure 4 Size distribution measured by laser diffraction of microbubbles after addition of non-PEGylated siPlexes (black squares) and attachment of 5 mol% DSPE-PEG₂₀₀₀-biotin containing siPlexes (grey circles). The data are the mean of three measurements and error bars represent standard deviations. Arrow indicates a peak of sub-micron sized particles.

Ultrasound induced release of PEG-siPlexes from microbubbles

It has been shown that coupling of polystyrene beads to the surface of microbubbles via a biotin-avidin bridge, results in local delivery of the beads upon ultrasound radiation³⁸. However, in contrast to these inert beads, self-assembled siPlexes may undergo physicochemical alterations during the ultrasound triggered release, which may influence their biological performance. Therefore, we determined the size, zeta potential and siRNA complexation of the siPlexes before attachment to the microbubbles and after ultrasound triggered release from the microbubbles.

The dark grey bars in Figure 5A show that, before binding to the microbubble surface the size of the siPlexes was independent of the PEGylation degree and averaged 130 nm. In contrast, the surface charge lowered with increasing degree of PEGylation (dark grey bars in Figure 5B) varying from 50 mV for the non-PEGylated to 20 mV for the siPlexes containing 5 mol% DSPE-PEG₂₀₀₀-biotin. Fig. 5A also shows that binding and subsequent ultrasound assisted release of the PEG-siPlexes from

the microbubbles (light grey bars) had only a limited effect on the size of these PEG-siPlexes with a maximal increase of ~ 20 nm, in contrast to the clear increase in size of the non-PEGylated siPlexes.

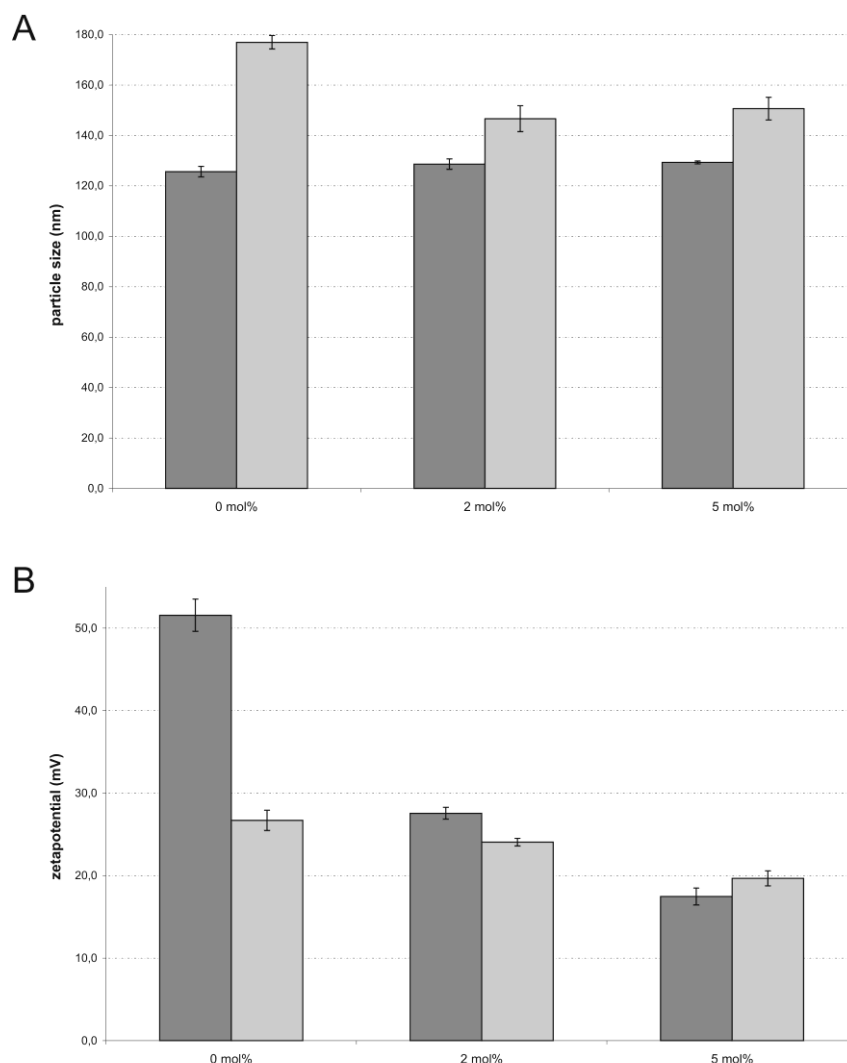


Figure 5 (A) Size and (B) zeta potential of the siPlexes containing 0 mol%, 2 mol% and 5 mol% DSPE-PEG₂₀₀₀-biotin before attachment to the microbubbles (dark grey bars) and after ultrasound assisted release from the siPlex loaded microbubbles (light grey bars). The data are the means of three independent measurements and the error bars represent standard deviations.

As observed for the size, the zeta potential (Figure 5B) of the PEG-siPlexes after being released from the microbubbles by ultrasound was not significantly altered, while the zeta potential of the non-PEGylated siPlexes was significantly lower. The change in size and zeta potential of the non-PEGylated siPlexes may be due the binding of negatively charged DSPE-PEG₂₀₀₀-biotin lipids from the imploded microbubbles to the non-PEGylated siPlexes.

Clearly, to keep their biological performance, the siPlexes may not dissociate (i.e. release their siRNA) upon exposure to ultrasound, as free siRNA is prone to nuclease degradation. Gel

electrophoresis revealed that ultrasound energy did not dissociate the siPlexes (data not shown). In conclusion, ultrasound mediated implosion of the PEG-siPlex loaded microbubbles and the induced microjets did not drastically influence the size, zeta potential and the complexation properties of the released PEG-siPlexes.

Cellular distribution of PEG-siPlexes

Next we studied the cellular distribution of PEG-siPlexes. Figure 6A till 6C show HuH-7 cells incubation with 5 mol% PEG-siPlexes. The z-scan in Figure 6A reveals that these PEG-siPlexes, after 20 min incubation at 37°C, were still located on top of the HuH-7 cells. This was confirmed by the images in Figure 6B and 6C. In these images, the green labelled PEG-siPlexes (Figure 6C) show exactly the same cellular distribution as the red labelled plasma membrane (Figure 6B). This confirms that PEGylation indeed has an effect on the cellular uptake of siPlexes³⁹, as non-PEGylated siPlexes were clearly taken up by the cells after 20 min (data not shown). Ultrasound irradiation did not change the cellular distribution of these free PEG-siPlexes (data not shown). Interestingly, PEG-siPlexes released from siPlex loaded microbubbles by ultrasound showed a totally different cellular distribution (Figure 6D till 6F). In this case, the green labelled PEG-siPlexes were localized inside the cells as shown by the z-scan (Figure 6D) and the membrane colouring (Figure 6E and 6F). These results suggest that PEG-siPlexes enter the cells via a different mechanism when they are released from the PEG-siPlex loaded microbubbles by ultrasound. Although further research is needed, we suppose that they enter cells via the transient cell membrane perforations that arise during the exposure to ultrasound⁴⁰. Indeed, such pores, which have been reported to be a few hundreds of nanometers in size^{34,41}, are large enough to allow the passage of the PEG-siPlexes released from the microbubbles. This implies that the negative effects of PEGylation on the cellular uptake as well as on the endosomal escape of PEG-siPlexes can be circumvented by attaching them to microbubbles and subsequently expose these siPlex loaded microbubbles to ultrasound.

Gene silencing efficiency of PEG-siPlex loaded microbubbles

Finally, we determined whether siRNA delivered by ultrasound mediated implosion of the PEG-siPlex loaded microbubbles could inhibit constitutive luciferase expression in HuH-7eGFPLuc cells (Figure 7). The black bars in Figure 7 show that the silencing capacity of the free siPlexes declines dramatically with increasing PEGylation degree. SiPlexes with a PEGylation degree of 2 mol% already showed a 3-fold reduced gene silencing capacity compared to the non-PEGylated siPlexes.

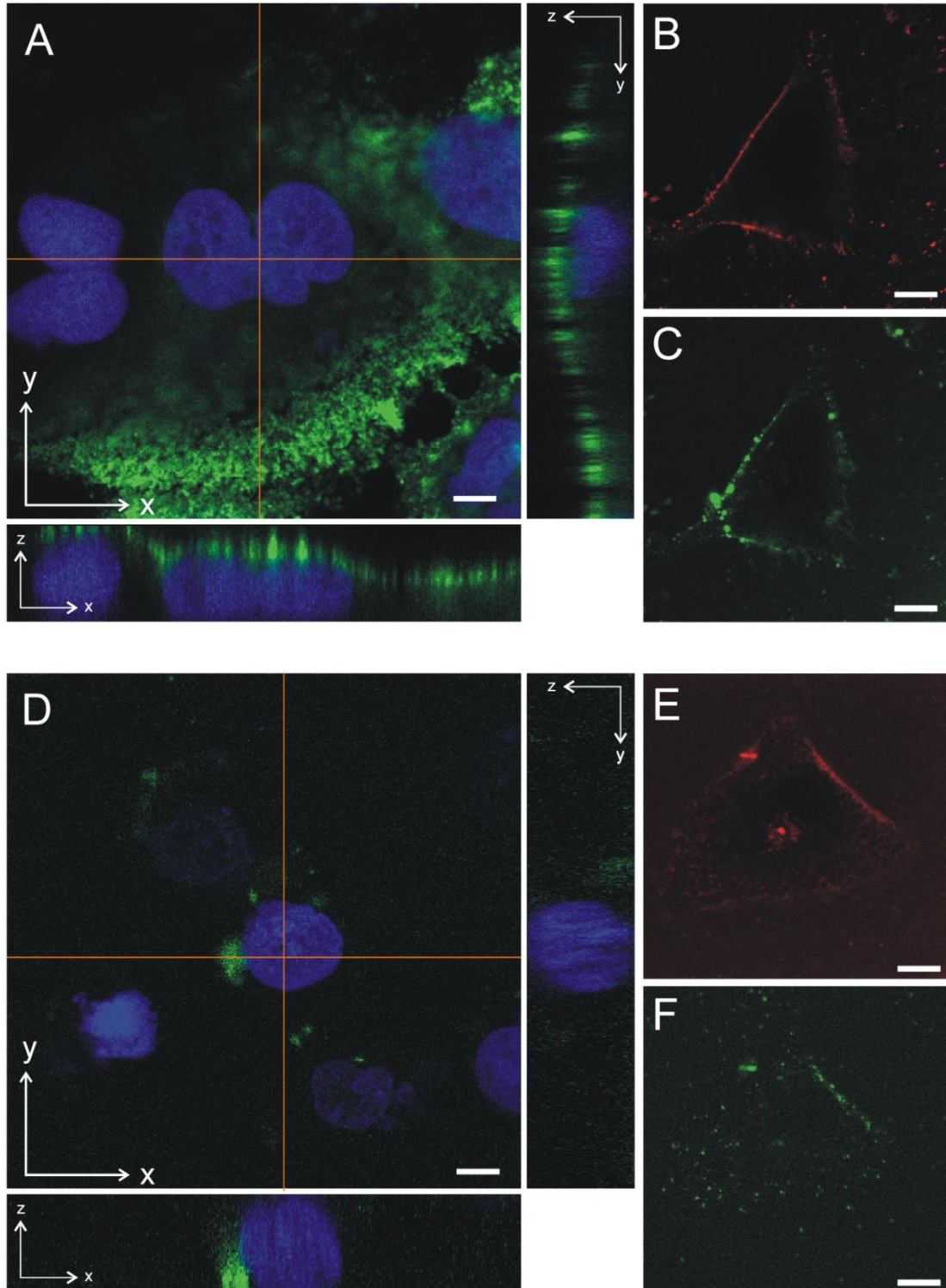


Figure 6 Cellular uptake and intracellular distribution of PEG-siPlexes (A till C) and ultrasound radiated PEG-siPlex loaded microbubbles (D till F). All PEG-siPlexes contain 5 mol% DSPE-PEG₂₀₀₀-biotin. Images A and D display confocal images and z-scans, at the positions indicated by the red lines, through HuH-7 cells with DraG5 labelled nuclei (blue) and incubated for 20 minutes with Atto488-labelled siPlexes (green). Confocal image (B) and (E) show the localisation of TRITC-concanavalin A (red), a plasma membrane marker. Confocal image (C) and (F) show the localisation of Atto488-labelled siPlexes (green) in the cells shown in image (B) and (E), respectively. The scale bars represent 10 μm .

Increasing the PEGylation degree to 5 mol% even completely blocked the silencing capacity of the siPlexes. This negative effect of PEGylation has intensively been studied for pDNA delivery and some groups suggest that the loss in transfection efficiency of highly PEGylated lipoplexes is due to a reduced cellular binding and uptake^{41,42}, while others believe that the PEG-lipids inhibit the endosomal release of the nucleic acids into the cytoplasm^{39,43-46}. The white bars in Figure 7 show that the negative effect of PEGylation on the gene silencing efficiency of the siPlexes containing 5 mol% DSPE-PEG₂₀₀₀-biotin can be completely counteracted by loading of these PEG-siPlexes on the surface of microbubbles followed by exposure of these microbubbles to ultrasound. Attachment of siPlexes containing 2 mol% DSPE-PEG₂₀₀₀-biotin to the microbubbles and subsequent exposure to ultrasound resulted in a similar silencing as the corresponding free PEG-siPlexes. For these PEG-siPlexes the number of PEG-siPlexes bound to the microbubbles is probably not enough to further increase their gene silencing efficiency. Indeed, as shown in Figure 3C, the 5 mol% DSPE-PEG₂₀₀₀-biotin containing siPlexes bind much more efficiently to the microbubble surface than the 2 mol% DSPE-PEG₂₀₀₀-biotin containing siPlexes (Figure 3B). Therefore, these data may indicate that the extent of gene silencing is governed by the amount of PEG-siPlexes that are released near the cell perforations. Figure 7 (dark grey bars) also shows that applying ultrasound energy, in the absence of microbubbles, could not enhance the gene silencing efficiency of the different siPlexes. Furthermore, microbubbles loaded with 5 mol% PEG-siPlexen were not able to cause gene silencing in the absence of ultrasound (Figure 7; light grey bars). This implies that the PEG-siPlex loaded microbubbles described in this work allow ultrasound controlled, i.e. targeted, intracellular delivery of siRNA.

CONCLUSION

In conclusion, we developed a novel delivery system in which PEG-siPlexes are attached to ultrasound responsive microbubbles via a biotin-avidin-biotin bridge. Exposure of these PEG-siPlex loaded microbubbles to ultrasound resulted in a massive release of unaltered PEG-siPlexes. Furthermore, PEG-siPlexes (containing 5 mol% DSPE-PEG₂₀₀₀-biotin) loaded on microbubbles were able to enter cells rapidly after exposure to ultrasound, while free PEG-siPlexes did not enter cells. Moreover, these PEG-siPlex loaded microbubbles caused, in the presence of ultrasound, a much higher gene silencing than free PEG-siPlexes. Interestingly, in the absence of ultrasound these PEG-siPlex loaded microbubbles did not cause any gene silencing. Therefore, the developed siRNA delivery system allows both space and time controlled gene silencing. Furthermore, the PEG-siPlex loaded microbubbles are expected to be suitable for systematic applications as ultrasound in combination with microbubbles is considered as a safe and already used in the clinic for diagnostic

purposes. Additionally, PEG-siPlexes are known not to aggregate in serum which is important to avoid blockage of small blood capillaries by aggregates⁴⁷. The developed siRNA delivery system may also allow the treatment of patients with metastasized tumours. Indeed, a recently developed device that combines magnetic resonance imaging (MRI) and ultrasound can both track down the metastasized tumours and guide the ultrasound energy to these tumours⁴⁸. So, the siRNA delivery system presented in this work may open up new perspectives for ultrasound controlled *in vivo* delivery of siRNA.

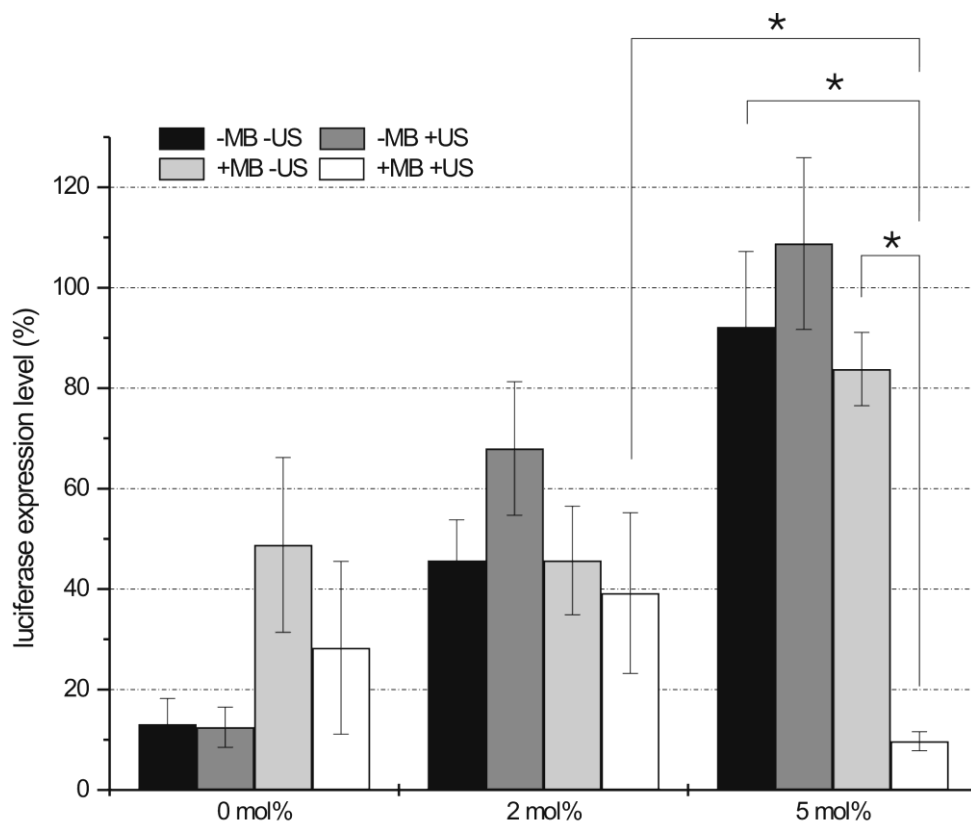


Figure 7 Silencing efficiency of free siPlexes and PEG-siPlexes in the absence and presence of ultrasound, and PEG-siPlex loaded microbubbles in the presence of ultrasound. The PEGylation (DSPE-PEG₂₀₀₀-biotin) degree of the siPlexes is represented in the x-axis. The black and the dark grey bars represent the gene silencing efficiency of free siPlexes in the absence and presence of ultrasound, respectively. The light grey and white bars represent the gene silencing of the siPlexes loaded on the microbubbles in the absence or presence of ultrasound. In all cases, the following ultrasound settings were used: 1 MHz, 10 % DC, 2 W/cm², 10 sec. The results are expressed as percentage of luciferase expression compared to mock siRNA transfected cells. The asterixes (*) represent significant differences with p < 0.05. (MB = microbubble; US = ultrasound)

ACKNOWLEDGMENTS

Niek Sanders is supported by the Fund for Scientific Research-Flanders (FWO). The financial support of this institute is acknowledged with gratitude. This work was supported by grants from Ghent University (BOF), FWO and the European Union (MediTrans). The HuH-7_eGFPLuc cells were kindly provided by Prof. Ernst Wagner, LMU University Munich.

REFERENCES

- (1) Elbashir S.M., Harborth J., Lendeckel W., Yalcin A., Weber K., & Tuschl T. Duplexes of 21-nucleotide RNAs mediate RNA interference in cultured mammalian cells. *Nature* **2001** 411(6836) 494-498.
- (2) Aagaard L. & Rossi J.J. RNAi therapeutics: principles, prospects and challenges. *Advanced Drug Delivery Reviews*. **2007** 59(2-3) 75-86.
- (3) Lewis D.L. & Wolff J.A. Systemic siRNA delivery via hydrodynamic intravascular injection. *Advanced Drug Delivery Reviews* **2007** 59(2-3) 115-123.
- (4) Lee S.H., Kim S.H., & Park T.G. Intracellular siRNA delivery system using polyelectrolyte complex micelles prepared from VEGF siRNA-PEG conjugate and cationic fusogenic peptide. *Biochemical and Biophysical Research Communications* **2007** 357(2) 511-516.
- (5) Akaneya Y., Jiang B., & Tsumoto T. RNAi-induced gene silencing by local electroporation in targeting brain region. *Journal of Neurophysiology* **2005** 93(1) 594-602.
- (6) Golzio M., Mazzolini L., Ledoux A. *et al.* In vivo gene silencing in solid tumors by targeted electrically mediated siRNA delivery. *Gene Therapy* **2007** 14(9) 752-759.
- (7) Kishida T., Asada H., Gojo S. *et al.* Sequence-specific gene silencing in murine muscle induced by electroporation-mediated transfer of short interfering RNA. *Journal of Gene Medicine* **2004** 6(1) 105-110.
- (8) Takabatake Y., Isaka Y., Mizui M. *et al.* Exploring RNA interference as a therapeutic strategy for renal disease. *Gene Therapy* **2005** 12(12) 965-973.
- (9) Chien P.Y., Wang J., Carbonaro D. *et al.* Novel cationic cardiolipin analogue-based liposome for efficient DNA and small interfering RNA delivery in vitro and in vivo. *Cancer Gene Therapy* **2005** 12(3) 321-328.
- (10) Eliyahu H., Serval N., Domb A.J., & Barenholz Y. Lipoplex-induced hemagglutination: potential involvement in intravenous gene delivery. *Gene Therapy* **2002** 9(13) 850-858.
- (11) Howard K.A., Rahbek U.L., Liu X. *et al.* RNA Interference in Vitro and in Vivo Using a Novel Chitosan/siRNA Nanoparticle System. *Molecular Therapy* **2006** 14(4) 476-484.

- (12) Schiffelers R.M., Ansari A., Xu J. *et al.* Cancer siRNA therapy by tumor selective delivery with ligand-targeted sterically stabilized nanoparticle. *Nucleic Acids Research* **2004** 32(19) e149.
- (13) Sorensen D.R., Leirdal M., & Sioud M. Gene silencing by systemic delivery of synthetic siRNAs in adult mice. *Journal of Molecular Biology* **2003** 327(4) 761-766.
- (14) Thomas M., Lu J.J., Ge Q., Zhang C., Chen J., & Klibanov A.M. Full deacylation of polyethylenimine dramatically boosts its gene delivery efficiency and specificity to mouse lung. *Proceedings of the National Academy of Sciences of the United States of America* **2005** 102(16) 5679-5684.
- (15) Urban-Klein B., Werth S., Abuharbeid S., Czubayko F., & Aigner A. RNAi-mediated gene-targeting through systemic application of polyethylenimine (PEI)-complexed siRNA in vivo. *Gene Therapy* **2005** 12(5) 461-466.
- (16) Sakurai F., Nishioka T., Yamashita F., Takakura Y., & Hashida M. Effects of erythrocytes and serum proteins on lung accumulation of lipoplexes containing cholesterol or DOPE as a helper lipid in the single-pass rat lung perfusion system. *European Journal of Pharmaceutics and Biopharmaceutics* **2001** 52(2) 165-172.
- (17) Choi Y.H., Liu F., Kim J.S., Choi Y.K., Park J.S., & Kim S.W. Polyethylene glycol-grafted poly-L-lysine as polymeric gene carrier. *Journal of Controlled Release* **1998** 54(1) 39-48.
- (18) Kunath K., von H.A., Petersen H. *et al.* The structure of PEG-modified poly(ethylene imines) influences biodistribution and pharmacokinetics of their complexes with NF-kappaB decoy in mice. *Pharmaceutical Research* **2002** 19(6) 810-817.
- (19) Ogris M., Brunner S., Schuller S., Kircheis R., & Wagner E. PEGylated DNA/transferrin-PEI complexes: reduced interaction with blood components, extended circulation in blood and potential for systemic gene delivery. *Gene Therapy* **1999** 6(4) 595-605.
- (20) Tam P., Monck M., Lee D. *et al.* Stabilized plasmid-lipid particles for systemic gene therapy. *Gene Therapy* **2000** 7(21) 1867-1874.
- (21) Wasungu L. & Hoekstra D. Cationic lipids, lipoplexes and intracellular delivery of genes. *Journal of Controlled Release* **2006** 116(2) 255-264.
- (22) Zuhorn I.S., Engberts J.B., & Hoekstra D. Gene delivery by cationic lipid vectors: overcoming cellular barriers. *European Biophysical Journal* **2007** 36(4-5) 349-362.
- (23) Bekeredjian R., Chen S., Frenkel P.A., Grayburn P.A., & Shohet R.V. Ultrasound-targeted microbubble destruction can repeatedly direct highly specific plasmid expression to the heart. *Circulation* **2003** 108(8) 1022-1026.
- (24) Duvshani-Eshet M., Adam D., & Machluf M. The effects of albumin-coated microbubbles in DNA delivery mediated by therapeutic ultrasound. *Journal of Controlled Release* **2006** 112(2) 156-166.
- (25) Kinoshita M., McDannold N., Jolesz F.A., & Hynynen K. Targeted delivery of antibodies through the blood-brain barrier by MRI-guided focused ultrasound. *Biochemical and Biophysical Research Communications* **2006** 340(4) 1085-1090.

- (26) Lentacker I., De Smedt S.C., Demeester J., Van Marck V., Bracke M., & Sanders N.N. Lipoplex-Loaded Microbubbles for Gene Delivery: A Trojan Horse Controlled by Ultrasound. *Advanced Functional Materials* **2007** 17(12) 1910-1916.
- (27) Manome Y., Nakayama N., Nakayama K., & Furuhashi H. Insonation facilitates plasmid DNA transfection into the central nervous system and microbubbles enhance the effect. *Ultrasound in Medicine and Biology* **2005** 31(5) 693-702.
- (28) Newman C.M., Lawrie A., Brisken A.F., & Cumberland D.C. Ultrasound gene therapy: on the road from concept to reality. *Echocardiography* **2001** 18(4) 339-347.
- (29) Pislaru S.V., Pislaru C., Kinnick R.R. *et al.* Optimization of ultrasound-mediated gene transfer: comparison of contrast agents and ultrasound modalities. *European Heart Journal* **2003** 24(18) 1690-1698.
- (30) Vannan M., McCreery T., Li P. *et al.* Ultrasound-mediated transfection of canine myocardium by intravenous administration of cationic microbubble-linked plasmid DNA. *Journal of the American Society of Echocardiography* **2002** 15(3) 214-218.
- (31) Kinoshita M. & Hynynen K. A novel method for the intracellular delivery of siRNA using microbubble-enhanced focused ultrasound. *Biochemical and Biophysical Research Communications* **2005** 335(2) 393-399.
- (32) Tsunoda S., Mazda O., Oda Y. *et al.* Sonoporation using microbubble BR14 promotes pDNA/siRNA transduction to murine heart. *Biochemical and Biophysical Research Communications* **2005** 336(1) 118-127.
- (33) Ogawa K., Tachibana K., Uchida T. *et al.* High-resolution scanning electron microscopic evaluation of cell-membrane porosity by ultrasound. *Medical Electron Microscopy* **2001** 34(4) 249-253.
- (34) Mehier-Humbert S., Bettinger T., Yan F., & Guy R.H. Ultrasound-mediated gene delivery: kinetics of plasmid internalization and gene expression. *J of Controlled Release* **2005** 104(1) 203-211.
- (35) Sanders N.N., Van R.E., De Smedt S.C., & Demeester J. Structural alterations of gene complexes by cystic fibrosis sputum. *American Journal of Respiratory and Critical Care Medicine* **2001** 164(3) 486-493.
- (36) Kinoshita M. & Hynynen K. Key factors that affect sonoporation efficiency in in vitro settings: the importance of standing wave in sonoporation. *Biochemical and Biophysical Research Communications* **2007** 359(4) 860-865.
- (37) Unger E.C., Porter T., Culp W., Labell R., Matsunaga T., & Zutshi R. Therapeutic applications of lipid-coated microbubbles. *Advanced Drug Delivery Rev.* **2004** 56(9) 1291-1314.
- (38) Lum A.F., Borden M.A., Dayton P.A., Kruse D.E., Simon S.I., & Ferrara K.W. Ultrasound radiation force enables targeted deposition of model drug carriers loaded on microbubbles. *Journal of Controlled Release* **2006** 111(1-2) 128-134.
- (39) Mishra S., Webster P., & Davis M.E. PEGylation significantly affects cellular uptake and intracellular trafficking of non-viral gene delivery particles. *European Journal of Cell Biology* **2004** 83(3) 97-111.

- (40) Prentice P., Cuschieri A., Dholakia K., Prausnitz M., & Campbell P. Membrane disruption by optically controlled microbubble cavitation. *Nature Physics* **2005** 1107-110.
- (41) Schlicher R.K., Radhakrishna H., Tolentino T.P., Apkarian R.P., Zarnitsyn V., & Prausnitz M.R. Mechanism of intracellular delivery by acoustic cavitation. *Ultrasound in Medicine and Biology* **2006** 32(6) 915-924.
- (42) Deshpande M.C., Davies M.C., Garnett M.C. *et al.* The effect of poly(ethylene glycol) molecular architecture on cellular interaction and uptake of DNA complexes. *Journal of Controlled Release* **2004** 97(1) 143-156.
- (43) Audouy S. & Hoekstra D. Cationic lipid-mediated transfection in vitro and in vivo (review). *Molecular Membrane Biology* **2001** 18(2) 129-143.
- (44) Meyer O., Kirpotin D., Hong K. *et al.* Cationic liposomes coated with polyethylene glycol as carriers for oligonucleotides. *Journal of Biological Chemistry* **1998** 273(25) 15621-15627.
- (45) Shi F., Wasungu L., Nomden A. *et al.* Interference of poly(ethylene glycol)-lipid analogues with cationic-lipid-mediated delivery of oligonucleotides; role of lipid exchangeability and non-lamellar transitions. *Biochemical Journal* **2002** 366(Pt 1) 333-341.
- (46) Song L.Y., Ahkong Q.F., Rong Q. *et al.* Characterization of the inhibitory effect of PEG-lipid conjugates on the intracellular delivery of plasmid and antisense DNA mediated by cationic lipid liposomes. *Biochimica and Biophysica Acta* **2002** 1558(1) 1-13.
- (47) Buyens K., Lucas B., Raemdonck K. *et al.* A fast and sensitive method for measuring the integrity of siRNA-carrier complexes in full human serum. *Journal of Controlled Release* **2007** 126(1) 67-76.
- (48) Moonen C.T. Spatio-temporal control of gene expression and cancer treatment using magnetic resonance imaging-guided focused ultrasound. *Clinical Cancer Research* **2007** 13(12) 3482-3489.

Chapter 7

Design and evaluation of doxorubicin containing microbubbles for ultrasound triggered doxorubicin delivery: cytotoxicity and mechanisms involved

This chapter is submitted to Molecular Therapy.

Lentacker I.¹, Geers B.¹, Demeester J.¹, De Smedt S.C.¹ and Sanders N.N.²

¹ Laboratory of General Biochemistry and Physical Pharmacy, Department of Pharmaceutics Ghent University, B-9000 Ghent, Belgium.

² Laboratory of Gene Therapy, Department of Nutrition, Genetics and Ethology, Ghent University, Heidestraat 19, B-9820 Merelbeke, Belgium

ABSTRACT

This paper describes the design and working mechanism of doxorubicin (DOX) loaded microbubbles for ultrasound mediated delivery of DOX. Compared to DOX-liposomes, DOX loaded microbubbles, prepared by attaching DOX-liposomes to the lipid shell of microbubbles killed melanoma cells significantly stronger after exposure to ultrasound. After treatment of the melanoma cells with DOX-liposome loaded microbubbles and ultrasound, DOX was mainly present in the nuclei of the cancer cells, while it was mainly detected in the cytoplasm of cells treated with DOX-liposomes. Exposure of cells to DOX-liposome loaded microbubbles and ultrasound caused an almost instantaneous cellular entry of the DOX. At least two mechanisms were identified which explain the fast uptake of DOX and the superior cell killing of DOX-liposome loaded microbubbles and ultrasound. First, exposure of DOX-liposome loaded microbubbles to ultrasound results in the release of free DOX which is more cytotoxic than DOX-liposomes. Second, the cellular entry of the released DOX is facilitated due to sonoporation of the cell membranes.

Chapter 7

Design and evaluation of doxorubicin containing microbubbles for ultrasound triggered doxorubicin delivery: cytotoxicity and mechanisms involved

INTRODUCTION

Doxorubicin (DOX), also called adriamycine, is one of the most frequently used anti-cancer drugs. DOX is used for the treatment of different solid and haematopoietic cancers such as breast cancer, osteosarcomas, aggressive lymphomas and leukemias. Different mechanisms explain its cytotoxic activity¹. They include DNA intercalation, lipid peroxidation and inhibition of topoisomerase II. The use of free DOX is rather limited because of the severe side-effects. Indeed, besides damaging tumours it also causes cardiotoxicity and nephrotoxicity¹. Additionally, the efficacy of free DOX is also hampered by multidrug resistance, originating from the P-glycoprotein and topoisomerase II resistance¹. Because of these problems associated with free DOX treatment, DOX has been encapsulated inside liposomes. These liposomes contain PEG (polyethylene glycol) chains at their surface to prevent recognition by the reticuloendothelial system (RES) (so-called stealth liposomes). This results in the passive accumulation of stealth liposomes in the tumour vasculature due to the enhanced permeability and retention effect (EPR)². In 1995 the liposomal DOX formulations Doxil[®] and Caelix[®] became FDA approved for the treatment of AIDS related Kaposi's sarcoma and ovarian cancer. Although Doxil[®] strongly reduced the cardiac toxicity of DOX in clinical trials, other side effects occurred. Several patients suffered from mucositis and the hand and foot syndrome, due to the localization of the liposomes in skin capillaries¹. Therefore, many research groups try to enhance

the targeting of DOX to the tumours by attaching ligands or antibodies to DOX loaded vehicles or by incorporating DOX in stimuli responsive carriers like pH and temperature responsive nanocarriers^{1,3}.

In the past ultrasound has been used as an external trigger to induce drug release from drug loaded carriers. In these experiments low frequency (<1 MHz) ultrasound was used. However, the clinical applicability of low frequency ultrasound is limited by its low penetration depth in the body. More recently it has been demonstrated that high frequency ultrasound (1-10 MHz), when combined with diagnostic microbubbles, can enhance the intracellular delivery and extravasation of drugs⁴⁻⁷. These effects have been attributed to inertial cavitation of the microbubbles. Cavitation is the alternate growing and shrinking of microbubbles under the influence of an ultrasonic field⁸. When the ultrasound intensity is high enough, microbubbles can implode due to the inertia of the intruding fluid (inertial cavitation). As a result, fluid streams and microjets transiently perforate the membranes of nearby cells and hence enhance the intracellular uptake of drugs^{6,7,9,10}. This phenomenon is called sonoporation. Additionally, it has been shown that such microjets can also transiently perforate blood vessels and thus induce extravasation of large molecules^{11,12}.

Several papers report on the synergistic effect of doxorubicin and ultrasound¹³. However, these papers mainly focused on ultrasound assisted intracellular delivery of respectively free doxorubicin^{14,15} or DOX encapsulated in micelles or liposomes¹⁶⁻²². The forces associated with the inertial cavitation of the microbubbles may (a) massively release the encapsulated drug from the nanocarriers and (b) improve the intracellular uptake of DOX due to sonoporation of the cell membranes. However, a major drawback of co-injecting DOX liposomes and microbubbles is the fact that DOX liposomes extravasate and thus still accumulate in undesired tissues (not exposed to ultrasound) which explains that a high amount of DOX liposomes remains necessary to achieve a sufficiently high concentration in the ultrasound treated region. This study aimed to further improve ultrasound mediated delivery of DOX-liposomes. Therefore we designed "doxorubicin loaded microbubbles" through avidin-biotin binding of doxorubicin containing liposomes to the lipid shell of microbubbles (DOX-liposome loaded microbubbles)(Figure 1). DOX delivery by such constructs could be attractive as it would take profit of both the sonoporation effect and targeting potential of ultrasound. Indeed, micobubbles carrying DOX-liposomes at their surface are expected to be too large to extravasate in undisered tissue (i.e. not treated by ultrasound). This papers shows the killing of tumour cells by DOX-microbubbles and explains the underlying mechanisms.

MATERIALS & METHODS

Preparation and characterization of lipid microbubbles containing DSPE-PEG-biotin

Liposomes containing DPPC (dipalmitoylphosphatidylcholine) and DSPE-PEG-biotin (1,2-distearoyl-sn-glycero-3-phosphoethanolamine-N-(biotinyl(polyethyleneglycol)2000)) in a 85:15 molar ratio were prepared as previously described⁶. Briefly, the in chloroform dissolved lipids were put in a round-bottomed flask and the solvent was removed via evaporation followed by flushing with nitrogen. The obtained lipid film was subsequently hydrated in HEPES buffer (20 mM HEPES, pH 7.4) at a final lipid concentration of 5 mg/mL and incubated overnight at 4°C to allow the formation of liposomes. The resulting liposomes were first extruded through a polycarbonate membrane (pore size of 0.2 µm) using a mini-extruder (Avanti Polar Lipids, Alabaster, AL, USA). Subsequently, the extruded liposomes were sonicated with a 20 kHz probe (Branson 250 sonifier, Branson Ultrasonics Corp., Danbury, CT, USA) in the presence of perfluorobutane gas (C₄F₁₀, MW 238 g/mol, F2 chemicals, Preston, Lancashire, UK). After sonication the microbubbles were washed (to remove the excess of lipids) with 3 mL fresh HEPES buffer and finally resuspended in 5 mL fresh HEPES buffer. To allow the attachment of biotinylated DOX-liposomes, the biotinylated microbubbles were incubated with 500 µL avidin (10 mg/mL) and incubated for 10 min at room temperature. Subsequently, the microbubbles were centrifuged and washed again with 3 mL fresh HEPES buffer. Finally the microbubbles were resuspended in 5 mL HEPES buffer. The mean size of these microbubbles was around 2 µm and their size distribution ranged between 0.5 and 10 µm.

Preparation and characterization of biotinylated doxorubicin liposomes

Liposomes containing DPPC, cholesterol and DSPE-PEG-biotin in a 60:40:5 molar ratio were prepared as described above. Liposomes were loaded with doxorubicin following the method previously established by Bolotin *et al.*²³ After removal of the chloroform, the lipid film was hydrated with ammonium sulphate buffer (250mM). The resulting liposomes were extruded through a polycarbonate membrane (pore size of 0.1µm) as described above. Subsequently, the liposomes were dialysed against pure distilled water overnight in a dialysis bag (MWCO 10.000, Spectra/Por Biotech, Spectrum laboratories, CA, USA) to remove the ammonium sulphate between the liposomes. Liposomes were loaded with DOX by mixing 1 mL of liposomes with 1 mg of DOX. This mixture was incubated for 4 h at 65°C. Afterwards, the free DOX was removed by passing the DOX loaded liposomes over a Sephadex column (Sephadex G75). Loading efficiency was determined by

measuring the absorbance of DOX in the DOX-liposome fraction and the free DOX at 450nm and was around 90%. The average hydrodynamic diameter of the PEGylated DOX-liposomes was determined by dynamic light scattering (DLS; Autosizer 4700, Malvern).

Attachment of biotinylated DOX-liposomes to avidinylated microbubbles

50 μ L of biotinylated DOX-liposomes was mixed with 1 mL avidinylated microbubbles and incubated at room temperature for 5 min. The attachment of DOX-liposomes to the microbubbles was visualized using a Nikon EZC1-si confocal laser scanning microscope (Nikon, Brussels, Belgium) equipped with a 40x objective. The 491nm line of this microscope was used to excite the doxorubicin and the doxorubicin was detected with the 580nm detector.

Cell culture

BLM-cells (melanoma cells)²⁴ were cultured in Dulbecco's modified Eagle's medium (DMEM) with the growth factor F12 and phenol red containing 2mM glutamine, 10% heat deactivated foetal bovine serum (FBS), 1% penicillin-streptomycin (Gibco, Merelbeke, Belgium) and HEPES buffer (20mM, pH 7.4).

Cytotoxicity measurements

Cells were grown to 90% confluency in Opticell units (Biocrystal, Westerville, OH, USA) in a humidified incubator at 37°C and 5% CO₂. Subsequently, cells were washed with 10 mL of phosphate buffered saline (PBS; Gibco, Merelbeke, Belgium) and respectively DOX-liposome loaded microbubbles, DOX-liposomes or free DOX (all in Optimem, Gibco, Merelbeke, Belgium) were added to the cells. Therefore we first mixed an appropriate amount of biotinylated DOX-liposomes (containing 10, 30, 50 or 100 μ g of DOX) with 1 mL of the avidinylated microbubbles. After 5 min of incubation at room temperature, Optimem (Gibco, Merelbeke, Belgium) was added to a final volume of 10 mL. The medium was prepared in a similar way for the experiments without microbubbles except that the microbubbles were substituted by an equal amount of Optimem. The 10 mL medium was completely added to the Opticell units (area 50 cm²). Subsequently the cells were placed in a water bath at 37°C with an absorbing rubber at the bottom and immediately subjected to ultrasound radiation. The ultrasound radiation was performed by moving in 15s a 22 mm ultrasound probe (sonitron 2000 (RichMar, Inola, OK, USA) over the whole surface of the Opticell. In all the experiments with ultrasound we used the following settings: 1 MHz, 50% duty cycle and an

ultrasound intensity of $2\text{W}/\text{cm}^2$. Unless otherwise stated, cells were immediately treated with ultrasound after addition of respectively DOX-liposomes, DOX-liposome loaded microbubbles or free DOX. Four hours after the addition of the DOX-liposomes, the DOX-liposome loaded microbubbles or free DOX we removed the medium and washed the cells two times with PBS, before adding fresh culture medium. 48 hours later the cells were incubated with $0.5\text{ mg}/\text{mL}$ MTT labeling reagent (Cell Proliferation Kit I, Roche diagnostics, Vilvoorde, Belgium) for 4 h. Afterwards the solubilisation solution was added and cells were incubated overnight at 37°C . The next day, the absorbance of each plate was measured at respectively 590nm (OD_{590}), to determine the amount of formed formazan, and at 690nm as a reference. The cell viability was calculated as follows:

$$\frac{(\text{OD}_{590} \text{ x} - \text{OD}_{590} \text{ phenol})}{(\text{OD}_{590} \text{ blank} - \text{OD}_{590} \text{ phenol})}$$

Experiments were performed at least three times and the results shown here are representative of the results obtained in the different cytotoxicity measurements. The error bars in the graphs are originating from different samples that were taken from one Opticell plate and separately measured at 590nm and 690nm .

Cellular uptake of DOX in the BLM cells

Cells were incubated with respectively DOX-liposomes, DOX-liposome loaded microbubbles and free DOX according to the protocols described above. The DOX in cells was visualized with a Nikon EZC1-si confocal microscope equipped with a $60\times$ objective. The 491nm line of this microscope was used to excite the doxorubicin and the doxorubicin was detected with the 580nm detector.

Statistical analysis

All the data in this report are expressed as mean \pm standard deviation (SD). For the transfection results, the Student's t-test was used to determine whether data groups differed significantly from each other. A p-value lower than 0.05 was considered statistically significant.

RESULTS & DISCUSSION

Design and characterization of DOX-liposome loaded microbubbles

As schematically presented in Figure 1, we aimed to construct lipid microbubbles loaded with doxorubicin-liposomes. Therefore, we first prepared doxorubicin-containing liposomes composed of 55 mol% DPPC, 40 mol% cholesterol, and 5 mol% DSPE-PEG-biotin. After loading the liposomes with doxorubicin and GPC purification, DOX-liposomes with an average diameter of 147 nm were obtained. We also prepared lipid microbubbles that contained 15 mol% DSPE-PEG-biotin in their shell. The biotinylated microbubbles were subsequently incubated with an excess of avidin, to saturate the biotin molecules at their surface. After removal of the excess of avidin the microbubbles were incubated with the biotinylated DOX-liposomes to couple the DOX-liposomes on the microbubbles via an avidin-biotin bridge (Figure 1). The binding of the DOX-liposomes, which are fluorescent due to the presence of doxorubicin, on the microbubbles was confirmed via confocal laser scanning microscopy (CLSM): Figure 2 clearly shows that the surface of the microbubbles becomes surrounded by doxorubicin-containing liposomes. The amount of DOX-liposomes that was bound to the microbubbles was estimated by removing the unbound DOX-liposomes from the microbubbles via centrifugation. We calculated that 65% of the DOX-liposomes was attached to the microbubbles. Knowing that we mixed about 1×10^9 microbubbles with 50 μg of doxorubicin encapsulated in liposomes, each microbubble is expected to contain about $3,25 \times 10^{-8}$ μg doxorubicin.

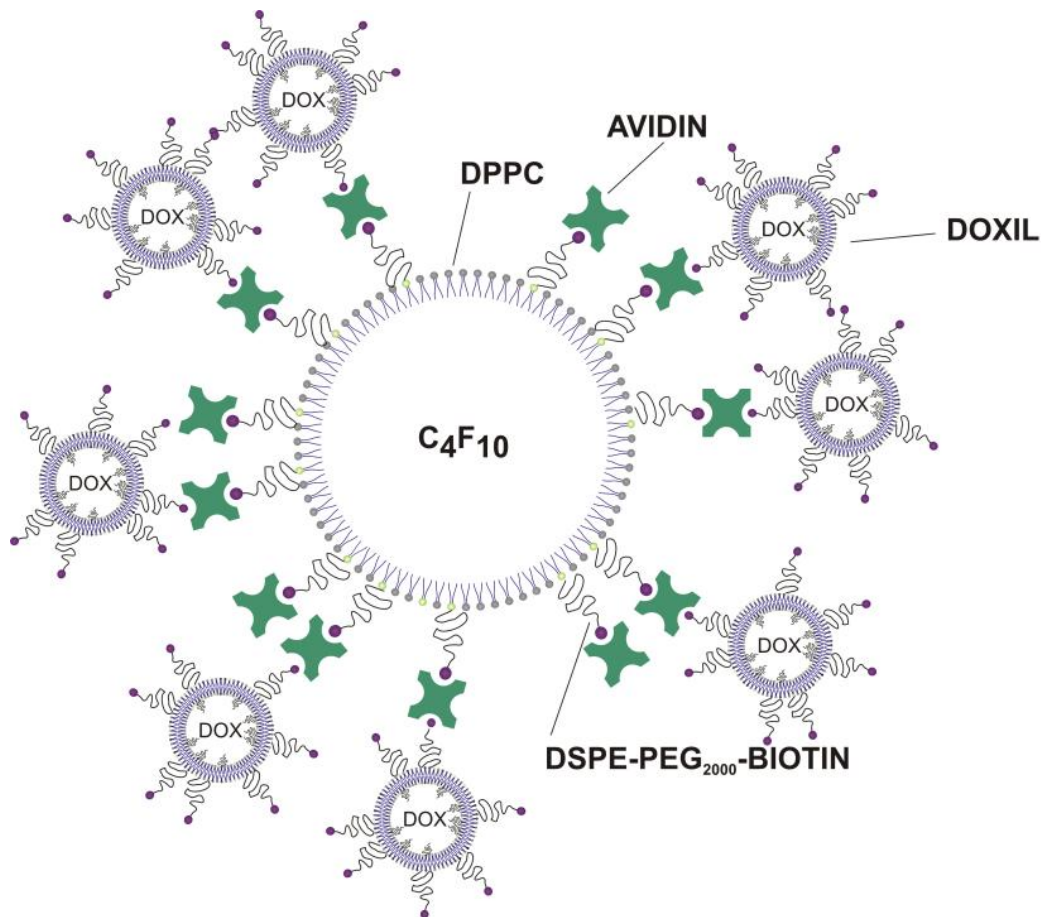


Figure 1 Schematic presentation of a DOX-liposome loaded microbubble.

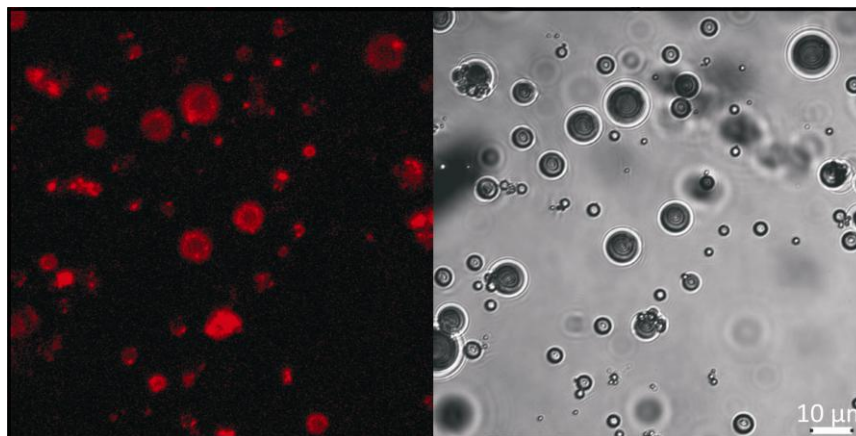


Figure 2 Confocal laser scanning microscopy image and corresponding transmission image of DOX-liposome loaded microbubbles. The DOX-liposomes were visualized using the fluorescence of the encapsulated doxorubicin.

Efficacy of DOX-liposome loaded microbubbles after ultrasound treatment

In Figure 3 the killing of cancer cells by respectively DOX-liposome loaded microbubbles, in the presence of ultrasound, and DOX-liposomes is compared. The cell killing by DOX-liposomes (light grey bars) was rather limited; the highest concentrations (50 and 100 $\mu\text{g}/\text{mL}$) killed about 50 % of the cells. In contrast, DOX-liposomes attached onto the microbubbles (white bars) were by far more toxic to the cells after ultrasound application. We also observed a nice correlation between the liposome concentration present on the DOX-liposome loaded microbubbles and the cell viability, which was less clear in case DOX-liposomes were used.

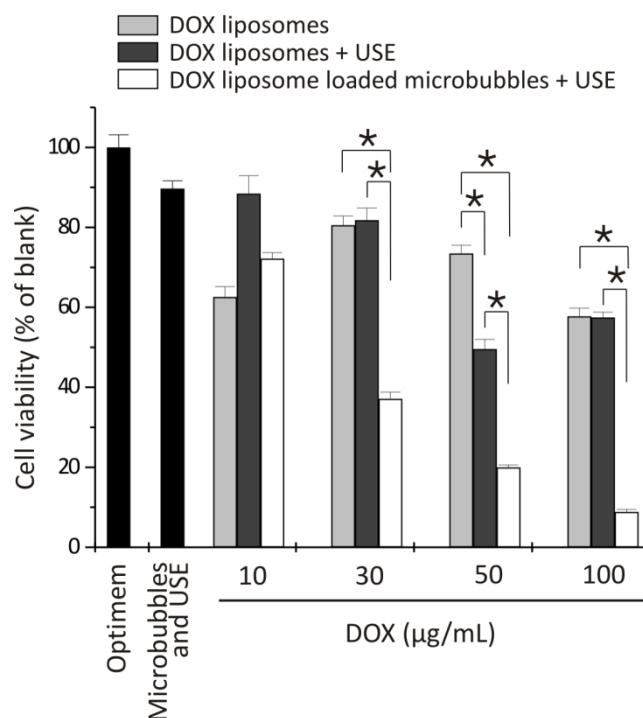


Figure 3 Cell viability of the melanoma cells after treatment with DOX-liposomes without (light grey bars) and with ultrasound exposure (USE) (dark grey bars) and DOX-liposome loaded microbubbles after ultrasound exposure (white bars) as a function of the DOX concentration. * $p < 0,05$

Some groups described a synergistic effect of ultrasound on the killing of cells by DOX-liposomes²⁵ and DOX-micelles^{20,26-28}. Though we did not observe an outspoken improvement of the cell killing by DOX-liposomes when ultrasound was applied (Figure 3: dark gray bars). Most authors use low frequency ultrasound (20-100kHz), which is known to favour cavitation at relatively low intensities, even in the absence of microbubbles. In our experiment we exposed the DOX-liposomes to 1MHz frequency ultrasound in the absence of microbubbles. Under these ultrasound conditions it is well known that cavitation is limited and probably too low to release the doxorubicin from the

liposomes or to perforate cell membranes. In contrast, DOX-liposome loaded microbubbles in the presence of ultrasound significantly lowered the overall viability of the melanoma cells. We observed previously that the ultrasound conditions used in this study may detach a (small) part of the cells from the Opticell membrane. Therefore, we also studied the effect of microbubbles (not loaded with DOX-liposomes) and ultrasound on the viability of the melanoma cells. As Figure 3 shows, this reduced the cell viability with about 10%. Though, even if we take this into account, DOX-liposome loaded microbubbles and ultrasound seemed much more efficient in killing cancer cells than free DOX-liposomes.

Intracellular localization of DOX

We tried to gain more insight into the intracellular doxorubicin concentrations in the melanoma cells (Figure 4). Different concentrations of respectively DOX-liposomes and DOX-liposome loaded microbubbles were added to the cells. After 4 hours the cells were washed and DOX uptake was visualized by CSLM. At the lowest DOX concentration (30 µg/mL) we could detect more DOX in cells exposed to DOX-liposome loaded microbubbles and ultrasound than in cells exposed to DOX-liposomes. This was less obvious at higher DOX concentrations used. The intracellular distribution of doxorubicin seemed to strongly depend on the way the doxorubicin was delivered to the cells. It was almost exclusively localized in the nuclei when the cells were treated with the DOX-liposome loaded microbubbles and ultrasound, while doxorubicin was found in both the cytoplasm and the nucleus of cells treated with DOX-liposomes. Sometimes a punctuated pattern could be seen in the cytoplasm of these cells (indicated by white arrows in Figure 4), which suggests that the doxorubicin locates in endosomes. Two simultaneously occurring phenomena may explain the different intracellular distribution of doxorubicin. First, after exposure of cells to DOX-liposome loaded microbubbles and ultrasound, free DOX (released from the liposomes destroyed by the ultrasound) probably enters the cells and accumulates in the nucleus because of its high affinity for DNA²⁹, which is abundantly present in the nucleus. Second, Schlichler et al³⁰ recently described the existence of exocytosis after exposure of cells to ultrasound and microbubbles to reseal the pores in the cell membranes. The transport of vesicles from the inside to the outside of the cell may limit endocytosis and thus reduce the amount of free doxorubicin or DOX-liposomes that is taken up by endocytosis.

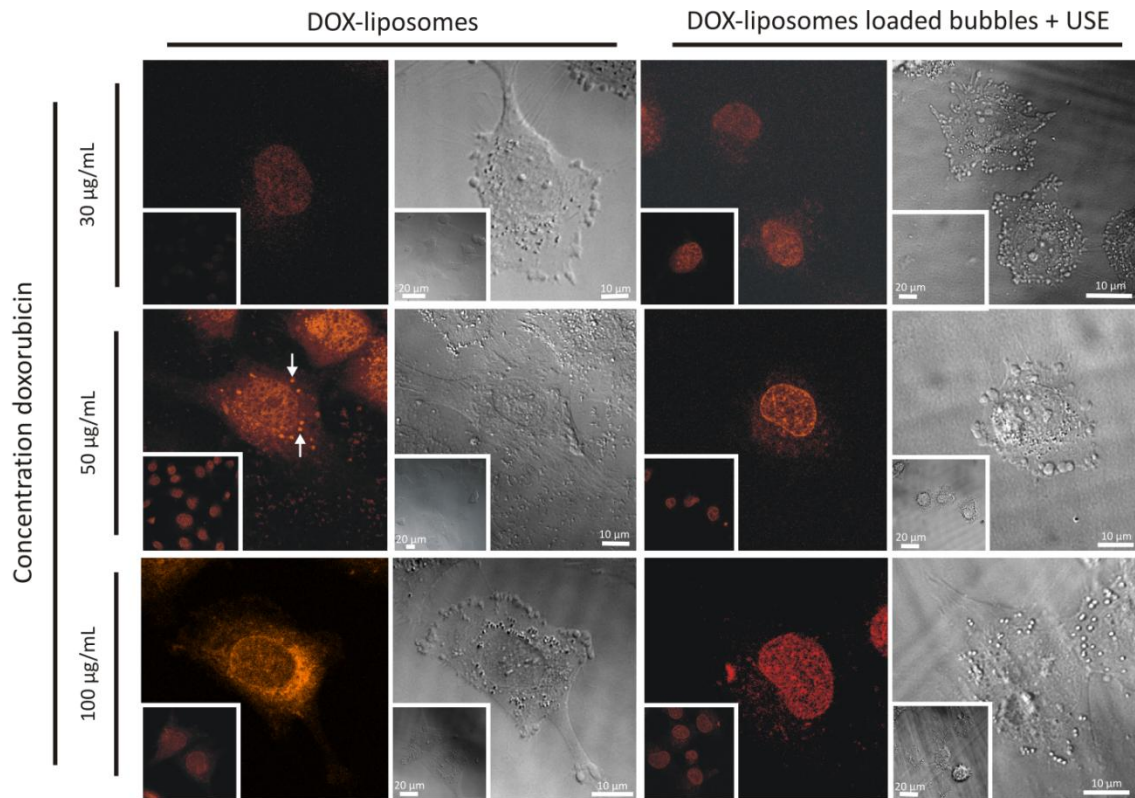


Figure 4 Confocal laser scanning microscopy images and corresponding transmission images of the uptake of DOX in melanoma cells treated with DOX-liposomes and DOX-liposome loaded microbubbles after ultrasound exposure. Cells were treated and incubated for 4 hours. Subsequently the cells were washed and immediately visualized with the confocal microscope. The same laser intensities were used to visualize the uptake of the same DOX concentrations in the two different formulations. For the uptake experiments of the 100 µg/mL DOX, a lower laser intensity was used as for the lower concentrations. For this reason it looks like there has been less DOX internalized at a higher concentration.

The higher amount of doxorubicin in the nuclei after exposure of the cells to DOX-liposome loaded microbubbles and ultrasound suggests the following delivery mechanism. Applying ultrasound destroys the liposomes on the microbubbles releasing free doxorubicin near the cell membranes, which can enter cells more easily than DOX-liposomes. Secondly, ultrasound may also increase the amount of free doxorubicin and DOX-liposomes that enter the cells via perforations in the membranes. In the following paragraphs we further investigated the mechanisms which may explain the stronger cell killing by doxorubicin loaded microbubbles and ultrasound.

Is the stronger cell killing by DOX-liposome loaded microbubbles due to an ultrasound mediated release of free DOX from the liposomes?

Several hypotheses have been proposed to explain the synergistic effect of ultrasound on the biological activity of anticancer drugs. The first mechanism postulates that ultrasound treatment of DOX-liposomes results in the release of doxorubicin from the liposomes which subsequently enters the cells via passive diffusion and pinocytosis³¹. To verify this hypothesis a direct effect of the cavitating microbubbles on the cell membrane should be avoided so that only the cytotoxic effect coming from doxorubicin can be taken into account. Therefore we performed an experiment in which the DOX-liposome loaded microbubbles were first exposed to ultrasound (using the same settings as in Figure 3) in an 'empty' Opticell (i.e. without melanoma cells). Subsequently, this 'medium' (i.e. the debris of radiated DOX-liposome loaded microbubbles) was transferred to an Opticell in which melanoma cells were growing. In this experiment sonoporation of the melanoma cells (by cavitating and imploding microbubbles cavitating) was thus avoided. After 4 hours of incubation, the 'medium' was removed and the cell viability was measured 48 hours later. Figure 5 shows that the debris of radiated DOX-liposome loaded microbubbles (white bars) showed a stronger tumour cell killing than DOX-liposomes (light grey bars). These data indicate that exposure of DOX-liposome loaded microbubbles to ultrasound most likely results in a release of free doxorubicin, which is known to cause a stronger cell killing than DOX-liposomes. Figure 5 reveals that the killing of melanoma cells by the debris of radiated DOX-liposome loaded microbubbles was significantly lower than that of DOX-liposome loaded microbubbles and ultrasound (especially at higher doxorubicin concentrations). It suggests that the cell killing by DOX-liposome loaded microbubbles and ultrasound is explained by both the release of free doxorubicin and the cavitation of the microbubbles which perforates the cell membranes.

We recently loaded PEGylated pDNA containing liposomes (lipoplexes) onto the same type of microbubbles as reported in this study⁶. We could show by dynamic light scattering that exposure of the lipoplex loaded microbubbles resulted in the release of intact lipoplexes. However, after exposure of the DOX-liposome loaded microbubbles to ultrasound we were no longer able to detect DOX-liposomes. This further suggests that indeed a substantial part of the DOX-liposomes becomes destroyed upon applying ultrasound to the DOX-liposome loaded microbubbles. Probably this results in the release of free doxorubicin that can enter the cells either via passive diffusion or through the perforations in the cell membranes, as discussed in the next paragraph.

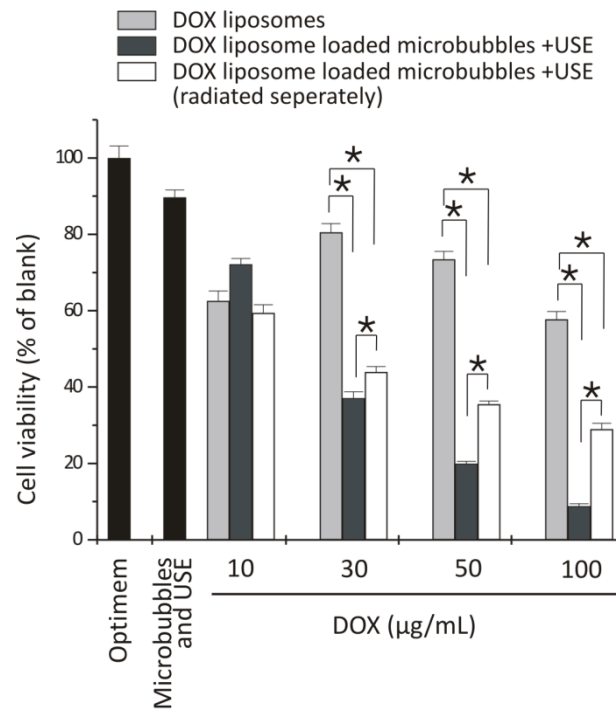


Figure 5 Cell viability of melanoma cells after treatment with DOX liposomes (light grey bars) and DOX-liposome loaded microbubbles with ultrasound exposure (dark grey bars). Cells were also treated with DOX liposome loaded microbubbles that were radiated with ultrasound before addition to the cells (white bars). *p<0,05.

Is the stronger cell killing by DOX-liposome loaded microbubbles due to an improved cellular uptake of DOX?

Several groups have studied the perforation of cell membranes by ultrasound^{9,30,32,33}. SEM images and uptake of fluorescent molecules after sonoporation have proven that cavitating microbubbles can indeed transiently disrupt cell membranes which allows compounds to enter cells. In our study pore formation might enhance the intracellular uptake of both free doxorubicin and doxorubicin liposomes. To further evaluate this hypothesis we studied the cellular uptake of doxorubicin shortly (i.e. 15-30 minutes) after exposure of melanoma cells to (1) DOX-liposome loaded microbubbles and ultrasound (Figures 6a-d), (2) DOX-liposomes (Figures 6e-h) and (3) free doxorubicin (Figures 6i-l). Almost immediately after exposure of the melanoma cells to DOX-liposome loaded microbubbles and ultrasound a substantial part of the cells contained very high levels of doxorubicin in their nuclei (Figures 6a,c). In sharp contrast, melanoma cells exposed to DOX-liposomes hardly contained doxorubicin after 15 minutes (Figures 6e,g). Free doxorubicin is known to be easily taken up by cells through a combined process of passive diffusion and active transport mechanisms³¹. Therefore, we also studied the uptake of free doxorubicin (Figures 6i-l). After 15

minutes cells treated with free doxorubicin contained clearly visible amounts of doxorubicin (Figures 6i,k) in the cytoplasm with only very little fluorescence in the nucleus of the cells. However, the amount of doxorubicin internalized by the cells was still much lower than the doxorubicin content in the cells exposed to DOX-liposome loaded microbubbles and ultrasound. Note that in the case of DOX-liposome loaded microbubbles a part of the cells had taken up extreme amounts of doxorubicin 15 minutes after exposure to ultrasound (these were probably the cells which were in contact with cavitating and imploding microbubbles), while the others were only weakly fluorescent (Figures 6a). In the case of free doxorubicin the fluorescence was rather equal in all cells which suggests that doxorubicin uptake occurred to the same extent in all cells.

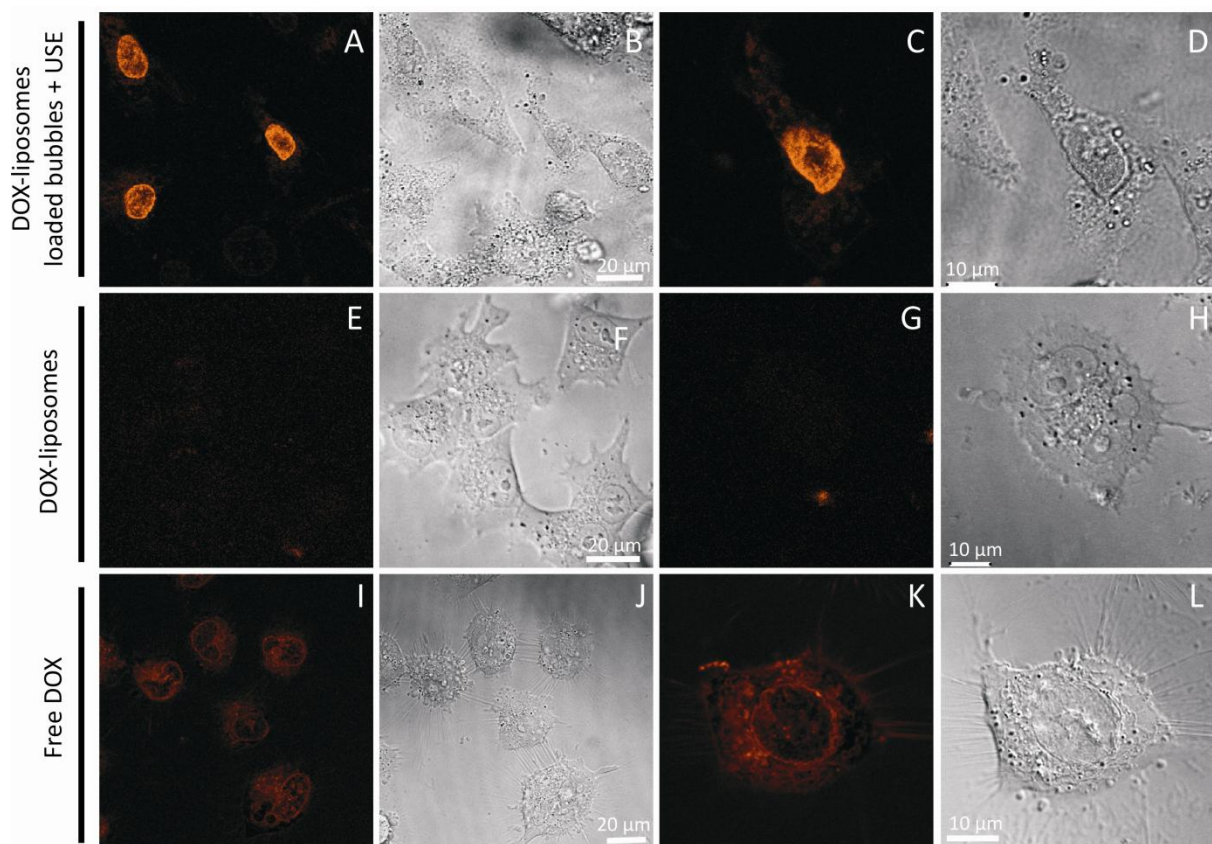


Figure 6 Confocal laser scanning microscopy image (A,C,E,G, I and K) and corresponding transmission image (B, D, F, H, J and L) of the uptake of doxorubicin after 15 minutes incubation with DOX-liposome loaded microbubbles and ultrasound exposure (A-D), DOX-liposomes (E-H) or free DOX (I-L). Image C,D,G,H,K and L present a close-up of a single cell.

Several papers have reported the instant uptake of larger molecules after sonoporation³⁴⁻³⁶. It has been shown that the microstreams developing around a cavitating microbubble, and especially the shock waves and microjets associated with microbubble cavitation, can result in the formation of transient pores in the cell membrane^{37,38}. Pore sizes between 100nm and a few μm in size have been

reported^{30,33}, implying that a rather small molecule like DOX should be able to enter the cell through such cell membrane pores. To further evaluate the hypothesis that microbubbles in the presence of ultrasound enhance the cellular uptake of doxorubicin we compared the killing of cells that had been exposed to respectively free doxorubicin and a mixture of free doxorubicin, microbubbles and ultrasound. As presented in Figure 7, microbubbles in combination with ultrasound significantly enhanced the cytotoxicity of free doxorubicin (dark gray bars). This supports the hypothesis that sonoporation indeed improves the cellular uptake of free doxorubicin. We also performed a second experiment in which we first exposed the melanoma cells to free DOX; After the 4 hours incubation time, the cells were carefully washed and treated with microbubbles and ultrasound. As can be seen in Figure 7 (white bars), this even resulted in a stronger killing which may be due to the fact that a certain time after internalization of free DOX melanoma cells become more sensitive to sonoporation. Cells treated with microbubbles and ultrasound are often irregularly shaped³². This was also observed in our experiments (Figure 6d). Despite their clearly damaged cell membrane, most cells are capable of resealing their membrane wounds^{32,39}, which was confirmed in our MTT experiment: only 10% of the BLM cells was metabolic inactive after exposure of the cells to microbubbles and ultrasound (Figure 3). It might be possible that due to the DOX induced cytotoxicity, the cells are less able to generate cell repair mechanisms, necessary to repair the cell membrane after sonoporation.

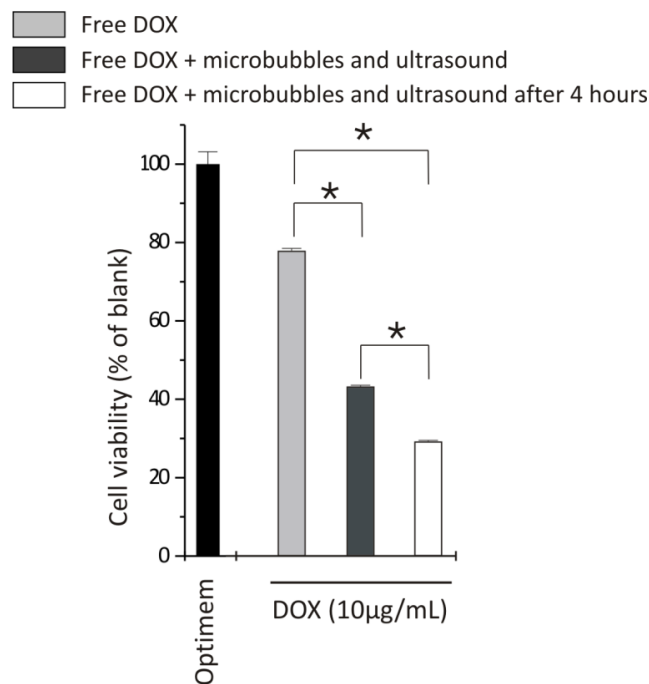


Figure 7 Cell viability of melanoma cells after treatment with free DOX (light grey bars) and free DOX with microbubbles and ultrasound exposure (dark grey bars). Cells were also incubated with free DOX for 4 hours, washed and then treated with microbubbles and ultrasound (white bars). *p<0,05

CONCLUSIONS

We succeeded in coupling doxorubicin containing liposomes onto the lipid shell of gas-filled microbubbles. DOX-liposome loaded microbubbles plus ultrasound killed much more tumour cells than DOX-liposomes. We showed that this is due to: (1) an ultrasonic triggered release of DOX from the DOX-liposomes present on the microbubbles, and (2) an enhanced uptake of the released DOX by the cells. The latter most likely results from temporary pores in the cell membranes induced by the imploding microbubbles (sonoporation). Based on the results in this manuscript we hypothesize that DOX-liposome loaded microbubbles in combination with ultrasound may significantly improve the *in vivo* efficacy of Doxil[®] being the liposomal doxorubicin formulation which is nowadays used in the clinic. Indeed, a local ultrasound triggered release of free doxorubicin in the tumour may enhance the cell killing by Doxil[®] as free DOX is expected to be more efficient than DOX-liposomes. Also, DOX-liposome loaded microbubbles may show less side-effects than Doxil[®] as in tissues not exposed to ultrasound the micron sized DOX-liposome loaded bubbles (1) will stay intact and thus will not release DOX-liposomes and (2) will not extravasate into these tissues. Moreover, the cavitation and implosion of the microbubbles in the tumour microvasculature may perforate endothelial cells and enhance the extravasation of the released doxorubicin^{11,12}. As demonstrated in Figure 8, the enhanced cellular uptake of doxorubicin in endothelial cells may improve doxorubicin to slow down angiogenesis and to break down the nutrient supply of the tumour cells⁴⁰. The *in vivo* biological response of the DOX-liposome loaded microbubbles may be further enhanced by attaching ligands to the microbubbles that specifically bind to the tumour endothelium^{41,42}.

Although several papers describe the use of ultrasound to improve drug release from nanoparticles and to enhance cellular uptake^{18,26,28,43-45}, only few have been published on the combined use of ultrasound and drug loaded microbubbles to improve antitumor treatment^{46,47}. Tartis *et al.* already developed a paclitaxel containing ultrasound contrast agent⁴⁷. In this study, the paclitaxel was dissolved in triacetin oil, which makes this type of microbubbles unsuited for hydrophilic drugs like DOX. Gao and colleagues were the first to report the design of a DOX loaded microbubble that was able to release the DOX upon ultrasound treatment⁴⁶. The doxorubicin was present in the shell of perfluorocarbon nanoparticles that vaporized and formed doxorubicin carrying microbubbles upon warming till 37 °C. Although they obtained good results both *in vitro* and *in vivo*, we believe that clinical application of the DOX-liposome carrying microbubbles described in our study may be more straightforward as as both DOX-liposomes (Doxil[®]) and lipid microbubbles (e.g. the contrast agent Definity[®]) are already used in clinical settings. Another advantage of the DOX-liposome loaded microbubbles is their high DOX loading efficiency. We estimated the

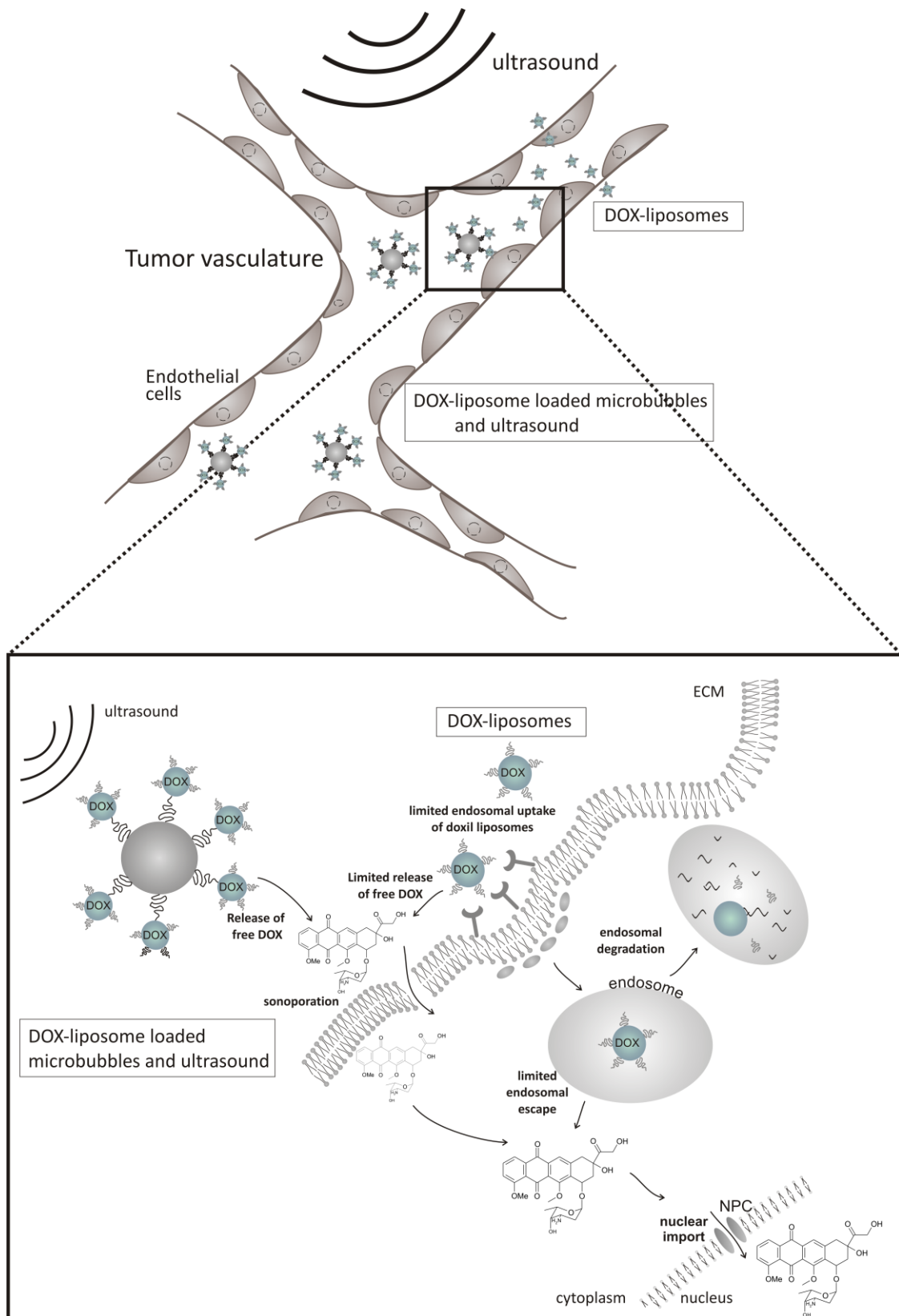


Figure 8 Schematic representation of the working principle of DOX-liposome loaded microbubbles compared to free DOX-liposomes in the tumor vasculature. When the microbubbles are exposed to ultrasound, the liposomes locally release the encapsulated doxorubicin. The cavitating and imploding microbubbles also increase the cell membrane permeability and hence increase the amount of doxorubicin that is taken up by especially the blood vessel cells.

encapsulated doxorubicin attached to one microbubbles to be 3.25×10^{-8} μg . Doxil[®] is given as a single dose of 20 mg/m^2 . This corresponds to a dose of 40 mg for an adult of about 80 kg. To reach amount of this dose we should administer about 1.23×10^{12} DOX-liposome loaded microbubbles. The recommended dose of Definity[®], which contains 1.2×10^{10} microbubbles/ml, is $10 \mu\text{l/kg}$ body weight which makes 10^{10} microbubbles for a person of 80 kg. This is about 100 times lower than the number of DOX-loaded microbubbles we must inject to administer 40 mg of doxorubicin. However, it has been demonstrated that Definity[®] doses that are 1000 times higher than the recommended dose are well tolerated in primates^{48,49}. Also, the locale release of the doxorubicin in the tumour after exposure of the DOX-liposome loaded microbubbles to ultrasound will most likely allow us to reduce the dose below 40 mg. The calculations above demonstrate that we may expect clinical effects in humans at a typically used microbubble dose.

ACKNOWLEDGMENTS

Ine Lentacker is supported by the Fund for Scientific Research - Flanders (Belgium). The financial support of institution is acknowledged with gratitude. Fien Vandeputte is thanked for the practical assistance. The financial support of the European Union (via the FP7 projects Arise and SonoDrugs) is acknowledged.

REFERENCES

- (1) Patil R.R., Guhagarkar S.A., & Devarajan P.V. Engineered nanocarriers of doxorubicin: A current update. *Critical Reviews in Therapeutic Drug Carrier Systems* **2008** 25(1) 1-61.
- (2) Maeda H., Wu J., Sawa T., Matsumura Y., & Hori K. Tumor vascular permeability and the EPR effect in macromolecular therapeutics: a review. *Journal of Controlled Release* **2000** 65(1-2) 271-284.
- (3) Andresen T.L., Jensen S.S., & Jorgensen K. Advanced strategies in liposomal cancer therapy: Problems and prospects of active and tumor specific drug release. *Progress in Lipid Research* **2005** 44(1) 68-97.
- (4) Ferrara K.W. Driving delivery vehicles with ultrasound. *Advanced Drug Delivery Reviews* **2008** 60(10) 1097-1102.
- (5) Frenkel V. Ultrasound mediated delivery of drugs and genes to solid tumors. *Advanced Drug Delivery Reviews* **2008** 60(10) 1193-1208.

- (6) Lentacker I., De Smedt S.C., Demeester J., Van Marck V., Bracke M., & Sanders N.N. Lipoplex-loaded microbubbles for gene delivery: A Trojan horse controlled by ultrasound. *Advanced Functional Materials* **2007** 17(12) 1910-1916.
- (7) Vandembroucke R.E., Lentacker I., Demeester J., De Smedt S.C., & Sanders N.N. - Ultrasound assisted siRNA delivery using PEG-siPlex loaded microbubbles. *Journal of controlled release* **2008** 126(3) 265-273.
- (8) Sboros V. Response of contrast agents to ultrasound. *Advanced Drug Delivery Reviews* **2008** 60(10) 1117-1136.
- (9) Duvshani-Eshet M., Baruch L., Kesselman E., Shimoni E., & Machluf M. Therapeutic ultrasound-mediated DNA to cell and nucleus: bioeffects revealed by confocal and atomic force microscopy. *Gene Therapy* **2006** 13(2) 163-172.
- (10) Pitt W.G., Husseini G.A., & Staples B.J. Ultrasonic drug delivery-a general review. *Expert Opinion on Drug Delivery* **2004** 1(1) 37-56.
- (11) Price R.J., Skyba D.M., Kaul S., & Skalak T.C. Delivery of colloidal, particles and red blood cells to tissue through microvessel ruptures created by targeted microbubble destruction with ultrasound. *Circulation* **1998** 98(13) 1264-1267.
- (12) Vancraeynest D., Havaux X., Pouleur A.C. *et al.* Myocardial delivery of colloid nanoparticles using ultrasound-targeted microbubble destruction. *European Heart Journal* **2006** 27(2) 237-245.
- (13) Yu T.H., Wang Z.B., & Mason T.J. A review of research into the uses of low level ultrasound in cancer therapy. *Ultrasonics Sonochemistry* **2004** 11(2) 95-103.
- (14) Siu T., Jackson J., Burt H., & Chiao M. Drug uptake enhancement using sonodynamic effects at 4 MHz - A potential application for micro-ultrasonic-transducers. *Ieee Transactions on Biomedical Engineering* **2007** 54(6) 1153-1156.
- (15) Yu T.G., Huang X.L., Hu K., Bai J., & Wang Z.B. Treatment of transplanted adriamycin-resistant ovarian cancers in mice by combination of adriamycin and ultrasound exposure. *Ultrasonics Sonochemistry* **2004** 11(5) 287-291.
- (16) Gao Z.G., Fain H.D., & Rapoport N. Controlled and targeted tumor chemotherapy by micellar-encapsulated drug and ultrasound. *Journal of Controlled Release* **2005** 102(1) 203-222.
- (17) Husseini G.A., Rapoport N.Y., Christensen D.A., Pruitt J.D., & Pitt W.G. Kinetics of ultrasonic release of doxorubicin from pluronic P105 micelles. *Colloids and Surfaces B-Biointerfaces* **2002** 24(3-4) 253-264.
- (18) Husseini G.A., Christensen D.A., Rapoport N.Y., & Pitt W.G. Ultrasonic release of doxorubicin from Pluronic P105 micelles stabilized with an interpenetrating network of N,N-diethylacrylamide. *Journal of Controlled Release* **2002** 83(2) 303-305.
- (19) Husseini G.A., Runyan C.M., & Pitt W.G. Investigating the mechanism of acoustically activated uptake of drugs from Pluronic micelles. *Bmc Cancer* **2002** 2
- (20) Husseini G.A. & Pitt W.G. Micelles and nanoparticles for ultrasonic drug and gene delivery. *Advanced Drug Delivery Reviews* **2008** 60(10) 1137-1152.

- (21) Rapoport N.Y., Herron J.N., Pitt W.G., & Pitina L. Micellar delivery of doxorubicin and its paramagnetic analog, ruboxyl, to HL-60 cells: effect of micelle structure and ultrasound on the intracellular drug uptake. *Journal of Controlled Release* **1999** 58(2) 153-162.
- (22) Rapoport N.Y., Christensen D.A., Fain H.D., Barrows L., & Gao Z. Ultrasound-triggered drug targeting of tumors in vitro and in vivo. *Ultrasonics* **2004** 42(1-9) 943-950.
- (23) Bolotin E.M. Ammonium Sulfate Gradients for Efficient and Stable Remote Loading of Amphipathic Weak Bases into Liposomes and Ligandoliposomes. *Journal of liposome research* **1994** 4(1), 455-479 .
- (24) Quax P.H.A., Vanmuijen G.N.P., Weeningverhoeff E.J.D. *et al.* Metastatic Behavior of Human-Melanoma Cell-Lines in Nude-Mice Correlates with Urokinase-Type Plasminogen-Activator, Its Type-1 Inhibitor, and Urokinase-Mediated Matrix Degradation. *Journal of Cell Biology* **1991** 115(1) 191-199.
- (25) Frenkel V., Etherington A., Greene M. *et al.* Delivery of liposomal doxorubicin (Doxil) in a breast cancer tumor model: Investigation of potential enhancement by pulsed-high intensity focused ultrasound exposure. *Academic Radiology* **2006** 13(4) 469-479.
- (26) Hussein G.A., de la Rosa M.A.D., Gabuji T., Zeng Y., Christensen D.A., & Pitt W.G. Release of doxorubicin from unstabilized and stabilized micelles under the action of ultrasound. *Journal of Nanoscience and Nanotechnology* **2007** 7(3) 1028-1033.
- (27) Hussein G.A. & Pitt W.G. The use of ultrasound and micelles in cancer treatment. *Journal of Nanoscience and Nanotechnology* **2008** 8(5) 2205-2215.
- (28) Rapoport N. Combined cancer therapy by micellar-encapsulated drug and ultrasound. *International Journal of Pharmaceutics* **2004** 277(1-2) 155-162.
- (29) Gewirtz D.A. A Critical Evaluation of the Mechanisms of Action Proposed for the Antitumor Effects of the Anthracycline Antibiotics Adriamycin and Daunorubicin. *Biochemical Pharmacology* **1999** 57, 727-741 .
- (30) Schlicher R.K., Radhakrishna H., Tolentino T.P., Apkarian R.P., Zarnitsyn V., & Prausnitz M.R. Mechanism of intracellular delivery by acoustic cavitation. *Ultrasound in Medicine and Biology* **2006** 32(6) 915-924.
- (31) Dai X., Yue Z., Eccleston M.E., Swartling J., Slater N.K., & Kaminski C.F. Fluorescence intensity and lifetime imaging of free and micellar-encapsulated doxorubicin in living cells. *Nanomedicine : nanotechnology, biology, and medicine* **2008** 4(1) 49-56.
- (32) Brayman A.A., Coppage M.L., Vaidya S., & Miller M.W. Transient poration and cell surface receptor removal from human lymphocytes in vitro by 1 MHz ultrasound. *Ultrasound in Medicine and Biology* **1999** 25(6) 999-1008.
- (33) Prentice P., Cuschierp A., Dholakia K., Prausnitz M., & Campbell P. Membrane disruption by optically controlled microbubble cavitation. *Nature Physics* **2005** 1(2) 107-110.
- (34) Karshafian R., Bevan P.D., Burns P.N. *et al.* Ultrasound-induced uptake of different size markers in mammalian cells. *IEEE Ultrasonics Symposium* **2005** 1-4 13-16.

- (35) Khanna S., Hudson B., Pepper C.J., Amso N.N., & Coakley W.T. Fluorescein isothiocyanate-dextran uptake by chinese hamster ovary cells in a 1.5 MHz ultrasonic standing wave in the presence of contrast agent. *Ultrasound in Medicine and Biology* **2006** 32(2) 289-295.
- (36) Kodama T., Doukas A.G., & Hamblin M.R. Shock wave-mediated molecular delivery into cells. *Biochimica et Biophysica Acta-Molecular Cell Research* **2002** 1542(1-3) 186-194.
- (37) Tachibana K., Uchida T., Ogawa K., Yamashita N., & Tamura K. Induction of cell-membrane porosity by ultrasound. *Lancet* **1999** 353(9162) 1409.
- (38) Wu J. & Nyborg W.L. Ultrasound, cavitation bubbles and their interaction with cells. *Advanced Drug Delivery Reviews* **2008** 60(10) 1103-1116.
- (39) Ross J.P., Cai X., Chiu J.F., Yang J., & Wu J.R. Optical and atomic force microscopic studies on sonoporation. *Journal of the Acoustical Society of America* **2002** 111(3) 1161-1164.
- (40) Molema G., Meijer D.K.F., & De Leij L.F.M.H. Tumor vasculature targeted therapies - Getting the players organized. *Biochemical Pharmacology* **1998** 55(12) 1939-1945.
- (41) Eliaz R.E., Nir S., Marty C., & Szoka F.C. Determination and modeling of kinetics of cancer cell killing by doxorubicin and doxorubicin encapsulated in targeted liposomes. *Cancer Research* **2004** 64(2) 711-718.
- (42) Sawant R.M., Cohen M.B., Torchilin V.P., & Rokhlin O. Prostate cancer-specific monoclonal antibody 5D4 significantly enhances the cytotoxicity of doxorubicin-loaded liposomes against target cells in vitro. *Journal of Drug Targeting* **2008** 16(7-8) 601-604.
- (43) Myhr G. & Moan J. Synergistic and tumour selective effects of chemotherapy and ultrasound treatment. *Cancer Letters* **2006** 232(2) 206-213.
- (44) Rosenthal I., Sostaric J.Z., & Riesz P. Sonodynamic therapy - a review of the synergistic effects of drugs and ultrasound. *Ultrasonics Sonochemistry* **2004** 11(6) 349-363.
- (45) Schroeder A., Avnir Y., Weisman S. *et al.* Controlling liposomal drug release with low frequency ultrasound: Mechanism and feasibility. *Langmuir* **2007** 23(7) 4019-4025.
- (46) Gao Z., Kennedy A.M., Christensen D.A., & Rapoport N.Y. Drug-loaded nano/microbubbles for combining ultrasonography and targeted chemotherapy. *Ultrasonics* **2008** 48(4) 260-270.
- (47) Tartis M.S., McCallan J., Lum A.F.H. *et al.* Therapeutic effects of paclitaxel-containing ultrasound contrast agents. *Ultrasound in Medicine and Biology* **2006** 32(11) 1771-1780.
- (48) Karshafian R., Bevan P.D., Williams S., Samac S., & Burns P.N. Sonoporation by Ultrasound-Activated Microbubble Contrast Agents: Effect of Acoustic Exposure Parameters on Cell Membrane Permeability and Cell Viability. *Ultrasound in Medicine and Biology* **2009** doi:10.1016/j.ultrasmedbio.2008.10.013 .
- (49) Unger E.C., Porter T., Culp W., LaBell R., Matsunaga T., & Zutshi R. Therapeutic applications of lipid-coated microbubbles. *Advanced Drug Delivery Reviews* **2004** 56(9) 1291-1314.

Summary & General Conclusions

Summary & General Conclusions

SUMMARY

Cancer is a genetic disease, caused by mutations in the genome of normal cells. Chemical and physical damage to the cellular genome can induce these mutations resulting in the transformation of a healthy cell into a tumor cell. Over the past years, researchers have acquired a basic understanding of tumor onset. Several important proto-oncogenes and proteins involved in angiogenesis have been identified, leading to the development and clinical use of several new anticancer agents.

In **chapter 1** we summarized the different chemotherapeutic drugs that are currently available for cancer treatment. Until now, the responsiveness of tumor cells to the current chemotherapeutic drugs is hampered by the development of tumor resistance genes and limited drug doses. The non-specificity of these drugs often results in severe side-effects e.g. neutropenia limiting the acceptable drug doses. Cancer gene therapy can be employed to suppress oncogenes, substitute defect tumor suppressor genes, improve the patient's immune system or selectively promote the transformation of non-toxic pro-drugs into highly potent drugs. The different approaches in cancer gene therapy are briefly discussed in this chapter together with a short overview of the most common genetic drugs. Due to the heterogeneity in tumor vasculature and interstitial transport, current cancer treatments are hampered by a non-uniform and insufficient delivery of chemotherapeutic and genetic drugs to the tumor. To achieve an efficient cancer therapy several important extracellular and intracellular barriers have to be conquered. It was recently suggested that ultrasound and microbubbles can be used to efficiently transport drugs into target cells. The microstreams and shock waves that develop around a cavitating or imploding microbubble are able to temporally disturb the cell membrane, resulting in the formation of transient pores through which drugs can enter the cell. As microbubble cavitation and implosion is limited to ultrasound treated areas, drug delivery can be targeted simply by applying ultrasound on the desired region. Because in most cases drugs and microbubbles are injected separately in the bloodstream there is still a risk that drugs are taken up, although less efficient, in unwanted areas. To reduce unwanted side-effects and lower drug doses it could be even

more advantageous to design a drug loaded microbubble. In this way drug release may become strictly limited to ultrasound treated areas, improving ultrasound targeting even more. Furthermore, associating drug and microbubble can assure that more drug molecules are available at the sonoporation site, enhancing drug uptake in the sonoporated cells. In this thesis we tried to develop drug-loaded microbubbles which are able to selectively deliver their drugs to cancer cells after ultrasound exposure.

Due to their negatively charged backbone it is interesting to couple genetic drugs like plasmid DNA electrostatically to the microbubble shell. For this purpose we developed cationic microbubbles in **chapter 2**. Albumin microbubbles were incubated with the cationic polymer poly-(allylamine hydrochloride) (PAH), enabling electrostatic loading of pDNA onto the microbubble shell. Polymer coating of the microbubbles was confirmed with zeta potential measurements and confocal laser scanning microscopy images using fluorescently labeled PAH. The polymer layer around the microbubble shell slows down gas diffusion and results in a 7-fold longer life-time of the microbubbles. pDNA loading onto the microbubble shell was demonstrated using confocal microscopy with a pDNA loading capacity of 0,1 pg pDNA per microbubble. As evidenced in our gel electrophoresis experiments, the pDNA bound onto the polymer shell was resistant to DNase I degradation.

In **chapter 3** we studied the gene transfection efficiency of the uncoated and polymer-coated albumin microbubbles. Despite their high pDNA loading efficiency and capacity to protect the adhered pDNA against degradation, the polymer coated microbubbles did not succeed in transfecting primary endothelial or melanoma cells. Gel electrophoresis experiments revealed that the pDNA was still complexed to microbubble shell fragments after ultrasound induced implosion of the microbubbles. Additional confocal microscopy images of the imploded microbubbles, showed the existence of very large (several μm) and heterogeneous aggregates consisting of microbubble shell fragments and pDNA. The large size and heterogeneity of these fragments make it rather unlikely that they will be taken up through cell membrane pores. Moreover, even if part of these fragments would be able to enter the cellular cytoplasm, the transfection capacity of the pDNA will be limited by a difficult intracellular dissociation from the polymer.

For gene delivery purposes, the microbubble should be able to locally release its genetic material in the ultrasound treated area, whereupon it should become available for cellular uptake through the cell membrane pores. As we discovered that an electrostatic loading of microbubbles with pDNA hampered the transfection efficiency due to a poor pDNA release, we searched for a different approach to develop drug loaded microbubbles. It was previously shown that ultrasound is capable of breaking avidin-biotin bonds between microbubbles and nanoscopic polystyrene beads. For this reason we prepared lipid microbubbles to which well-defined pDNA or siRNA containing

nanoparticles were attached with the aid of an avidin-biotin bond, as reported in **chapters 4 and 6**. The pDNA or siRNA molecules were first complexed with DSPE-PEG-biotin containing cationic liposomes, leading to the formation of PEGylated lipoplexes with a biotin molecule attached to the end of their PEG-tails. Also, biotinylated lipid microbubbles were prepared containing the same biotinylated lipid. After incubation of the microbubbles with an excess of avidin, confocal microscopy images showed the coupling of these lipoplexes onto the microbubble shell and proved that lipoplex loading could be improved by increasing the biotinylation degree of the lipoplexes. Ultrasound exposure of lipoplex loaded microbubbles resulted in the release of intact lipoplexes, with an unaltered size and surface charge. Also, pDNA and siRNA complexation properties of the lipoplexes were not changed after ultrasound induced release from the microbubbles. The gene transfection efficiency (**chapter 4**) or silencing efficiency (**chapter 6**) of the lipoplexes was significantly improved after microbubble coupling and ultrasound exposure, in contrast to free lipoplexes. Interestingly, in the absence of ultrasound the lipoplex loaded microbubbles did not result in gene transfection or gene silencing, allowing both a space and time controlled delivery.

PEGylation of lipoplexes is known to be essential for *in vivo* use, to avoid a rapid clearance from the blood stream and to prevent the development of immune responses. However, it has also been demonstrated that the presence of the PEG-chains around lipoplexes reduces their gene transfection capacity due to a reduced uptake by cells and inefficient escape from endosomes. As the lipoplex loaded microbubbles were able to restore these gene transfer capacity in the presence of ultrasound we wondered how the lipoplexes, released from the microbubbles, were taken up by cells (**chapter 5**). We first evaluated whether the lipoplexes entered the cell via an endocytic pathway. Pre-incubation of the cells with the endocytic inhibitor methyl- β -cyclodextrin only reduced the transfection efficiency of free lipoplexes, while the transfection efficiency of the lipoplex loaded microbubbles remained unchanged. Methyl- β -cyclodextrin hampered the endocytic uptake of free lipoplexes as evidenced with confocal microscopy. We also studied the effect of a photosensitizer, which destroys endosomal membranes, on the transfection efficiencies. Disrupting the endosomes only improved the transfection efficiency of free lipoplexes, indicating that the lipoplexes released from the microbubbles are taken up by an endocytosis independent pathway. Confocal imaging revealed that the free lipoplexes mainly adhered onto the cell membranes and were only visible in the endosomes after a longer incubation time. In contrast, the membranes of cells exposed to lipoplex loaded microbubbles and ultrasound became immediately disturbed and lipoplexes were detected inside the cell membrane, protruding in the cellular cytoplasm.

The clinical use of doxorubicin liposomes (Caelix[®] and Doxil[®]) is up till now hampered by a limited therapeutic efficacy, as the available dose mainly depends on the passive diffusion of free doxorubicin (released from the liposomes) into the cancer cells. Several research groups have

therefore focused on the development of an active delivery system for doxorubicin, aiming at an improved therapeutic efficacy. In **chapter 7** of this work we used the same microbubble concept to couple doxorubicin containing liposomes (DOX-liposomes) on the shell of lipid microbubbles to obtain an ultrasound controlled doxorubicin delivery system. While ultrasound exposure of free DOX-liposomes did not result in an enhanced cell killing, we saw an important increase in DOX cytotoxicity after ultrasound exposure of the DOX-liposome loaded microbubbles. Confocal images showed the immediate uptake of DOX in the nucleus of melanoma cells exposed to DOX-liposomes loaded microbubbles and ultrasound. In contrast, the DOX coming from the free DOX-liposomes was mainly located in vesicles in the cellular cytoplasm, suggesting an endosomal uptake. Our findings also suggested that three different phenomena are responsible for the stronger activity of DOX-liposomes. First, the ultrasound induced implosion of the microbubbles destroys at least a part of the attached liposomes, resulting in the release of free DOX. Second, due to the sonoporation effect, more free DOX or DOX-liposomes are able to enter the melanoma cells. Third, there is a combined cytotoxic effect of DOX and sonoporation, as exposure of the melanoma cells to DOX makes the cells less resistant to microbubble and ultrasound exposure.

GENERAL CONCLUSIONS

In conclusion, we succeeded in preparing microbubbles which are able to carry genetic (pDNA, siRNA) and chemotherapeutic (doxorubicin) drugs. We proved that these microbubbles can selectively deliver their genetic or chemotherapeutic drugs to melanoma cells upon ultrasound exposure. We also showed that the activity of currently available drug carriers (pDNA or siRNA lipoplexes and doxorubicin-liposomes) was significantly improved by microbubble coupling and ultrasound exposure. This enables us to obtain a space and time controlled drug delivery guided by ultrasound. The fact that ultrasound and microbubbles have already been approved for ultrasound contrast imaging and are currently used in daily clinic, makes it very plausible that the microbubble concept reported in this thesis may find its way as an advanced drug delivery system.

Samenvatting & Algemene Besluiten

Samenvatting & Algemene Besluiten

SAMENVATTING

Kanker is een genetische aandoening die veroorzaakt wordt door mutaties in het genoom van normale cellen. Chemische en fysische schade aan het cellulair genoom kunnen mutaties induceren die leiden tot de transformatie van een gezonde cel in een kankercel. De laatste jaren zijn wetenschappers erin geslaagd om een aantal oorzaken in het ontstaan van kanker te ontrafelen. Verschillende belangrijke proto-oncogenen en angiogenese controlerende proteïnen werden geïdentificeerd, wat heeft geleid tot de ontwikkeling van verschillende nieuwe antikanker geneesmiddelen.

In **hoofdstuk 1** van dit doctoraat werden in eerste instantie de belangrijkste klassen van chemotherapeutica die momenteel voorhanden zijn samengevat. Tot vandaag is de therapeutische werking van deze geneesmiddelen nog steeds beperkt omwille van hun weinig specifieke aard. Naast de kankercellen worden veel snel delende cellen getroffen, wat onder andere kan leiden tot een tekort aan witte bloedcellen. Hierdoor is de maximale dosis beperkt, wat kan resulteren in de vorming van geneesmiddelresistente kankercellen, waardoor de therapie niet meer aanslaat of de patiënt hervalt. Anderzijds kan genterapie gebruikt worden om oncogenen te onderdrukken, defecte tumor suppressor genen te vervangen, de selectieve omzetting van onschadelijke pro-drugs naar chemotoxische geneesmiddelen te stimuleren of om het immuunsysteem van de patiënt te verbeteren zodat kankercellen vernietigd kunnen worden. De verschillende genterapie-strategieën ter behandeling van kanker worden kort besproken, samen met een overzicht van de meest courante genetische therapeutica. Om een efficiënte kankertherapie te kunnen bereiken is het noodzakelijk om verschillende barrières in het lichaam te overwinnen. Recent werd aangetoond dat ultrasound en microbubbels kunnen aangewend worden om geneesmiddelen in cellen te brengen. Wanneer microbubbels blootgesteld worden aan een ultrasoon veld, beginnen ze te caviteren, waarna ze eventueel ook kunnen imploderen. De stromingen en schokgolven die ontstaan tijdens cavitatie en zeker tijdens de implosie van de microbubbels kunnen de celmembraan van de cel tijdelijk verstoren,

wat resulteert in de vorming van tijdelijke poriën in de celmembranen waardoor geneesmiddelen kunnen opgenomen worden. Doordat microbubbel-cavitatie en -implosie enkel kan gebeuren in de ultrasound bestraalde zones, kan de geneesmiddeltoediening selectief gestuurd worden door alleen de zieke weefsels aan ultrasound bloot te stellen. Omdat geneesmiddel en microbubbels meestal afzonderlijk worden geïnjecteerd, bestaat nog steeds het risico dat het geneesmiddel, zij het minder efficiënt, ook in ongewenste weefsels wordt opgenomen, wat kan leiden tot neveneffecten. Om de geneesmiddeldosis en neveneffecten van geneesmiddelen te beperken, is het nog meer aangewezen om microbubbels te ontwerpen die het geneesmiddel bevatten zodat het enkel in de ultrasound bestraalde weefsels beschikbaar wordt voor opname. Bovendien kan een geneesmiddel beladen microbubbel ervoor zorgen dat de geneesmiddelconcentratie ter hoogte van de celmembraan perforaties hoger is, waardoor meer geneesmiddel kan opgenomen worden in de doelcellen. Het doel van dit doctoraat was om geneesmiddel beladen microbubbels te ontwerpen die in staat zijn om hun geneesmiddel lokaal vrij te stellen na ultrasound bestraling en de selectieve opname van dit geneesmiddel in kankercellen te bevorderen.

Omwille van hun negatieve lading is het zeer interessant om nucleïne-zuren zoals plasmide DNA (pDNA) elektrostatich aan de microbubbel wand te koppelen. Voor deze reden werden positief geladen microbubbels aangemaakt in **hoofdstuk 2**. Albumine microbubbels werden bedekt met een positief geladen polymeer poly-(allylamine hydrochloride) (PAH), zodat het pDNA elektrostatich kon binden op de microbubbel wand. De aanwezigheid van het PAH-polymeer rond de microbubbel werd aangetoond door de oppervlaktelading van de bubbel te meten en via fluorescentie microscopie (na het fluorescent markeren van het PAH). We toonden aan dat de polymeerlaag rond de microbubbel zorgt voor een vertraagde gasdiffusie uit de microbubbel, waardoor de stabiliteit van de microbubbel aanzienlijk verlengd kan worden. De koppeling van pDNA aan de microbubbel wand werd geverifieerd met confocale microscopie en de maximale beladingsgraad werd geschat op 0,1 pg pDNA per microbubbel. Bovendien konden we uit gelelectroforese experimenten afleiden dat het gebonden pDNA beschermd was tegen degradatie door DNase I.

In **hoofdstuk 3** bestudeerden we de transfectie efficiëntie van onbedekte en polymeer omhulde albumine microbubbels. Ondanks hun hoge pDNA beladingsgraad en bescherming van het pDNA tegen degradatie waren de polymeer omhulde microbubbels niet in staat om primaire endotheelcellen of melanoma cellen te transfecteren. Gelelectroforese experimenten toonden aan dat het pDNA na ultrasound geïnduceerde implosie van de microbubbels nog steeds gebonden zit aan microbubbelfragmenten. Via confocale microscopie werd duidelijk dat na implosie van de microbubbels, grote, heterogene aggregaten (enkele micrometers groot) overblijven die bestaan uit microbubbel-wand en pDNA. Door hun grootte en heterogeniteit is het zeer onwaarschijnlijk dat deze fragmenten in staat zijn om opgenomen te worden door de celmembraan perforaties. Zelfs in

het geval dat een deel van deze fragmenten het cytoplasma van de cel kan bereiken, zal de transfectie wellicht verhinderd worden door de moeilijke intracellulaire dissociatie, waardoor het pDNA de nucleus niet kan bereiken.

Om een efficiënte genexpressie te bekomen dient de microbubbel zijn pDNA vrij te geven na ultrasound bestraling, waarna het beschikbaar komt voor cellulaire opname door de celmembraan poriën. Omdat we in hoofdstuk 3 aantoonden dat de elektrostatische binding van nucleïnezuren aan de microbubbel wand de transfectie verhinderd door een geringe dissociatie, werd gezocht naar een alternatieve strategie. Eerder werd aangetoond dat ultrasound in staat is om polystyreen nanopartikels die via een avidine-biotine-binding aan het oppervlak van microbubbels zitten lokaal vrij te stellen. Hierop voortbouwend werden nieuwe microbubbels aangemaakt waarbij pDNA (**hoofdstuk 4**) of short interfering RNA-bevattende (siRNA) (**hoofdstuk 6**) nanopartikels aan het oppervlak van een lipide microbubbel gekoppeld werden met behulp van een avidine-biotine binding. De pDNA of siRNA moleculen werden eerst gecomplexeerd met DSPE-PEG-biotine bevattende liposomen. Dit zorgde voor de vorming van gePEGyleerde pDNA of siRNA bevattende lipoplexen met een biotine molecule gekoppeld aan het uiteinde van de PEG-staarten. Daarnaast werden ook lipide microbubbels aangemaakt die hetzelfde gebiotinyleerde lipide bevatten. Confocale microscopie toonde aan dat de lipoplexen eenvoudig aan het oppervlak van de microbubbels gekoppeld konden worden na incubatie met avidine en dat de beladingsgraad van de microbubbels verhoogd kon worden door de biotinylatiegraad van de lipoplexen te verhogen. Ultrasound bestraling van deze lipoplex beladen microbubbels resulteerde in een massale vrijstelling van intacte lipoplexen, met een onveranderde grootte en oppervlaktelading. Ook de pDNA of siRNA complexatie eigenschappen van de lipoplexen bleven onveranderd, wat aangetoond werd met gelelectroforese. De transfectie efficiëntie (**hoofdstuk 4**) of onderdrukkingsefficiëntie (**hoofdstuk 6**) van de lipoplexen steeg enorm na koppeling aan de microbubbels en ultrasound bestraling, dit in tegenstelling tot de vrije lipoplexen. Zonder ultrasound bestraling waren de met lipoplex beladen microbubbels niet in staat om de cellen te transfecteren, wat toelaat om de genexpressie of genonderdrukking volledig te controleren door ultrasound.

Het is algemeen bekend dat PEGylatie van lipoplexen noodzakelijk is voor *in vivo* applicaties, daar dit een snelle bloedklaring van de lipoplexen en ongewenste immunologische reacties verhindert. Daarentegen is het ook aangetoond dat PEGylatie van lipoplexen hun transfectie-efficiëntie verlaagt doordat het de opname in de cellen en de vrijstelling van partikels uit de endosomen bemoeilijkt. Omdat we in hoofdstuk 4 aantoonden dat het gebruik van lipoplex beladen microbubbels de transfectie-efficiëntie van de gePEGyleerde lipoplexen kan herstellen na ultrasound bestraling, onderzochten we in een volgende stap van dit project hoe de lipoplexen afkomstig van de lipoplex beladen microbubbels werden opgenomen door melanoma cellen (**hoofdstuk 5**). Eerst

bestudeerden we of de lipoplexen opgenomen werden via endocytose. Hiervoor gingen we het effect na van de endocytotische inhibitor methyl- β -cyclodextrine op de transfectie efficiëntie van vrije lipoplexen en lipoplex beladen microbubbels na ultrasoundbestraling. Pre-incubatie van de cellen met methyl- β -cyclodextrine verlaagde enkel de transfectie efficiëntie van de vrije lipoplexen, wat suggereert dat de lipoplexen afkomstig van de microbubbels worden opgenomen via een endocytose onafhankelijke weg. Via confocale microscopie zagen we dat methyl- β -cyclodextrine de cellulaire opname van de vrije lipoplexen verhinderde, wat niet het geval was voor de lipoplex beladen microbubbels. Wanneer we de membranen van de endosomen tijdens de transfectie fotochemisch verstoorden, veroorzaakte dit alleen een verhoging van de gentransfer door de vrije lipoplexen. Dit bevestigde dat de lipoplexen afkomstig van de lipoplex beladen microbubbels niet via endocytose in de cel worden opgenomen. Confocale fluorescentie microscopie-beelden toonden aan dat de vrije lipoplexen voornamelijk aanwezig waren ter hoogte van het celmembraan en enkel na een langere incubatietijd zichtbaar werden in de endosomen. In tegenstelling hiermee zorgde ultrasound bestraling van de lipoplex beladen microbubbels voor een onmiddellijke verstoring van het celmembraan en waren de lipoplexen, kort na bestraling, al zichtbaar in de celmembraan en het cytoplasma van de cel.

De klinische bruikbaarheid van doxorubicine liposomen (DOX-liposomen) (Doxil[®], Caelix[®]) wordt tot vandaag gehinderd door de beperkte diffusie van doxorubicine uit de liposomen. Daarom zoeken verschillende onderzoeksgroepen naar een actief toedieningssysteem voor doxorubicine. In **hoofdstuk 7** van dit doctoraat gebruikten we hetzelfde microbubbel concept, zoals hierboven beschreven, voor de gerichte afgifte van doxorubicine (DOX). Hiervoor werden gebiotinyleerde DOX-liposomen gekoppeld aan het microbubbel oppervlak. Hoewel ultrasound bestraling van de vrije DOX liposomen niet resulteerde in een verhoogde celdood, zorgde bestraling van de DOX-liposoom beladen microbubbels voor een sterke stijging van de doxorubicine toxiciteit. Confocale opnames toonden aan dat het DOX afkomstig van de microbubbels bijna onmiddellijk zichtbaar was in de kern van de melanomacellen. Daarentegen duurde het veel langer vooraleer vrij DOX of vrije DOX-liposomen werden opgenomen. Bovendien was het DOX hierbij eerder zichtbaar in het cytoplasma van de cel en veel minder in de celkern. Onze resultaten bevestigden ook dat de verhoogde cytotoxiciteit van de DOX-liposoom bevattende microbubbels veroorzaakt wordt door drie verschillende redenen. Ten eerste wordt een deel van de liposomen beschadigd bij microbubbel implosie, wat leidt tot een versnelde vrijstelling van DOX. Ten tweede wordt het doxorubicine sneller opgenomen door de cellen door de celmembraan-perforaties die ontstaan tijdens microbubbel implosie. Tenslotte is er een gecombineerd cytotoxisch effect van DOX en sonoporië.

Algemene besluiten

Onze resultaten tonen aan dat het mogelijk is om microbubbels aan te maken die gePEGyleerde pDNA of siRNA bevattende nanopartikels aan hun oppervlak dragen, alsook liposoom bevattende chemotherapeutica (doxorubicin). Na ultrasound bestraling zijn deze microbubbels in staat om hun genetisch of chemotherapeutische geneesmiddelen efficiënt toe te dienen aan melanomacellen. De therapeutische werkzaamheid van verschillende geneesmiddelen (pDNA, siRNA, doxorubicin) kan sterk verhoogd worden door koppeling aan de microbubbels en ultrasound bestraling. Bovendien kan dit zorgen voor een tijd- en plaatsgecontroleerde afgifte, volledig gecontroleerd door ultrasound. Doordat microbubbels en ultrasound al gebruikt worden voor ultrasone beeldvorming in de dagelijkse klinische praktijk, is het microbubbel concept bestudeerd in dit proefschrift een veelbelovende strategie voor toekomstige geneesmiddeltoediening in de klinische praktijk.

Curriculum Vitae

Curriculum Vitae

PERSONALIA

Name	Lentacker
First name	Sabine Maria Alfons
Nationality	Belgian
Place and date of birth	Lokeren, 20/05/1981
Marital status	Married
Children	Siebe, 26/06/2007
Private address	E. Van Hoorebekestraat 62 9050 Ledeberg
Telephone	+32 (0)9 224 00 15
Professional address	Harelbekestraat 72 9000 Ghent
Telephone	+32 (0)9 264 80 78
Fax	+32 (0)9 264 81 89
E-mail	Ine.Lentacker@UGent.be
URL	http://www.biofys.UGent.be

DEGREES

June, 2004	Ghent University – Pharmacist with great distinction
-------------------	--

PEER REVIEWED PUBLICATIONS

Lentacker I., De Geest B.G., Vandenbroucke R.E., Peeters L., Demeester J., De Smedt S.C. and Sanders N.N. Ultrasound-responsive polymer-coated microbubbles that bind and protect plasmid DNA. *Langmuir* 2006 22(17) 7273-7278. **(SCI 4)**

Lentacker I., De Smedt S.C., Demeester J., Sanders N.N. Lipoplex-loaded microbubbles for gene delivery: a Trojan horse controlled by ultrasound. *Advanced Functional Materials* 2007 17(12) 1910-1916. **(SCI 7,5)**

Vandenbroucke R.E.*, **Lentacker I.***, Demeester J., De Smedt SC, Sanders N.N Ultrasound assisted siRNA delivery using PEG-siplex loaded microbubbles. *Journal of controlled release* 2008 126(3) 265-273. **(SCI 4,7)**

* **Equal contribution.**

Sanders N.N., Peeters L., **Lentacker I.**, Demeester J., De Smedt S.C. Wanted and unwanted properties of surface PEGylated nucleic acid nanoparticles in ocular gene transfer. *J. Control Release* 2007 122(3) 226-235. **Invited. (SCI 4,7)**

Peeters L., **Lentacker I.**, Vandenbroucke R.E., Lucas B., Demeester J., Sanders N.N., De Smedt S.C. Can ultrasound solve the transport barrier of the neural retina? *Pharmaceutical Research* 2008 25(11) 2657-2665. **(SCI 2,7)**

Lentacker I., Vandenbroucke R.E., Lucas B., Demeester J., De Smedt S.C., Sanders N.N. New strategies for nucleic acid delivery to conquer cellular and nuclear membranes. *Journal of controlled release* 2008 132(3) 279-288. **Invited. (SCI 4,7)**

Lentacker I., Wang N., Vandenbroucke R.E., Demeester J., De Smedt S.C., Sanders N.N. Ultrasound exposure of lipoplex loaded microbubbles facilitates direct cytoplasmic entry of PEGylated lipoplexes. *Molecular Pharmaceutics* 2009 6(2) 457-467. **(SCI 3,5)**

Lentacker I., De Smedt S.C., Sanders N.N. Drug loaded microbubble design for ultrasound triggered delivery. *Soft Matter* 2009 DOI: 10.1039/b823051j. **Invited. (SCI 4,7)**

Lentacker I., Geers B., Demeester J., De Smedt S.C., Sanders N.N. Design and evaluation of doxorubicin containing microbubbles for ultrasound triggered doxorubicin delivery: cytotoxicity and mechanisms involved. Submitted to Molecular Therapy. **(SCI 5,8)**

CONFERENCE PROCEEDINGS

Lentacker I., De Smedt S.C., Demeester J., Sanders N.N. Microbubbles which bind and protect DNA against nucleases. Journal of Controlled Release 2006 116(2) 73-75. **(SCI 4,7)**

Lentacker I., De Smedt S.C., Demeester J., Sanders N.N. Lipoplex loaded microbubbles for gene delivery: a Trojan horse controlled by ultrasound. Human Gene Therapy 2007 18(10) 1046. **(SCI 4,33)**

Vandenbroucke R.E., **Lentacker I.**, Demeester J., De Smedt S.C., Sanders N.N. Loading of PEGylated siRNA-plexes on microbubbles restores their siRNA delivery capacity in the presence of ultrasound. Human Gene Therapy 2007 18(10) 1046. **(SCI 4,33)**

Lentacker I., De Smedt S.C., Sanders N.N. Circumventing the endocytic uptake of highly PEGylated lipoplexes using lipoplex loaded microbubbles and ultrasound can drastically increase their transfection efficiency. Human Gene Therapy 2008 19(10) 1095. **(SCI 4,33)**

CONFERENCES WITH LECTURE (presenting author)

Lentacker I., De Geest B.G., De Smedt S.C., Sanders N.N. Development and characterization of Layer-by-Layer coated microbubbles as gene delivery system. Biofarmaciedag, Janssen Pharmaceutica Beerse, May 22th 2006.

Vandenbroucke R.E., **Lentacker I.**, Demeester J., De Smedt S.C. and Sanders N.N. Loading of PEGylated siRNA lipoplexes on microbubbles restores their siRNA delivery capacity in the presence of ultrasound. GTRV Summer School, La Grande Motte, France September 6th-8th 2007

Vandenbroucke R.E., **Lentacker I.**, De Geest B.G., Lucas B., Demeester J., De Smedt S.C., Sanders N.N. Nonviral Gene Therapy: battle against major drawbacks. Promega 2nd Signaling and bioluminescence conference, Brussels, Belgium November 14th 2007. **Invited.**

Lentacker I., Vandenbroucke R.E., Demeester J., De Smedt S.C., Sanders N.N. Lipoplex loaded microbubbles for gene delivery. Material Challenges for biomedical applications Ghent, Belgium November 27th 2007.

Sanders N.N., Vandenbroucke R.E., **Lentacker I.**, Lucas B. Demeester J., De Smedt S.C. New strategies for DNA and siRNA delivery. 10th European symposium on Controlled Drug Delivery (ESCDD), Noordwijk aan zee, The Netherlands. April 2nd- 4th 2008. **Invited.**

Lentacker I., Demeester J., De Smedt S.C., Sanders N.N. Shooting PEGylated lipoplexes into the cell membrane with ultrasound responsive lipoplex loaded microbubbles. 11th Annual Meeting of the American Society of Gene Therapy, Boston, USA May 28th - June 1st 2008.

Lentacker I., De Smedt S.C., Sanders N.N. Liposome loaded microbubbles for ultrasound targeted drug delivery. International Sonothrombolysis Conference, Mannheim/Heidelberg, Germany July 4th- 5th 2008.

Lentacker I., De Smedt S.C., Sanders N.N. Circumventing the endocytic uptake of highly PEGylated lipoplexes by using lipoplex loaded microbubbles and ultrasound can drastically increase their transfection efficiency. XVIth Annual Congress of the European Society of Gene and Cell Therapy, Brugge, Belgium, November 13th-16th 2008.

Lentacker I., De Smedt S.C., Sanders N.N. Nanoparticle loaded microbubbles for ultrasound assisted gene delivery. Microbubbles for ultrasound imaging and Drug delivery: New applications with bursting bubbles. Philips Research, Eindhoven, The Netherlands, November 28th 2008. **Invited.**

Lentacker I., Vandenbroucke R.E., Demeester J., De Smedt S.C., Sanders N.N. Drug loaded microbubbles for ultrasound assisted drug delivery. 14th European symposium on ultrasound contrast imaging. Rotterdam, The Netherlands, January 22th-23th 2009. **Invited.**

CONFERENCES WITH POSTER PRESENTATION (presenting author)

Lentacker I., De Geest B.G., Vandenbroucke R.E., Peeters L., Demeester J., De Smedt S.C., Sanders N.N. Development and characterization of ultrasound responsive microbubbles for gene delivery.

- Biofarmaciedag, Gent, Belgium, May 20th 2005.
- Biofarmaciedag, Utrecht, The Netherlands, December 2nd 2005.
- Ninth European symposium on Controlled Drug Delivery, Noordwijk-aan-Zee, The Netherlands, April 5th-7th 2006.
- 9th Annual meeting of the American Society of Gene Therapy, Baltimore, Maryland, USA, May 31th June 4th 2006.

Lentacker I., De Smedt S.C., Demeester J., Sanders N.N. Lipoplex loaded microbubbles for ultrasound targeted gene delivery.

- Biofarmaciedag, Leiden , The Netherlands, November 27th 2006.
- 12th European Symposium on Ultrasound Contrast Imaging, Rotterdam, the Netherlands, January 25th-26th 2007.

Lentacker I., De Smedt S.C., Demeester J., Sanders N.N. Lipoplex loaded microbubbles for ultrasound targeted gene delivery. ESGCT 15th annual meeting, Rotterdam, The Netherlands, October 27th -30th 2007.

Vandenbroucke R.E., **Lentacker I.**, Demeester J., De Smedt S.C., Sanders N.N. Loading of siRNA lipoplexes on microbubbles can overcome the low transfection efficiency of highly PEGylated siRNA lipoplexes.

- Pre-Satellite Meeting of the 3rd Pharmaceutical Sciences World congress (PSWC 2007), Amsterdam, The Netherlands, April 20th-21th 2007.
- ESGCT 15th annual meeting, Rotterdam, The Netherlands, October 27th -30th 2007.

Lentacker I., Vandenbroucke R.E., Demeester J., De Smedt S.C., Sanders N.N. Loading of siRNA lipoplexes on microbubbles can overcome the low transfection efficiency of highly PEGylated siRNA lipoplexes.

- 10th annual meeting of the American Society of Gene Therapy, Seattle, USA May, 30th - June 3th 2007.
- Summer School on Therapeutic Ultrasound, Cargèse, France, April 10th-13th 2007.

Lentacker I., De Smedt S.C., Demeester J., Sanders N.N. Lipoplex loaded microbubbles for Gene delivery: a Trojan horse controlled by ultrasound.

- Summer School on Therapeutic Ultrasound, Cargèse, France, April 10th-13th 2007.
- Pre-Satellite Meeting of the 3rd Pharmaceutical Sciences World congress (PSWC 2007), Amsterdam, The Netherlands, April 20th-21th 2007.
- 10th annual meeting of the American Society of Gene Therapy, Seattle, USA May, 30th - June 3th 2007.

CONFERENCES WITHOUT LECTURE OR POSTER PRESENTATION

11th European Symposium on Ultrasound Contrast Imaging, Rotterdam, the Netherlands, January 20th-21th 2005.

RESEARCH VISITS

September 2005 - Cardiovascular Research Unit, Northern General Hospital, Sheffield University –
“Transfection experiments on Vascular Smooth Muscle cells”